THESE DE DOCTORAT DE
L'UNIVERSITE PIERRE ET MARIE CURIE

Spécialité :
Informatique

présentée par

Corina IOVAN

pour obtenir le grade de
DOCTEUR DE L'UNIVERSITE PIERRE ET MARIE CURIE

Détection et caractérisation de la végétation en milieu urbain à partir d'images aériennes haute résolution

Detection and Characterisation of Vegetation in Urban Areas from High Resolution Aerial Imagery

soutenue publiquement le 30 novembre 2009
devant le jury composé de :

Didier BOLDO	Chargé de Recherche à l'Institut Géographique National	*encadrant*
Matthieu CORD	Professeur à l'Université Pierre et Marie Curie (Paris 6)	*directeur de thèse*
Patrick GALLINARI	Professeur à l'Université Pierre et Marie Curie (Paris 6)	*examinateur*
Michel ROUX	Maître de Conférences à Télécom ParisTech	*examinateur*
Nicole VINCENT	Professeur à l'Université Paris Descartes (Paris 5)	*rapporteur*
Josiane ZERUBIA	Directrice de Recherche INRIA Sophia Antipolis	*rapporteur*

Acknowledgement Trees

During the study years spent at the French National Mapping Agency (IGN) and the Pierre et Marie Curie University (UPMC), I have met many people who have provided priceless contribution to this work. Fortunately, I could always rely on their support, sympathy and wisdom and they deserve my most tender acknowledgment.

To my family for love and support (Paris, December 2009).

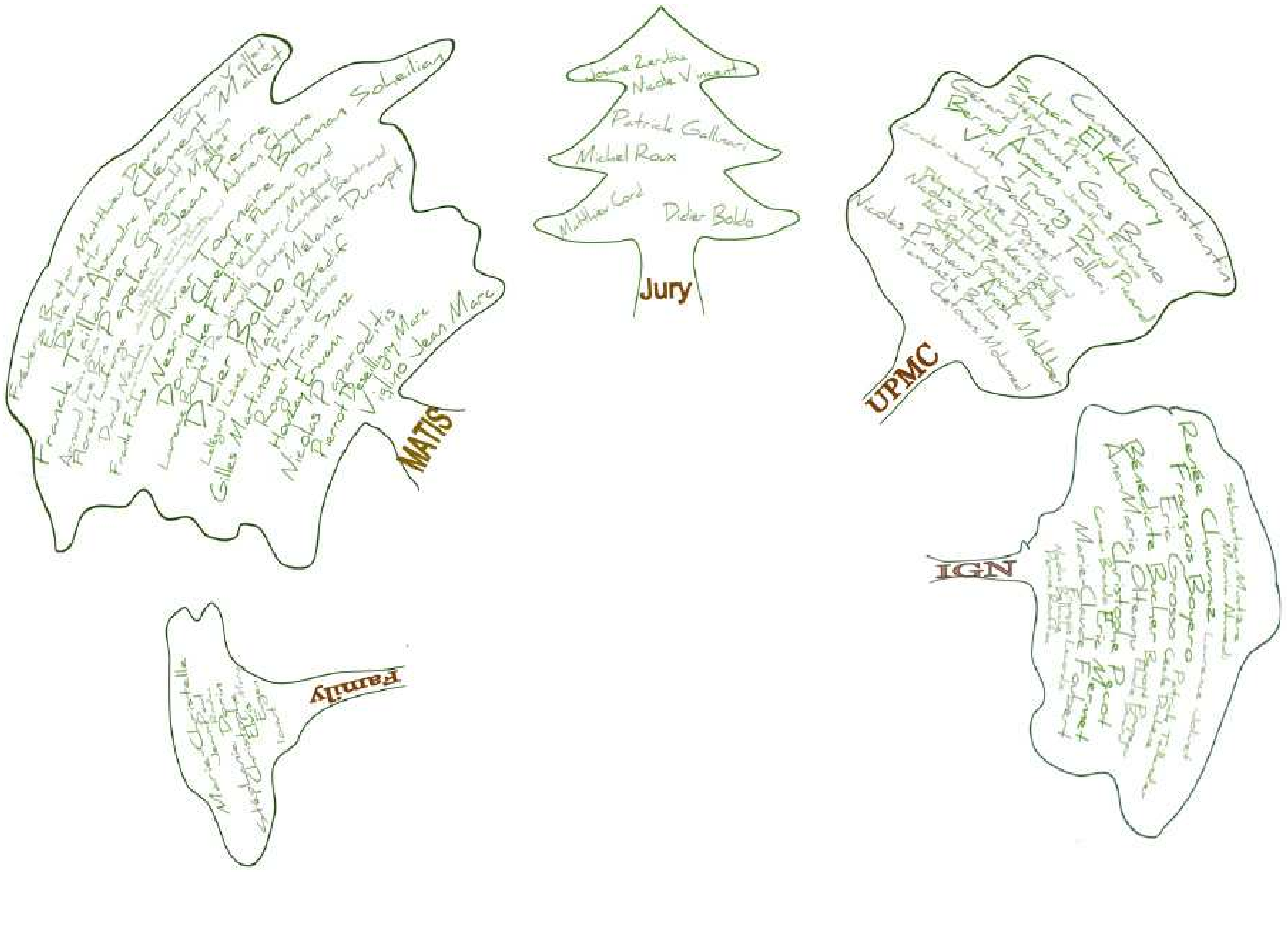

Contents

List of Figures

List of Tables

Chapter 1

Introduction

1.1 General context

Over the past centuries, the production of maps depicting the Earth's surface was hindered by lack of detailed sources of geographic information. Since remote sensing data became available in the 1930s accurate topographic mapping at large scales replaced traditional topographic tools and allowed to map in detail a multitude of new environments (e.g. wetland, agricultural land, forest and urban or built-up land) [Robinson *et al.*, 1995].

One of the primary challenges to understand the dynamics of the Earth system is an accurate assessment of the relationships between human population and the other components of the system [Small and Miller, 1999]. As the global rate of urbanisation increases [United Nations, 2007], so does the relative importance of the urban environment to the global population.

Vegetation is of particular interest as it presents a versatile resource for effectively managing and moderating a variety of problems associated with urbanisation. The spatial distribution and abundance of urban vegetation, for example, is recognised as a key factor influencing numerous biophysical processes of the urban environment. Given the associations between vegetated land cover and the biophysical and social processes of urban systems there exists an ongoing demand for effective urban vegetation mapping and classification techniques [Tooke *et al.*, 2009], [Zhang and Feng, 2005].

Progress in computer science and its wide use produced a major increase in the speed and efficiency of the mapping process. Nowadays, when a person sitting in front of a computer calls forth data in map format, much of this information comes from geographical databases storing information most probably obtained by remote sensing techniques [Robinson *et al.*, 1995]. The detail level stored in geographical databases on each land cover environment depends on the analysed environment. Urban areas contain residential zones, industrial and commercial complexes, lawn areas and parks, gardens and fragments of natural landscapes, bare soil, streets, and other types of urban land cover classes. Information on these geographic entities such as building footprints, and height, building superstructures or streets are stored in three dimensional (3D) databases and can be used for urban modelling applications.

Recently the need for 3D data describing urban areas increased. This data is useful for a variety of applications such as city planning, architecture, micro-climate investigations or planning in telecommunication. All these applications need 3D city models, but of course the requirement concerning the quality of description is are as various as the applications. If research concerning building reconstruction has reached maturity [Durupt and Taillandier, 2006], the most acute problem is distinguishing between building and vegetation areas.

1.2 Specific context of the thesis

Since the 1990s, the MATIS laboratory of IGN conducts research on automatic or semi-automatic production and updating of geographical databases from remote sensed data. Research on automatic 3D reconstruction of urban areas focused on building reconstruction [Taillandier, 2004] and streets [Ruskoné, 1996], [Tournaire, 2007]. These urban features have been successfully integrated into final products [Flamanc *et al.*, 2003], and recently the operational system BATI-3D ®, for 3D urban area modelling [IGN, Institut Géographique National, 2008].

Vegetation is another important feature of urban areas with environmental and social effects. They are an issue of primary importance in fields such as urban planning, disaster management or telecommunications planning. Accurate information on the position of trees and their species is mandatory for green area and tree stand management in urban areas and essential for a realistic modelling of the urban environment. 3D city models could be enriched by integrating detailed information on the vegetation component. The modelling of vegetation is a considerable challenge due to the complex nature and its intricate distribution between other urban features. Trees are especially difficult to represent because of their complex structure and their interaction with other trees as well as with other objects, such as buildings or cars present on the streets.

The works presented in this thesis were conducted at the MATIS laboratory of the French National Mapping Agency (Institut Géographique National, IGN) as part of the Cap Digital Business Cluster, Terra Numerica project [Ministry for the Economy, Industry and Employment, 2009]. The aim of this thesis is to develop a system for the analysis of urban vegetation able to detect vegetation areas, separate them into distinct vegetation classes (lawns and trees), delineate individual tree crowns, estimate 3D tree parameters and perform tree species classification. The system should meet the following requirements:

- *completeness* currently, most algorithms generating 3D city models do not take into account the vegetation component of a city. Their interest in vegetation go rarely beyond detecting it in order to discard it as it is considered as noise for building reconstruction algorithms. The vegetation analysis system should provide enough information on urban vegetation so that it could be suppressed in a first time to allow a better reconstruction of buildings and thereafter vegetation models should be re-inserted into the 3D city model.

- *robustness* accurate information on urban vegetation obtained by means of the vegetation analysis system will find applications in urban planning where accurate information on vegetation species are of high importance in order to find the best moment to perform vegetation lopping.

1.3 Image analysis systems for vegetation detection

1.3.1 Related works

Ever since Earth observation satellites were launched, one challenging application was the analysis of urban settlements from remotely sensed data. With the increased spatial resolution of remote sensed data, applications vary from land cover and land use analysis to delineating built-up land features [Xu, 2008] and estimating vegetation cover [Buyantuyev *et al.*, 2007]. Urban landscape is also analysed and characterised from high-resolution digital aerial imagery and LIght Detection and Ranging (LIDAR) data [Zhou and Troy, 2008], [Haala and Brenner, 1999], [Knudsen, 2005], [Zhang, 2001], [Rutzinger *et al.*, 2007], [Weinacker *et al.*, 2004].

Pinz [1991] describes the concept of a computer vision system capable of finding trees in infrared aerial photographs. Generic description of a type of object is integrated with the image object where an object is, in this case, a tree. The tree recognition results from aerial photographs taken at different resolution scales and under various conditions are also integrated at the feature, namely tree, level.

Gerke *et al.* [2001] used a tree model combining geometric and radiometric features and neighbourhood relations for trees in urban environments from colour infrared aerial images and normalised digital surface models.

At the moment this work began and to the best of the author's knowledge, there were not a lot of complete and functional systems aiming at dealing with vegetation in urban areas. Works closest to the ones presented in this thesis, both from an input data point of view and from the output objectives are the ones of Straub *et al.* [2003]. They proposed a system dealing with automatic extraction of trees for 3D city models from images and height data. In a first step, trees are extracted based on radiometric and geometric models of trees. Trees are later on separated into individual units by using the watershed segmentation algorithm. Tree crown boundaries are measured with active contours and 3D city models benefitting from 3D views of trees are finally generated.

1.3.2 Research Strategy

The works presented in this thesis seek to provide a further contribution for the analysis of urban vegetation by proposing a complete hierarchical approach to analyse vegetation in urban areas. The strategy developed is a hierarchical one: regions of interest containing vegetation are extracted in a first step and category of objects present therein are analysed in following steps either through segmentation or classification approaches. This type of strategy was successfully adopted on other type of urban features, such as buildings [Baillard *et al.*, 1998], [Cord and Declercq, 2001]. The methodological approach adopted in this research is composed of three main steps:

- *step 1* detection of vegetation areas
- *step 2* segmentation into low- and high- height vegetation and tree crown delineation
- *step 3* characterisation of vegetation for an accurate 3D tree description in urban areas

A global view of the complete hierarchical system developed to analyse urban vegetation is given in Figure 1.1. The proposed system extracts all vegetation areas, separates them into high- and low-height vegetation, delineates individual tree crowns, extracts 3D tree parameters (such as crown diameter, height, trunk localisation) and classifies them according to their species. The results of this system are used to create realistic urban virtual environments.

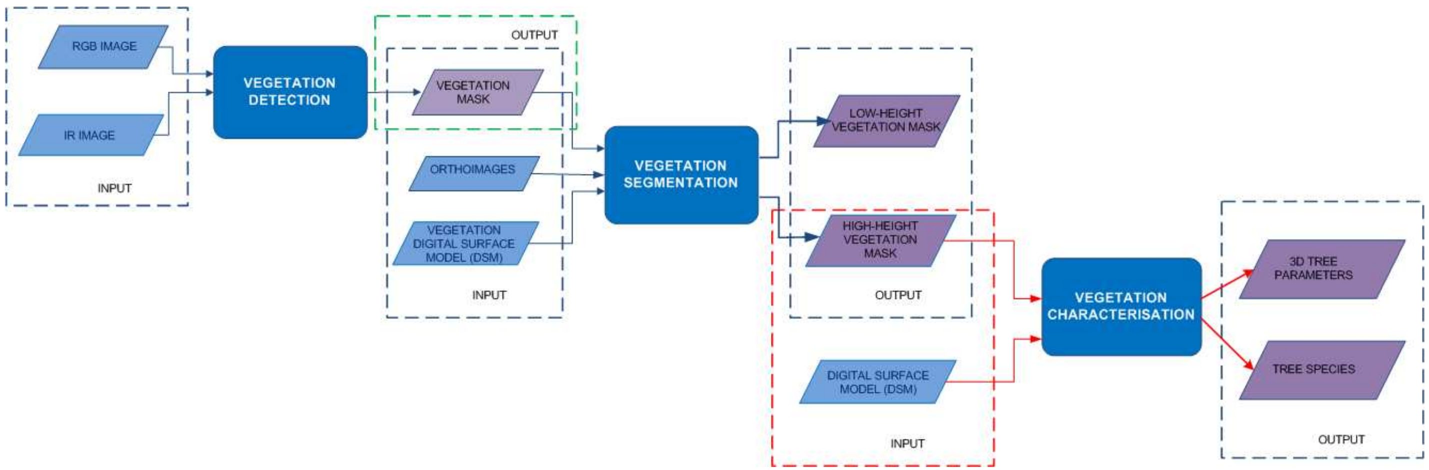

Figure 1.1: Hierarchical system developed to analyse urban vegetation. The first module of the proposed system extracts vegetation areas from high resolution aerial input data of urban areas. Vegetation masks are processed by the following module which separated them into high- and low-height vegetation areas and performs individual tree crown delineation. The third module is used to estimate 3D parameters of trees and to classify them according to their species.

1.4 Contributions

The main contributions of this thesis are listed in the following:

- We propose a vegetation mapping and management tool that from high resolution remote sensed data of urban areas locates vegetation areas, separates them into lawn and trees, delineates individual tree crowns, estimates 3D tree attributes and performs tree species classification.
- To *detect vegetation in urban areas*, we propose an approach based on supervised learning techniques, using a Support Vector Machines (SVM) classifier on multispectral features [Iovan *et al.*, 2007].
- To *delineate individual tree crowns*, we propose a robust method for finding *seed regions* based on height data [Iovan *et al.*, 2007], [Iovan *et al.*, 2008a] which will be grown to represent tree crown regions by integrating individual tree height data.
- We show that provided an accurate ground truth database, *tree species classification* in urban areas can be accurately performed by using spectral and spatial feature vectors computed on different colour spaces [Iovan *et al.*, 2008a].
- We collected reference data on tree species from the city of Marseille, France and formed the first *tree species reference database* useful for testing different classification systems.
- Research work presented in this thesis has been successfully integrated in IGN's BATI-3D ® production line [IGN, Institut Géographique National, 2008] for the creation of realistic 3D virtual representation of a city's vegetation component [Iovan *et al.*, 2009].

1.5 Outline

The body of this thesis is divided into six chapters, the first of which is this introduction (Chapter 1). The remainder of the manuscript is organised in such a way that each chapter deals with a relatively independent issue. Specific topics for the following chapters are summarised as follows:

- *Chapter 2* presents data used in this thesis, details on the study area and acquisition conditions and illustrates reference data set used to perform tree species classification.

- *Chapter 3* investigates spectral reflectance of vegetation in urban areas for vegetation detection by means of two approaches, a first one based on spectral indexes and a second one using a Support Vector Machines (SVM) classifier.

- *Chapter 4* details image segmentation algorithms for segmentation of low- from high-height vegetation areas and for individual tree crown delineation.

- *Chapter 5* describes the methods used to estimate 3D tree parameters and returns to the task of classification by presenting the spectral and spatial feature vectors computed on different colour models to perform tree species classification.

- *Chapter 6* gives concluding remarks, summarises the research as well as points out the possible directions for future studies.

Finally, Appendix A presents the theory of the SVM supervised classifier used throughout this thesis and a summary of the classifier evaluation protocol and of tools used for accuracy assessment, whereas Appendix B illustrates reference data set used to perform tree species classification.

CHAPTER 2

Data and Study Area

2.1 Data

In this section data used in this research will be presented, starting from the acquisition, going on to the pre-processing and the methods used to obtain derived data. Data used in this thesis represents standard types of data produced for 3D city modelling applications. No specific data acquisition is required to obtain vegetation areas, low- and high height vegetation masks and tree crown contours.

2.1.1 Images

The aerial images were acquired by the digital cameras developed at IGN's LOEMI research laboratory according to a flight plan containing *flight strips* ensuring an overlap of 60% between images taken within each strip and 60% between two adjacent strips. This ensures that all the points of the studied area are visible on at least four to nine images. The CCD (Charged-Coupled Device) matrix is made up of more than 16 millions pixels (4096×4096) each having a size of 9 μm [Thom and Souchon, 1999]. The four channels (red (R), green (G), blue (B) and near-infrared (IR)) were acquired simultaneously by four different acquisition heads of a four-head camera system [Paparoditis *et al.*, 2006].

Figure 2.1 illustrates the acquisition system used for recording images of the Marseille study area.

The data set is made up of high-resolution georeferenced aerial images with a resolution of 20 cm per pixel and were acquired according to the flight plan presented in Figure 2.2.

2.1.2 Derived Data

The multiview properties of the acquisition system are exploited to produce the digital surface model, described in the following sections. Figure 2.3 gives an overview of data derived from the multiple view images.

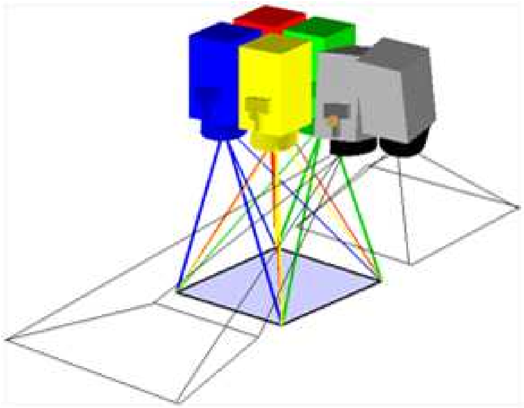

Figure 2.1: The system was developed in the LOEMI Laboratory [LOEMI, 2009] and it is the result of coupling one classical camera system with four acquisition heads for the R, G, B and near-infrared bands with one two-head forward-backward camera with no overlapping between the areas covered by the two heads.

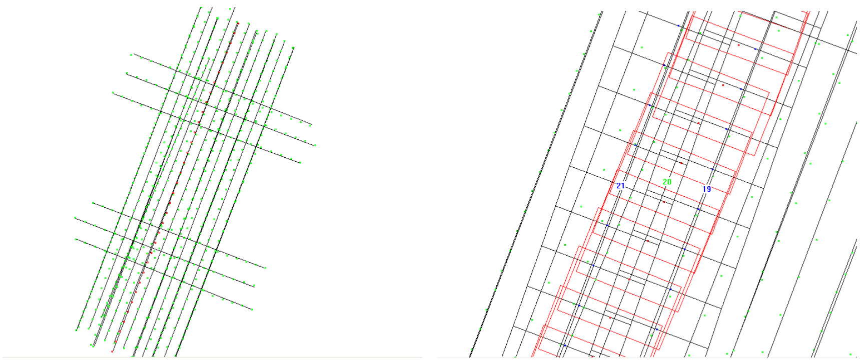

(a) (b)

Figure 2.2: Flight plan for the 2004 aerial-image acquisition campaign for the city of Marseille. (a) A total of 23 flight-strips were flown, 6 of which are perpendicular. Dots on each flight strip stands for the position where an image was captured. (b) Enlarged detail of flight strips 19, 20 and 21 illustrating the 60% overlap between images taken on the same strip and 60% between two adjacent strips. Areas covered by images taken in each strip is presented by a bounding rectangle.

2.1.2.1 Orthoimages

Orthoimages (also called orthophotographs) are planimetrically correct aerial images [Robinson *et al.*, 1995] combining the geometric utility of a map with the extra real-world image information provided by a photograph [Lillesand *et al.*, 2008]. They do not contain the scale, tilt and relief distortions characterising normal aerial photographs. Figure 2.4 illustrates a three channel RGB orthoimage and its corresponding IR orthoimage which were generated from the vertical and oblique

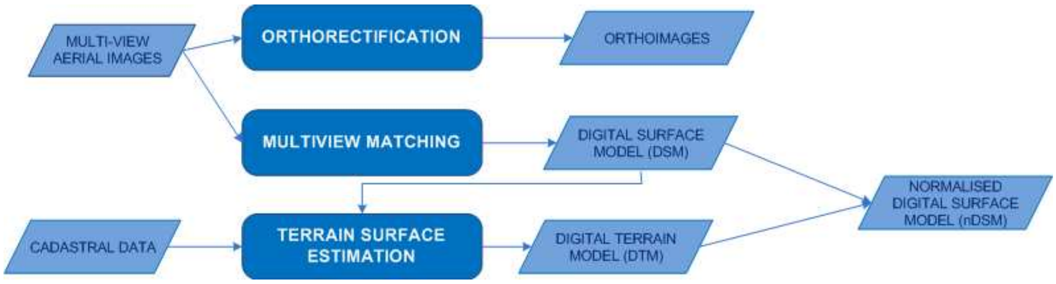

Figure 2.3: Flow diagram of data set creation. Aerial images and cadastral data are used to obtain additional data. Due to the important overlap between aerial images, the DSM obtained is accurate enough for 3D object analysis problems.

RGB and IR images.

2.1.2.2 DSM, DTM, nDSM

A dense Digital Surface Model (DSM) is computed from multiple images using the MICMAC [1] multi-view matching algorithm [Pierrot-Deseilligny and Paparoditis, 2006]. Buildings are masked on the DSM, and the resulting depth map is further on used to estimate the terrain surface, thus obtaining a Digital Terrain Model (DTM) [Champion and Boldo, 2006] which is a digital representation of the topographic surface. A Normalised Digital Surface Model (nDSM), containing the height of above ground objects, is computed as the difference between DSM and DTM.

Figure 2.5 shows a *Digital Surface Model* (DSM), also referred to as a *Digital Elevation Model* (DEM). The DSM is similar to a digital image, with the digital number at each pixel representing a surface elevation rather than a radiance value [Lillesand *et al.*, 2008]. In Fig. 2.5 the brightness of each pixel is represented as being proportional to its elevation, so light-toned areas are topographically higher and dark toned areas are lower.

2.2 Study Areas

Marseille

The study area is located in the city of Marseille, situated in the south-east of France. Marseille's climate is Mediterranean, with a great variety of vegetation species. It is a complex urban area, with many greened and treed resting places, highly intermingled with buildings. Figure 2.6 presents the ortho-image of the

[1] http://www.micmac.ign.fr

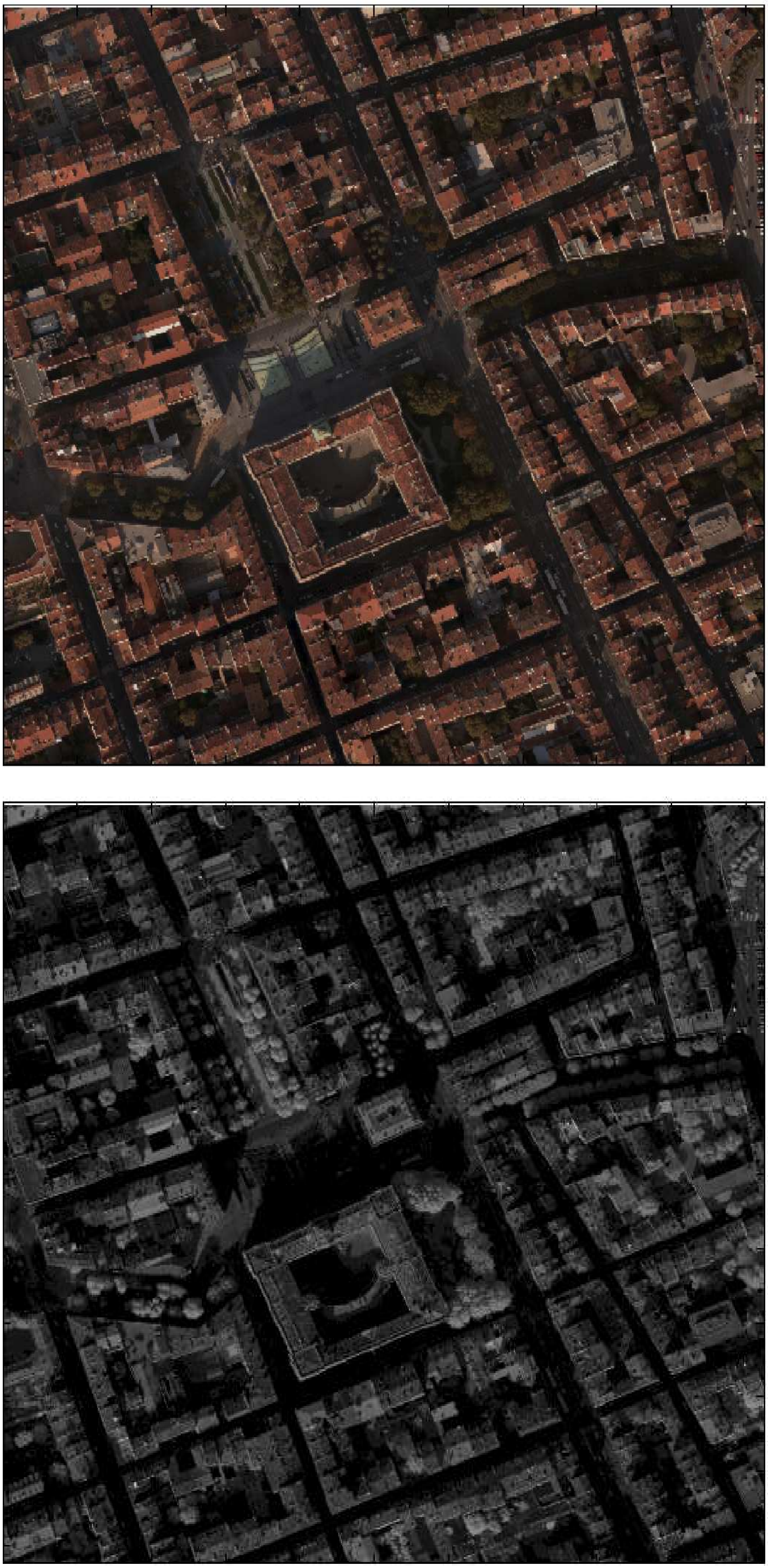

Figure 2.4: RGB and IR orthoimages of Marseille site B.

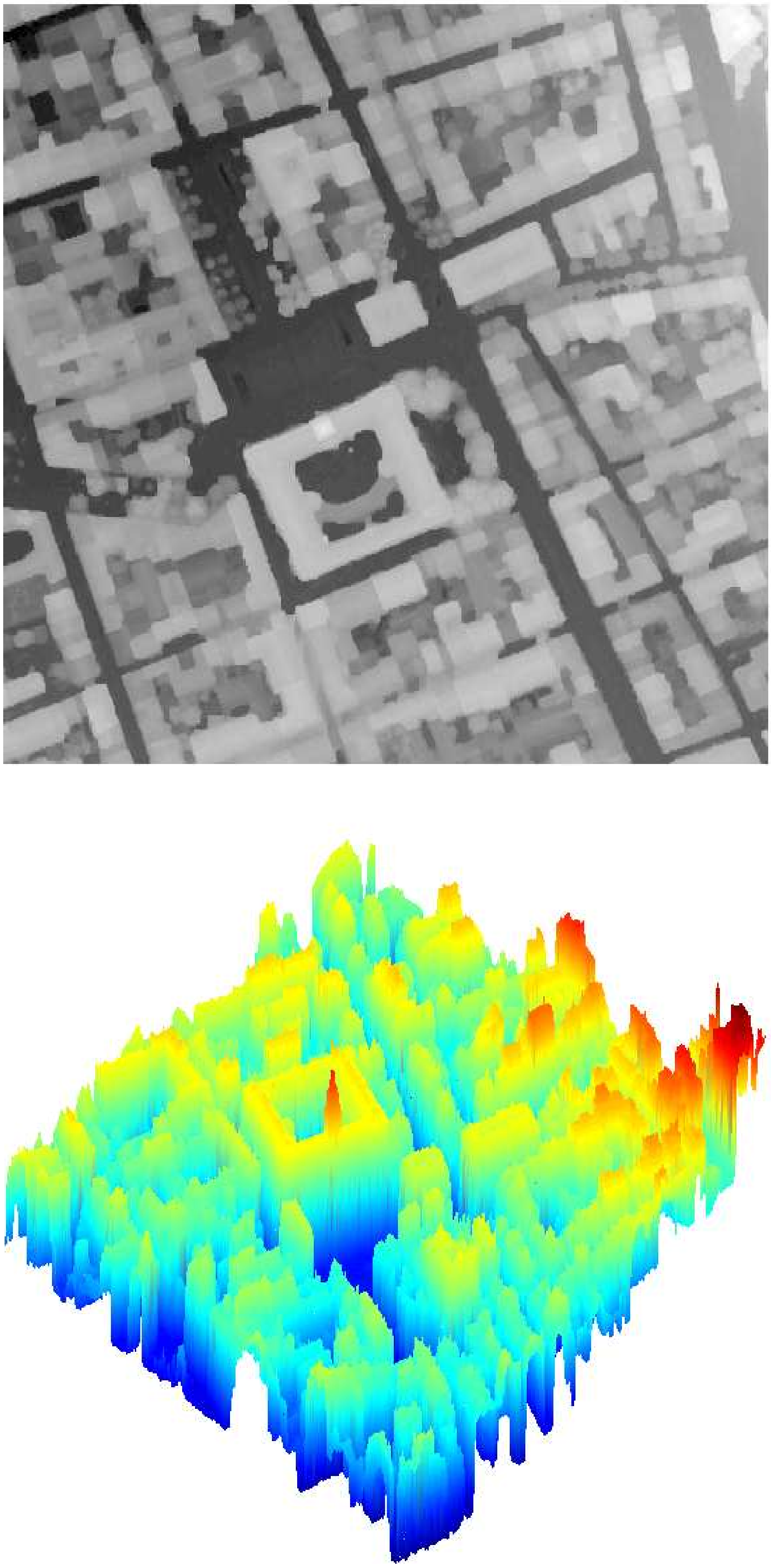

Figure 2.5: Digital Surface Model of Marseille with brightness proportional to elevation.

study area and highlights the three sites used in this thesis. Larger crops of each site are given below in Figures 2.7, 2.8 and 2.9.

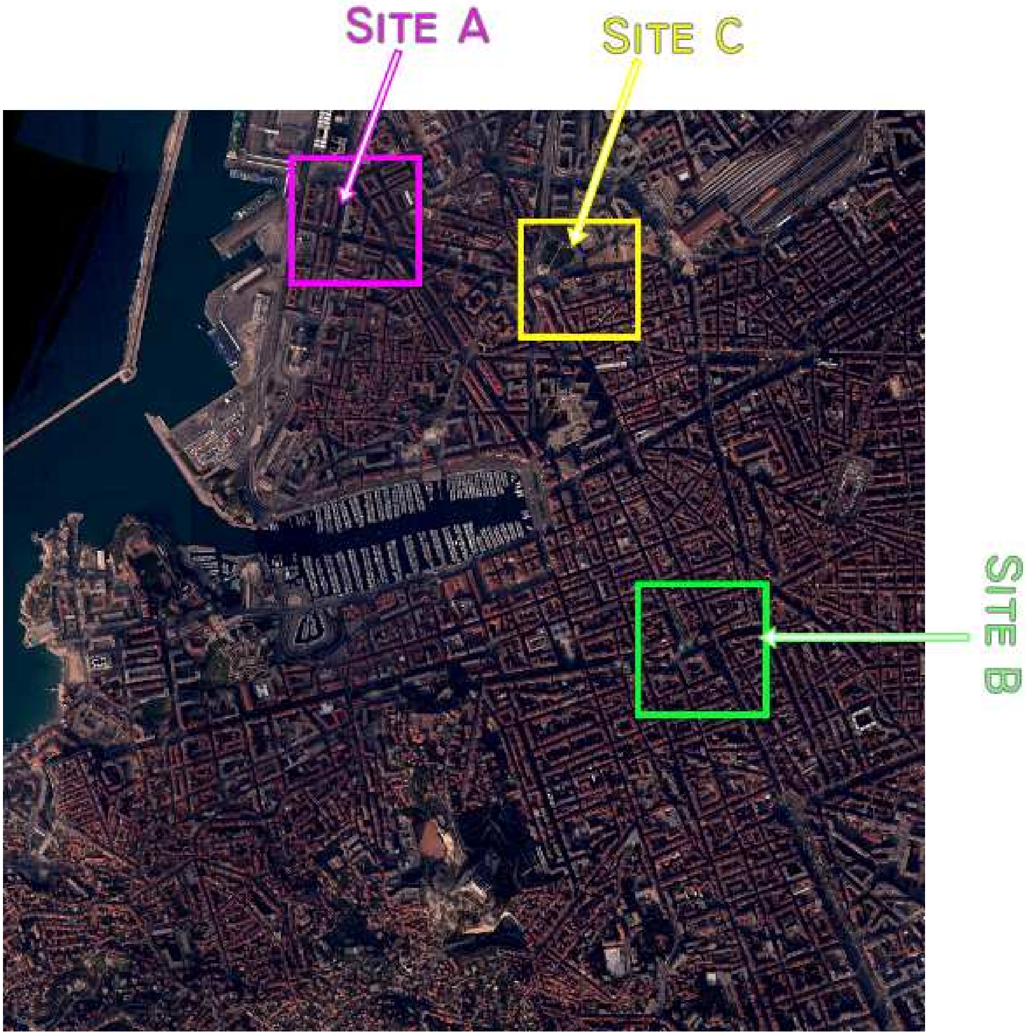

Figure 2.6: Orthoimage of Marseille study area illustrating the three sites used to test algorithms presented in this study.

Figure 2.7: Orthoimage of Marseille study area site A showing a portion of ≈ 167 000 m^2 of urban area, where 1 pixel corresponds to 20 cm.

Figure 2.8: Orthoimage of Marseille study area site B illustrating a portion of ≈ 167 000 m^2 of urban area, where 1 pixel corresponds to 20 cm.

Figure 2.9: Orthoimage of Marseille study area site C showing a portion of ≈ 167 000 m^2 of urban area, where 1 pixel corresponds to 20 cm.

2.3 Reference Data

Remotely sensed data is rarely employed without the use of some form of *reference data*, often referred to by the term *ground truth* [Lillesand *et al.*, 2008]. In this work, the second term will be employed both to denote reference data acquired on ground (such as the tree species reference data) and by means of photo interpretation (such as the tree crown delineations) generated by a qualified human interpreter. This data is used to verify information extracted from remote sensing data by the algorithms proposed in this thesis. The acquisition of reference data involves collecting measurements or observations about the objects and areas that are being sensed remotely [Lillesand *et al.*, 2008]. The collection of reference data is often a difficult, expensive and time consuming task.

In the context of this thesis, an experienced photo-interpreter with no *a priori* knowledge on the scene was given the task of partitioning images of the three sites into a number of homogeneous polygons all containing one type of urban vegetation, either lawns or individual tree crowns. This was done by means of stereo restitution. The operator was supplied with images used to generate the orthoimages and with the help of a digital stereo plotter, ground herbaceous regions and individual tree crown contours were delineated. A total of 29 hours of work were necessary to annotate vegetation areas in sites A, B and C.

Reference data for tree species identification was collected in September 2006 during a field acquisition campaign in the city of Marseille, France. Field data was collected for each tree having its crown delineated by photo-interpretation. Field data consisted of a set of three images: one image of the tree's trunk, one of its leaves and one of the whole tree, including trunk and crown. Tree species in the entire set of images were identified by their scientific and common names by the *Inventaire Forestier National*, IFN (French National Forest Inventory). A total of 15 different tree species were identified in the sites A, B and C. The collection of a tree species data set is a premier for the IGN and could be exploited to evaluate tree species classification performances for different classification systems. More details and several images depicting ground truth data are presented in Appendix B.

Chapter 3

Vegetation Detection and Localisation

3.1 Introduction

The goal of this chapter is to present the techniques developed to detect vegetation in urban areas from high resolution colour infrared aerial imagery (cf. Chapter 2). After a brief review of state of the art techniques aiming at differentiating between vegetation and non vegetation in remotely sensed images (section 3.2), a detailed description of the proposed approach is given (section 3.3). Results obtained on test areas will further on be presented together with a quantitative evaluation of the quality of the detection module. A comparison with results obtained by applying state-of-the-art techniques for vegetation detection is presented in section 3.3.1 and finally the advantages and drawbacks of the proposed method will be highlighted (section 3.4).

Vegetation detection aims at grouping together semantically coherent regions and localising them in aerial images.

In other terms, the purpose of this module is to answer to the following two questions:

- *does the remotely sensed data contain information characterising vegetation?*
- *where in the data is this information located?*

Consider the images in Figure 3.1 and try to identify the objects present therein. What are the clues you use to interpret these images? What information is recovered from an image in order to recognise vegetation? Intuitively, colour/tone is a fundamental feature to look for to separate vegetation from man-made objects in an urban environment. But as we can see from the example presented in Figure 3.1-(a) vegetation is not always green. This is also the case when data is recorded under leaf-on/leaf-off conditions.

Shape is another cue which might be taken into consideration to distinguish vegetation from non-vegetation areas. We could separate man-made objects from

(a) (b)

Figure 3.1: Given the images on the left, what clues are useful to extract objects on the right? (a) *Vegetation is not always green. (b) Not every green object is vegetation.*

natural ones by describing the later ones as having irregular shapes and boundaries and the former ones, geometric (square or circular) shapes and distinct boundaries. Figure 3.2 contradicts this assumption by presenting a grass covered building having geometric boundaries. Other cases introducing uncertainty when using shape as criteria in the recognition of vegetation are building balconies or terraces on top of buildings having trees in plant pots.

Texture could be an important feature to recognise different objects in aerial images, with smoothness indicating surfaces of similar height whereas coarseness, irregular height surfaces. But, as vegetation is composed both of grass (low height) and trees (high-height), texture could not be a reliable indicator to separate between vegetation and non vegetation areas.

From a conceptual point of view, answering to the above mentioned questions implies:

- *developing an algorithm or model which relates vegetation parameters to its radiance as measured by a remotely located sensor*
- *inverting the algorithm or model to extract the vegetation parameters from the measured radiance*

Delineation of vegetation cover in urban areas can be realised by means of image interpretation techniques based on either the reflectance properties of the vegetation cover, its colour properties or its structure. Pixel wise statistical interpretation completely neglects the shape and context aspects of the image information, which are the main clues for a human interpreter. Shape, texture and context are particularly important in the interpretation of images of high spatial resolution.

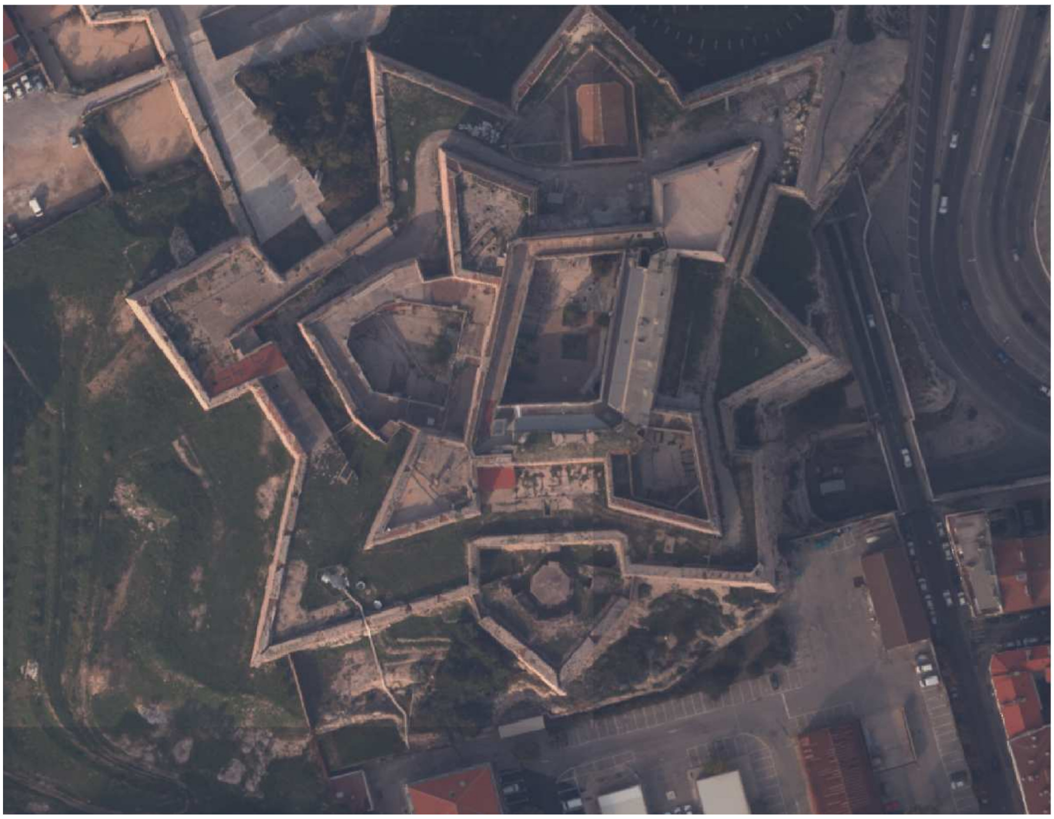

Figure 3.2: Grass covered building reflecting sources of incoherence when assuming that vegetation areas have irregular contours.

Taking into account the input data, our objectives can be fulfilled by exploiting either its spectral characteristics, spatial ones or both types of characteristics.

Taking into account the spectral characteristics of objects is a preferred way of analysing and interpreting remotely sensed data as it is founded on solid physical laws.

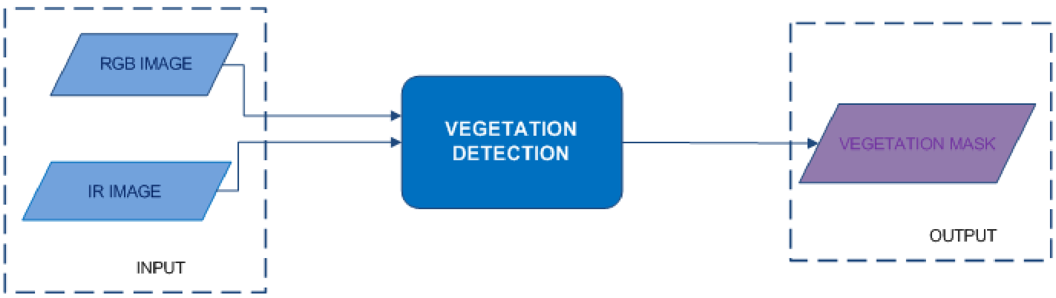

Figure 3.3: Vegetation detection module.

Figure 3.3 gives an overview of the system developed to detect vegetation cover in urban areas. The system takes as input RGB and IR images of the urban areas and outputs binary masks for vegetation areas.

Before presenting our approach to detect vegetation, we will synthesise in the following section other approaches to detect vegetation from optical remotely sensed data. Information about remotely sensed data collected by LIDAR systems is outside the scope of this thesis, but the following reference gives a good insight into the subject [Mallet and Bretar, 2009].

3.2 Related Works

After the review on major features to be exploited by vegetation detection algorithms, a more detailed presentation of methods developed to extract vegetation from remote sensing imagery is given in the following part of this section. These methods will be grouped according to exploited features. The presentation will be detailed on studies focusing on vegetation in urban areas and restrained to algorithms developed for land cover/land use applications.

First studies on satellite imagery were applied to natural/agricultural areas which can generally be considered as homogeneous, compared to urban areas [Michel and Lortic, 1992]. Colour/tone was intensively used to distinguish between vegetation and non vegetation in such areas. Since objects, including vegetation have their unique spectral signature, they can be identified according to their spectral characteristics, mostly by vegetation indexes (VIs). VIs are spectral transformations of two or more bands designed to enhance the contribution of vegetation properties. As a simple transformation of spectral bands, they are computed directly without any bias or assumptions regarding land cover class, soil type, or climatic conditions [Huete *et al.*, 2002]. Pre-processing of data is a necessary step prior to vegetation extraction based on spectral indexes. Pre-processing steps commonly comprises a series of operations such as radiometric correction, geometric correction, image enhancement [Xie *et al.*, 2008].

Various authors have used indices with slightly different spectral bands or with variations in the algebraic form [Perry and Lautenschlager, 1984]. According to Jackson *et al.* [1983] the ideal vegetation index should be particularly sensitive to vegetative covers, insensitive to soil colour and to soil brightness and little affected by atmospheric effects, environmental effects and solar illumination geometry and sensor viewing conditions. Table 3.1 gives the most used VIs in the literature.

Table 3.1: Different vegetation indexes (adapted from [Bannari *et al.*, 1995])

Index	Abbreviation	Formula	Author & year
Ratio Vegetation Index	RVI	$\frac{R}{NIR}$	Pearson and Miller, 1972
Vegetation Index Number	VNI	$\frac{NIR}{R}$	Pearson and Miller, 1972
Normalised Difference Vegetation Index	NDVI	$\frac{NIR-R}{NIR+R}$	Rousse et al., 1974
Transformed Vegetation Index	TVI	$\sqrt{NDVI+05}$	Rousse et al., 1974
Perpendicular Vegetation Index	PVI	$\sqrt{(\varphi_{soil}-\varphi_{vegetation})_R^2+(\varphi_{soil}-\varphi_{vegetation})_{NIR}^2}$	Richardson and Wiegand, 1977
Transformed Vegetation Index	TVI	$\frac{(NDVI+0.5)}{\lvert NDVI+0.5\rvert}\sqrt{\lvert NDVI+0.5\rvert}$	Perry and Lautenschlager, 1984
Differenced Vegetation Index	DVI	$(NIR-R)$	Clevers, 1986
Normalised Difference Greenness Index	NDGI	$\frac{G-R}{G+R}$	Chamad et al., 1991
Redness Index	RI	$\frac{R-G}{R+G}$	Escadafal and Huete, 1991

The most frequently used VI for vegetation mapping is the Normalised Difference Vegetation Index (NDVI), introduced by Deering [1978] and Tucker [1979] and defined in 3.1.

$$NDVI = \frac{\varphi_{IR} - \varphi_{R}}{\varphi_{IR} + \varphi_{R}} \tag{3.1}$$

where φ_{IR} and φ_{R} denote reflectances in the near infrared and the red bands respectively.

The NDVI is based on the theory that as the leaf area of a vegetation canopy increases, red reflectance decreases, because of the higher level of absorption by chlorophyll, and near infrared reflectance increases, because of enhanced scattering from multiple leaf layers. The NDVI uses linear combinations of data in these two wave bands and its computational and theoretical simplicity has led to its widespread application in a range of environments and at a range of spatial scales.

Terrettaz and Collet [1997] evaluate the interest of the PVI index as a biomass indicator in separating residential areas in SPOT satellite images. They conclude that the PVI index is not reliable to distinguish between built-areas and other urban land cover classes and suggest that results of separating urban land cover classes should be improved by integrating texture to spectral information.

While all these indexes were developed for different applications and particular types of input data and acquisition conditions (which can be incompatible with the urban environment), there is no ideal index designed to characterise the urban environment [Bannari *et al.*, 1995].

The urban environment is a mixture of different proportions of lawns, shrubs, treed areas, bare soil, building areas as well as streets. Therefore, the spectral response of urban vegetation is altered by the presence of such different types of elements, having similar spectral signatures. Moreover, the atmospheric conditions over urban areas are greatly influenced by the presence of pollutants and dust issued from industrial plants which are mainly located around big cities. All these factors induce great variations in the spectral reflectance of the same urban material.

Besides vegetation indexes, other classification algorithms have been applied on spectral features to classify vegetation. They can be divided into supervised and unsupervised classification approaches. The most widely used supervised classification algorithm for satellite imagery is the Maximum Likelihood Classifier (MLC). Xu *et al.* [2005] uses a decision tree classifier to determine class proportions within a pixel for land cover classification remote sensing data. Classification accuracy achieved by decision tree regression is compared with those obtained by the maximum likelihood classifier, implemented in the soft mode, and a supervised version of the fuzzy c-means classifier. The results of classifications from a synthetic image and a Landsat ETM+ image show that decision trees give higher accuracy as compared to the conventional MLC applied in a soft mode and the supervised FCM, especially when the data contains a large proportion of mixed pixels.

Methods for unsupervised classification most frequently used are the K-means and the ISODATA (Iterative Self-Organising Data Analysis Technique) clustering algorithms [Xie *et al.*, 2008]. Duda and Canty [2002] investigate several unsupervised classification algorithms for land cover classification of multispectral satellite data. The clustering algorithms examined are K-means, extended K-means, agglomerative hierarchical, fuzzy K-means and fuzzy maximum likelihood and fuzzy clustering is found to perform best on satellite data. Spectral and spatial information are combined by Tso and Olsen [2005] into hidden Markov models (HMM) for unsupervised image classification of satellite multispectral data of an agricultural/urban area. The proposed approach incorporates 2D spatial information into a one-dimensional linear HMM and results show that it outperform the k-means clustering approach using spectral data.

A fuzzy classification approach is used in [Zhang and Foody, 1998] to perform land-cover classification from satellite imagery of a suburban area. Results show that a fuzzy classification strategy may enable a suitable and effective classification of data presenting the mixed-pixel problem, often encountered in mid-level resolution satellite data.

Due to the spectral mixture of a pixel in an urban environment, approaches based on spectral indexes do not guarantee to perform correctly. Therefore, other approaches rely not only on spectral information to detect vegetation but integrate other kind of information into the detection process. Zhu *et al.* [2003] build a hierarchical multiresolution structure and analyse vegetation cover by analysing the relationship between objects, layers, and hierarchical structures at various scales. Bicego *et al.* [2003] use colour segmentation followed by a region growing approach to extract vegetation information. Besides spatial information, height is another kind of information integrated into vegetation extraction process. Myeong [2005] states that to improve the accuracy of vegetation classification techniques, traditional spectral pattern recognition techniques can be improved by adding height information extracted from derived remote sensing data, such as the Digital Elevation Model, into the classification process. Haala and Brenner [1999] add height information obtained from a Laser DEM to spectral information to improve classification results obtained using the ISODATA algorithm [Richards, 1993]. Berberoglu *et al.* [2000] adds texture to spectral information into a neural networks classifier to perform land cover mapping from satellite data. Medium/low resolution satellite data with mixed pixels is analysed in [Zhu et al., 2005] by a Support Vector Machines (SVM) classifier approach using spectral, texture and vegetation index to extract green space information. Results indicate that the SVM approach can efficiently be used to identify urban green space.

In recent years, more advanced methods reflecting the latest remote sensing techniques used in vegetation mapping are seen in literature. Hyperspectral imagery is increasingly studied to extract vegetation cover as its wider spectral bands allow a better differentiation of individual species than multispectral data [Xie et al., 2008]. The potential of airborne hyperspectral data for automated spectrally based classification of urban surfaces into ecologically relevant categories is investigated. Hung and Ridd [2002] developed a supervised classifier based on a maximum-likelihood approach to estimate ground component composition of urban areas at the sub pixel level from satellite images of urban areas. They propose a solution to the mixed-pixels (pixels containing more than one category of land cover) problem by using the Bayes algorithm for estimating land cover composition and expert system rules. Hyperspectral data is analysed by Bochow et al. [2007] to classify urban biotopes by building fuzzy logic models of biotope types. Maximum likelihood based classification follows a feature selection stage and a stage during which membership functions are designed for each biotope. Segl et al. [2003] proposes to fusion spectral and shape features for identification of urban surface cover types using reflective and thermal hyperspectral data. Wania [2008] evaluates the potential to detect and characterise urban vegetation using hyperspectral images by means of different vegetation indexes and established that indices including both the influence of the underlying soil and atmospheric effects perform better tan the commonly used ratio indices.

3.3 Vegetation detection in urban areas

This section presents the approaches investigated in this thesis to detect vegetation in urban areas. The first approach makes use of spectral indices whereas in the second one, a SVM classifier exploits spectral characteristics of vegetation and non vegetation areas.

The first approach studied exploits the NDVI vegetation index as well as additional spectral indices, which will be presented in the following paragraphs. For the rest of the presentation we will call this first approach *the spectral indices method* as several spectral indices are used to identify vegetation areas. In the second approach, reflectance values of vegetation and non vegetation areas are used by a Support Vector Machines (SVM) classifier to build radiometric models for the two

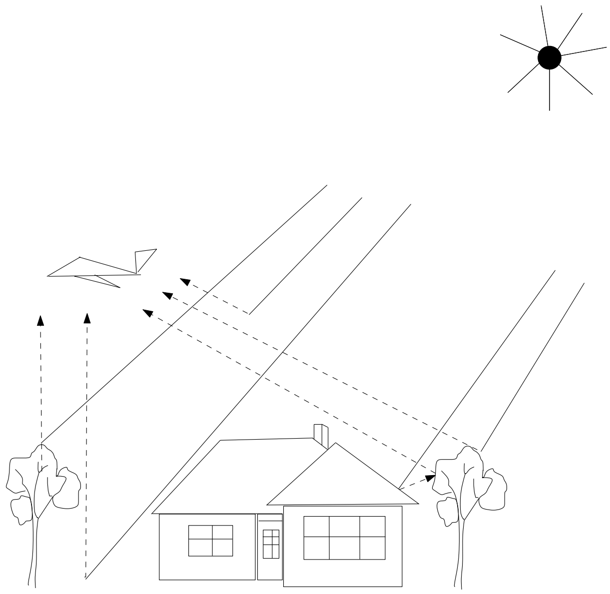

Figure 3.4: Spectral mixture at sensor level. Vegetation indexes such as the NDVI are greatly affected by the great spectral mixture at sensor level over urban areas Bannari *et al.* [1995].

classes. Details on each of the approaches will be given in the following along with a comparison between results obtained by the two methods and a discussion on the advantages and drawbacks of each one.

3.3.1 Vegetation detection based on spectral indices

The urban environment is a mixture of different proportions of lawns, shrubs, treed areas, bare soil, building areas as well as streets. Therefore, the spectral response of urban vegetation is altered by the presence of such different types of elements, having similar spectral signatures.

As described in [Xie *et al.*, 2008], pre-processing of aerial images prior to vegetation extraction is essential to increase the interpretability of the image data. This is particularly true when an area is encompassed by many images since it is essentially important to make these images are spatially and spectrally compatible. The ideal result of image pre-processing is that all images after image pre-processing should appear as if they were acquired by the same sensor. Two types of radiometric corrections were performed on images contained in the data set. The first one aims at correcting atmospheric effects and the second one, performs gray level balance.

3.3.1.1 Radiometric Corrections of Digital Aerial Imagery

Radiometric correction of remote sensing data involves the process of correcting radiometric errors or distortions of digital images to improve the fidelity of the brightness values.

Radiometric correction of atmospheric effects on the four channels of the raw images significantly reduces image brightness variations, allowing meaningful computation of radiometric indexes for the vegetation detection application. Radiometric corrections address variations in the pixel intensities that are not caused by the object or scene being scanned. *Atmospheric haze reduction* is a simple method that assumes that some image pixels should have a reflectance of zero [Lillesand *et al.*, 2008]. Actual values of zero pixels result from atmospheric scattering. Haze correction consists in subtracting the histogram offset from all pixels in a specific band. Result of the atmospheric correction is depicted in Figure 3.5-(b).

(a) Original image (b) Atmospheric correction (c) Atmospheric correction and gray balance

Figure 3.5: Results of radiometric corrections on a RGB image of site B from the Marseille data set before and after the corrections. (a) depicts raw RGB data. (b) illustrates results of atmospheric haze reduction performed on the image in (a). (c) depicts the results of atmospheric haze reduction and gray level balance.

The second correction is the gray level balance. It is based on the observation of reference targets whose radiometry is supposed to be known. It is a relative radiometric correction method that applies one image as a reference and adjusts the radiometric properties of subject images to match the reference [Hall *et al.*, 1991]. It consists in taking the value of asphalt areas in direct sun light on the red channel of our data as reference and adjusting the radiometric values of pixels in other channels (green , blue and infra-red) by this coefficient. It is founded on the assumption that asphalt areas in direct sunlight should be grey and that grey shades should have the save radiometric values in all spectral bands. The output is a set of calibrated images appearing as is they were collected by the same sensor. Result of the gray level balance applied on the image presented in Figure 3.5-(b) is depicted in Figure 3.5-(c).

Once the radiometric corrections performed and the availability of high radiometric accuracy of the data, we proceed to choosing the appropriate radiometric indexes to compute in order to detect vegetation.

3.3.1.2 Choice of vegetation indexes

To detect vegetation areas, *the spectral indices method* combines a couple of spectral indices. The first index computed for each pixel in our images is the NDVI (Normalised Difference Vegetation Index) [Gong *et al.*, 2003]. It allows the creation of a gray-level image, the NDVI image, by computing for each pixel the NDVI index, according to equation 3.1. This index highlights areas with a higher reflectance in the infrared band than in the red band (i.e. vegetation). Figure 3.6 presents the NDVI image obtained for a subset of site B, Marseille data set. Applying a threshold on the NDVI image gives a coarse segmentation of the urban scene in vegetation and non-vegetation areas, as depicted in Figure 3.6-(b).

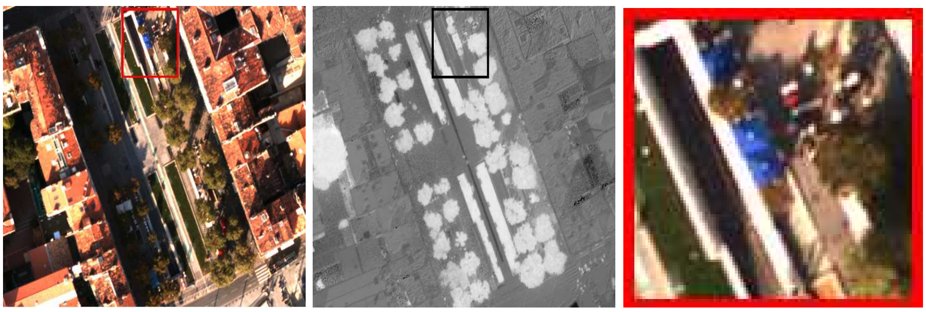

(a) (b) (c)

Figure 3.6: Spectral indices used for vegetation detection on a subset of site B, Marseille data set. (a) RGB channels of a subset of site B, Marseille data set. (b) NDVI image highlighting vegetation areas, represented by white tones in this figure. (c) Enlarged excerpt from the RGB image illustrating pixels classified as vegetation by the NDVI index which correspond to parasols.

The highlighted patch in Figure 3.6-(b) presents an area classified as vegetation by the NDVI index, which in fact corresponds to non-vegetation areas (blue parasols) as can be noticed in Figures 3.6-(a) and (c).

As there are also other materials present in an urban environment with a high reflectance in the infrared band, we refine vegetation classification results using a second spectral index computed for each pixel, according to:

$$SI = \frac{\varphi_R - \varphi_B}{\varphi_R + \varphi_B} \tag{3.2}$$

This is the saturation index (SI) [Mathieu *et al.*, 1998] and the image obtained for this index for each pixel is presented in Figure 3.7–(a). Results obtained for the NDVI and the SI indices are fused by arithmetic combination into the vegetation mask presented in Figure 3.7–(b).

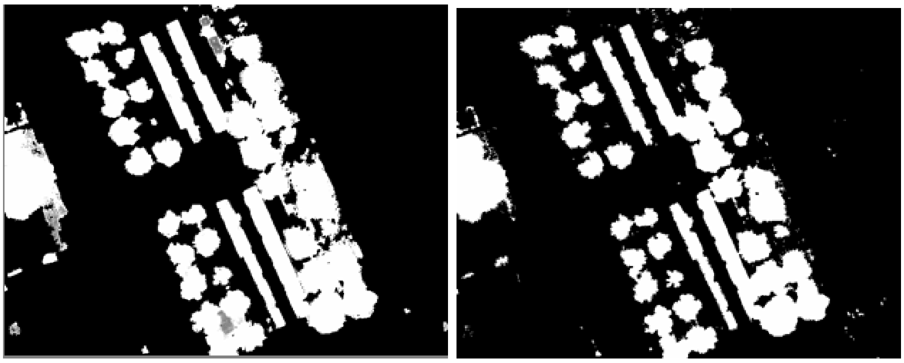

(a) (b)

Figure 3.7: Spectral indices used for vegetation detection on a subset of site B, Marseille data set. (a) Saturation Index (SI) image. (b) Vegetation mask obtained by combining results obtained by thresholding the NDVI image and results obtained by thresholding the SI image.

The methodological approach applied for computing the vegetation mask by means of spectral indices is summarised as follows:

- RGB and IR raw data are radiometrically corrected (atmospheric haze correction and gray balance).
- Radiometric indices are derived. The NDVI and the SI indices are computed. Images containing for each pixel the value of the index are derived and thresholded to produce masks of the corresponding areas.
- Arithmetical combination of the two masks is done to produce an unique vegetation mask.

The spectral indexes approach for vegetation detection in urban areas is summarised in Figure 3.8.

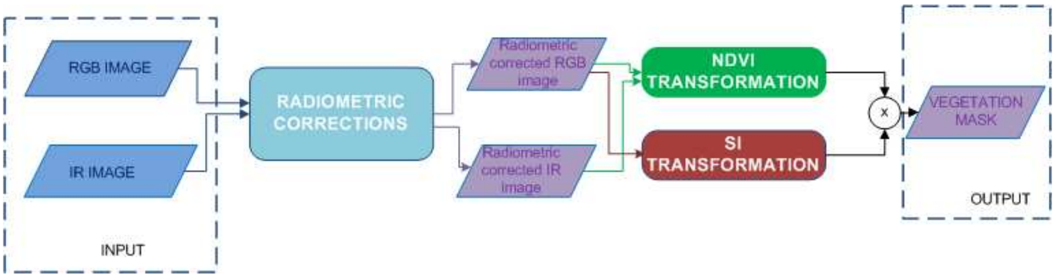

Figure 3.8: Overview of the spectral indices method. Raw data is first corrected with a radiometric correction model that requires external information such as gray level of asphalt areas for the calibration part. Corrected data are then used to calculate values of spectral indices. Resulting images are thresholded based on histogram methods and final vegetation mask is obtained by arithmetically combining results obtained by the two indices.

To illustrate the limitations of the *spectral indexes method* we report results on another area from the Marseille data set, depicted by Figure 3.9.

(a) (b) (c)

Figure 3.9: Vegetation detection on a new subset of the Marseille data set, site C. (a) False colours image of a second test area for the NDVI index, depicting in reddish tones areas with high reflectance in the infrared channel. (b) NDVI image of the area presented in Figure 3.9(a). (c) Vegetation mask obtained by thresholding the NDVI index.

Results obtained on the new data looked satisfying at first but soon revealed that the tennis court in the upper right part of the image was depicted as vegetation while its ground is synthetic and painted in a green colour (cf. Fig. 3.9-(c)).

To overcome the limitations of the *spectral indexes method* combining the NDVI and the SI indexes, other vegetation indexes were tested. The one performing best on the tennis court was the *"Green NDVI"* introduced by Gitelson *et al.* [1996] and given in Equation 3.3.

$$GNDVI = \frac{\varphi_{IR} - \varphi_G}{\varphi_{IR} + \varphi_G} \tag{3.3}$$

According to Gitelson *et al.* [1996], the Green Normalised Difference Vegetation Index (GNDVI) has wider dynamic range than the NDVI and is, on average, at least five times more sensitive to chlorophyll concentration. While NDVI is sensitive to vegetation fraction and to rate of absorption of photosynthetic solar radiation, the GNDVI can be used to sense the concentration of chlorophyll, to measure the rate of photosynthesis and to monitor plant stress. Figure 3.10 presents the GNDVI image of the test area presented in Fig. 3.9(a).

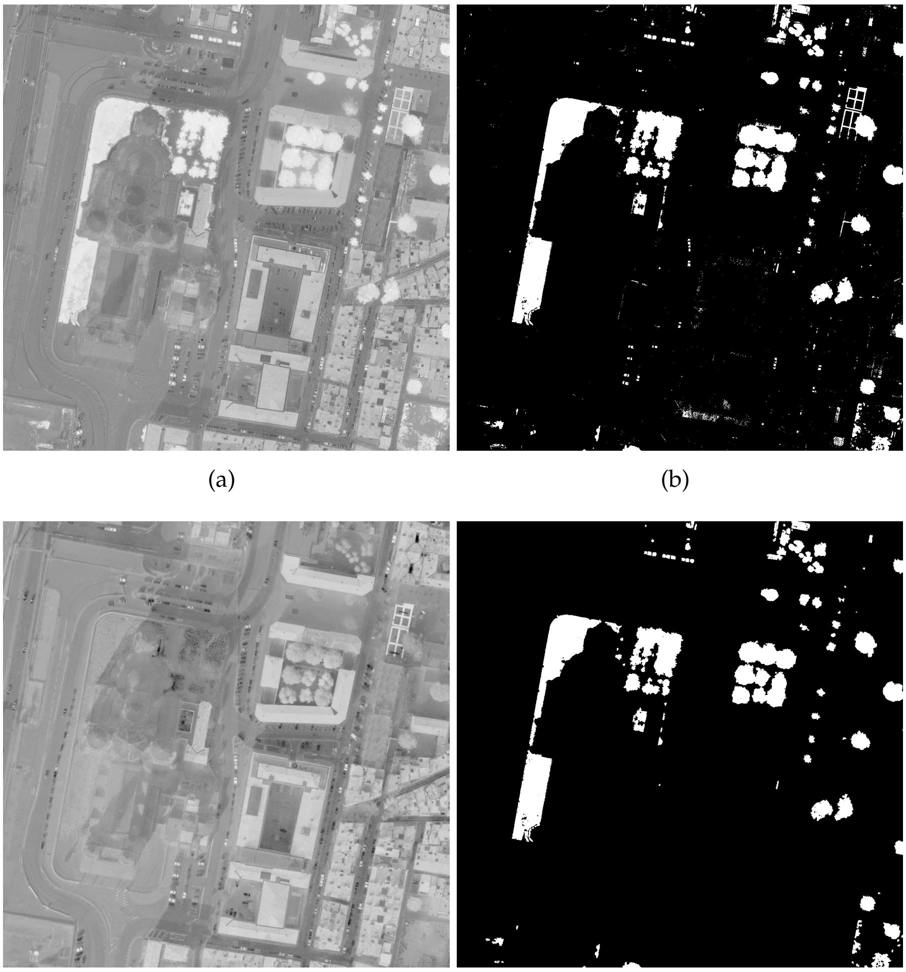

(a) (b) (c) (d)

Figure 3.10: Spectral indices used for vegetation detection on a subset of site C, Marseille data set. (a) GNDVI image of the test area presented in (a). (b) Vegetation mask obtained by thresholding the GNDVI image. (c) SI image. (d) Vegetation mask obtained by combining the GNDVI and the SI masks.

Figure 3.10(b) demonstrates that the GNDVI index is more adapted to this image than the NDVI index as it performs better in delineating the tennis court. On the other hand, it is not self sufficient in detecting vegetation as parts of the tennis court (ground area outlines) are still misclassified as vegetation. The usage of the SI is therefore necessary as it allows a correct delineation of the outlines of the tennis court (cf. Fig. 3.10(c)). The final vegetation mask presented in Fig. 3.10(d) is obtained by combining results obtained by the GNDVI and the SI index.

In order to propose a method to extract vegetation in urban areas resistant to atmospheric effects and insensitive to spectral variations of objects in different areas, a supervised classification approach based on spectral features and a Support Vector Machines (SVMs) classifier is presented in the following section.

3.3.2 Vegetation Detection based on SVM Classifier

This section presents the approach developed to detect vegetation in urban areas. The proposed approach belongs to the class of supervised classification ones and is based on spectral characteristics of vegetation in urban areas.

The classifier used is based on Support Vector Machines (SVMs), introduced in 1992, by Boser, Guyon and Vapnik [Boser *et al.*, 1992]. In recent years, support vector machines have received considerable attention from the machine learning community because of their outstanding performance in pattern recognition and computer vision applications [Cord and Cunningham, 2008], [Campbell, 2002]. Performances obtained by SVMs on real world data, often outperforming state of the art applications, making them a powerful tool in the supervised classification framework.

Principles of SVMs are presented in Appendix A. A complete formulation of the classification method can be found in a great number of publications, such as [Vapnik, 1995; Cortes and Vapnik, 1995; Cristianini and Shawe-Taylor, 2000; Theodoridis and Koutroumbas, 2003].

Main characteristics of the proposed approach are described in the following sections and its capacities in combining spectral information to separate vegetation from other objects in urban areas are evaluated on sample data sets.

3.3.2.1 Feature Vector

The first step for any supervised classification system is the choice of discriminant information characterising each of the two classes of our binary classification problem. This will form the *Feature Vector* used to train the SVM classifier.

To separate vegetation areas the *Feature Vector* is composed of reflectance values of each pixel in the infrared(IR), red(R), green(G) and blue(B) bands.

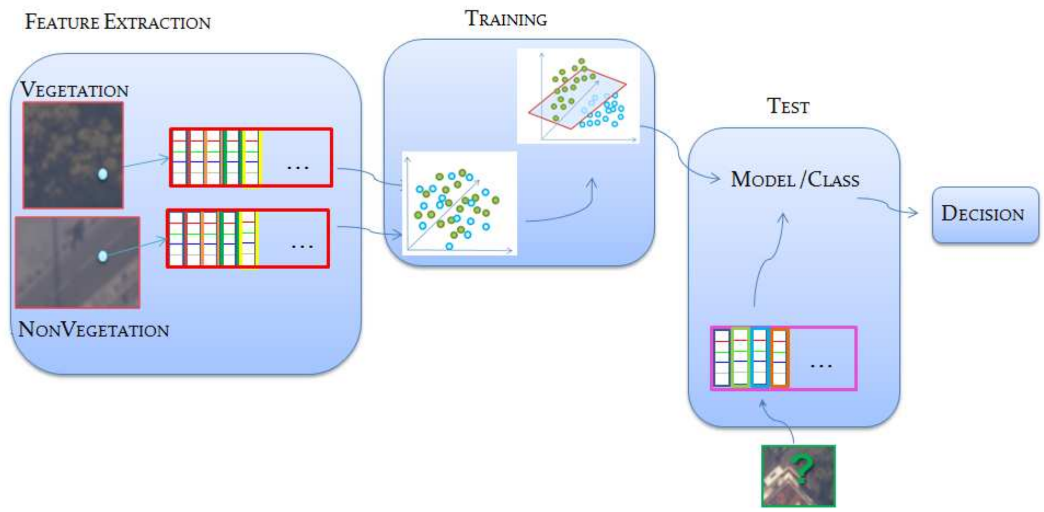

Figure 3.11: Vegetation detection based on a SVM classifier - system overview.

Several colour transformations have been applied to the R, G and B components of the feature vector. Components of the *HSV*, *XYZ* and *Lab* colour spaces were used in addition to the IR channel to perform vegetation detection. Literature is abundant with reference publications on consideration of different colour metrics. For more details on colour spaces, we suggest the reader reference works such as [Green, 2002].

3.3.2.2 Similarity Kernel

For binary classification problems, SVMs are used to learn from a set of labelled examples a classification rule which should be used to predict the class of new unlabelled examples. Geometrically, this rule could be expressed as the hyperplane that separates the input space into two half-spaces, and the prediction of the class of a new point depends on the position of this point on one or the other side of the hyperplane. SVMs learn a classification function that, among all separating hyperplanes, maximises the distance to the closest data point from the training data set.

The discriminative power of SVMs can be enriched via kernel functions which allow the mapping of data points from the original space to another space, where linear classification between data sets might be possible. As the kernel defines a distance between data points, it can be seen as a measure of similarity between them: the larger the kernel, the closer data points are in the initial feature space.

Several kernels were analysed: *linear*, *polynomial* and *Radial Basis Function*. For the classifier implementation, the LIBSVM [Chang and Lin, 2001] library was used.

3.3.2.3 Training and test data sets

Training and tests were performed on manually delineated samples of vegetation and non-vegetation areas. Training areas were delineated on site B of the Marseille data set and test ones, on the site A of the Marseille data set. These areas were used also as training and test samples for the classifier and to measure classifier accuracy. Table 5.3 gives the total number of pixels used for training and test stages for the vegetation detection module.

Table 3.2: Size of training and test data sets for vegetation detection.

	Training	Test
	# pixels	# pixels
Vegetation Areas	100,000	250,000
Non-vegetation Areas	100,000	1,000,000
TOTAL	200,000	1,250,000

Training was performed on the same amount of pixels for the vegetation and non vegetation classes, in order to build reliable models. As for the test data set, the differences between the sizes of the two classes comes from the absence of enough ground truth pixels to test models on larger data sets.

In the following section, results will be given both in a visual and a quantified form. A comparison to the NDVI is also made in order to have an estimate of how the NDVI index performs on the same test areas.

3.3.3 Results, Evaluations and Comparison

Figure 3.12 gives a comparative overview of vegetation detection by the NDVI and the linear kernel SVM classifier with feature vectors computed on the Lab colour space. Results are presented on a subset of site C of the Marseille data set.

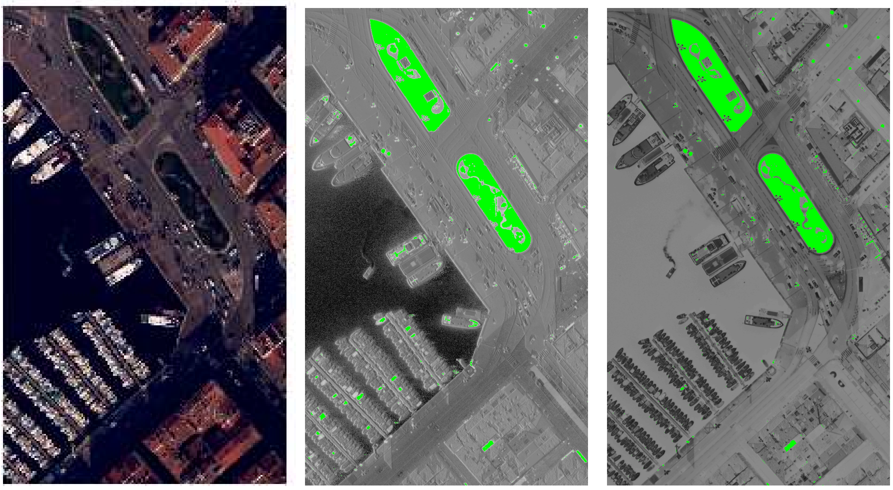

(a) RGB (b) NDVI (c) SVM linear on Lab

Figure 3.12: Vegetation detection results for a subset of site C of the Marseille data set. This area is close to the "old harbour" part of the city. False positive rate was set to $FP = 1 \times 10^{-3}$ accepted misclassified pixels for both methods. Green pixels in Figures (b) and (c) indicate pixels classified as vegetation. A large number of such green pixels can be noticed on the boats in the lower part of Figure (b) compared to the same area in Figure (c).

The harbour area is a challenging area for vegetation detection as the ships present therein introduce several misclassified pixels due to reflexions and mixture of materials. Green pixels are in Fig. 3.12(c) and 3.12(b) used to mark vegetation pixels. Compared to results of the SVM method presented in Fig. 3.12(c), results obtained by the NDVI method produce over-detections, especially on ships.

Table 3.3 presents a comparison of accuracies for vegetation classification for the NDVI method and the SVM approach. Feature vectors for the SVM approach are computed on different colour spaces and the SVM classifier is tested with different kernels (linear, polynomial and Gaussian - Radial Basis Function). Vegetation detection performances of the two methods are compared by means of True Positives (TP) rates for three False Positives (FP) cases: $FP = 0.0001$, $FP = 0.001$, $FP = 0.01$, meaning, respectively, that one pixel out of 10000, 1000 and 100 is misclassified. These values correspond to three distinct functioning points on the correspondent Receiver Operator Characteristic (ROC) curves, which are presented in Figures 3.13, 3.14, 3.15, 3.16. For the SVM approach, several kernels (linear, polynomial (poly) and Radial Basis Function (rbf)) are used for feature vectors computed in different colour spaces *RVB*, *HSV*, *XYZ* and *Lab*. Details on colour spaces can be found in [Green, 2002].

Table 3.3: Results for vegetation detection by SVM classifier and comparison to the NDVI index. Feature vectors are computed in different colour spaces. True Positives (TP) rate is presented for three values of False Positives (FP) rate.

Colour space	kernel	FP=1e-4	FP=1e-3	FP=1e-2
NDVI	–	0.0882	0.907	**0.998**
RGB	linear	0.57	0.903	0.997
RGB	poly	0.848	**0.993**	0.997
RGB	rbf	0.498	0.811	0.981
HSV	linear	0.539	0.76	0.979
HSV	poly	**0.867**	0.99	0.994
HSV	rbf	0.467	0.939	0.988
XYZ	linear	0.398	0.661	0.792
XYZ	poly	0.467	0.696	0.816
XYZ	rbf	0.397	0.649	0.776
Lab	linear	0.629	0.991	**0.998**
Lab	poly	0.859	0.98	0.994
Lab	rbf	0.678	0.967	**0.998**

Table 3.3 emphasises the great potential of the SVM-based approach for vegetation detection in urban areas compared to the traditional NDVI-based approach.

For a fixed FP rate of 0.0001, i.e. one out of 10000 pixels is misclassified, performances of the NDVI-based approach are inferior to performances of all other SVM-based approaches for vegetation detection. For a FP rate of 0.001, the SVM-based approach still outperforms the NDVI one, by an approximately 9% increase of the TP rate for the *RGB* colour space and a polynomial kernel. For FP rates of 0.01, the NDVI-based approach performs equally to the SVM-based one, for the *Lab* colour space with linear or rbf kernels.

Figures 3.13, 3.14, 3.15, 3.16 present detection ROC curves obtained for the SVM classifier compared to the NDVI index, for the three colour spaces analysed for vegetation detection in urban areas. Curves are plotted on each colour space for each of the three SVM similarity kernels: *linear*, *poly*, *rbf*. Functioning points presented in Table 3.3 are marked on each ROC curve by an emphasised dot of the respective colour.

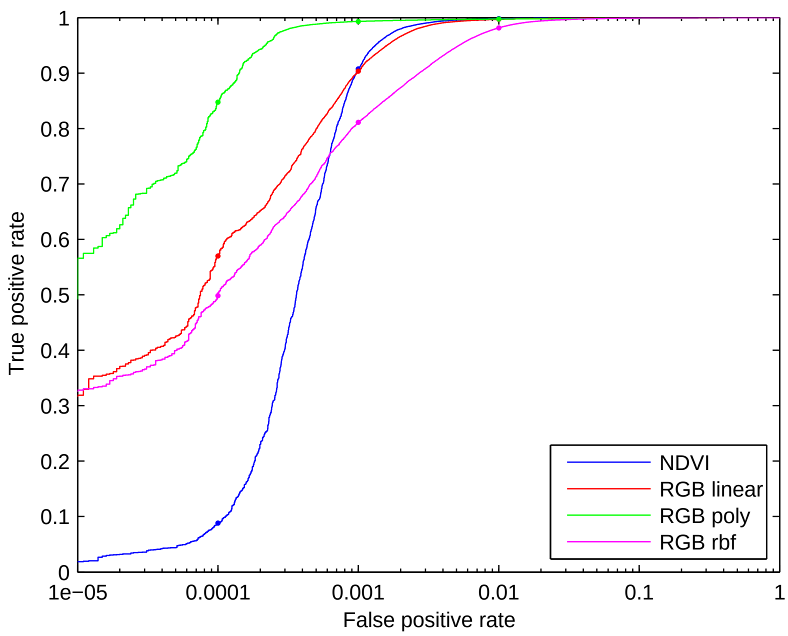

Figure 3.13: Vegetation detection ROC curves on RGB colour space.

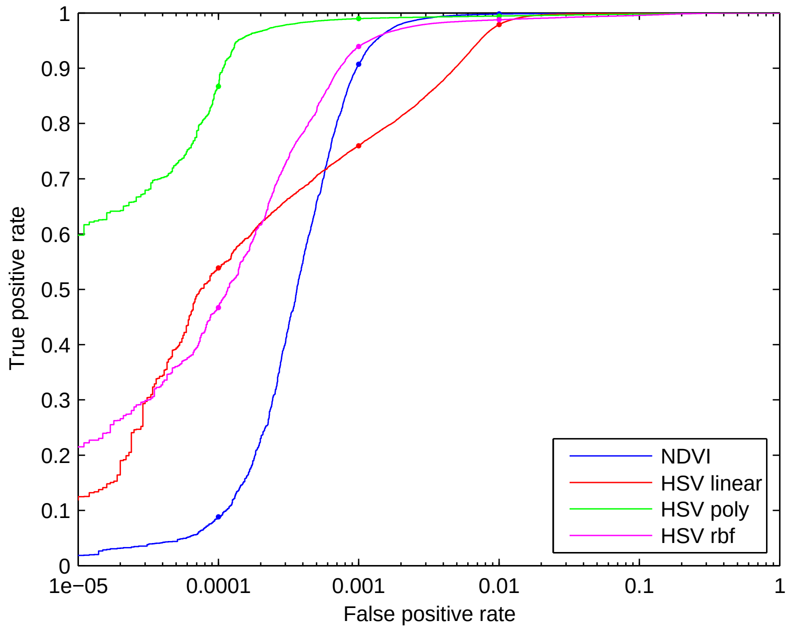

Figure 3.14: Vegetation detection ROC curves on HSV colour space.

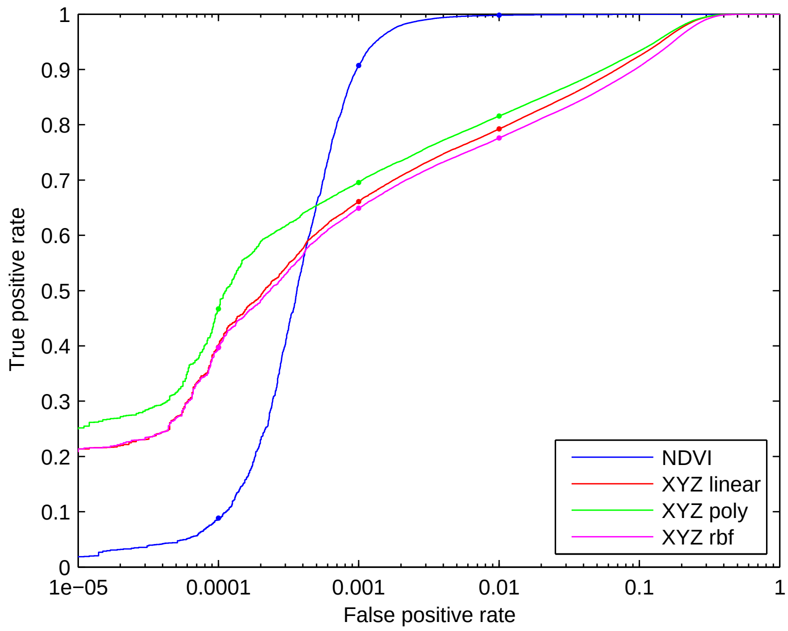

Figure 3.15: Vegetation detection ROC curves on XYZ colour space.

The **linear kernel** gives very good results for the feature vector computed in the *Lab* colour space, which could be the result of the non-linear relationships

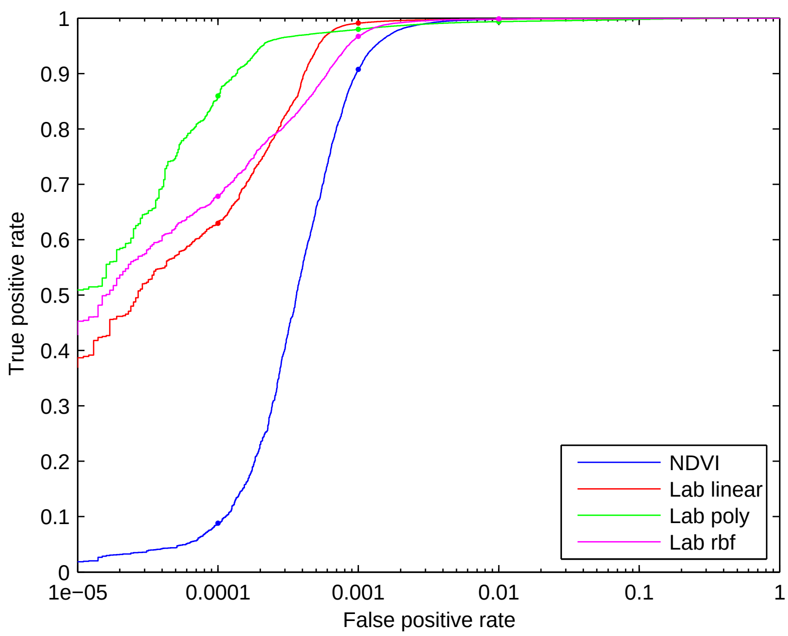

Figure 3.16: Vegetation detection ROC curves on Lab colour space.

between the L, a and b components of the colour space as they intend to mimic the logarithmic response of the eye.

The **polynomial kernel** gives equally good performances for the RGB and the Lab colour spaces whereas the **radial basis function** kernel gives best performances on the Lab colour space.

Results obtained on the *RGB* colour space for a **polynomial kernel** and on the *Lab* space for a **linear one** show an improvement approximately 9% compared to the NDVI method. The linear kernel, by its simple interpretation is preferred over the polynomial one, having a higher number of parameters to be set. Further evaluations should be performed in order to test the generalisation capacities of the SVM method. Vegetation models learnt by the SVM classifier on site C of the Marseille data set could have good generalisation capacity when applied on the whole Marseille data set. Yet, evaluation is a difficult task as supplementary ground truth data should be acquired for this. Therefore evaluation of the obtained results is not performed and thus not presented herein.

3.4 Conclusions

This chapter presented approaches developed to locate vegetation information in urban areas. This is done by interpreting high resolution multispectral aerial images based on spectral reflectances of vegetation and non vegetation areas.

After reviewing state of the art methods, the approaches developed to detect vegetation in urban areas are presented. The first one combines several spectral indices, such as the NDVI, the GNDVI and the SI. Overall accuracy obtained by the *spectral indices* method is considered satisfactory for most applications. Experiments performed on images acquired on the same day and by the same acquisition system over urban areas showed the necessity of combining different spectral indexes to obtain accurate vegetation masks. Moreover, the sensitivity of the *spectral indices* method to different materials in the urban environment emphasised the need of constantly adapting the choice of indices used to detect vegetation to the study area.

The second approach presented in this chapter uses a SVM classifier and spectral feature vectors. Combinations of four colour spaces and three types of kernels for the SVM classifier were analysed. This is a robust method to perform vegetation/non-vegetation classification in urban areas. The best-results configuration for the linear kernel was obtained for the feature vector computed on the *Lab* colour space.

To sum up, the NDVI method needs an adjustment of the spectral indexes used to detect vegetation to the study area. We could not establish an unique combination of spectral indexes working for all the areas belonging to the same data set. Compared to this, the SVM based method is robust to data belonging the same data set (i.e. images acquired by the same system, on the same day and over the same area) as it shows good generalisation performances. Furthermore, it has the advantage that no radiometric corrections are necessary prior to performing the training stage. On the other side, on data acquired by another acquisition system, on a different area and under different illumination conditions, training of the SVM classifier might be necessary.

In terms of the entire system developed to analyse vegetation in urban areas, this chapter presented the first module, which gives localisation areas for urban vegetation and will represent input data for the following component. These masks are used to focus only on vegetation areas and to mask out other urban features, such as buildings, streets, etc.

Chapter 4

Segmentation

4.1 Introduction

This chapter describes methods developed to identify trees and lawns in the urban vegetation areas previously detected. Detecting specific objects in a scene requires them to be defined according to the type of input data available. But how does one define lawns and trees? Figure 4.1 illustrates several samples of trees and lawns extracted from colour aerial images.

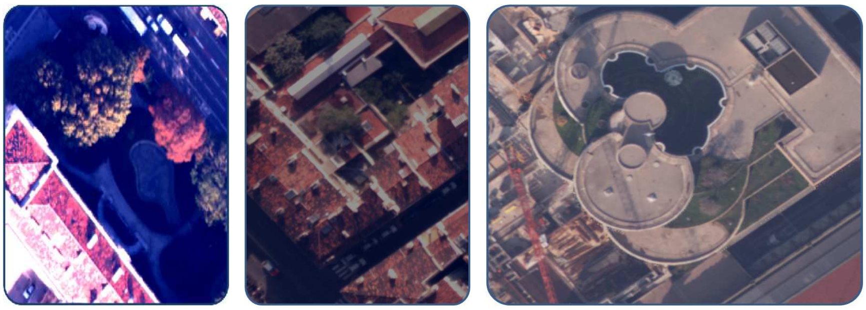

(a) (b) (c)

Figure 4.1: Urban vegetation ambiguities. How can an algorithm discern between a tree and a tall bush Fig. 4.1(a)? What about strips of grass on top of buildings Fig. 4.1(c) or trees lying on balconies. 4.1(b) and trees on the ground?

Urban vegetation includes vegetation in either public or private space and/or the juxtaposition of these types. There is a variety of ways to classify vegetation in urban areas. According to McBride and Reid [1988] vegetation in developed areas includes the following categories: tree groves, street strip trees, shade trees/lawns, and shrub cover. *Tree groves*, have a continuous canopy but vary in height, tree spacing, crown shape, and understory conditions. *Street strips* show variations in spacing of trees, depending upon species and structure. Both continuous and discontinuous canopies are observed. *Shade trees and lawns* vary widely in species and structure. Lawns are structurally the most uniform type of urban habitat. *Shrub cover* is the most limited in vegetation type and also contains a variety of species and structures.

4.2 Objectives

4.2.1 Which type of urban vegetation are we interested in?

Given the great mixture of vegetation types in the urban landscape, highly intermingled to each other, we will in the following focus on:

- *Trees situated on the public domain with a crown size superior to one square meter.* This could be strip trees or trees located in public parks or squares.
- *Lawns or grass areas belonging to public land.* We are not interested in lawns located on top of buildings but on those located at ground level, which have an impact on the 3D city model.

4.2.2 What accuracy should we achieve?

Our interest in urban vegetation types is twofold :

- *A visualisation one*: to accurately represent vegetation in 3D city models, we are interested in representing the exact number of trees on the public domain. Therefore, over-detections are not allowed : we cannot accept to represent two trees in the 3D city model if a single tree is present on the ground.
- *A characterisation one*: the segmentation step should be accurate and detailed enough so that information extracted for each vegetation type could be used to extract 3D parameters (tree diameter and height) and for a pattern analysis characterisation of vegetation species.

After reviewing related works (section 4.3) we present our approach to delineate the two urban vegetation types which are of interest in our study, i.e. lawns and individual tree crowns (section 4.4) as well as the obtained results (section 4.4.2.3). After a comparison of the proposed method to delineate individual tree crowns against state of the art techniques (section 4.6), we evaluate these results also against ground truth data (section 4.5) and we finally draw concluding remarks (section 4.7).

4.3 State of the Art

This section provides an overview of methods developed to identify trees and lawns, from remotely sensed aerial imagery. It begins with a presentation of research works aiming at identifying grass areas and continues with algorithms developed for individual tree crown delineation. To highlight important issues and limitations, this section includes an overview of a variety of tree crown delineation algorithms applied on different kind of remotely sensed data although not all are the subject of this thesis.

4.3.1 Lawn delineation

Lawn (herbaceous regions) delineation is often performed in land cover studies and is rarely a stand alone goal. In forestry applications, tree crown delineation is the main objective. In urban area ones, and especially when it comes to 3D city models, grass areas represent regions of interest on their own, as their representation greatly differs in the end product from that of trees.

Our goal is to distinguish lawn areas from other urban vegetation classes, so that each of the vegetation areas could be more accurately characterised. In other words, we are interested in localising lawn areas in previously delineated urban vegetation class.

Depending on the type of input data and on their resolution, researches have mainly used spectral charactheristics, texture or height information to achieve similar goals. Vegetation has an unique spectral signature which enables it to be distinguished from other types of land cover classes using spectral reflectance properties in different spectral bands. Green spaces in urban areas, such as grass and tree classes are often confused in spectral based classification.

[Bicego *et al.*, 2003] combines colour segmentation with a region growing approach to extract field areas, forests and buildings from aerial images over a rural study area. This study exploits the property that fields and forests in rural areas are broad regions with regular shape and homogeneous colour. Therefore, the image is first segmented in the HSI (Hue, Saturation, Intensity) colour space and a growing algorithm merging pixels adjacent to the pixels issued from the first segmentation is applied to create regions of homogeneous colour. Results obtained are found to be encouraging through visual inspection yet no qualitative evaluation is presented.

Urban cover mapping from high-spatial resolution colour infrared aerial imagery is studied in [Myeong *et al.*, 2003]. Their method combines spectral and texture information to distinguish between five cover types using maximum likelihood decision rule. Classification confusion between objects with similar spectral responses such as water and dark impervious surfaces, concrete and bare soil, and grass and trees occurred. Classification results were greatly improved in [Myeong, 2005] by adding height information to separate treed areas.

[Stefanov *et al.*, 2001] also studies land cover classification in urban areas using

Landsat Thematic Mapper (TM) data. They developed an expert system from ERDAS Imagine software and used it to classify land cover in urban areas. This allowed the integration of remotely sensed data with land use data, spatial texture, and digital elevation models to improve classification accuracy.

[Zhang, 2001] developed an algorithm integrating textural and spectral information of high-resolution colour infrared images to extract urban treed areas. Tree features are detected with higher accuracy than common texture algorithms by combining directional variance and local variance information.

Vegetation classification in urban areas from high-resolution colour infrared IKONOS data is studied in [Yansong *et al.*, 2004]. A pre-processing step for shadow correction is first performed before vegetation is classified. Three methods to derive vegetation information are compared and texture information appears highly efficient in vegetation classification.

[Shackelford and Davis, 2003] add texture properties to the classification process to increase the discrimination between spectrally similar urban land cover classes. By combining both spectral and spatial information into a hierarchical fuzzy classification approach classification accuracies are up to 11% larger than those from the traditional maximum-likelihood approach.

4.3.2 Tree Crown Delineation

Many researches deal with tree crown delineation techniques and a wide range of such methods have been proposed recently. The extraction of crown boundary maps from remote sensed data has mainly been investigated for forestry applications. Part of these methods were extended to urban area ones. Table 4.1 presents some of the output parameters of tree crown delineation approaches developed for forestry and urban area applications depending upon the input data type.

The goals for tree detection in forestry applications and in urban area ones are very different. Detecting tree position may be sufficient for forestry application but when it comes to 3D city modelling, several other information have to be extracted, such as tree crown diameters, tree height, tree species.

Automated crown mapping is the process of defining crown boundaries in digital data. Literature is abundant with works presenting this process, under different names, such as *individual tree crown delineation* [Gougeon and Leckie, 2003; Gougeon, 1998, 1995b], *tree crown extraction* [Perrin *et al.*, 2005], *automatic tree extraction* [Straub and Heipke, 2001], *crown segmentation* [Erikson, 2003; Lamar *et al.*, 2005], *tree crown delineation* [Culvenor *et al.*, 1998], *individual tree detection* [Pitkänen *et al.*, 2004; Wulder *et al.*, 2004], *canopy segmentation* [Turner, 2006], *single*

Acquisition system	Applications	Output parameters
Satellite imagery	Forestry	Vegetation cover Species classification Tree crown maps Tree crown parameters Stem counting
Aerial imagery	Forestry	Tree crown maps Species classification Tree crown parameters Stem counting
	Urban areas	Tree crown maps Species classification Tree crown parameters Stem counting 3D tree models
LiDAR data	Forestry	Tree crown maps Species classification Tree crown parameters Stem counting
	Urban areas	Tree crown maps Species classification Tree crown parameters Stem counting
Multispectral data	Forestry	Tree crown maps Species classification
Hyperspectral data	Forestry	Tree crown maps
RADAR data	Forestry	Tree crown maps

Table 4.1: Tree crown delineation approaches: output parameters are data- and application- dependent.

tree delineation [Weinacker *et al.*, 2004], *auto-interpretation* [Pitt *et al.*, 1997].

In the following we will employ the term "individual tree crown delineation" as it emphasises the segmentation of the high-height vegetation areas into individual units, representing tree crowns. According to [Gougeon and Leckie, 2003], individual tree crown delineation techniques provide one of the following three types of information: *tree location*, *tree location and crown dimensions* or *full crown delineation*. The different approaches proposed for individual tree crown delineation can be divided into the following conceptual approaches:

Top-down methods

- model-based methods

Bottom-up methods

- contour based methods
- local maxima methods
- valley-following algorithms
- region growing methods

These methods vary in complexity depending on the type of remote sensing data (optical spectral reflectance or lidar height data) and on the application they were designed for (forest inventories vs. crown parameters estimation). The following sections review these techniques, highlighting relevant advantages and limitations.

4.3.3 Bottom-up methods

Bottom-up segmentation approaches use different image-based criteria and search algorithms to find homogeneous segments within the image.

4.3.3.1 Local-maxima methods

These methods use local maxima information to estimate tree top position and the number of trunks [Pinz, 1998; Wulder *et al.*, 2000], rather than tree crown borders. These approaches are based on the assumption that reflectance is highest for crown tops and decreases towards crown boundaries.

[Wulder *et al.*, 2000] proposes a local-maxima filter to automate the extraction of individual tree locations from high spatial resolution remotely sensed imagery. A kernel is moved over the image and trees are located when the central digital value in the kernel window is higher than all other values. Results obtained are strongly linked to the size of the kernel window, which has to be optimised according to the size of the trees in a study region. One of the drawbacks of local maxima methods for tree detection is handling tree crowns of different sizes. To tackle this problem, several authors proposed adaptive methods in finding local maxima in LiDAR data, by linking the crown-width to the tree-height [Popescu *et al.*, 2003; Pitkänen *et al.*, 2004]. By making the assumption "the higher a tree, the bigger its crown width", the result is a local maximum search algorithm with a dynamic search radius, depending on the height of the analysed point. [Popescu *et al.*, 2003] predicted crown width from tree height on a canopy height model, to adjust the window size used for finding the local maxima. [Pitkänen *et al.*, 2004] detected tree tops as local maxima on a smoothed LiDAR canopy height model smoothed by with the different degree of smoothing selected based on canopy height.

[Korpela, 2004] proposed a semi-automatic tree top positioning method for aerial images. Multiple image-matching techniques are used to find tree tops inside a predefined 3D search space in the canopy volume. Tree top positions are identified as local maxima on correlation images obtained by template matching [Pollock, 1996]. A volumetric correlation is used to detect 3D maxima which correspond to tree top positions. This approach is also applied to LiDAR data in [Korpela, 2006] and is found to be very sensitive to variations in the size of the trees.

[Dralle and Rudemo, 1996] developed semi-automated approach to estimate tree top positions by detecting local maxima on smoothed panchromatic aerial imagery of Norway spruce forests. The method performs well with nadir view images and for strongly thinned forest plots, where displacement errors of 65 cm in object spaced affected 95 % of the trees.

Local maxima methods are strongly influenced by illumination conditions, occlusions or shadings introducing intensity variations in the the appearance of similar objects. They are based on the assumption that each tree crown has one dominant peak represented by the brightest pixel of the canopy image. These are limiting assumptions when applied to urban area trees which are often cut to geometrical shapes and can therefore have multiple peaks or and poor apical dominance [Gougeon and Leckie, 2003].

4.3.3.2 Valley-following (local minima)

Valley-following algorithms exploit shadows around tree crowns to delineate their contour Gougeon and Leckie [2001]. They are based on the assumption that trees are represented on high resolution imagery by bright areas surrounded by darker regions of shade [Gougeon, 1998]. Pixels representing shaded areas appear like "radiometric valleys" [Culvenor, 2003] which are joined to delineate tree crowns. The individual tree crown (ITC) algorithm for crown delineation in high resolution aerial imagery was introduced by Gougeon [1995b,c, 1998]; Gougeon and Leckie [2001]. It consists of two steps: first, a valley-following process connects local minima pixels into a continuous network of crown boundaries [Culvenor, 2003]. Then, a rule-based stage refines crown boundaries by dealing with gaps in crown boundaries. Using the same topographic structure, [Culvenor *et al.*, 1998] identifies local maxima and grows them out to regions of minima representing shade to determine crown boundaries. Both these methods work best in dense canopies where there is shade between trees.

The ITC approach was also applied by [Leckie *et al.*, 2003] on a LiDAR canopy height model and on multispectral imagery to delineate trees in coniferous forests, with the accuracy of the obtained results ranging from 80% to 90%. This study showed that complementary data sources may provide more accurate tree isolation results than data sources taken apart.

[Warner *et al.*, 1998] delineate individual trees in deciduous forests by exploiting the shadows between crowns on an illumination image derived from colour aerial images. First shadow areas between tree crowns are isolated and connected based on orientation information obtained from a direction of minimum texture algorithm.

The main weakness of this approach is directly related to the strong assumptions it is based on. As tree crowns are not always separated by a gap, the results of this approach could be limited when applied on urban trees.

4.3.3.3 Region growing methods

Region growing methods generally include two steps: a first one in which starting points (or seed points) are located in the input data, which are expanded in the second step to regions homogeneous with respect to some characteristics.

[Culvenor *et al.*, 1998] developed the Tree Identification and Delineation Algorithm (TIDA) to delineate individual tree crowns in high resolution images of Eucalyptus forests by combining information on spectral maxima and minima, representing crown centres and boundaries respectively. Local maxima within a neighbourhood of pixels from the infrared portion of the spectrum is used to estimate seed points. A four-way linear search (0°, 45°, 90°, 135°) is performed for each pixel in the image to find peaks. To take into consideration different resolutions of the input data, the distance of this search is user defined. Once seed points identified, local minima are identified by a similar search as crown boundaries. This algorithm has a great accuracy (92% of trees were correctly identified), but is strongly dependent on variations in remotely sensed data introduced by illumination and viewing geometry.

[Erikson, 2004b] developed region growing algorithms to extract individual tree crowns from colour infrared aerial photographs of forests. They are based on fuzzy rules, Brownian motion and random walks respectively and consist of two steps, a first one designed to find seed points which are grown to regions in the second step. To find seed points, the first band of the input image is thresholded and a distance transform is performed on the resulting image. This distance image is smoothed with a Gaussian filter and local maxima are detected as seeds. During the growing step, a series of constraints decide on the rapidity of a pixel aggregation to a region.

Several studies use the watershed [Vincent and Soille, 1991] segmentation technique to delineate tree crowns in remote sensed data. [Mei and Durrieu, 2004] applied it on an inverted LiDAR canopy surface model over a mixed species stand. The accuracy of the segmentation varied from 63% for Olive tree stands to 90% for Poplar plantations. [Lamar *et al.*, 2005] extracted hemlock crowns from aerial imagery by developing a five-step spatial segmentation approach including watershed segmentation. [Kanda *et al.*, 2004] applied it to segment high spatial resolution aerial imagery whereas [Komura *et al.*, 2004] delineate tree crowns in satellite images by applying the watershed algorithm on an inverted radius distribution image created after estimating tree crown radius through circle expression. [Schardt *et al.*, 2002] segment tree crowns on a LiDAR tree height model of forests by detecting local-maxima as seed points for a watershed segmentation algorithm applied on a smoothed tree height model. [Hyyppa *et al.*, 2001] performed a low-pass filtering to smooth the LiDAR canopy height model before detecting trees as local maxima points above a user-defined threshold in a specific neighbourhood and applying a watershed algorithm to delineate single trees. This algorithm was later used in Maltamo *et al.* [2004]; Yu *et al.* [2004] to delineate individual trees in LiDAR data. Marker controlled watershed segmentation was also applied by [Chen *et al.*, 2006] to isolate individual trees in a savanna woodland in small footprint LiDAR data. Treetops detected as local maxima on canopy maxima model were used to compute a distance-transform image used in the segmentation step. The accuracy of the obtained results was of 64.1%. [Weinacker *et al.*, 2004] delineate single trees in mixed forests by a region growing algorithm applied on LiDAR data. Seed points are local-maxima on the smoothed LiDAR digital surface model. An inverted watershed algorithm is used to grow regions from the extracted seed points. The obtained results are refined to tree crown regions by additional processing steps. Height information is used to threshold the obtained regions into high- and low-trees. Geometric knowledge on area and distance between neighbour trees is used to merge small regions to larger ones. Consequently, large regions are split into circles based on minimal area, anisometry, and height information. Finally, tree crown borders are located by a ray-tracing algorithm refining crown borders based on crown slope estimates along search rays from crown tops to the previously extracted border. Even though tree crown borders are slightly overestimated by this algorithm, with 61,7 % of correctly segmented trees.

An approach similar to the watershed algorithm was proposed by [Persson *et al.*, 2002] to delineate trees in LiDAR data was adapted by [Pouliot *et al.*, 2005] for the segmentation of crowns in high resolution aerial imagery of mixed coniferous forest. In this method, each pixel in the image is considered a seed point and is forced to follow the local upward gradient until a local maximum point is reached. This seed pixel is then assigned to the cluster correspondent to that local maximum position. This algorithm provides the segmentation of tree crowns based on clusters defined by the pixels that climbed to a given local maximum point.

[Secord and Zakhor, 2006] developed a region growing algorithm to detect trees in LiDAR data and aerial imagery of urban areas. A similarity analysis of eight connected data points is performed and regions are grown if the similarity is above a threshold and stops if it is below the threshold. The similarity is composed of weighted features from aerial image and LiDAR, such as height, texture map, height variation, and normal vector estimates and their weights are determined using a learning method on random walks.

[Solberg *et al.*, 2006] also developed a region growing algorithm to delineate single trees in LiDAR data of heterogeneous spruce forest. Seeds were detected as local maxima on the smoothed canopy surface model and grown to segments representing individual trees by successive expansions according to slope and shape constraints.

A region growing algorithm was proposed by [Tiede *et al.*, 2005, 2006] for tree identification and tree crown delineation in raw laser point data. First, a *tree finding algorithm* based on a regression model [Pitkänen *et al.*, 2004; Popescu *et al.*, 2003] is used to find local maxima which will be used ad seed points for a region growing algorithm developed to delineate tree crowns. Growing is performed for points neighbour to the tree top with respect to height and crown-width conditions.

[Pekkarinen, 2002] developed a co-occurrence segmentation method for multi-source forest inventory applied on imaging spectrometer image composed of 30 spectral channels. The proposed method consists of a low-level segmentation step carried out by means of clustering connected components in the feature space followed by co-occurrence-based region merging. This type of merging makes it possible to combine in a meaningful way segments which have spectrally different properties.

Some of the main benefits of region growing approaches lie in the results obtained, which can easily be derived to extract tree species parameters. Results obtained are on the other side strongly influenced by the choice of the seed points from which regions are grown. The challenge is to develop a tree delineation algorithm that can account for the most significant sources of variation in remotely sensed data [Culvenor *et al.*, 1998].

4.3.3.4 Contour based methods

These methods are designed to detect crown edges of individual trees and use high-order active contours Horváth *et al.* [2006a], edge-detection filters or multi-scale analysis Brandtberg and Walter [1998] to delineate tree crowns.

[Horváth *et al.*, 2006a] introduced prior shape information into the segmentation to model circular objects and applied it to find tree crowns in colour infrared aerial images. An energy minimisation method using local minima information to define circles was first proposed and later on changed to energy inflexion points in [Horváth *et al.*, 2006b].

[Brandtberg and Walter, 1998] propose to delineate individual tree crowns in high spatial resolution aerial imagery by following edges created by gradient operator and analysing their curvature at multiple scales using variable smoothing filters. Primal tree crown sketches (representing circles) are created at each scale and summed into a final primal sketch image. Crown peaks are identified by a local maxima filter and are grown into regions respecting a minimum brightness rule. Seven out of ten tree crown were identified but the algorithm was subject to omission and commission errors in structurally complex forest canopies.

Straub, Gerke and Pahl [2003] developed an algorithm combining optical imagery and LiDAR canopy surface model for the automatic extraction of trees both in forest areas[Straub, 2003b] as well as in urban areas [Straub, 2003a, 2004; Straub and Heipke, 2001; Wolf (Straub), B. M. and Heipke, C., 2007]. A multi-scale representation of the height data is segmented using the watershed algorithm [Vincent and Soille, 1991] to detect tree tops with an ellipsoidal tree model [Pollock, 1994]. Fuzzy functions are used to choose the best hypotheses from the results of all levels based on the tree model. Finally, crown boundaries are refined using active contours. The approach was tested on different data sets and acquired with different sensor characteristics and were found promising given an adequate resolution for the digital surface model.

[Wang *et al.*, 2004] detected treetops in high spatial resolution aerial imagery by combining spectral and spatial prior knowledge about tree tops. These tree tops are used as seeds for a marker-controlled watershed segmentation of individual coniferous tree crowns. An edge-based method is first used to delineate crown boundaries. For each previously detected crown contour, a treetop is located as the point having the maximum intensity and located in the centre of the contour. They are further on used as markers for a watershed segmentation applied on a distance image.

[Ouma and Tateishi, 2008] extracts urban trees from Quickbird imagery by using a multi-scale filtering approach and non-parametric classifier on spectral and textural wavelet decomposition.

4.3.4 Top-down methods

Top-down image segmentation approaches include object information or top-down cues into the segmentation algorithm, in contrast to bottom-up approaches, which use mainly the continuity of grey-level, texture, and bounding contours.

Model-based methods

These methods exploit object-recognition techniques such as template matching and shape detection to locate synthetic generated models of tree crowns (templates) in remotely sensed data. Templates generated for standard tree crown shapes are searched over the input data to locate similar objects [Pollock, 1994] whereas shape detection involves recognising objects based on their geometry.

Pollock [1996] located tree tops in aerial photographs of coniferous forests based on crown templates generated using geometric and radiometric criteria. The model also incorporates knowledge about sensing geometry and scene illumination. Although this kind of approaches give good results, prior knowledge about tree crown size and shape has to be exploited, which can be rather difficult in an urban environment. Furthermore, as presented in [Pollock, 1998] the accuracy of this approach is strongly altered when applied to mixed species stands containing tree crowns occluded by neighbour trees or irregular tree crown shapes.

Larsen [1997] extend the approach proposed by Pollock [1998] by designing a correlation based crown template algorithm for Norway Spruce in high resolution panchromatic aerial imagery. Besides proposing a model integrating crown size and shape, the algorithm adapted to background brightness variation by simulating the expected shadow cast by trees. Although this approach performs well when tree crowns are consistent, problems can occur with irregular crown shapes and sizes.

[Olofsson *et al.*, 2003] use field measurements to generate a library of tree crowns template which are combined with the template matching technique for single tree detection in digital imagery of coniferous forests. Examples from the template library are matched against the image to produce a correlation map in which local maxima give estimates for tree positions. This method was reliable for detecting most visible trees (79.3%) but does not account for small or shaded trees.

[Perrin *et al.*, 2005] proposes an approach to extract tree tops and tree crown parameters from Colour InfraRed (CIR) aerial images of poplar plantations using stochastic geometry. This approach yields an energy minimisation problem. Regions of interest extracted by Gabor filters are modelled by marked point processes of ellipses. Both interactions between the geometric objects and the grey levels of the image inside and outside the objects were taken into consideration for the energy formulation. This energy formulation is used to extract the best configuration of objects.

[Gong *et al.*, 2002] developed a 3D model-based tree measurement method from high resolution aerial images. Trees are modelled as 3D semi-ellipsoids with five parameters: treetop coordinates, trunk base height, crown depth, crown radius and crown surface curvature. Treetops are manually identified and tree models are automatically matched on the images. The accuracy of the measurements depend on stand complexity, image quality and the accuracy of tree top location on the images.

Object-based techniques were also developed for LiDAR data. [Andersen *et al.*, 2002] proposed a complex crown template matching approach based on Bayesian object recognition and Markov chain Monte Carlo simulation applied directly on laser point vectors. Typical tree crown shapes (generalised ellipsoids) were used to determine the intersections between LiDAR data and tree crowns. As laser pulses penetrate into the canopy, probability models were used to model tree distributions and interactions (internal or outer crown strike). Point spatial configurations were compared to a prior probability model to identify structures associated with individual tree crowns. Given the constraints of the generalised ellipsoidal crown model, crowns with asymmetrical or irregular shapes could be difficult to detect. A LIDAR-based canopy segmentation algorithm for use on eucalyptus forests is proposed in [Turner, 2006]. It operates by matching a vertical crown template model with crowns from a 3D canopy surface models. Template matching approach has the advantage that view angle differences are handled in an integrated way [Olofsson *et al.*, 2003].

4.4 Our approach

This section presents the methods developed to produce an urban vegetation thematic map containing two categories, i.e. lawns and trees. It also presents the algorithm developed to delineate individual tree crown borders. In the following, the approaches developed to partition the previously obtained vegetation map will be positioned to state of the art methods. Then, the methods developed to produce each thematic class will be detailed.

The proposed approach consists of a two-step strategy, starting with lawn delineation and continuing with individual tree crown delineation, and is summarised in Figure 4.2. Given the vegetation mask previously obtained (cf. Chapter 3) and the DSM (cf. Chapter 2), height information is the main source of information exploited to separate lawns from trees, and to individually separate tree crowns.

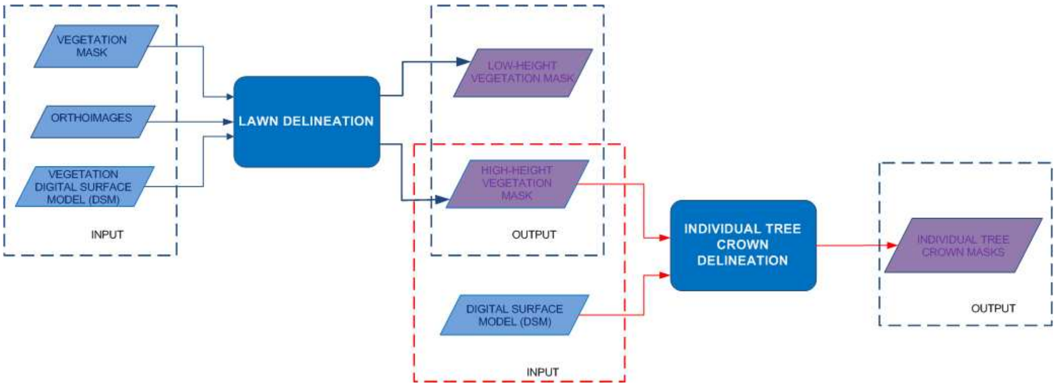

Figure 4.2: Input data and objectives for the "segmentation" module. Vegetation mask, orthoimages and vegetation digital surface model are used by the "lawn delineation" module to produce high- and low- height vegetation masks. The high-height vegetation mask and the digital surface model are used by the "individual tree crown delineation" module to produce individual tree crown masks.

Lawn delineation

From the different approaches proposed by literature on similar data types to delineate grass regions, we developed a method based on spatial characteristics computed on height data to delineate lawns in urban areas.

As reflectance properties of different types of vegetation, such as trees and grass, are very close and texture classification highly depends on the illumination conditions (the position of the solar light source) and the position of the sensor view angle relative to the imaged area, we compute texture characteristics on vegetation height data. The proposed method is presented in section 4.4.1.

Individual Tree Crown Delineation

At the output of the lawn delineation step, two thematic classes are isolated from the vegetation class. The first one contains lawn areas and the second, trees. Taking into consideration the available data to perform tree crown delineation, two state of the art approaches could have been taken into account, i.e. template matching and region growing ones.

Template matching methods rely on an input model for tree crowns. Given the high-variability in shape of urban trees, due to the tree's age or as a result of human interventions (like pruning, shaping or replacing trees) an unique type of tree model adapted to different climatic regions would be difficult to develop.

To delineate individual tree crown boundaries from the tree class, the developed method belongs to the class of region growing methods exploiting tree height continuity criteria and thus belonging to bottom-up segmentation methods. This approach consists of two steps: the first one is used to detect seed points which are grown to regions corresponding to individual tree crowns in the second step.

Figures 4.3 and 4.4 illustrate input data and output objectives for each of the two modules described in this chapter. Results obtained by the proposed methods are used to illustrate the goal of each component.

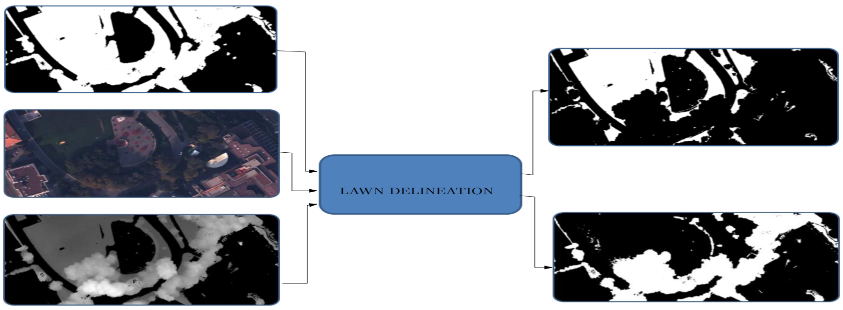

Figure 4.3: Overview of input data sources and output objectives for the "lawn delineation" module. The vegetation mask obtained from the "vegetation detection" module is used together with orthoimages and digital surface model corresponding to vegetation areas to produce high- and low- height vegetation masks.

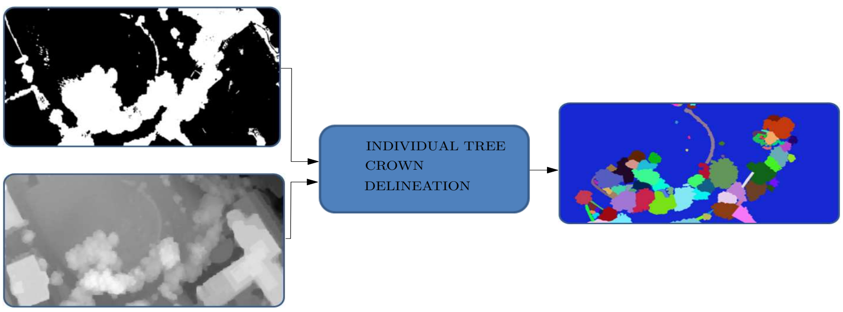

Figure 4.4: Overview of input data sources and output objectives for the "individual tree crown delineation" module. The high height vegetation mask obtained as output of the "lawn delineation" module is used together with the digital surface model to produce individual tree crown masks.

4.4.1 Lawn Delineation

Separating lawn areas from trees comes down to developing an algorithm capable of distinguishing between two spectrally close classes. From a radiometric point of view, the challenge is to find discriminant features characterising each of the two classes. Besides spectral features, texture characteristics could be used to improve classification accuracy. As for the geometric characteristics, shape alone is not an eligible criteria when it comes to vegetation in urban areas, often cut to shapes such as circles and rectangles. Height information on each vegetation class could also be used as discriminant characteristics. This is available only if accurate DSM and DTM data are available so that a normalised DSM could be obtained.

According to available input data, we chose to exploit texture characteristics computed on the DSM to characterise and differentiate between grass and trees. The proposed method exploits texture characteristics on the DSM to segment vegetation according to height variation. Based on such features, decision is made by simple thresholding techniques.

To extract lawns from the vegetation areas previously delineated we compute the local height variance on the vegetation areas corresponding to the Digital Surface Model (DSM). This texture feature accentuates large changes in height values between adjacent pixels. Variance texture is computed using the unbiased empirical estimator V, according to

$$V = \sum_{x_{ij} \in W} \frac{(x_{ij} - M)^2}{(n-1)} \tag{4.1}$$

where x_{ij} is the height value of pixel *(i,j)* on the DSM; n equals the number of pixels in a sliding window, W, and M is the mean value of the moving window computed by $M = \frac{\sum x_{ij}}{n}$.

The algorithm for lawn delineation can be resumed into the following steps:

(1) first, the digital surface model (DSM) of the area is used to compute variance by equation C.1,
(2) the vegetation mask is used on the image obtained after the first step to hide all non-vegetation areas,
(3) the resulting image is passed on to a decision module which separates lawns from trees,
(4) the output is saved as binary images representing lawn and tree areas.

4.4.1.1 Results

Height local variance was computed by using a sliding window of an empirically determined size of 11×11 pixels. This settings allowed us to capture both fine-scale and coarser-scale height characteristics of urban vegetation. The variance texture data was separated into low- and high- values using a histogram-based thresholding method.

Figure 4.5-(a) depicts the variance image computed on the vegetation area extracted from the DSM on a subset of site B, Marseille data set. Figures 4.5-(b) and (c) depict results of the segmentation between tree areas and lawns.

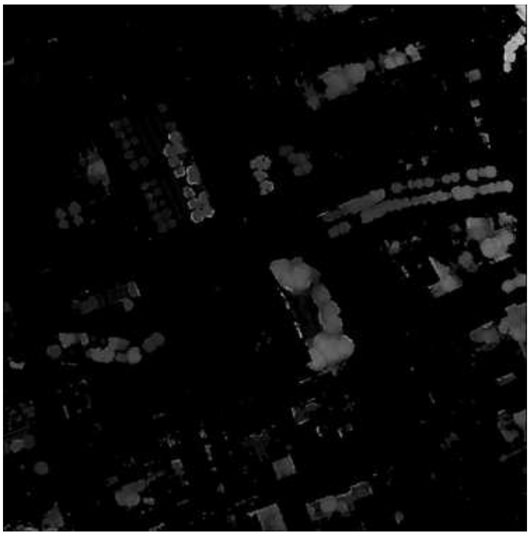

(a)

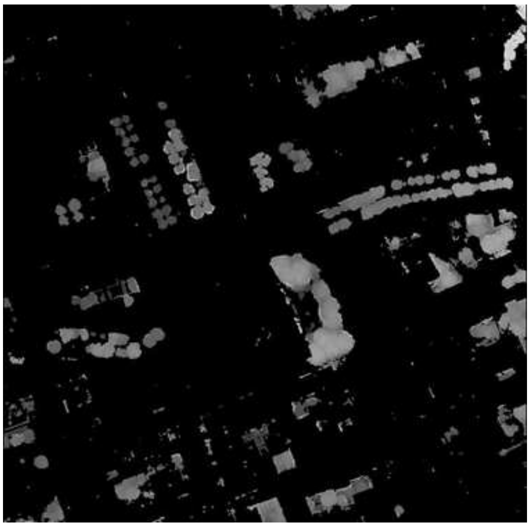

(b)

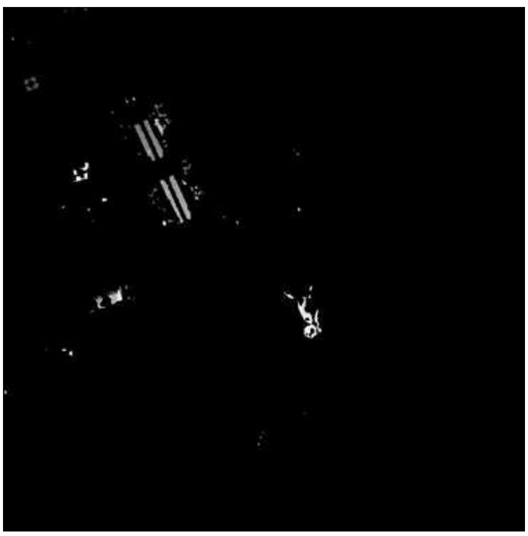

(c)

Figure 4.5: Differentiation between grass and tree areas. (a) Vegetation areas on the DSM corresponding to the height local variance. (b) Tree areas. (c) Lawn areas.

The accuracy of the results obtained was visually assessed and proved to correctly separate low- from high- height vegetation areas. Extensive experiments were run on different subsets the Marseille data set and the method successfully passed the visual inspection proving reliable in each test.

Provided an accurate DSM is available, the method gives reliable results for separating lawn areas from trees. In the context of our application, results obtained by applying this method to separate trees from lawns proved highly satisfactory.

The main limitation of the proposed method is the size of the sliding window which has to be adjusted for different DSM resolutions. This also implies that the method is sensitive to the value of the threshold used to separate low and high height vegetation areas. In order to select the optimal parameter set, the accuracy of the obtained results should be evaluated against reference data.

4.4.2 Individual Tree Crown Delineation

Traditionally, region growing (RG) methods developed for image segmentation start by arbitrarily choosing seed pixels which are grown into regions composed of all neighbouring pixels satisfying a similarity criterion. This process continues until all pixels belong to some region. It is possible to split the segmentation procedure in two steps, one in which seed points are chosen, and a second one, when a region is grown.

The performance of this type of segmentation method is highly dependent on the number of seeds (as the number of detected regions is equal to the number of seed points) and on the choice of the similarity criteria used (which can be based on any characteristic of the regions in the image).

The method we developed uses a set of seed points with a one-to-one correspondence with the number of trees in the image, which are grown into regions made of pixels lying on the same surface.

4.4.2.1 Seed Points

To obtain one seed point for each tree crown, we use the DSM to estimate tree tops. To reduce the number of possible candidates for a tree top, a Gaussian filter is used as a smoothing filter on the DSM with an empirically determined mask, approaching the average size of the trees in the image. To determine tree tops, we evaluate the maximum height of the trees present in the DSM and we consider all points having the same height as tree tops. In the first iteration we obtain points corresponding to the highest trees in the stand. Therefore, we iteratively decrease the analysis altitude, h. At each step, we analyse all points at greater heights than

h and detect a new seed when a new region appears and it doesn't touch pixels previously labelled as seeds. A graphical illustration of this algorithm is presented in Figure 4.6.

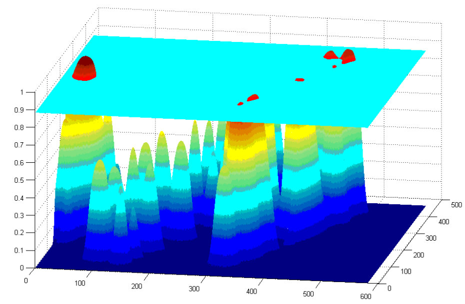

(a)

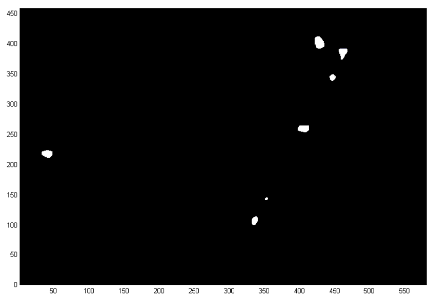

(b)

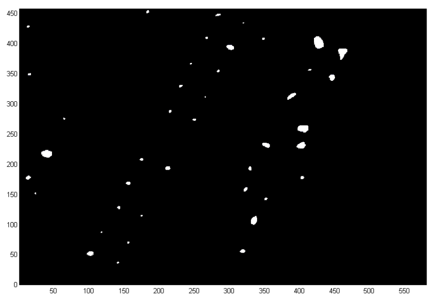

(c)

Figure 4.6: Detecting seed regions on the DSM of a tree stand region from site B, Marseille data set. (a) 3D view of the DSM: all points higher than the analysis altitude h are evaluated for tree top estimation. (b) 2D view of the 30th iteration. (c) Seed points detected after the final iteration: we can notice that we obtain one seed region for each tree.

The *find seed* algorithm applied on the digital surface model of trees is resumed by the following steps:

1. the digital surface model (DSM) correspondent to the high-height vegetation mask is smoothed by a Gaussian blur filter,

2. for h from max(smoothed DSM) down to 0,

   - assign into a new labelled image (seed labelled image), an unique label to all pixels above a current height and with no assigned label

3. for i from 0 to max(seed labelled image),

   - search for connected regions

4. deal with the connected regions and generate output seed labelled image.

The Find Seed algorithm performs two passes through the smoothed DSM of high-height vegetation areas. In the first pass, the image is processed from maximum to minimum intensity values to generate labelled seed regions. In the second pass, labelled regions are scanned to detect connected regions which are dealt with in a final step to ensure uniqueness of seed region labelling.

Let $dsm(p)$ be a function of grey levels representing a digital image with the domain $\Omega \subset \mathbb{Z}^2$. Each pixel $p \in \Omega$ has a grey level $dsm(p)$, four direct neighbours, $N_4(p)$ and four diagonal neighbours, $N_D(p)$. Eight-neighbours, $N_8(p)$ of pixel p consist of the union of $N_4(p)$ and $N_D(p)$. Let R^h be a set of pixels such as $\forall p \in R^h \exists p' \in R^h$ such as $p' \in N_8(p)$ and $dsm(p) = h$. $L(R^h)$ represents the label assigned to pixels forming the region R^h.

Algorithm 1: *FindSeed* Algorithm

Input: DSM of high-height vegetation mask : dsm
Output: seed labelled image : *seed_lbl*
Initialisation: $smooth\_dsm \leftarrow GaussianFilter(dsm, \sigma)$;
$label \leftarrow 0$; $seed\_lbl \leftarrow -1$; $l \leftarrow -1$;
$h_{MAX} \leftarrow Max(smooth\_dsm)$, $L \leftarrow -1$;
for $h = h_{MAX}$ *to* 0 **do**
  for $(\forall\ p \in R^h)$ *such as* $(smooth\_dsm(p) > h)$ *AND* $(seed\_lbl(p) == -1)$ **do**
    */*Get the set of detected seed regions*/*;
    $R_1^h, \ldots, R_n^h$;
  end
  for $i = 1$ *to* n **do**
    */*Assign a label to each region*/*;
    $L(R_i^h) \leftarrow l$;
    $l \leftarrow l + 1$;
  end
  for $i = 1$ *to* n **do**
    if $\forall\ p \in R_i^h\ (\nexists\ p')$ *such as* $(p' \in N_8(p))$ *AND* $p' \in R_j^h$ *with* $(L(R_j^h) \neq -1)$ **then**
      */*Get the set of isolated seed regions*/*;
      $\mathscr{I} \leftarrow R_i^h$;
    end
    for *region* $R_r^h \in \mathscr{I}$ **do**
      */*Assign a label to all pixels of region* R_r^h**/*;
      $seed\_lbl(p) \leftarrow label$;
      $label \leftarrow label + 1$;
    end
  end
end

4.4.2.2 Region Growing

Starting from the previously labelled tree tops, tree crown borders are obtained by a region growing approach based on geometric criteria of the trees. This approach is similar to the previous one, based on a height descent. The altitude analysis h is iteratively decreased, and for each step, the pixels corresponding to a height of $h \pm \triangle h$ are iteratively aggregated to the adjacent region.

4.4.2.3 Results

Tree crown delineation is performed on tree areas previously identified. The segmentation algorithm belongs to the family of region-growing algorithms and uses tree seed regions depicted in Figure 4.6-(c) as input.

The input RGB image for the individual tree crown delineation contains a tree stand from a subset of site B of the Marseille data set and is presented in Figure 4.7-(a) while the reference manual delineation of tree crowns is presented in Figure 4.7-(b).

The results of this algorithm are illustrated in Figure 4.8 on a subset of site B, of the Marseille data set, depicted in Figure 4.7-(a). The reference manual delineation presented in Figure 4.7-(b) for the same tree stand is used for evaluation purposes.

A visual assessment of the tree crown delineation results shows little over-segmented regions. Most trees are identified by a unique tree crown segment (cf. Figure 4.8). A more thorough evaluation of the quality of the segmentation algorithm is given in the following section (Section 4.5). Evaluation measures are first presented and are followed by the assessment of the accuracy of the canopy segmentation.

4.5 Evaluation

4.5.1 Evaluation Measures

The approach used for the evaluation is similar to the one presented in [Mei and Durrieu, 2004]. A statistical analysis is first performed taking into consideration the total number of trees in the ground truth and the omission (omitted trees) and commission errors (segments not associated with a tree). We take into consideration the following cases for the spatial analysis of the segmentation : pure segments, over-segmented trees, under-segmented trees. Figure 4.9 illustrates these evaluation measures. Pure segments (Figure 4.9-(a)) correspond to correctly identified trees. We consider that a segment is 100% pure if it corresponds to one and only one segment in the ground truth and vice versa, with an overlap area greater than 80%. Over-segmented trees (Figure 4.9-(b)) correspond to the case when more then one segment is associated with the ground truth delineation. Under segmented trees (Figure 4.9-(c)) correspond to segments which include a significant part (> 10%) of more than one tree crowns.

4.5.2 Canopy Segmentation Accuracy

As with most segmentation methods, the quality of the segmentation is evaluated against reference data. Partitions of an image were evaluated by finding correspondences between pixels in the reference and the ones belonging to regions obtained after segmentation. The accuracy assessment results are presented in Table 4.2.

Table 4.2: Tree Crown Delineation Accuracy Assessment

	Quantity	**% of the total number of trees**
Trees correctly segmented	33	89.1
Trees over-segmented	1	2.7
Trees under-segmented	2	5.4
Trees omitted	1	2.7
Total number of detected trees	37	

From the total of 41 ground truth trees, some of the trees are forgotten. This happens for trees with a small-area crown and is due to the smoothing step preceding the segmentation. It is directly dependent to the size of the Gaussian Blur filter size. Trees with small crowns, hardly noticeable in DSM data, are completely deleted by the GB filter. This is the main limitation for the tree delineation algorithm which cannot correctly delineate trees with small tree crowns, due to the smoothing step.

As we evaluate the quality of the segmentation, trees omitted after the smoothing step are not taken into account as they are not relevant for assessing the quality of the segmentation algorithm. Therefore, accuracy assessment is computed for the 37 trees present in the DSM after the smoothing step. According to the evaluation measures previously described, a total of 33 trees were correctly segmented, accounting for 89.1% of the trees detected from the stand. Only one tree is over-segmented, 2 are under segmented and one is omitted by the algorithm.

Other limitations are those intrinsic to the correlation algorithm giving the precision of the DSM and to the distance between two neighbour tree crowns. If parts of the tree crown are not visible in images used to generate the DSM (as the tree lies in shadows or is occluded by narrowing buildings) these parts will not be visible in the DSM and thus the segmentation algorithm will produce crown borders smaller that the real size of the tree crown. If two trees are very close to each other, the algorithm stops the growing of the respective tree crowns before all pixels belonging to the tree crown are taken into consideration. These will often result in under-segmented tree crowns.

As one of the main limitations of the algorithm is related to the DSM smoothing step, the sensitivity of the canopy segmentation algorithm to the size of the Gaussian blur filter is analysed hereafter. Table 4.3 presents the sensitivity analysis of the algorithm for delineating individual tree crowns to the size of the Gaussian blur filter applied on DSM data.

Table 4.3: Sensitivity of Gaussian Blur (GB) filter size (number of tree crowns in the Ground Truth data)

GB filter size	10	15	20	25	**30**	35	40	50	60
Trees correctly segmented	28	32	33	33	**33**	32	30	30	27
Trees over-segmented	7	3	2	1	**1**	1	1	1	0
Trees under-segmented	1	1	1	2	**2**	2	4	4	6
Trees omitted	1	1	1	1	**0**	0	0	0	0

Different sizes were evaluated for the Gaussian filter which varied from 10 to 60 pixels on a basis of 5 pixels at each step. Best performances in terms of correctly segmented trees were obtained for sizes 20, 25, end 30 pixels. Equal performances in terms of over- and under- segmented trees were obtained for sizes 25 and 30. The best overall configuration is given by a filter size of 30 pixels as no trees are omitted. For a filter size superior to 30 pixels, both the number of correctly segmented trees and the number of under segmented trees increase compared to a filter size of 30. For filter sizes of 10 and 15 pixels, the performances of the tree delineation algorithm decrease, both in the number of correctly segmented trees and over segmented ones.

4.6 Comparison

We compared the proposed approach to delineate tree crowns with two state of the art image segmentation approaches. The first approach, developed by Erickson [Erikson, 2004a] in his PhD thesis, is the random walk segmentation algorithm aiming at individually delineate tree crowns from very high resolution aerial images. The second, is the watershed segmentation algorithm presented in Vincent and Soille [1991]. The following paragraphs briefly summarise each of these approaches and present some of the obtained results.

4.6.1 Random walk image segmentation algorithm

The *TreeAnalysis* program is a package containing the research code developed by Mats Erickson in his PhD thesis. It was retrieved from the author's web site `http://hem.bredband.net/b109016/download.html` on the 31st of July, 2006. The program delineates tree crowns using a random walk segmentation algorithm starting from seed points representing tree tops. Seed points can either be found automatically (using the scale-space theory) or manually positioned by the user.

4.6.1.1 Algorithm description

The random walk image segmentation algorithm is based on the assumption that neighbour tree crowns are separated by dark pixels. The algorithm contains two steps, a pre-processing and an expansion one. During the pre-processing step, seed points are extracted and used as stating points for the random walk algorithm. This first steps' output will be used in the expansion step to regroup pixels belonging to individual tree crowns into individual segments.

Seed point extraction Seed points are found by using the scale-space theory. A distance transform is first computed on the input image. This image is later on smoothed and used to extract the seed points, by local maxima detection. The value of each seed point in the distance image is used as a ranking for the analysis order of each seed - the higher its value, the higher the chance it corresponds to tree tops.

Creation of a random walk image To simulate the random walk for a particle the original input image is used. Each of the seed points are starting points for the particle movements. To illustrate the movements, a neighbourhood of variable size is considered around each seed point. The size of the neighbourhood is computed based on user-defined number of grey level values. The particle moves to a new randomly chosen position in the neighbourhood if the gray level of the new position is lower than the gray level of the current position. This step is repeated until a valid new position for the particle is found. During this step, a particle is likely to move several times to the same position. Statistics about the number of times each point in the neighbourhood is visited are saved in a new image, in which the values of each pixel count for the number of times a particle moved to correspondent position.

Expansion for creating the segmentation output The final segmented image obtained through the random walk segmentation algorithm is first initialised with an unique label for each seed point. Each seed point is expanded to a circle having a radius proportional to the distance value correspondent to the seed point in the statistics image obtained in the previous step. Points having values different than zero in the statistics image which are border pixels to only one region are included in the newly created segments. All other pixels with a value different than 0 and which are border pixels to more regions are considered to be dividing lines between tree crowns. Regions are iteratively expanded to include all pixels having a lower gray level than the mean of the gray levels in the seed's neighbourhood computed on the input image.

4.6.1.2 Experimental details

Tests were performed on a subset of site B, from the Marseille data set (cf. Chapter 2). Two types of trials were conducted. The main difference lies in the type of input data. The first trial was conducted on three channel orthorectified photographs, whereas the second one exploits the canopy height information from the DSM. Figure 4.10 presents input data used for the two trials.

The *TreeAnalysis* program either takes user defined seed points as starting points to build regions or automatically extracts them from the input data. In order to evaluate the sensitivity of the random walk segmentation algorithm to seed points, two types of trials were conducted on each of the data types presented in Figure 4.10 - one using automatically positioned seed points and the second one using a manual initialisation of seed points. The set of manually positioned seed points, presented in Figure 4.11-(a), were obtained by means of stereo photo interpretation. Particular attention was payed to the initialisation step such as one seed point was assigned to a single tree crown. Figure 4.11 presents input seed points used for the two trials, automatically extracted and manually positioned ones. Great difference is noted in the number and position on the automatically located seeds and the manually positioned ones, with great impact on the number and size of the resulting tree crown units.

(a)

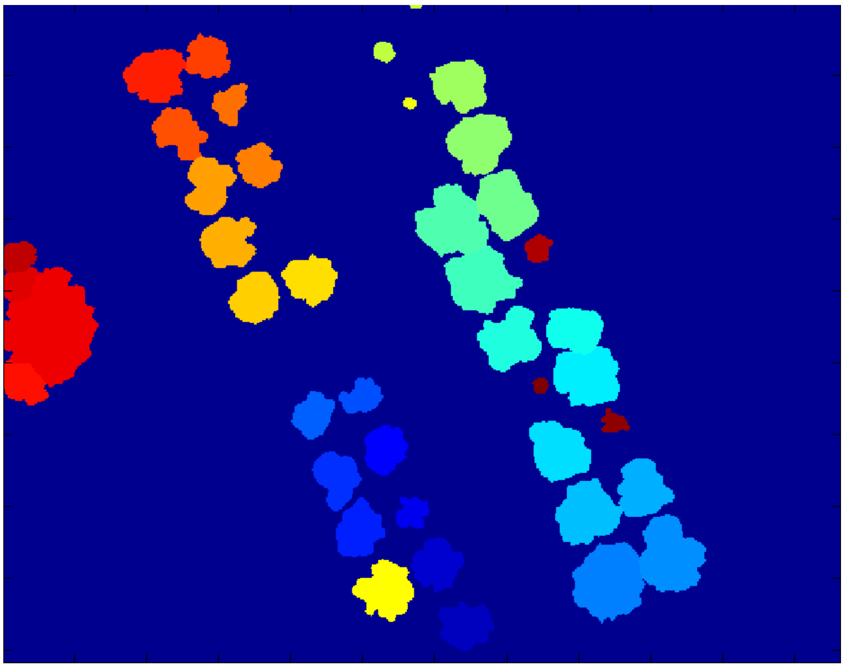

(b)

Figure 4.7: Input data and reference manual delineation of tree crowns for a tree stand of site B, Marseille data set. (a) RGB image depicting a tree stand from site B, Marseille. (b) Reference delineation of tree crowns hand-made by a qualified photo interpreter from IGN by means of stereo restitution. Individual tree crowns are depicted by different colours.

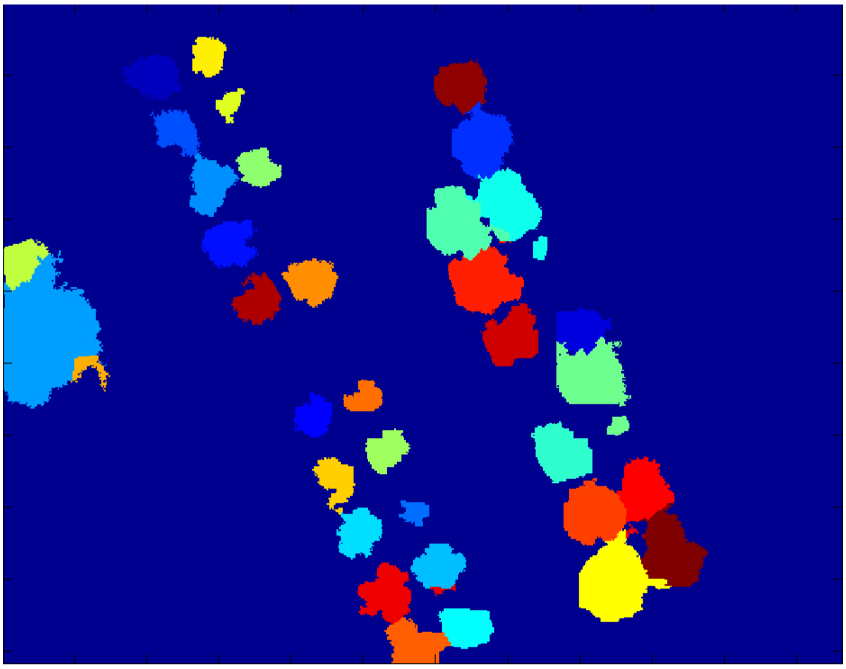

Figure 4.8: Automatic tree crown delineation results for the proposed RG method on a tree stand of site B, Marseille data set. Individual tree crowns are depicted by different colours.

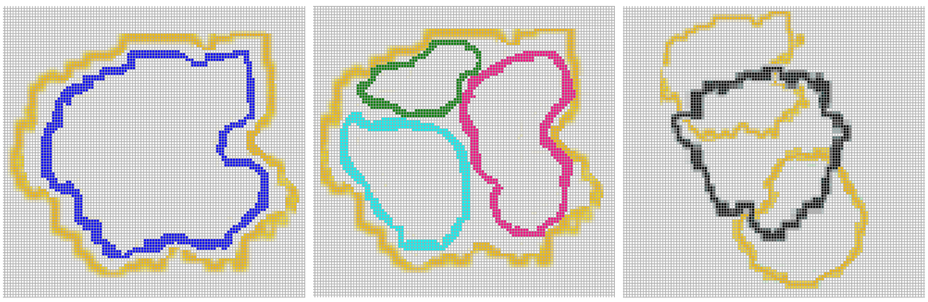

(a) (b) (c)

Figure 4.9: Evaluation measures defined for tree crown delineation accuracy assessment. Yellow shapes represent ground truth delineation of tree crowns. (a) Pure segments. (b) Over-segmented trees. (c) Under segmented trees.

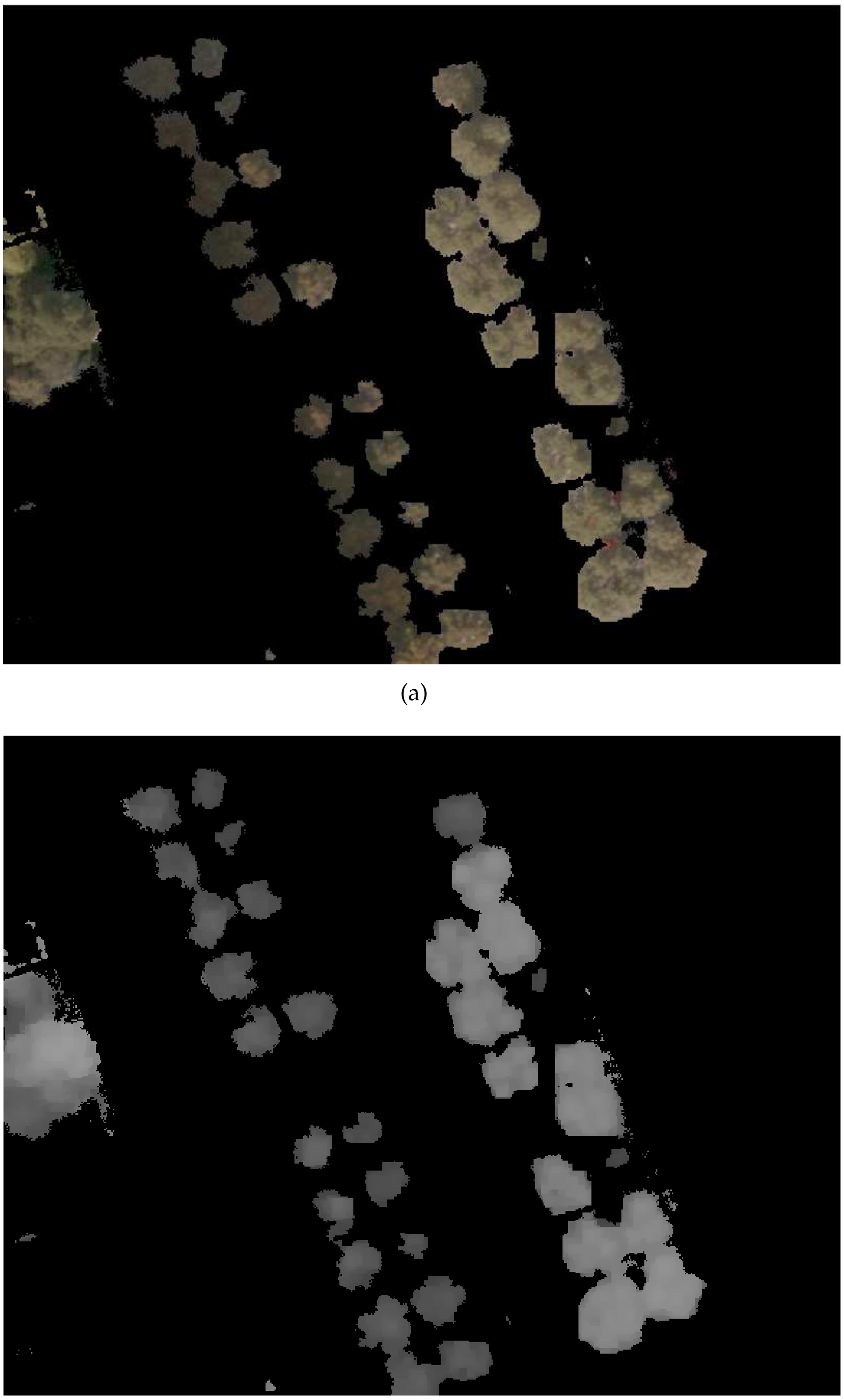

(a)

(b)

Figure 4.10: Input data used for the random walk region growing trials. (a) RGB orthorectified image. (b) Canopy height information from the DSM.

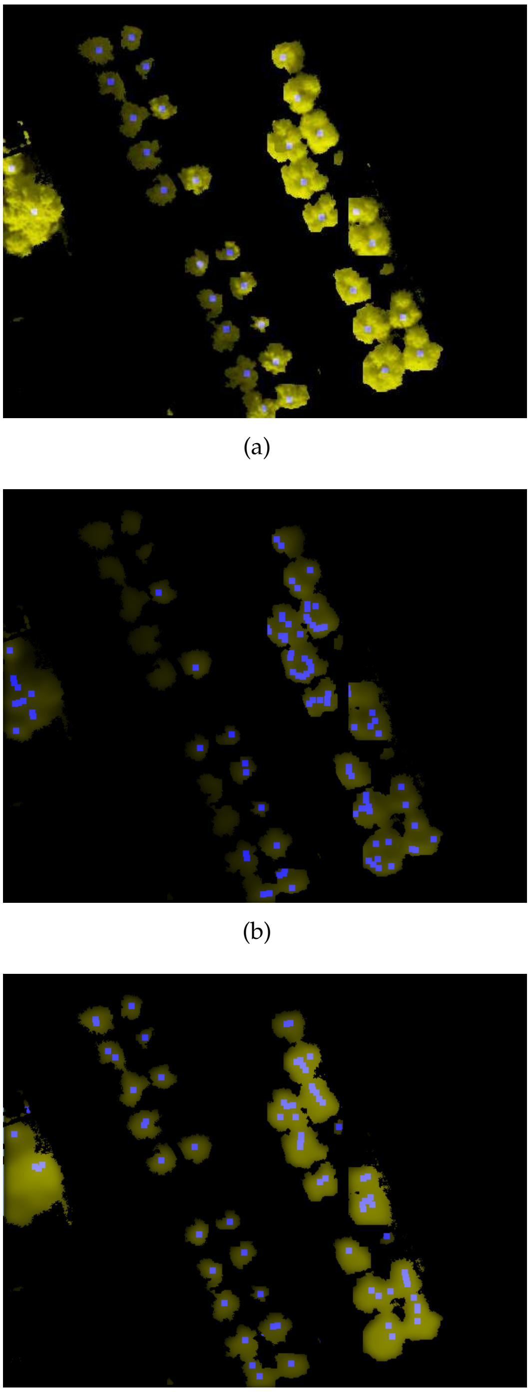

(a)

(b)

(c)

Figure 4.11: Seed points used for the random walk region growing trials on a tree stand from site B, Marseille data set. (a) Manually positioned seed points (marked by a blue square) over-imposed on tree crowns to be delineated. (b) Automatically extracted seed points for the RGB orthoimage. (c) Automatically extracted seed points from the DSM correspondent to the tree area. Seed points are marked by a blue square in both images.

Figure 4.12 summarises the experiments performed with the *TreeAnalysis* program. Two types of input data are taken into consideration. The first one is an RGB orthoimage and it corresponds to classic input data for the *TreeAnalysis* software. The second one is the DSM correspondent to high height vegetation areas. These images are first used for seed point extraction, thus generating a set of automatically extracted seed points. The second one, is the set of manually positioned seeds, used as the first one, to initiate the random walk region growing algorithm. Output of the *TreeAnalysis* trials is composed of tree crown units. A total of four types of results will be presented and analysed for all types of input data and each case of seed point initialisation.

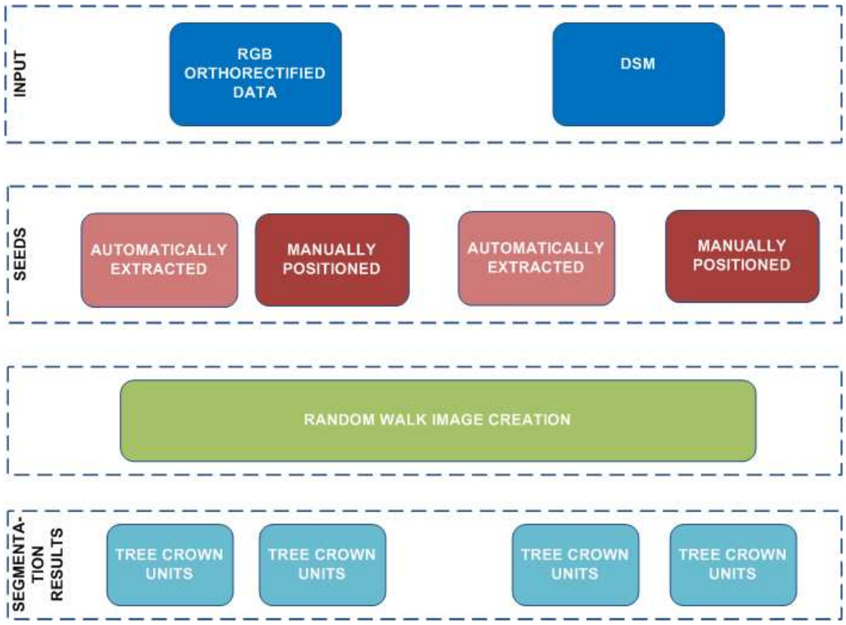

Figure 4.12: Summary of the trials performed on the input data presented in Figure 4.10 for seed points data depicted in Figure 4.11

.

The following paragraphs present results obtained by applying the random walk region growing algorithm on the two types of input data, both using automatically positioned seed points as well as manually positioned ones.

4.6.1.3 Results

Orthorectified data

Figure 4.13 presents tree crowns delineated by the *TreeAnalysis* program initialised with seed points extracted from the RGB orthoimage (presented in Figure 4.11-(b) and (c)). Results obtained by using manually positioned seeds are presented in Figure 4.13-(b) whereas segmentation results obtained by automatically extracted seeds are presented in Figure 4.13-(a).

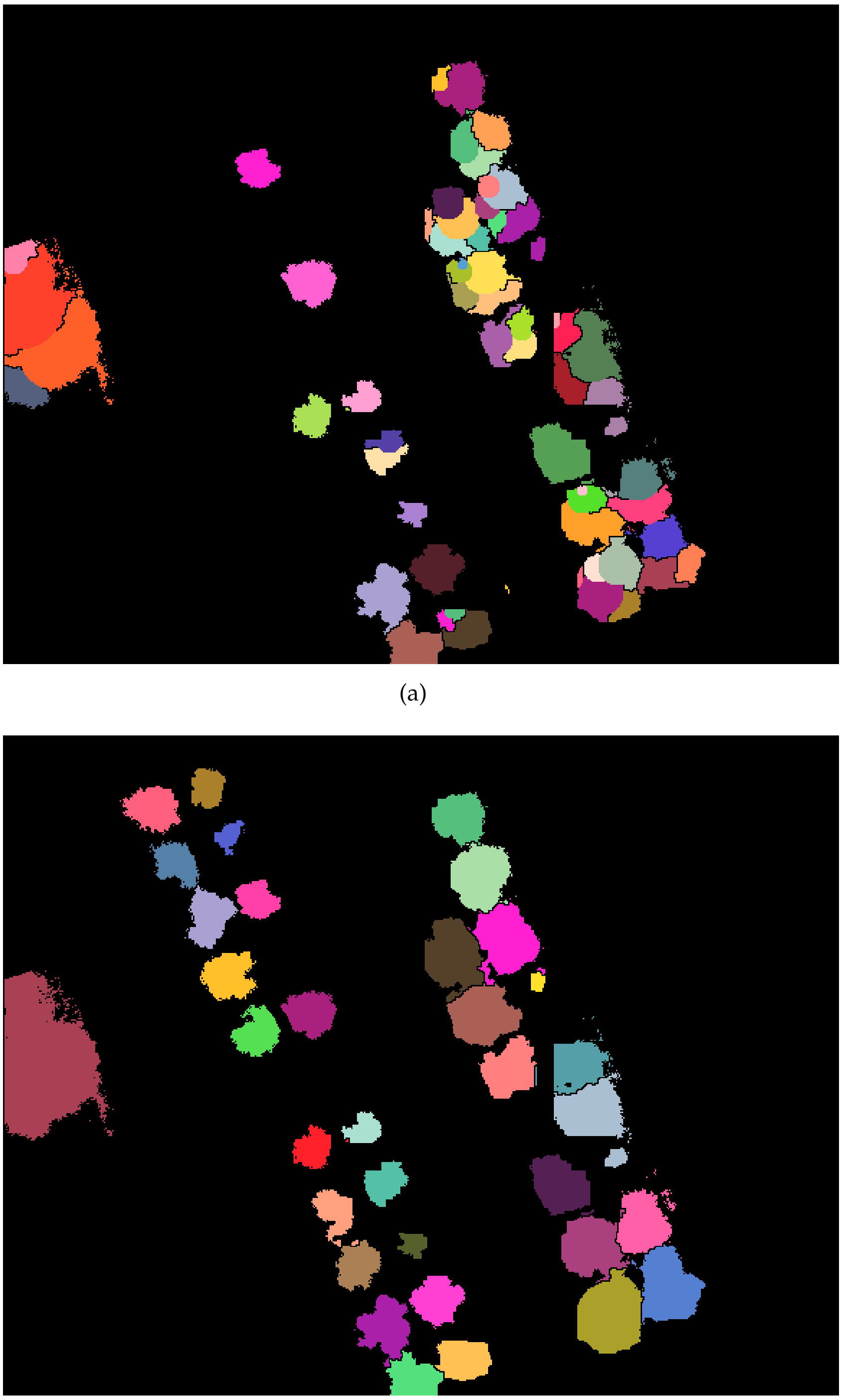

(a)

(b)

Figure 4.13: Segmentation results for the random walk region growing algorithm applied on orthorectified data of a tree stand from site B, Marseille data set. (a) Results obtained by using automatically located seeds. (b) Tree crown units extracted from the RGB orthoimage by using manually placed seed points.

For both manually positioned seed points and automatically positioned ones we used the same parameter when testing the *TreeAnalysis* program. The obtained results are quite realistic, with several over segmented tree crown regions for the automatically positioned seed points (Fig. 4.13-(a)). Generally speaking, segmentation results for automatically positioned seed points are less accurate than when dealing with manually positioned seed points (Fig. 4.13-(b)). The accuracy of the tree crown segmentation strongly depends on the position of seed points. The number of tree crown regions obtained as an output depends on the number of input seed points. A correct initialisation of the seeds, leads to accurate segmentation results.

Canopy Height Data - DSM

Output obtained from the previous trials highlight the strong influence of accurate seed points on the accuracy of the segmentation results. In this paragraph, the random walk region growing algorithm is evaluated on the DSM, thus exploiting tree height information. As for the previous type of input data, two trials ware conducted on the DSM, the first one evaluates the algorithm's accuracy by using automatically positioned seed points whereas the second one uses the manually positioned set of seed points.

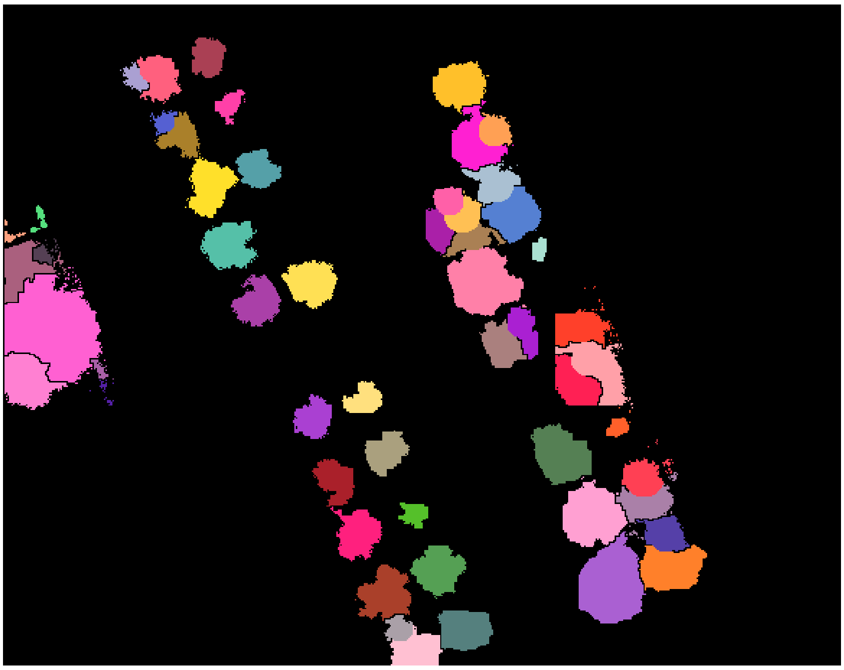

(a)

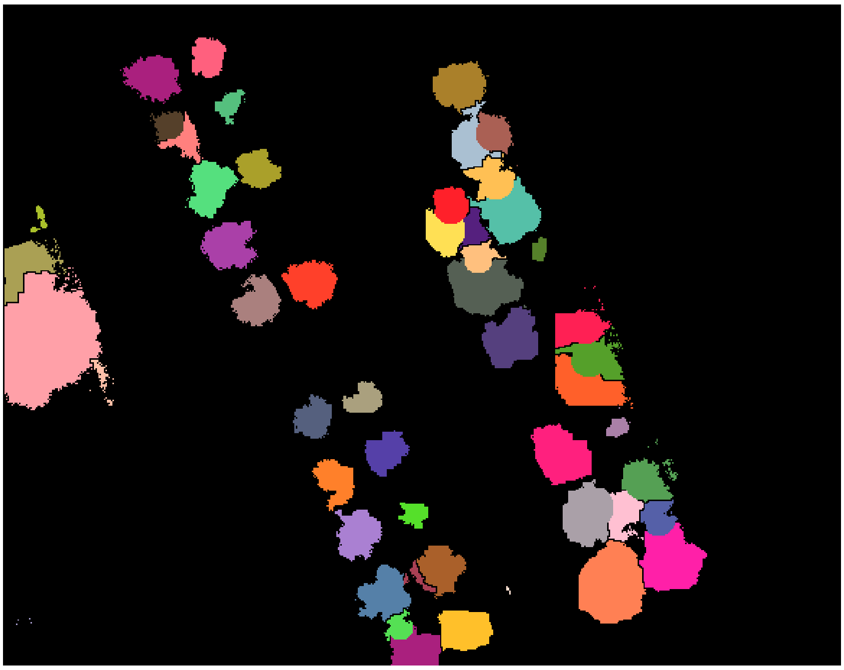

(b)

Figure 4.14: Segmentation results for the random walk region growing algorithm applied on canopy height data of a tree stand from site B, Marseille data set. (a) Tree units obtained from automatically detected seeds. (b) Results obtained by using a manual initialisation of seed points.

Compared to results obtained for RGB orthoimage data, we note the higher accuracy of the random walk segmentation algorithm when applied on the height data. This is mainly due to the higher accuracy of the seed points automatically positioned on the DSM (presented in Fig.4.11-(c)). Border lines between neighbour trees mostly follow realistic tree crowns although some geometric-shape effects can still be observed.

Segmentation Accuracy

Results obtained for the random walk region growing algorithm were compared against ground truth data in order to assess segmentation accuracy. Table 4.4 presents accuracy assessment results for DSM input data and automatically positioned seed points. Motivations for the choice of this configuration were two-fold:

- automatically initialised seed points were chosen so that algorithm comparison could be made in equivalent conditions.
- DSM input data was evaluated both to establish similar conditions for the algorithms and as visual assessment of the results showed a lower number of over-segmented trees compared to using RGB orthoimage.

Table 4.4: Random Walk Region Growing Algorithm - Segmentation Accuracy

	Quantity	**% of the total number of trees**
Trees correctly segmented	23	62.1
Trees over-segmented	11	29.7
Trees under-segmented	4	10.8
Trees omitted	0	
Total number of detected trees	37	

Segmentation accuracy was evaluated using the evaluation measures presented in section 4.5. Out of the total of 37 trees present in the DSM, only 62.1 % were correctly segmented and 29.7 % were over-segmented. Compared to the tree delineation algorithm proposed in this thesis, there were no omitted trees for the *TreeAnalysis* program run on the DSM with automatically extracted seed points.

4.6.1.4 Conclusions

This study revealed the importance of the DEM channel for tree crown segmentation. Important difference was noted in the segmentation results of the same area were obtained for the RGB images compared to data containing the DEM channel.

Results obtained by the *TreeAnalysis* program are very much dependent on the seed points used. There is no perfect initialisation of the seed points but the performed experiments show that accurate initialisation of seed points gives better segmentation results than an automatic initialisation of the seeds.

The use of the DSM channel as input data for the random walk region growing algorithm gives better results for automatically positioned seed points. As can be noticed from Figure 4.14 segmentation results on canopy height data have higher accuracy than the ones for the RGB orthoimage (Figure 4.13).

This trial shows that the main problem is finding accurate seed points. We can notice in Figures 4.13(b) and 4.14(b) that accurate initialisation of the seeds leads to accurate segmentation results. On the other side, over-segmentation from Figure 4.13(a) is directly related to multiple seeds automatically extracted from the RGB orthoimage and presented in Fig. 4.11(b).

4.6.2 Comparison to watershed algorithm

The watershed algorithm is an image segmentation algorithm using the watershed transform to delineate homogeneous regions. It is a powerful tool used in many different image processing applications and is nowadays part of several image processing software libraries (e.g. the Image Processing Toolbox of Matlab). After a concise description of the watershed transform, we will present in the following of this section results obtained by using this algorithm to isolate individual tree crowns from the canopy height model of trees. This section will end with a discussion of the advantages and limitations of this approach compared to the algorithm we proposed.

4.6.2.1 Algorithm description

The watershed transform has its origins in the areas of topography and hydrology. It was first introduced to the image processing community using a mathematical morphology formalism by [Digabel and Lantuejoul, 1978] in 1978. As an extension of morphological transforms it is a powerful tool for image segmentation applications.

For the watershed transformation, an image is considered as a topographic relief where gray levels correspond to altitude information, the dark and light structures of the image correspond to the valleys and the domes of the relief. The plateaus located at the top of the domes and the bottom of the valleys respectively correspond to regional maxima and minima.

Given this formalism, watersheds can be defined in terms of flooding by considering that regional minimas are holes and that the surface is slowly immersed into a lake which we consider of infinite extent. Water will progressively pass through the holes starting with the lowest minima and will progressively flood the relief. At any moment of the flooding, different lakes delineated on the topography contain the same water quantity.

Suppose we will prevent water coming from different lakes (thus different regional minima) to merge into a single lake by building dams on the topographical surface wherever this might occur. When the surface is completely underwater, only dams separating lakes equal in number to regional minima are still visible. These dams are the watersheds whereas the lakes represent the catchment basins associated to a regional minima.

4.6.2.2 Experimental details

Experiments were performed on the canopy height model data by using the Matlab implementation of the watershed algorithm, included in the Image Processing Toolbox. Segmentation results are presented in the following paragraph and accompanied by a quantitative and qualitative evaluation against ground truth data.

4.6.2.3 Results

Segmentation works best for smooth convex objects that don't overlap too much. Some of the tree borders obtained by applying this image segmentation algorithm are straight lines and do not follow irregularly shaped tree crown borders. This is due to the way the watershed transform builds up the digs preventing water to flow into the neighbour regions.

Segmentation Accuracy

Segmentation accuracy was assessed by comparing results obtained for the watershed algorithm against ground truth data. Evaluation measures presented in section 4.5 were used to quantify segmentation results for the watershed algorithm, which are presented in Table 4.5.

Performances of the watershed algorithm are close to the ones of the algorithm proposed in this thesis for tree crown delineation with 78.3 % of tree crowns correctly segmented and are identical in terms of over- and under- segmented

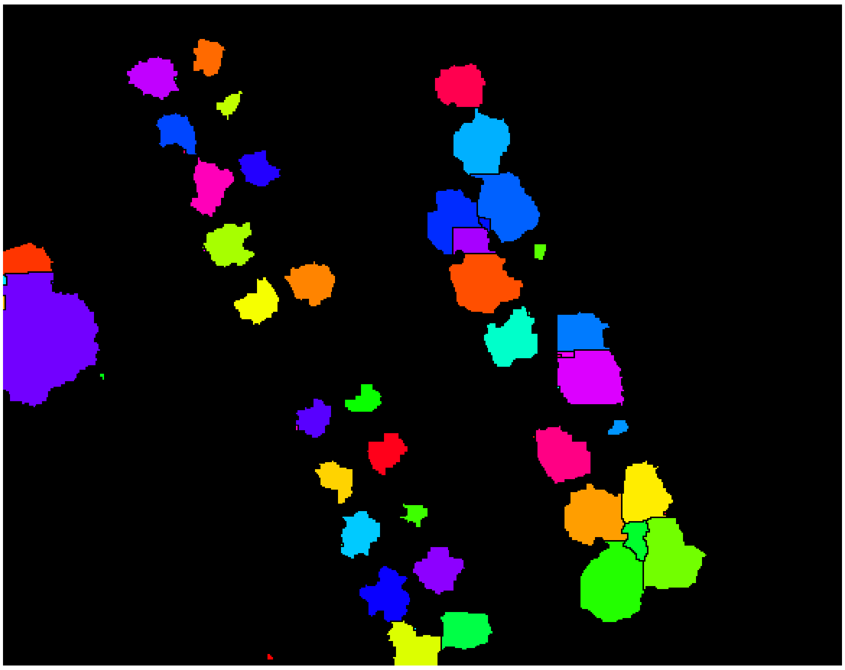

Figure 4.15: Tree crown delineation results obtained by applying the watershed image segmentation algorithm on the canopy height model of a tree stand fro site B, Marseille data set.

Table 4.5: Watershed Algorithm - Segmentation Accuracy

	Quantity	**% of the total number of trees**
Trees correctly segmented	29	78.3
Trees over-segmented	1	2.7
Trees under-segmented	2	5.4
Trees omitted	5	13.5
Total number of detected trees	37	

trees. However, the main drawback of the watershed algorithm is made up of the 13.5 % omitted trees.

4.7 Conclusions

This chapter gives an overview of the methods developed to cope with object recognition in urban vegetation areas. This chapter englobes the image segmentation procedures developed on one hand to separate tree areas from lawn ones and on the other side to delineate tree crown borders.

After reviewing state of the art approaches, the methods developed to perform lawn individual tree crown delineation are presented. The first module of this chapter deals with lawn delineation by processing the vegetation mask and the digital surface model to separate high and low height vegetation areas. The high vegetation mask and its corresponding part of DSM are further processed by the second module, to delineate individual tree crown borders. The output of the module presented in this chapter consists of individual segments for each tree crown and will be exploited by following chapters to both achieve an accurate representation of vegetation in 3D city models and to perform vegetation characterisation.

Lawn delineation is performed by computing local variance on the DSM and thresholding the resulting image. Applied to flat urban areas, this method gives promising results but is strongly dependent on the window-size and the threshold used to separate lawn from trees, especially when dealing with sloping regions. These two parameters have to be set according to the spatial resolution of the input data and prior knowledge on landscape relief. One of the most disturbing aspects when processing aerial images of urban areas is the presence of multiple shadows and multiple reflection. One of the advantages of the proposed method is the fact that such effects have minor influence on the accuracy obtained as it is applied on the DSM.

Tree crown delineation is performed on *high-height* vegetation mask and its corresponding part of the DSM. The method developed belongs to bottom-up segmentation methods and exploits tree height continuity criteria to delineate tree crowns into individual units. Results obtained are highly accurate, both from a quantitative point of view and as well as from a qualitative one. Performances of the proposed method are compared to two state of the art methods mostly used for similar goals, the random walk image segmentation and the watershed algorithm. Results obtained by the three methods are close with higher quantitative results for the proposed method compared to the random walk image segmentation algorithm and with a more realistic delineation results compared to the watershed algorithm.

As tree crown delineation is performed on 3D height information, it is not influenced by shadings, occlusions or intensity variations. Nevertheless, a precise DSM is needed to obtain accurate tree crown delineation results as due to the Gaussian blur applied on it, trees having small crowns cannot be detected after the smoothing process. Given such a DSM, the limitations remaining are the ones corresponding to particular tree shapes. This is the case with road-alignment trees, having highly intermingled tress crowns and which may be delineated as one unique tree crown.

Future works could focus on the development of top-down segmentation approaches involving marked point processes, as the ones developed in [Perrin *et al.*, 2006]. By introducing *a priori* knowledge into the segmentation process, like contextual and topological relationships for trees, results obtained for individual tree crown delineation could be improved.

The following chapter will use the individual tree crown units extracted with the algorithms presented in this chapter to perform tree characterisation for realistic 3D urban vegetation representation in virtual city models (Chapter 5).

CHAPTER 5

Vegetation Characterisation

5.1 Introduction

This chapter deals with vegetation characterisation, i.e. identifying specific characteristics of trees corresponding to the individual tree crown units previously obtained (cf. Chapter 4). The detail level of vegetation characterisation differs with respect to potential uses of the output results. For inventory purposes, one could be interested in species cover whereas visualisation applications only require morphology characteristics. But what tree characteristics can be measured from remote sensed data?

A combination of objectives of a study and available input data will determine what characteristics are to be measured for an effective description of vegetation. The goal of this chapter resumes to an analysis of each tree crown unit at different detail levels, obtained by answering to the following questions:

WHAT ARE THE OBJECTIVES OF THE STUDY?

As stated in the previous chapter and given our interest in urban vegetation, two levels of increasing complexity are brought forward:

- *Individual Tree Crown Attributes Estimation* First level of analysis, where parameters such as tree height and crown diameter are used to shape virtual 3D tree models to be placed into 3D city models.
- *Tree Species Classification* The most detailed level of analysis, tree species are specified by classification techniques on areas where species distribution data is available.

WHAT TYPE OF INPUT DATA IS AVAILABLE?

To obtain results from a specific level of analysis, particular input data must be available besides high resolution remote sensed data.

- *Cartographic data* For visualisation purposes specific mapping information has to be available to correctly position virtual tree models into the 3D city model.

- *Ground truth data* Accurate ground truth data needs to be available to evaluate classification algorithms.

The flowchart presented in Fig. 5.1 gives input data and output results obtained by the vegetation characterisation module. Given individual tree crown masks obtained by the segmentation module presented in Chapter 4, image data and height information, the first component which will be presented in this chapter extracts morphology attributes for each tree crown. This set of information can be used for visualisation needs, e.g. to shape virtual 3D tree models before inserting them into the 3D city model. The second component, deals with tree species classification by means of supervised machine learning techniques. Given ground truth data of tree species, tree crown masks previously obtained and image information, spectral and spatial characteristics are used to perform tree species classification.

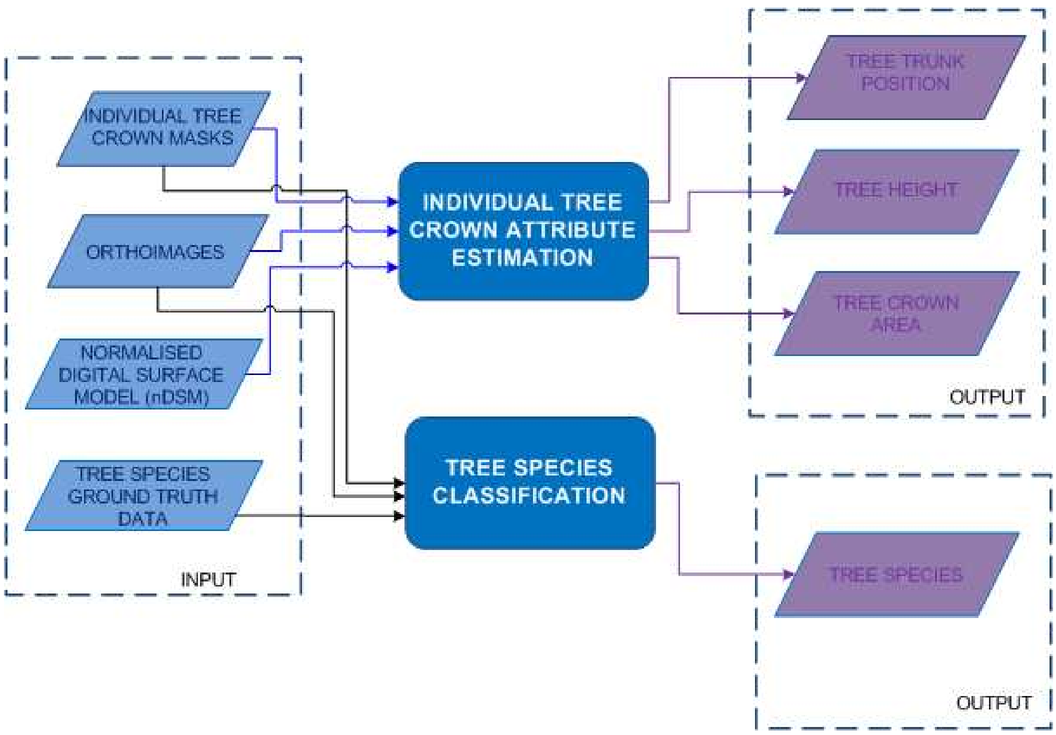

Figure 5.1: Flowchart depicting input data for each processing stage and output results for the vegetation characterisation module. Two independent stages for vegetation characterisation are presented. The first one estimates 3D tree parameters whereas the second one deals with tree species classification.

In this chapter, we will first present, in section 5.2, attributes computed for each individual tree crown unit. Section 5.3 shows how spectral and texture descriptors computed on different colour spaces are used by an SVM classifier to perform tree species classification. Finally, conclusions and perspectives are drawn in section 5.4.

5.2 Individual Tree Crown Attributes Estimation

Measurements of vegetation characteristics have been made for more than a century, and techniques developed to obtain these measurements are numerous [Bonham, 1989]. There are many characteristics that can be measured on a tree. A combination of the objectives of a study and the available input data will determine what characteristics are to be measured for an effective description of vegetation.

This section is dedicated to the estimation of 3D tree parameters for a realistic representation of trees in 3D city models. Tree measures to be extracted are presented before describing the measuring method and presenting results obtained for a stand of trees from site B of the Marseille data set. Finally, a discussion on limitations of the methods used for tree parameters estimation will be made.

5.2.1 Tree characteristics estimation

Measuring tree attributes from aerial data often underestimate real tree parameters [Brack, 1997], such as tree height and tree crown size, because parts of the crown are too small for resolution or are obscured by other trees. We focus on three particular type of parameters, namely tree crown dimensions, tree height and tree crown surface.

Figure 5.2 presents tree characterisation measures estimated for individual tree crown units. Each characteristic aims to describe tree units by particular geometric properties. Each property is associated with one or more measures, for instance, area, perimeter, length or width can measure the geometric characteristic of a tree crown.

Tree crown diameter and tree height, are estimated for each tree using the segments obtained from the tree crown delineation method presented in Chapter 4. Figure 5.3 depicts the parameters estimated for a tree, from the corresponding tree crown segment.

PROPERTY	MEASURE
Size	
Shape	
Position	

Figure 5.2: Selected measures for tree characteristics measurements. Each measure is presented next to the geometric property it describes. Tree crown area is given by its size, *width*/*length* ratio gives the tree crown shape and a tree crown's barycentre stands as an estimate for trunk position.

(a) (b) (c)

Figure 5.3: Parameters estimated for an individual tree. (a) Crown surface estimation. (b) Tree crown diameter. (c) Tree height.

5.2.1.1 Crown size and area

The width (diameter) of a crown can be measured by assuming the tree's outline is a circle. The tree crown's diameter is estimated by vertically projecting the edges of the crown on the ground and measuring the length along one axis from edge to edge through the crown centre (cf. Fig. 5.3 -(a) & (b)).

5.2.1.2 Crown height

Tree height (cf. Fig. 5.3 -(c)) is estimated as the distance from the base of the tree to the tree top and is directly computed on the Normalised Digital Surface Model (nDSM) (cf. Chapter 2, section 2.1.2.2).

5.2.1.3 Trunk position

The position of the trunk of the trees on the ground is estimated as the barycentre of the crown surface. The barycentre was computed as the average of all points of the surface. The projection of this point on the orthoimage gives the centre of the region in geographical coordinates.

5.2.2 Results

Tree crown parameters - tree trunk coordinates, crown area and tree height - estimated for several trees in site B of the Marseille data set are given in Table 5.1.

Table 5.1: Results for tree crown attributes estimation - site B, Marseille data set.

Tree Sample	Trunk Position		Crown Area	Tree Height
	X	Y	(m^2)	(m)
1	846924.182	3114689.582	18.24	4.10
2	846901.934	3114739.846	18.35	3.59
3	846917.59	3114686.904	17.56	2.26
4	846898.226	3114747.056	19.21	2.95
5	846912.646	3114715.744	17.07	2.66
6	846921.298	3114698.44	17.21	2.98
7	846915.118	3114695.556	17.60	2.05
8	846912.44	3114721.718	16.98	2.65
9	846897.196	3114729.134	16.67	3.30
10	846895.754	3114736.55	16.81	3.54
11	846902.346	3114721.512	16.01	2.88
12	846909.556	3114704.826	15.53	2.78

As no ground truth data containing tree height, tree crown area and exact geographic coordinates for tree trunks was available, the accuracy of some of the results presented in this section was visually assessed. This was done for tree trunk position estimations, for the twelve trees presented in Table 5.1. The estimated position of a tree's trunk is marked by a red cross overimposed on the orthoimage depicting site B of the Marseille data set in Fig. 5.4.

Figure 5.4: Tree trunk position estimation on a tree stand from site B of the Marseille data set. Estimated tree trunk positions (marked by a red cross) are over-imposed on the RGB orthoimage of the stand.

Tree crown diameter, tree height and trunk position are estimated for each tree from tree crown outlines extracted previously. Such morphological information on each tree are used to enhance virtual 3D city models with realistic representation of vegetation. A sample scene from site B of the Marseille data set is presented in Fig. 5.5 where trees are represented by 3D billboards exploiting parameters estimated for each tree crown and given in Table 5.1. Tree models were automatically inserted into the 3D city model according to position, diameter and height parameters. Figure 5.5 testifies for the accurate positioning of tree trunks in the 3D city model by the presenting a view of the tree trunk positioned in the centre of the tree crown projection on the ground, underneath the tree model.

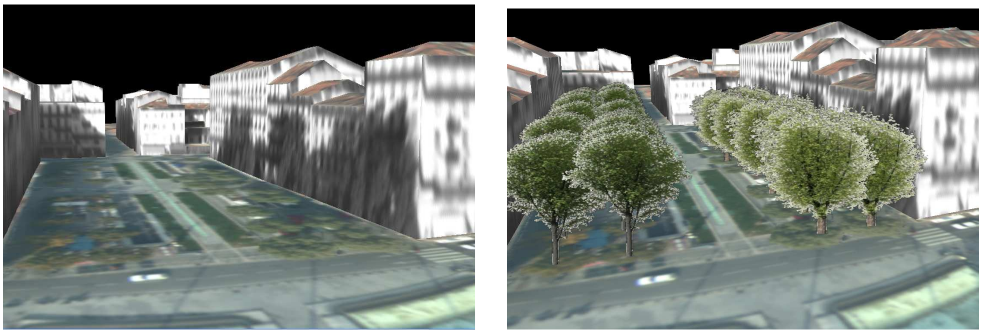

Figure 5.5: 3D tree modelling over Marseille - site B. Left: 3D city model containing buildings. Right: Automatic generated 3D city model containing buildings and realistically rendered trees according to vegetation information obtained by the proposed methods for parameter estimation.

5.2.3 Extension of Vegetation Characterisation on Different Study Areas

Research code developed during this thesis has been integrated into IGN's BATI-3D ® production line. All modules presented so far, have been successfully integrated into the 3D city model production software. We are therefore able to present in this section some examples of 3D city models featuring vegetation exported by BATI-3D ® on other study areas. Figures 5.6 and 5.7 illustrate several views of 3D vegetation in the city of Montbéliard, France. The 3D city model was produced by the BATI-3D ® production line, with the vegetation component modelled by algorithms presented so far in this thesis. The entire city model was encoded into a KML (KeyHole Markup Language) file and displayed in the Google Earth © browser. Trees were modelled by photo realistic billboards inserted into the city model.

Figure 5.6: Two views of the 3D city model of Montbéliard, France. City model produced by BATI-3D ® and displayed in the Google Earth © browser. Images used to produce the city model are aerial images with a spatial resolution of 15 cm/pixel whereas background images in the viewer are satellite ones.

Figure 5.8 illustrates two views of IGN's head office and its neighbourhood, in Saint-Mandé, France. 3D city model is produced by the BATI-3D ® production line

Figure 5.7: Two views of the 3D city model of Montbéliard, France. City model produced by BATI-3D ® and displayed in the Google Earth © browser. Images used to produce the city model are aerial images with a spatial resolution of 15 cm/pixel whereas background images in the viewer are satellite ones.

form aerial imagery. The city model is displayed in a viewer developed by Erwann Houzay at the MATIS laboratory [MATIS, IGN, 2008]. The vegetation component is extracted and modelled by vegetation modules presented so far in this thesis.

The same 3D tree model is used for all tree samples in the view, found at [Work Group Computer Graphics and Media Design, Dresden University of Technology, 2007] and downloaded free of charge.

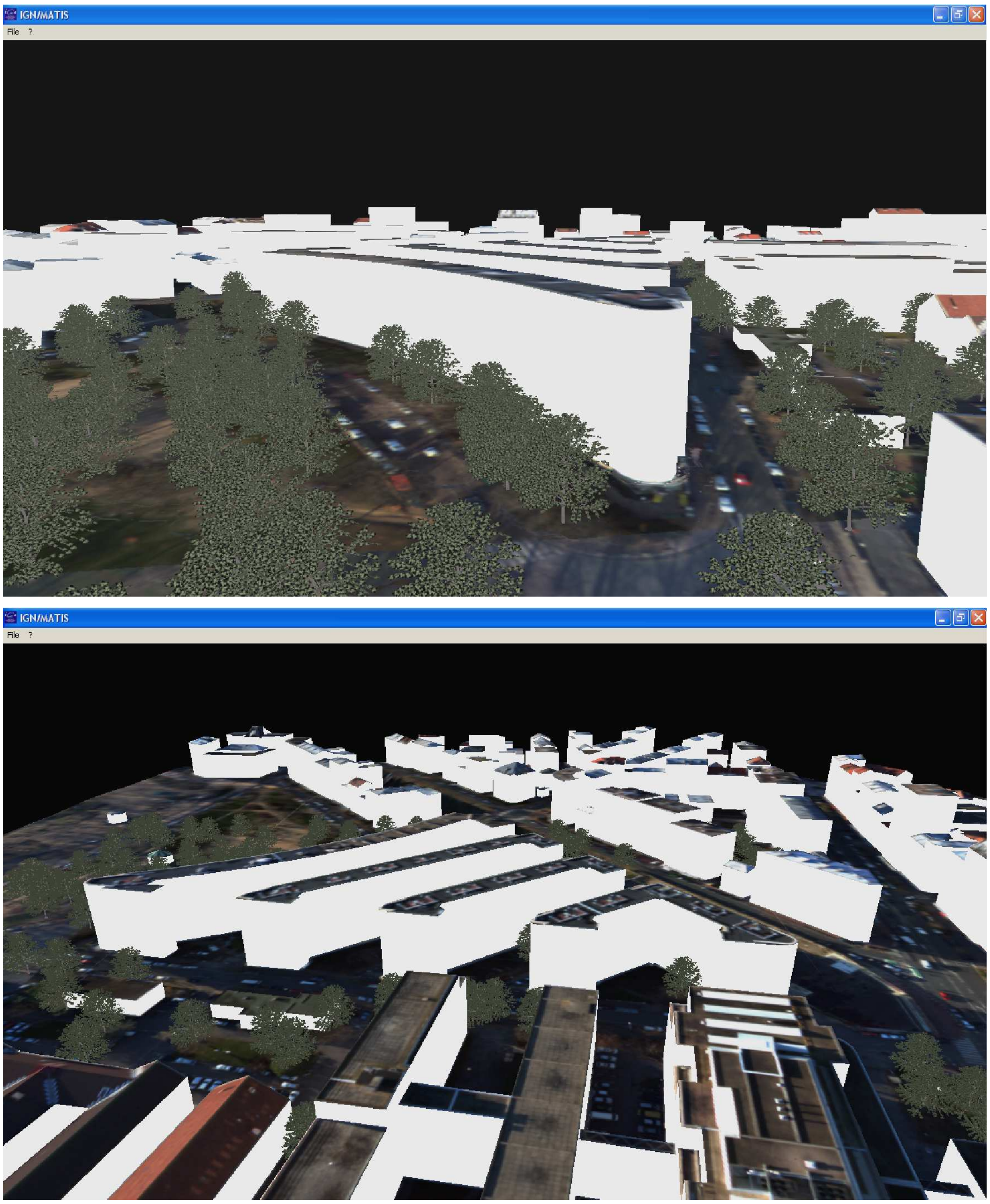

Figure 5.8: Two views of the 3D city model of IGN's head office and its neighbourhood in Saint-Mandé, France. City model produced by BATI-3D ® and displayed in in a viewer developed in the MATIS laboratory [MATIS, IGN, 2008].

5.3 Tree Species Classification

In this section, the most detailed level of characterisation, i.e. tree species classification is presented. To perform tree species classification, ground truth data has to be available. Details on ground truth data acquisition for tree species classification are given in Chapter 2 and Appendix B. In the following of this section, a brief state of the art will be presented followed by details on the supervised classification systems used and the features computed to perform tree species classification. Finally, results and conclusions will be presented.

5.3.1 Context

The problem of tree species classification was first issued in the field of forestry where digital interpretation techniques of aerial/satellite imagery have been used for the inventory and monitoring of forested areas [Gougeon, 1995b]. Depending on the spatial resolution of the input data, the goals of these studies cover a large range of applications. High spatial resolution imagery is used in pixel-based classification of individual tree crowns [Erikson, 2004a; Leckie, 1990; Meyer *et al.*, 1996; Beaubien, 1994] yet low spatial resolution imagery was mostly used to extract single species stands [Gillis and Leckie, 1993].

Spectral resolution is another important factor for tree species classification. The simplest form of multispectral sensing are colour infrared imagery [Korpela, 2004]. Such type of data is used in numerous type of applications, from forest tree species identification in [Rohde and Olson, 1972] to urban vegetation monitoring [Nichol and Lee, 2005]. Hyperspectral data collected by satellite sensors have been used to perform species classification in an African rainforest [Thenkabail *et al.*, 2004] while airborne AVIRIS data was used to identify and map species of urban trees [Xiao *et al.*, 2004].

[Wania, 2008] analysed the potential of hyperspectral data acquired by an airborne sensor for urban vegetation observation. The potential of detecting tree species was analysed and compared to that of multispectral data. Results are highly influenced by illumination conditions and the existence of mixed pixels (effects specific to urban area applications).

Temporal resolution (or multitemporal data) was compared in [Key *et al.*, 2001] to multispectral data to perform individual tree species classification in a temperate hardwood forest. Key *et al.* suggest that multitemporal data could be used to compensate for limited spectral resolution by combining multiple dates of low spectral resolution images.

There are numerous studies in the literature combining different types of data to perform tree species identification. Sugumaran *et al.* combined multispectral images with different spatial resolution and acquired at different dates to classify urban forest species [Sugumaran *et al.*, 2003]. Multi-temporal hyperspectral data and LIDAR data were combined in [Voss and Sugumaran, 2008] to perform tree species classification in an urban environment.

As presented in Lillesand *et al.* [2008], the visual image interpretation process for tree species identification from aerial or satellite data starts by eliminating those species whose presence in an area is impossible or improbable because of location or climate. Based on a knowledge of common species associations and their requirements, the second step is to establish which groups of species do occur in the area. The final stage is the identification of individual tree species based on a number of distinctive characteristics with varying scale such as shape, size, pattern, shadow, tone and texture.

Such type of characteristics have been exploited by researches on tree species classification either in forest or urban areas, by choosing an appropriate representation of species depending on the type of input data. Most tree species classification studies exploit spectral information [Rohde and Olson, 1972] , [Meyer *et al.*, 1996], [Leckie *et al.*, 2005], [Pinz, 1998], [Gougeon, 1995c], [Gerylo *et al.*, 1998], [Key *et al.*, 2001] to generate spectral signatures used in different classification approaches [Gougeon, 1995a]. Characteristics such as texture, structure and context have been exploited in [Brandtberg, 2002], [Pinz, 1990] while other researches propose classification systems combining different types of tree species information. Erikson [2004a] separates four types of trees from Swedish forests after delineating their tree crown borders [Erikson, 2004a]. Tree species belong to the deciduous and the coniferous taxonomic groups and their separation is done from colour infrared aerial photographs with very high ground resolution (3 to 15cm). Classification of tree species is performed by a rule based system taking into account shape and colour information specific to each species. On the same data set, Kulikova *et al.* [2007] improve classification accuracy by integrating radiometry, texture and shape criteria into the feature vector for a supervised classification system based on SVM [Kulikova *et al.*, 2007]. Tree crowns shape is added to the feature vector by proposing a shape description invariant to translation, rotation and scaling. Results show that shape descriptors improve the classification performances compared to the to a classifier based on radiometric and textural descriptors alone.

These and other studies represent a variety of forest conditions but few have specifically addressed species classification at a tree level in urban areas from remote sensed aerial imagery data, where the problem is challenging. Species identification is challenging when the number of features is reduced or if the features are shared by several species [Korpela, 2004].

Tree species discrimination in urban areas using remote sensing data is a difficult task, for several reasons:

- *complexity*: tree stands are very complex, having great height and shape variance (in urban areas trees of different ages, thus height, are often adjacent and crowns are often cut to different geometric shapes);
- *density*: the high density of trees, often intermingled to each other, leads to many hidden parts of crowns, to crown shadowing and differential crown illuminations;
- *diversity*: the great number of species in one genus form difficult cases and their discrimination can be difficult even on the field.

It is easy to enumerate cases, which are most likely unsolvable. Suppose we want to know the species of each of the tree crowns depicted by Figure 5.9. Which are the features suitable to discriminate between the two?

Figure 5.9: Tree crowns belonging to two different species. Assigning the correct species to each tree is a very difficult task, even for an advised photo interpreter. Finding features suitable to discriminate between two such similar patterns is even more difficult.

The higher the tree species number, the more difficult it is to find discriminant features. The case presented in Fig. 5.9 is the most simple case, in which only two species of trees are available. But, there are rarely only two species of trees in a city.

In this thesis we explore the possibility of distinguishing at canopy level several tree species from the Marseille data set based on ground truth data acquired on site. Specific objectives are as follows:

- *Evaluate separability within taxonomic groups of tree species*
- *Identify discriminant features for species classification*

The process of answering these specific objectives is formulated as a classification problem, whose task is to learn from a set of training data, a specific model for each class, which will be used to detect a particular class in unseen/test data sets.

A class is given by one tree species. The task of classification is to determine the presence or absence of a particular species within a set of tree crown units.

General considerations on classification systems and feature extraction are given in section 5.3.2. Section 5.3.4 presents the classification framework for tree species classification. It closely follows the description of the undertaken experiments for spectral 5.3.5 and spatial 5.3.6 feature vectors. Finally, section 5.3.7 presents results for an early fusion framework for tree species classification, shortly followed by a concluding discussion in section 5.3.8.

5.3.2 Considerations on features for tree characterisation

When humans visually interpret remotely sensed imagery, they take into account context, edges, texture and tonal variation or colour. A discrete tonal feature is a connected set of pixels that all have the same or almost the same gray shade (brightness value). When a small area of the image has little variation of discrete tonal features, the dominant property of that area is a gray shade. Conversely, when a small area has a wide variation of discrete tonal features, the dominant property of that area is *texture*.

Texture feature extraction is the procedure of generating descriptions of a textured surface in terms of measurable parameters. The expected features represent relevant properties of the surface [Wu, 2003].

There are several approaches to texture analysis. According to [Haralick, 1979] two categories can be identified:

- *Statistical* methods define texture in terms of grey-level statistics which are constant or slowly varying over a textured region. Different textures can be discriminated by comparing statistics computed over the regions.

- *Structural* methods aim at determining the primitives composing the texture. Extracted primitives and their placement rules are used in different texture recognition applications.

Statistical methods analyse the spatial distribution of grey values by computing local features at each point in the image and deriving a set of statistics from the distributions of the local features. Depending on the number of pixels defining the local feature, statistical methods can be divided into first-order (one pixel), second-order (two pixels) and higher-order (three or more pixels) statistics [Wu, 2003]. Statistical methods were used in this work to analyse tree crown texture for species classification based on SVM classification systems. Details on feature extraction and results obtained will be provided in the following of this section.

Most classification systems contain a two-stage procedure, a learning or training stage and a detection stage. In the training stage the useful features necessary for detection are extracted while in the detection stage the comparison of the test features to the reference ones is accomplished.

Classification systems take as input a vector, or pattern, of n components, or features. The features express species characteristics and patterns refer to a set of measurements obtained for each tree crown unit.

There are several classification procedures, depending on the type of input feature spaces. Spectral features refer to the family of classification procedures that utilises spectral information whereas spatial ones involve categorisation of image pixels on the basis of their spatial relationship with pixels surrounding them [Jensen, 1996].

In computer vision, attributes or properties of objects and scenes that are extractable from the image are called features. These attributes are sometimes classified to be either local or global. Within photogrammetry and remote sensing, however, the term *features* refers to recognisable objects or structures in the image, such as a road or a building [Sowmya and Trinder, 2000]. The term *features* is used here with the same meaning as in computer vision, referring to properties of objects.

Before presenting the features extracted for species classification, the following paragraph presents vegetation characteristics, from remote sensing data.

Characteristics of tree species

Tree species are defined by several characteristics, such as average height, crown shape, leaf shape and colour, stem density, crown spectral characteristics, and so on.

To classify different tree species present in a tree stand from a radiometric point of view, a detailed description of the canopy reflectance is needed. Plant canopy reflectance depends on measurement configuration, soil reflectance, leaf reflectance, plant architecture (dependent on leaf area index, leaf inclination distribution function, leaf size, canopy height and so on) and illumination conditions. Figure 5.10 presents measurement configurations of plant canopy reflectance in the optical domain. Plant architecture is given by Leaf Area Index, Leaf Inclination Distribution Function, leaf size/canopy height, cover fraction, etc. We present in the following an analysis on the way leaf and plant architecture influence tree canopy reflectance, based on the works presented in [Jacquemoud and Feret, 2007].

Spectral reflectance is the portion of incident radiation reflected by a non-transparent surface. The spectral signature of a material is a unique reflectance

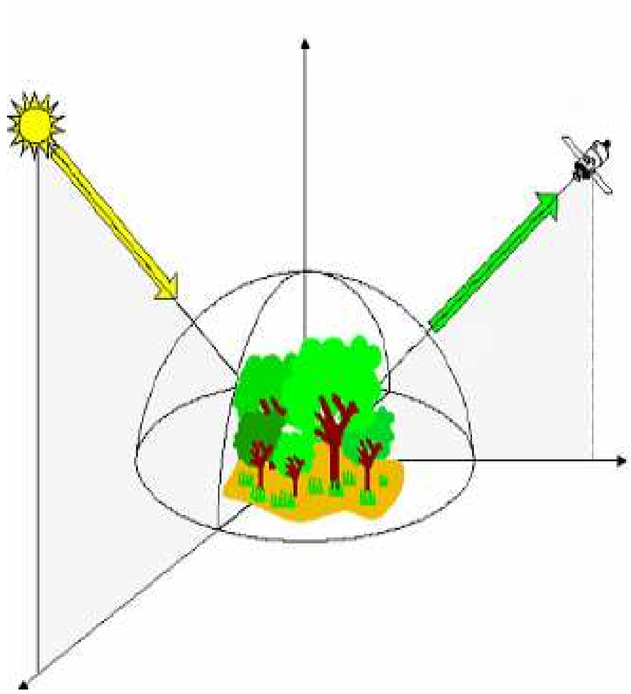

Figure 5.10: Plant canopy reflectance depends on measurement configuration, soil reflectance, leaf reflectance and transmittance, plant architecture and illumination conditions (adapted from [Jacquemoud and Feret, 2007])

value in a specific part of the spectrum. Vegetation has low reflectance in the visible bands of the spectrum and a much higher reflectance in the near infrared region. A tree's spectral signature depends on the spectral reflectance of tree leafs. A typical cell of a green leaf contains: water, dry matter, chlorophyll and pigments. In the blue and red regions the spectral reflectance of vegetation is low, due to absorption by chlorophyll, and has a peak at the green region which gives rise to the green colour of vegetation. But no matter the tree species, all leafs contain chlorophyll.

If we take into consideration the infrared region of the spectrum, tree spectral signatures depend on plant architecture characteristics. More precisely, they strongly depend on Leaf Area Index (LAI) or leaf density and leaf inclination distribution function. Theoretically speaking, we can distinguish between evergreen coniferous and deciduous trees, as the latter tree species family has an average leaf density three times higher than the first one. From a practical point of view, it is difficult to estimate these parameters on input data with our spectral resolution.

As for the geometric/shape characteristics such as tree height or tree crown width, it is a delicate matter to consider such characteristics as discriminant for species classification in the urban environment due, on one hand, to the fact that trees are often cut to different shapes and on the other hand to the great age diversity between trees belonging to the same species.

Features for Tree Species Classification

Images are composed of tone (i.e. spectral information) and texture (i.e. tonal variability in a given area), two interdependent characteristics [Baraldi and Parmiggiani, 1995; Haralick *et al.*, 1973]. The texture of an image contains information about the spatial and structural arrangement of objects [Tso and Mather, 2001]. There are two classes of texture measures: first order (occurrence) and second order (co-occurrence) statistics [Haralick *et al.*, 1973; Tuceryan and Jain, 1998]. First-order statistics are derived from the histogram of pixel intensities in a given neighbourhood (i.e. moving window), but don't take into consideration spatial relationship between pixels. Second-order statistics are computed from the Gray Level Co-occurrence Matrix (GLCM) which indicates the probability that each pair of pixels values co-occur in a given direction and distance [Haralick *et al.*, 1973; Tuceryan and Jain, 1998]. Other methods used to characterise image texture include Fourier analysis, wavelets, variograms, fractal dimension [Tso and Mather, 2001].

The distribution of feature vectors of each tree species could result in overlapping classes. By choosing an adequate representation space and classifier function, classes could be separated. It is not to be taken for granted that well separated classes in the feature space will be found, even if optimal features have been selected [Bernd, 1997]. Two types of features have been evaluated in this work to perform tree species classification: spectral and texture ones, detailed in sections 5.3.5 and 5.3.6, respectively.

5.3.3 Database description

The Marseille data set is composed of 15 different species of trees. More details on the taxonomy of species in the Marseille data set are presented in Appendix B. Only for six of these species a high enough number of samples was available to perform species classification. The retained species, are given in Table 5.2 by their common and scientific names and number of samples per species.

Table 5.2 presents the division of the samples per taxonomic group and species. The total of 267 tree crown contours was randomly divided into training and test subsets. Figure 5.11 presents randomly picked tree crowns for each of the six species from the data set.

Table 5.2: Number of samples per taxonomical group/species used for statistical analysis

Taxonomic group	Species		Samples	Total
	common name	*scientific name*		
Deciduous	Plane Tree	*Platanus sp.*	69	213
	Scholar Tree	*Sophora japonica L.*	32	
	Lime Tree	*Tilia sp.*	83	
	Mediterranean Hackberry	*Celtis australis L.*	29	
Coniferous	Stone Pine	*Pinus pinea L.*	36	54
	Italian cypress	*Cupressus sempervirens L.*	18	

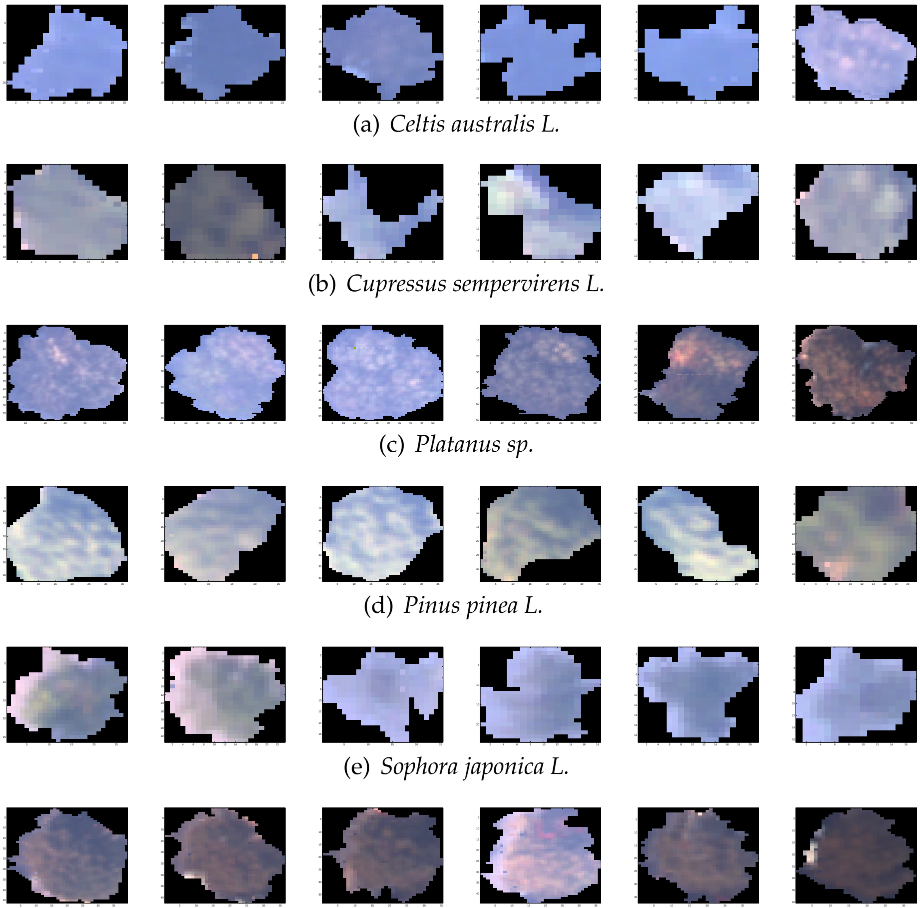

(a) *Celtis australis L.*

(b) *Cupressus sempervirens L.*

(c) *Platanus sp.*

(d) *Pinus pinea L.*

(e) *Sophora japonica L.*

(f) *Tilia sp.*

Figure 5.11: Six tree crown samples for each species from the Marseille data set: *Celtis australis L., Cupressus sempervirens L., Platanus sp., Pinus pinea L., Sophora japonica L., Tilia sp.*

Figures 5.12, 5.13 and 5.14 illustrate training and test samples from the Marseille data set. Tree samples for each species were randomly picked from three areas from the Marseille site in order to cover the full range of spectral variation. Training samples are generally indicated by a lighter tone of colour than test ones, except for the *Celtis australis L.* species for which train samples are indicated by a dark green colour and test ones are marked in yellow. The species of each tree crown unit is marked by a coloured mask over-imposed on the tree crown contour.

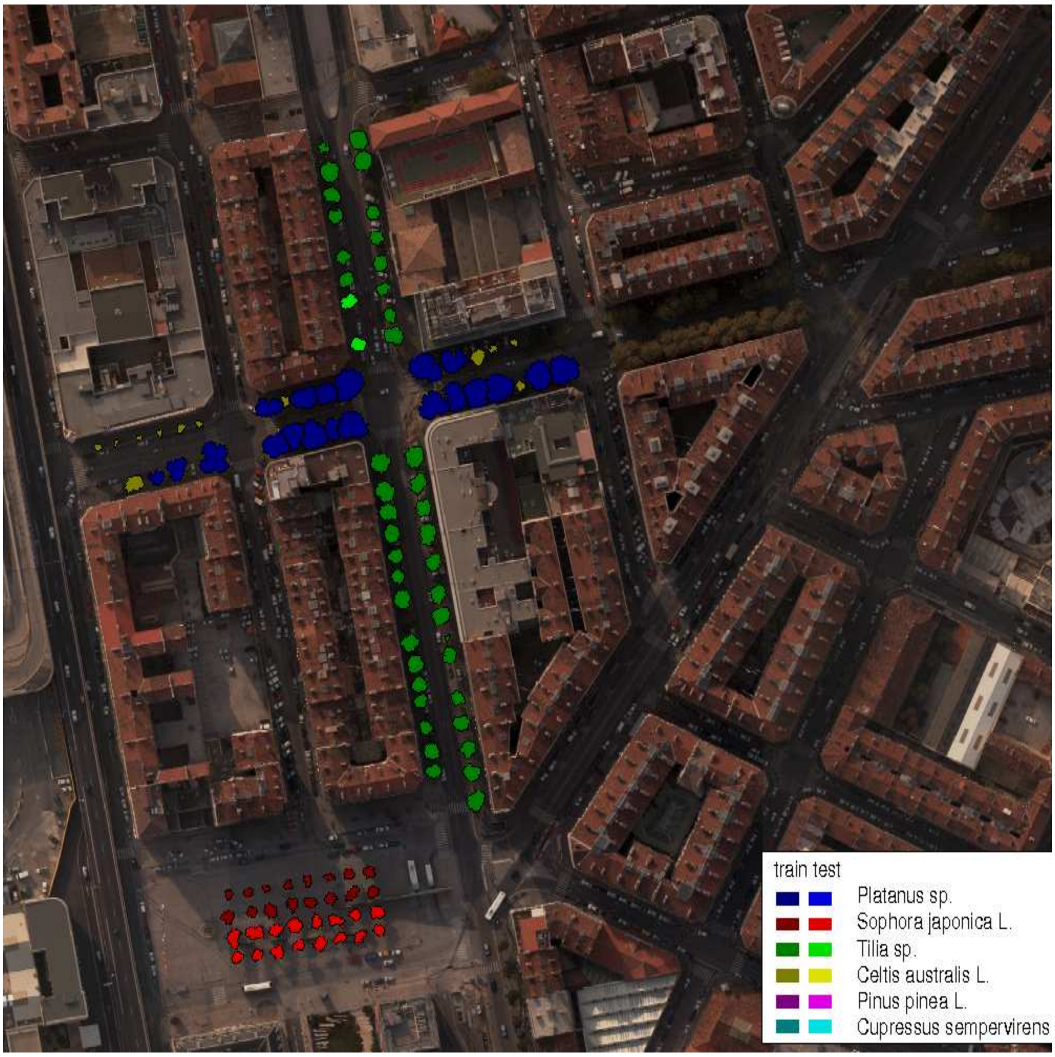

Figure 5.12: Training and test samples from site A of the Marseille data set. Training samples are marked by a lighter tone of colour than test ones.

Figure 5.12 depicts training and test samples for tree species classification from site A of the Marseille database. It contains four out of the six tree species present in the database, namely *Platanus sp.*, *Sophora japonica L.*, *Tilia sp.* and *Celtis australis L.* ones. Most samples from site A are used for the training stage. All *Sophora japonica L.* samples of the entire database can be seen in the bottom part of Figure 5.12, coloured in red.

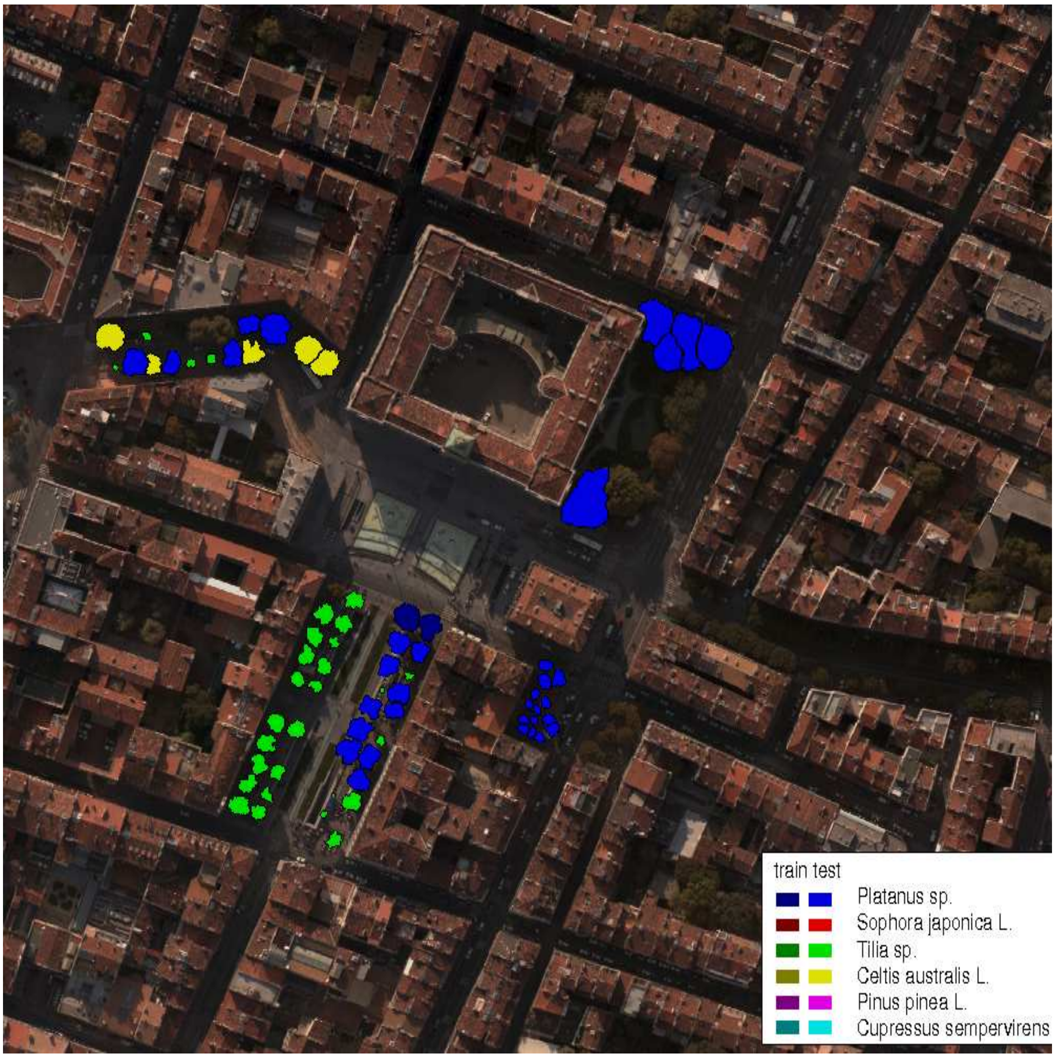

Figure 5.13: Training and test samples from site B of the Marseille data set. Training samples are marked by a lighter tone of colour than test ones.

Figure 5.13 depicts training and test samples from site B of the Marseille data set. There is a total of three species present in this site: *Platanus sp.*, *Tilia sp.* and *Celtis australis L.*. Most of the samples from this site are used to perform tests.

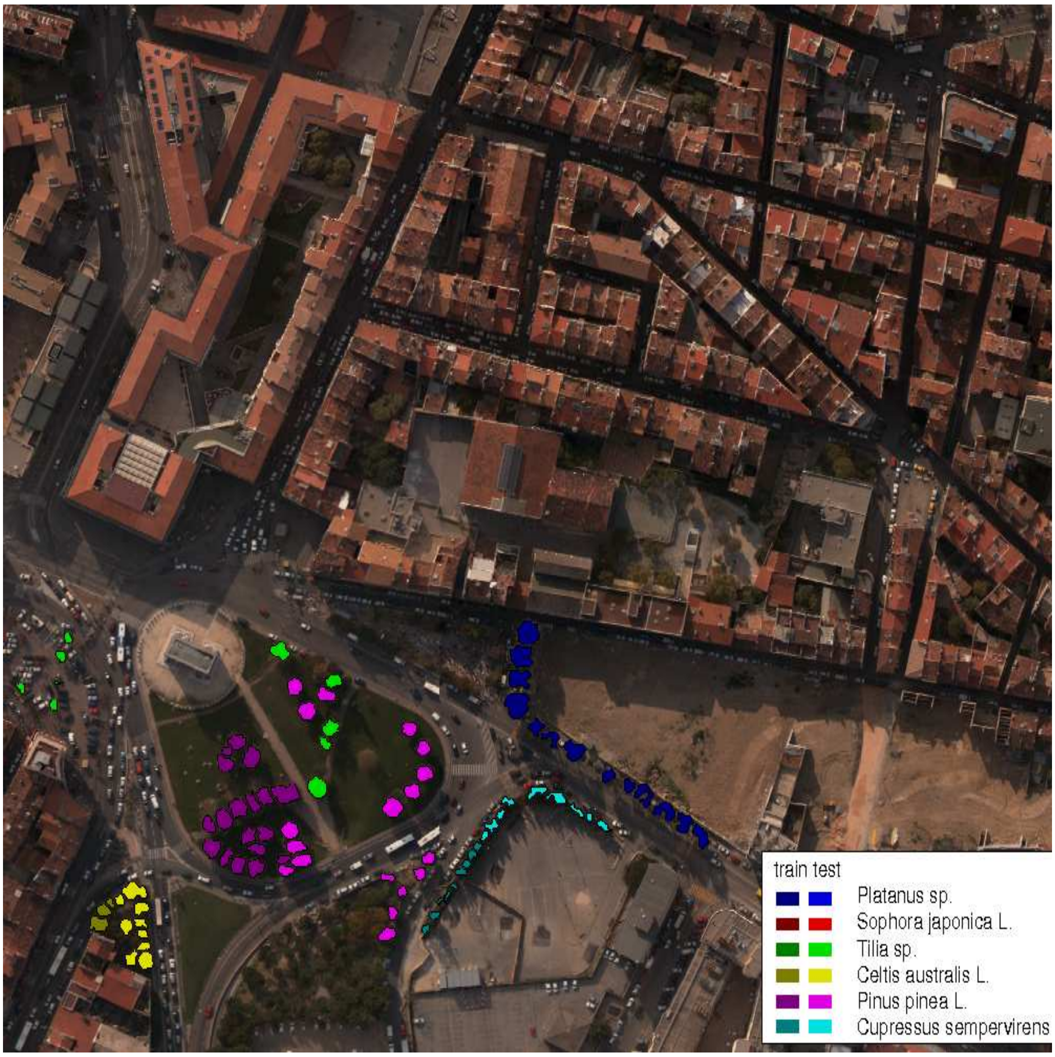

Figure 5.14: Training and test samples from site C of the Marseille data set. Training samples are marked by a lighter tone of colour than test ones.

Figure 5.14 illustrates tree samples from site C, Marseille data set. In this site, there are a total of five tree species, namely, *Platanus sp.*, *Tilia sp.*, *Celtis australis L.*, *Pinus pinea L.*, *Cupressus sempervirens L.*. The latter two species are coniferous species. All coniferous samples from the Marseille database are present in site C. *Pinus pinea L.* samples are coloured in violet whereas the *Cupressus sempervirens L.* ones, in turquoise.

Table 5.3 presents the sizes of the training and testing databases.

Table 5.3: Training and test data sets - species allotment.

Tree Species	Total Number of Samples	Training Samples	Test Samples
Platanus sp.	69	35	34
Sophora japonica L.	32	16	16
Tilia sp.	83	42	41
Celtis australis L.	29	15	14
Pinus pinea L.	36	18	18
Cupressus sempervirens L.	18	9	9

Ground truth data was available for all samples in the Marseille data set. Details on ground truth data acquisition are presented in Chapter 2 and Appendix B.

5.3.4 Classification framework

Given a set of labelled examples, building a classifier comes up to finding a rule, on the basis of features of available examples, that could be repeatedly used to assign a class-label to any new example.

Classification can be performed at a pixel- or object- level in image processing [Bernd, 1997]. In remote sensing applications, pixel-based classification approaches are appropriated for low spatial resolution data. Yet, with high spatial resolution imagery, single pixels no longer capture the characteristics of classification targets [Yu *et al.*, 2006] and adjacent pixels are more likely to belong to the same class [Trias Sanz, 2006]. The increase in intra-class spectral variability reduces statistical separability between classes and classification accuracy is reduced [Yu *et al.*, 2006]. Object-based classifiers are more appropriate with this type of data as they first segment an image into clusters of similar neighbouring pixels ("objects") and then classify the objects according to the features characterising the object [Cleve *et al.*, 2008].

Image objects are basic entities in an image and each pixel group possesses a relationship relating to the real world component it models. Such objects are in our case tree units delineated through the individual tree crown delineation algorithm previously presented (cf. Chapter 4).

In previous works [Iovan *et al.*, 2008a], [Iovan *et al.*, 2009], [Iovan *et al.*, 2008b] pixel-based classification approaches have been presented. Results showed that object-based classification outperformed pixel-based approaches. Therefore, we investigated in this thesis object-based classification approaches for tree species classification which will be presented in the following of this chapter. Tree crown units (objects) are already separated from the background and between each other and computation of features describing each sample belonging to a class is eased.

Figure 5.15 depicts the system used to perform tree species classification from spectral and spatial feature vectors.

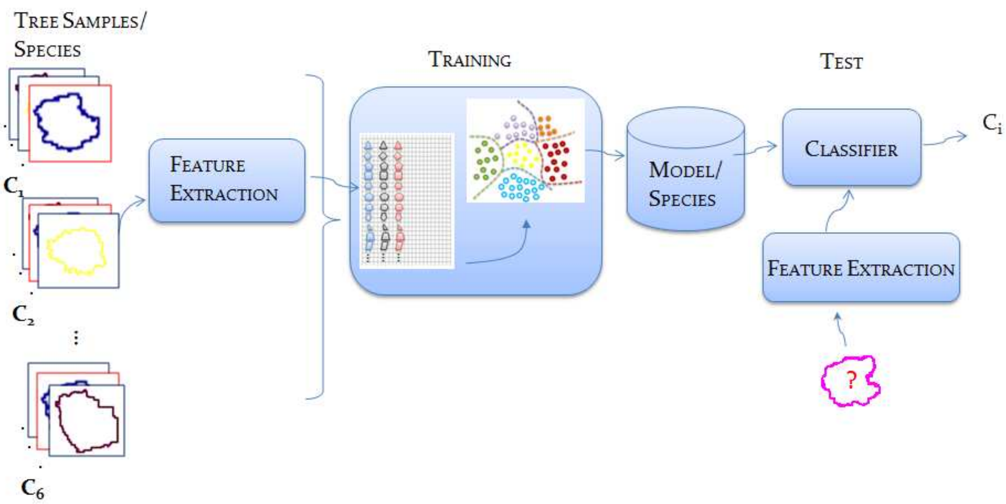

Figure 5.15: System overview for the spectral and spatial feature spaces.

Input tree crown samples of each tree species (class) are used to extract spectral and spatial features which will form the feature vector for the training stage. During training, feature vectors belonging to one species are used to find the boundary separating all samples belonging to the class taken in consideration from all other samples not belonging to the class. During the test stage, features of an unknown tree sample are compared to models computed for each species during the training stage. The sample is assigned to the class giving the highest membership probability.

The discriminative SVM classifier was used in a one-against-all configuration. Feature vectors were used in the training phase to build a set of binary classifiers able to separate each class from all others. This method trains N SVMs (where N is the number of classes) and there are N decision functions. In this work, $N = 6$

as there are six species of trees in the Marseille data set. An unknown tree sample is classified as belonging to the class for which the largest decision value was determined [Hsu and Lin, 2002].

The SVM classifier used was the one provided in [Chang and Lin, 2001]. For all colour spaces, *linear*, *polynomial* and *Gaussian - Radial Basis Function (RBF)* kernels were used to train and test specific classes.

Three sets of features have been evaluated in order to identify best features to perform tree species classification: spectral, spatial and combined (spectral and spatial) ones. Section 5.3.5 presents tree species classification based on spectral features. Classification based on spatial features is presented in section 5.3.6 and finally, classification based on combined features is given in section 5.3.7.

5.3.5 Classification based on spectral features

5.3.5.1 Feature extraction

Reflectance values of pixels belonging to tree crowns from each species are used to estimate the sample's mean and covariance matrix. For this, an assumption is made that the distribution of reflectance values of the sample in each spectral band is Gaussian (normally distributed). Under this assumption, the distribution of brightness values for a tree sample in one spectral band is described by the *mean vector* and the *covariance matrix*. For each tree sample belonging to a species, a feature vector composed of *the mean* of radiometries in each spectral band and *the covariance matrix* of radiometries between spectral bands.

For each tree crown unit belonging to a species, a feature vector containing the mean vector and covariance matrix is computed and used to form training data for the classifier.

5.3.5.2 Feature transformation

Since the aim of this study is to separate vegetation regions which look similar, it seems that using perceptually relevant colour spaces is important. Feature vectors were computed on four different colour spaces: *RGB, XYZ, Lab, HSV* [Ceccato *et al.*, 2001]. The literature on colour spaces is abundant and it is not the aim of this work to detail them. More details on colour spaces can be found in [Green, 2002]. For all colour spaces, the IR channel was also added to the colour bands for feature extraction.

5.3.5.3 Results

Results obtained for tree species classification by using spectral features, on the Marseille database will be presented for the best configuration between *colour space* and *similarity kernel*, evaluated in terms of overall accuracy. For this, we performed several experiments for feature vectors computed on several colour spaces and by using different kernels for the SVM classifier. Table 5.4 gives a summary of the overall accuracy results obtained.

Table 5.4: Overall accuracy (%) for different colour spaces and SVM kernels

Colour Space \ Kernel	linear	polynomial	rbf
RGB	66.0	56.8	62.0
HSV	62.9	61.1	60.1
XYZ	59.8	62.7	59.5
Lab	73.6	59.0	64.0

Each cell of the table contains overall accuracies results computed from the confusion matrix of each colour space. As can be noted, the linear kernel for the Lab colour space outperforms the other classifiers. Therefore, in the following, we present classification results resampled on the RGB images of each site for the best configuration (e. g. linear kernel and the *Lab* colour space).

Figures 5.16, 5.17 and 5.18 present a map of tree species obtained by the SVM classifier by using a spectral feature vector computed on the Lab colour space.

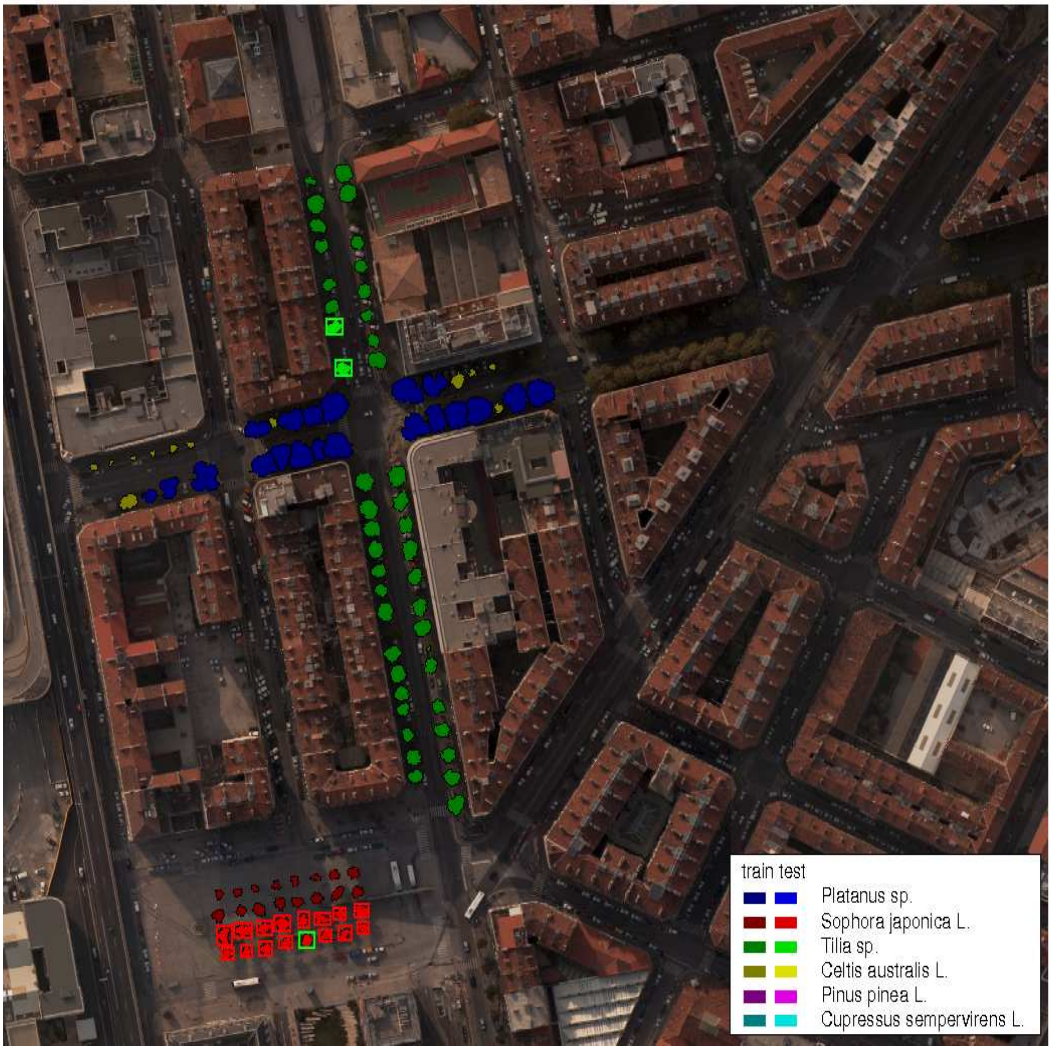

Figure 5.16: Tree species classification results obtained on the Marseille data set - site A with spectral feature vectors extracted on Lab colour space. Ground truth data is marked by a tree crown mask and classification results are bounded by rectangles coloured by appropriate species colour.

This figure illustrates tree species classification results for site A of the Marseille data set. Tree crown samples used for training are coloured by an appropriate colour, according to its species. Trees used for test, are coloured according to their species and bounded by a rectangle coloured by the colour associated to the species of tree as detected by the classifier. From the total number of trees present on site A, only 18 tree crowns were used for the test phase, 2 *Tillia sp.* and 16 *Sophora japonica L.*. Spectral features computed on the *Lab* colour spaces allowed a correct classification of the *Tillia sp.* trees and of 15 of the *Sophora japonica L.* trees. In the bottom of the image, we can observe a tree sample coloured in red (thus belonging to the *Sophora japonica L.* species) and bounded by a light green rectangle, meaning that the classifier classed it to the *Tillia sp.* species.

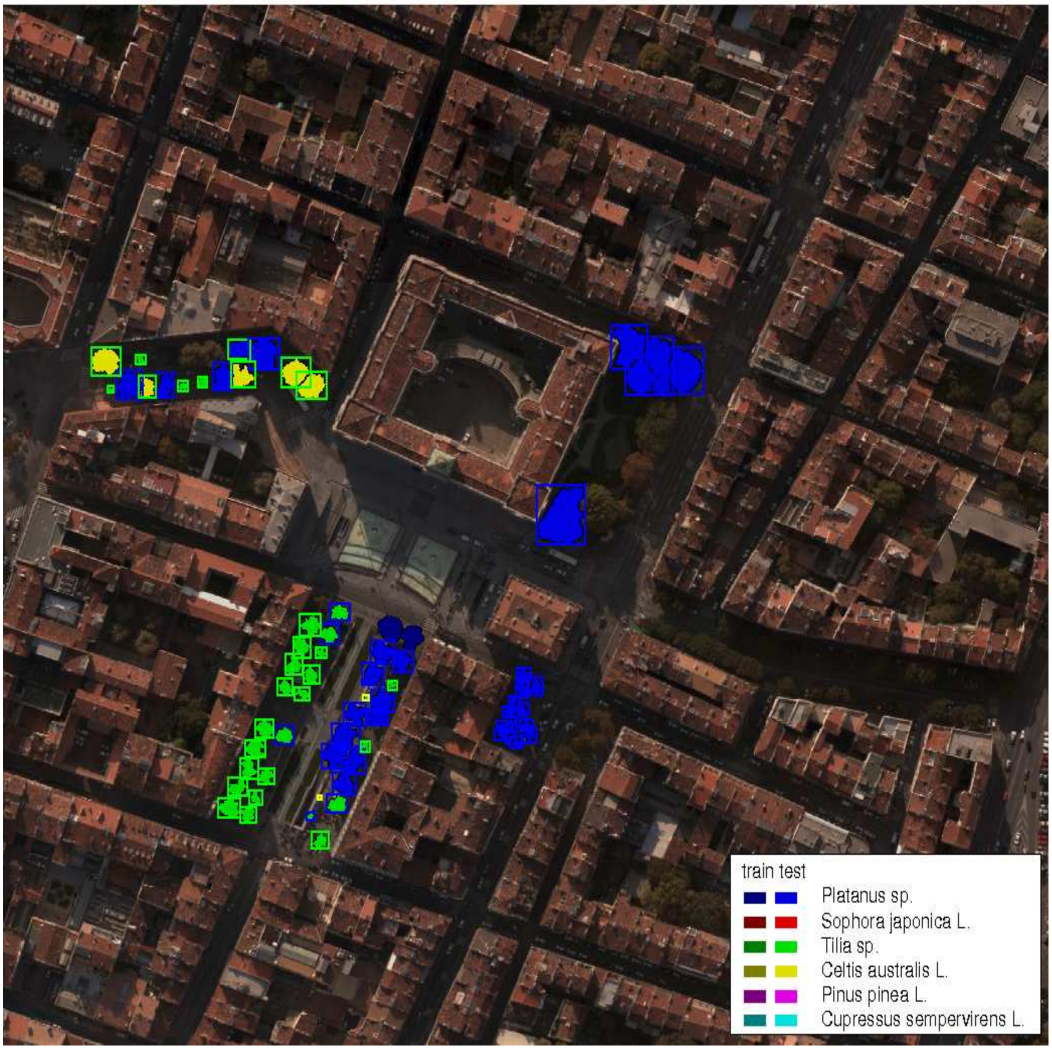

Figure 5.17: Tree species classification results obtained on the Marseille data set - site B with spectral feature vectors extracted on Lab colour space. Ground truth data is marked by a tree crown mask and classification results are bounded by rectangles coloured by appropriate species colour.

Classification results for site B of the Marseille data set are presented in Figure 5.17, for spectral feature vectors computed on the *Lab* colour space. Three different species of trees were present in this site, namely *Platanus sp.*, *Tilia sp.* and *Celtis australis L.*. Trees used for tests are bounded by rectangular boxes coloured by the colour associated to the species assigned by the classifier to the specific tree sample and have their tree crown coloured by the colour associated to the ground truth species. From the entire data set of trees present in site B, only 2 samples were used for training and the other ones were used for tests. Spectral features computed on the *Lab* colour space prove rather discriminative for *Platanus sp.* trees present in this site, with only one misclassified sample, in the upper left part of the image (the tree sample coloured in blue and bounded by a green colour box). 5 *Tilia sp.* trees were classified as *Platanus sp.* ones and 2 as *Celtis australis L.* trees. The worst results can be observed for the *Celtis australis L.* tree samples (marked by a yellow colour) which were all misclassified into *Tilia sp.* trees.

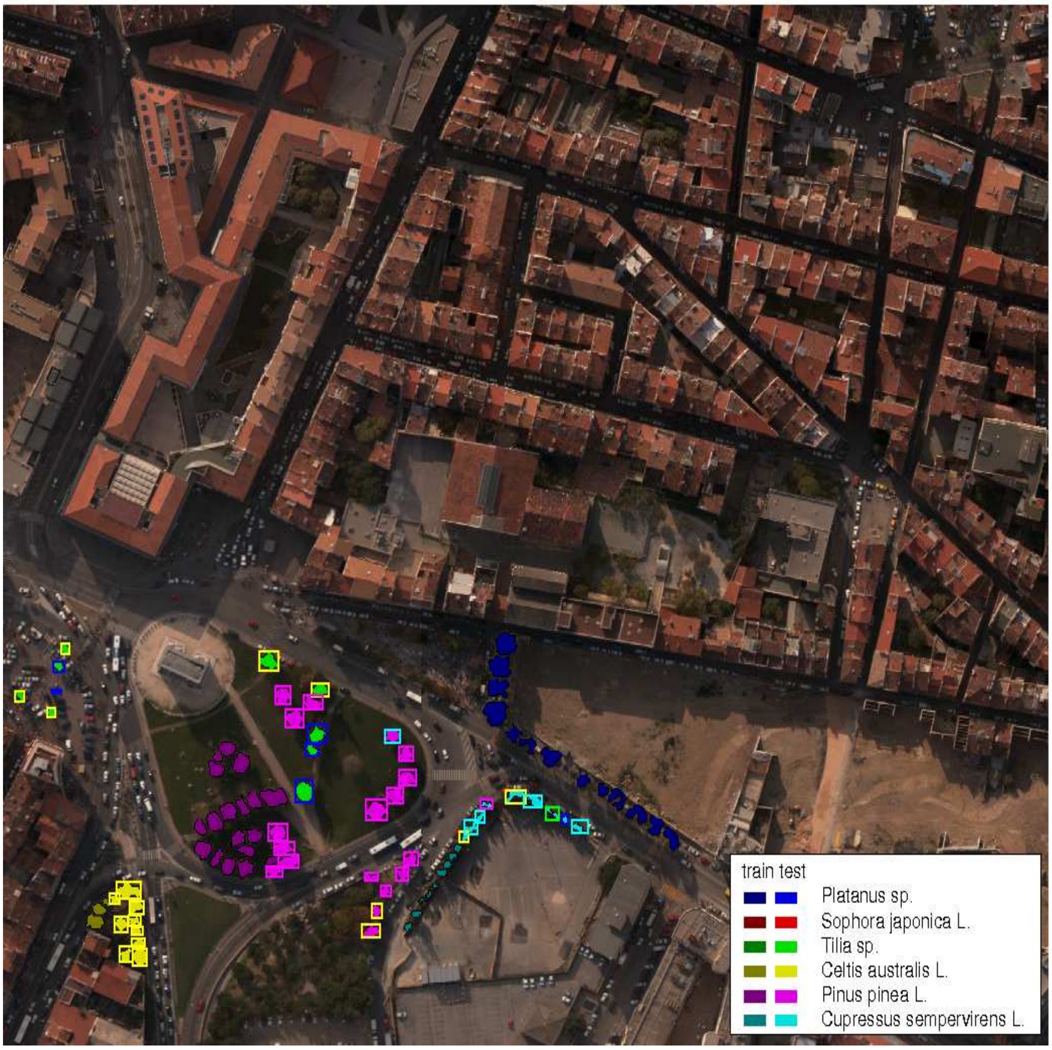

Figure 5.18: Tree species classification results obtained on the Marseille data set - site C with spectral feature vectors extracted on Lab colour space. Ground truth data is marked by a tree crown mask and classification results are bounded by rectangles coloured by appropriate species colour.

Figure 5.18 illustrates tree species classification results obtained on site C of the Marseille data set. All samples of *Pinus pinea L.* trees and of *Cupressus sempervirens L.* ones from the entire database are situated in this site, and are coloured by violet and respectively turquoise colours, in slightly different shades, according to train and test usage of each sample. These two species account for the taxonomic group of coniferous trees. Besides coniferous trees, site C of the Marseille data set also contains *Platanus sp.*, *Tilia sp.* and *Celtis australis L.* trees. Each *Tilia sp.* sample was misclassified either as *Celtis australis L.* or *Platanus sp.* tree species. All *Platanus sp.* tree sample contained in this site were used for the train phase. Only 4 *Cupressus sempervirens L.* samples were correctly classified by spectral features and at least one sample was assigned to each of the other tree species. 2 *Pinus pinea L.* trees were misclassified as *Celtis australis L.* and 1 as *Cupressus sempervirens L.* species.

5.3.5.4 Evaluation

Classification performances are presented in Figure 5.19 by means of ROC curves for the spectral feature vector computed in the Lab colour space. ROC curves obtained for the six tree species are depicted on the same graph by different colours. Details on ROC curves can be found in Appendix A.

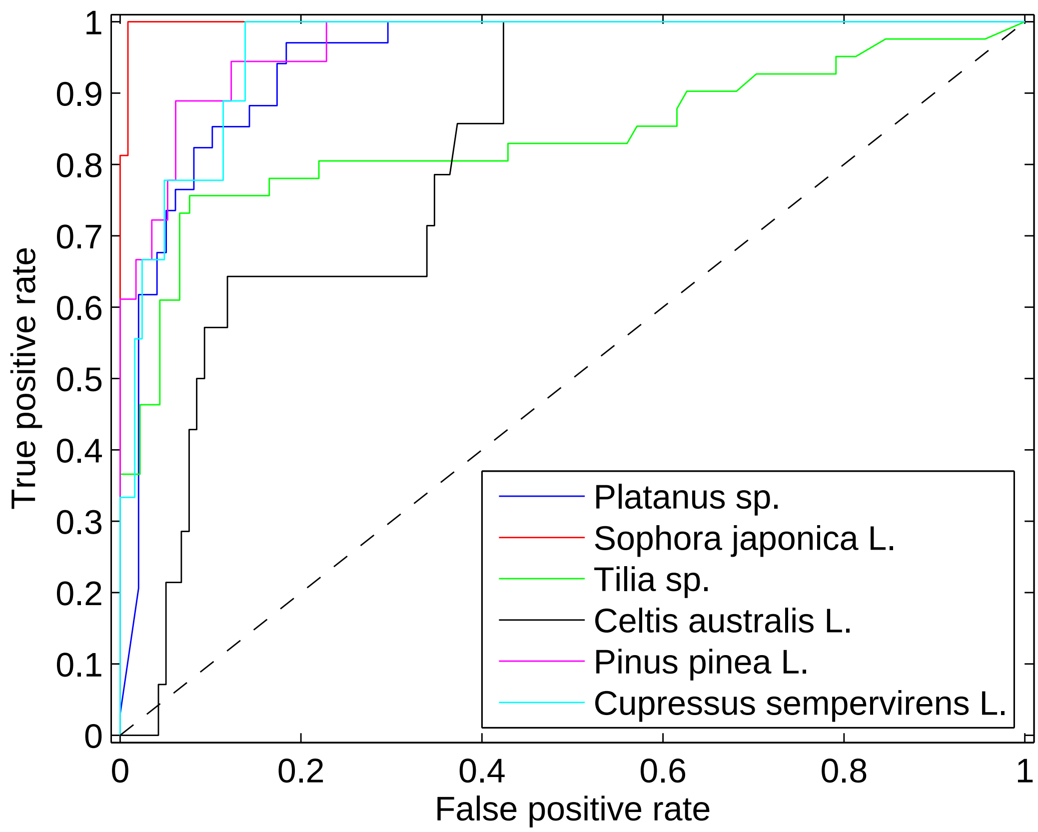

Figure 5.19: Classification performances for the spectral feature vectors obtained by the linear SVM classifier with spectral features extracted in the Lab colour space.

Generally speaking, the closer a ROC curve is to the upper left corner point, the better the performances of the classifier. Figure 5.19 illustrates the good performances of the *Sophora japonica L.* species detector followed by the *Pinus pinea L.* and *Platanus sp.* ones and on the other end of the performances scale, the *Tilia sp.* and the *Celtis australis L.* ones.

Assessment of Classification Accuracy

To asses the accuracy of the classification, confusion matrices and user's accuracy matrices are used, and are detailed in Appendix A. Table 5.5 gives the confusion matrix while Table 5.6 presents user's accuracy matrix obtained for the six tree species from the Marseille data set for a spectral feature vector computed on the Lab colour space and by using a linear kernel SVM classifier. *Platanus sp.* and *Sophora japonica L.* tree samples seem well separable from other tree species while *Celtis australis L.* and *Tilia sp.* sample are most often mistaken, as it is confirmed by the confusion matrix presented in the following.

Table 5.5: Confusion matrix for the linear SVM classifier and spectral feature vector on Lab colour space.

	Ground Truth						
	Platanus	Sophora	Tilia	Celtis	Pinus	Cupressus	# of Det. Trees
Platanus	**33**	0	10	0	0	1	44
Sophora	0	**15**	0	0	0	0	15
Tilia	1	1	**24**	5	0	1	32
Celtis	0	0	7	**9**	2	2	20
Pinus	0	0	0	0	**15**	1	16
Cupressus	0	0	0	0	1	**4**	5
# of G.T. Trees	34	16	41	14	18	9	132

Results presented in Table 5.5 can be transcribed in terms of user's accuracy, by dividing the number of correctly classified samples from each class by the total number of samples in the ground truth data. These results are reported in Table 5.6.

Table 5.6: User accuracy matrix for spectral features.

	Ground Truth					
	Platanus	Sophora	Tilia	Celtis	Pinus	Cupressus
Platanus	**75.0**	0	22.7	0	0	2.27
Sophora	0	**100**	0	0	0	0
Tilia	3.12	3.12	**75.0**	15.62	0	3.12
Celtis	0	0	35.0	**45.0**	10.0	10.0
Pinus	0	0	0	0	**93.8**	6.2
Cupressus	0	0	0	0	20.0	**80.0**

5.3.6 Classification based on spatial features

5.3.6.1 Feature extraction

To statistically analyse tree crown texture, we used a set of features extracted from the Gray Level Co-occurrence Matrix (GLCM) and introduced in [Haralick *et al.*, 1973]. In the following we briefly summarise the computation methodology of GLCM and introduce some necessary notations.

Consider an image $I(x, y)$ of size $N_x \times N_y$ containing L levels of gray. The GLCM is a $L \times L$ matrix given by:

$$P(i, j|d, \theta) = \sharp\{(x_1, y_1), (x_2, y_2) \in (N_x \times N_y) \times (N_x \times N_y) | I(x_1, y_1) = i, I(x_2, y_2) = j, \\ d = |x_2 - x_1|, \theta = |y_2 - y_1|)\} \quad (5.1)$$

This matrix is used to extract second order statistical texture features. A set of 14 texture features which can be extracted from the GLCM are suggested by [Haralick *et al.*, 1973]. A subset of 8 texture features were used to perform tree species classification.

To compare co-occurrence matrices extracted from two samples, the first step is a normalisation step transforming entries of the GLCM into probabilities of co-occurence, independent of window size. The following notations [Haralick *et al.*, 1973] will be used in the following:

$p(i, j)$ normalised element of the co-occurence matrix given by

$p(i, j) = P(i, j)/R$, R is the frequency of pairs of compared pixels in the co-occurrence matrix

$p_x(i)$,ith entry in the marginal probability matrix obtained by:

$$p(i,j) = \sum_{j=1}^{N_g} p(i,j)$$

N_g ,number of distinct gray levels in the quantified image

$$p_y(j) = \sum_{i=1}^{N_g} p(i,j)$$

$$p_{x+y}(k) = \sum_{i=1}^{N_g} \sum_{j=1, i+j=k}^{N_g} p(i,j), k = 2, 3, ..., 2N_g$$

$$p_{x-y}(k) = \sum_{i=1}^{N_g} \sum_{j=1, |i-j|=k}^{N_g} p(i,j), k = 0, 1, ..., N_g - 1$$

A subset of eight texture measures from the co-occurrence matrix were used to perform tree species classification. These features are given by:

Angular Second Moment

$$f_1 = \sum_i \sum_j \{p(i,j)\}^2$$

Contrast

$$f_2 = \sum_{n=0}^{N_g-1} n^2 \{p_{x-y}(n)\}$$

Correlation

$$f_3 = \frac{\sum_i \sum_j (ij) p(i,j) - \mu_x \mu_y}{\sigma_x \sigma_y}$$

where μ_x, μ_y, σ_x and σ_y are the means and standard deviations of p_x and p_y.

Sum of Squares: Variance

$$f_4 = \sum_i \sum_j (i - \mu)^2 p(i,j)$$

Inverse Difference Moment

$$f_5 = \sum_i \sum_j \frac{1}{1 + (i-j)^2} p(i,j)$$

Sum Average: Mean

$$f_6 = \sum_{i=2}^{2N_g} i p_{x+y}(i)$$

Sum Variance

$$f_7 = \sum_{i=2}^{2N_g} (i - f_8)^2 p_{x+y}(i)$$

Entropy

$$f_8 = -\sum_i \sum_j p_{i,j} log(p(i,j))$$

Four GLCM were computed for θ=0°, θ=45°, θ=90°, and θ=135°. For each spectral band of each colour space analysed, eight texture measures were computed over the four GLCM, yielding a measurement vector of $4 \times 8 = 32$ for each sample image. Computations of the *mean* and *range* of each feature over the four directions reduced the dimensionality to 16 features for each spectral band. Features computed for each spectral band were concatenated into one feature vector for each tree sample of a given species [Drimbarean and Whelan, 2001].

5.3.6.2 Feature transformation

Texture feature vectors were computed on the *RGB*, *HSV*, *XYZ* and *Lab* colour spaces.

For all colour spaces analysed for tree species classification, besides spectral bands, the *IR* band was also taken into consideration.

Choice of GLCM parameters

The choice of an appropriate distance d (cf. Equation 5.1) between pixels is closely related to the coarseness or the fineness of the texture being analysed. The coarser the texture, the more the distance between pixels can be increased. In order to use the most appropriate value for d, sensitivity of the overall classification rate to d was studied. The following table (Table 5.7) gives an analysis of the overall accuracy of a linear kernel SVM classifier with feature vectors computed in a RGB colour space and for a number of five gray levels in the co-occurrence matrix.

Table 5.7: Sensitivity of overall accuracy to d

d	1	2	3	4	5
Overall accuracy (%)	52.7	47.1	46.7	44.5	40.4

As can be noticed in Table 5.7, the best performances were obtained for $d = 1$. In the following of the experiments, d was set to 1 for all colour spaces and number of gray levels taken into consideration, allowing the texture to be characterised in its finest level of detail.

Overall accuracy varies also with the number of gray levels taken into consideration in the GLCM. In the following tables (Table 5.8, 5.9, 5.10, 5.11 and 5.12) overall accuracy for different colour spaces and types of SVM kernels is presented for $d = 1$ and for an increasing number of gray levels. The best case configuration is further on used to perform tree species classification based on spatial feature vectors.

Table 5.8: Overall accuracy (%) for different colour spaces and SVM kernels and 5 gray levels.

Colour space \ Kernel	linear	polynomial	rbf
RGB	52.7	44.8	47.5
HSV	45.5	47.3	51.9
XYZ	46.1	45.5	21.6
Lab	44.9	51.3	47.4

Table 5.9: Overall accuracy (%) for different colour spaces and SVM kernels and 6 gray levels.

Colour space \ Kernel	linear	polynomial	rbf
RGB	52.3	18	18.2
HSV	59.9	43.7	51.9
XYZ	44.6	43.2	21.9
Lab	44.7	45.5	21.1

Table 5.10: Overall accuracy (%) for different colour spaces and SVM kernels and 7 gray levels.

Colour space \ Kernel	linear	polynomial	rbf
RGB	46	17.7	45.3
HSV	**64.9**	52.5	61.8
XYZ	48.8	17.6	20
Lab	43.2	52.5	44.3

As can be noticed by analysing results reported in tables 5.8, 5.9, 5.10, 5.11 and 5.12, the best configuration is obtained for features computed on the HSV colour

Table 5.11: Overall accuracy (%) for different colour spaces and SVM kernels and 8 gray levels.

Kernel / Colour space	linear	polynomial	rbf
RGB	48.9	17.1	19.8
HSV	55.1	55.3	58.6
XYZ	43.8	17.1	21.5
Lab	43.5	50.6	45.3

Table 5.12: Overall accuracy (%) for different colour spaces and SVM kernels and 9 gray levels.

Kernel / Colour space	linear	polynomial	rbf
RGB	45.7	18.9	19.2
HSV	53.5	51.4	48.2
XYZ	44.1	17.1	21.5
Lab	41.5	43.3	44.1

space with a number of 7 gray levels in the GLCM and a linear kernel SVM classifier (cf. Table 5.10).

5.3.6.3 Results

Figures 5.20, 5.21 and 5.22 present a map of tree species obtained by the SVM classifier by using a spatial feature vector computed on the HSV colour space.

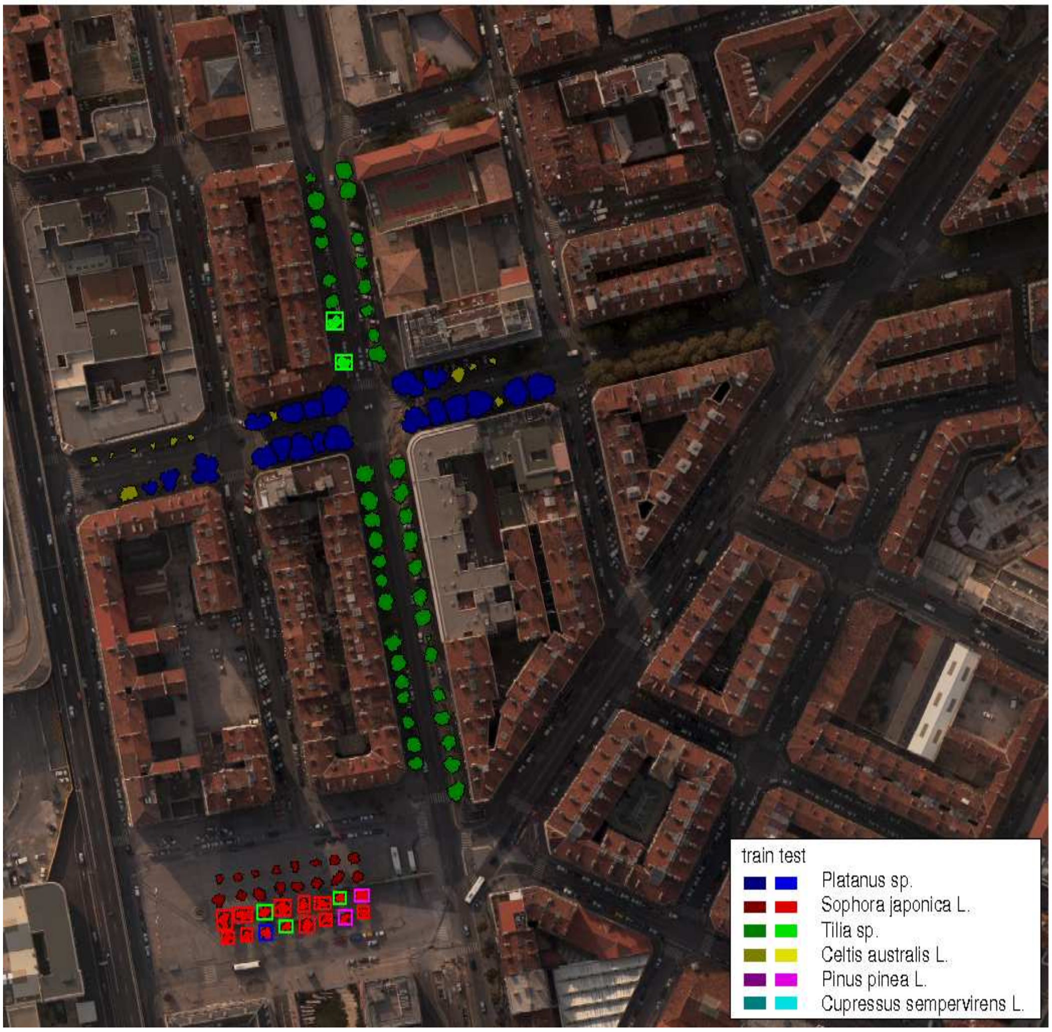

Figure 5.20: Tree species classification results obtained on the Marseille data set - site A with spatial feature vectors extracted on the HSV colour space. Ground truth data is marked by a tree crown mask and classification results are bounded by rectangles coloured by appropriate species colour.

Tree species classification results for site A of the Marseille data set are depicted in Figure 5.20. Tree crown samples used for training are coloured by an appropriate colour, according to its species. Tree samples used for test, are coloured according to their species and bounded by a rectangle coloured by the colour associated to the species of tree as detected by the classifier. Compared to tree species classification results presented in Figure 5.16 we note that the 2 *Tillia sp.* are also correctly classified. Yet, 6 out of the 16 *Sophora japonica L.* tree samples were misclassified by using spatial features computed on the HSV colour space, compared to only 1 misclassified sample for the spectral feature case. 3 *Sophora japonica L.* samples were misclassified as *Tillia sp.* trees, 2 as *Pinus pinea L.* and 1 as *Platanus sp*. species, as it can noticed in the lower part of the image, for tree samples coloured in red.

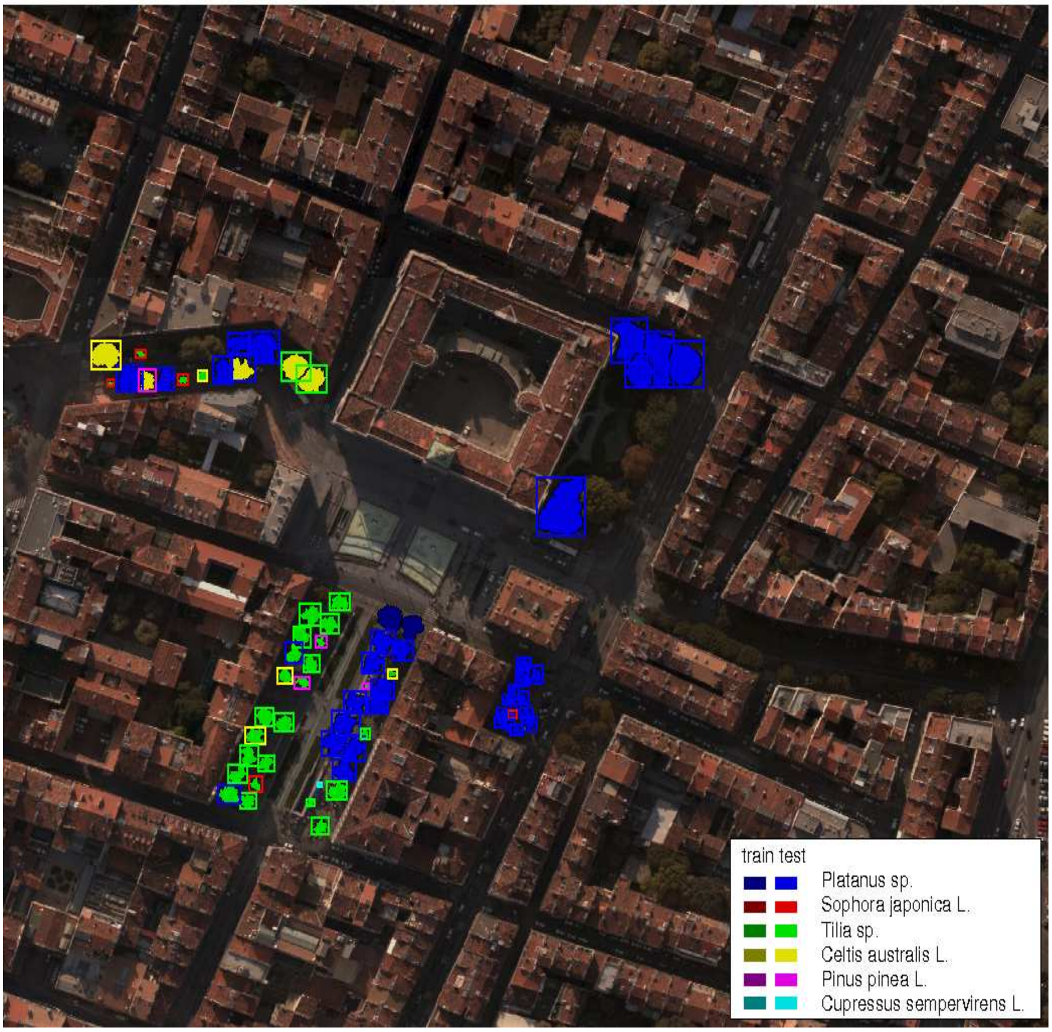

Figure 5.21: Tree species classification results obtained on the Marseille data set - site B with spatial feature vectors extracted on the HSV colour space. Ground truth data is marked by a tree crown mask and classification results are bounded by rectangles coloured by appropriate species colour.

Classification results for site B of the Marseille data set are presented in Figure 5.21, for spatial feature vectors computed on the *HSV* colour space. Classification results show the presence of six tree species in site B, whereas according to ground truth data there are only three species of trees present in the site. 1 *Platanus sp.* sample was classified as *Sophora japonica L.* species. 1 *Celtis australis L.* tree sample was correctly classified while all other one were either classified as *Tilia sp.*, *Platanus sp.* or *Pinus pinea L.*. Several misclassified samples of *Tilia sp.* can also been noticed and confusions occurred to all other tree species from the database. Visual assessment of the classification results reported in Figure 5.21 are less accurate than the ones reported for the spectral feature vector and presented in Figure 5.17.

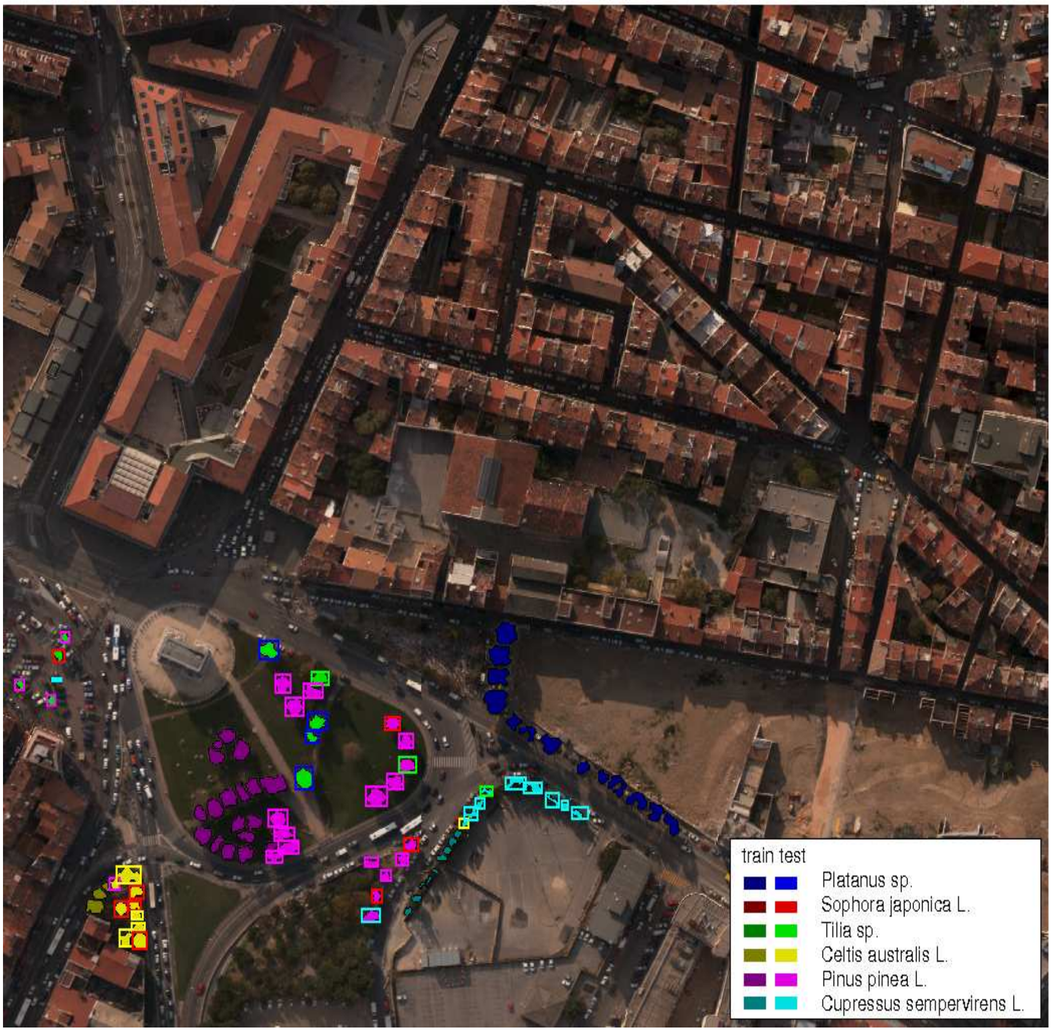

Figure 5.22: Tree species classification results obtained on the Marseille data set - site C with spatial feature vectors extracted on the HSV colour space. Ground truth data is marked by a tree crown mask and classification results are bounded by rectangles coloured by appropriate species colour.

Figure 5.22 illustrates tree species classification results obtained on site C of the Marseille data set. Although there are no *Sophora japonica L.* samples in the ground truth data collected for site C, we can notice that 8 samples of different species from the site were mistaken by it. Compared to results presented in Figure 5.18 we notice an improvement in results obtained for the *Cupressus sempervirens L.* and the *Pinus pinea L.* species, as less samples were misclassified. Several *Celtis australis L.* samples depicted in yellow, were misclassified as *Sophora japonica L.* or *Pinus pinea L.* tree species. Only 1 *Tilia sp.* sample was correctly classified and the other ones were assigned either to *Platanus sp.*, *Sophora japonica L.*, *Pinus pinea L.* or *Cupressus sempervirens L.* tree species.

5.3.6.4 Evaluation

Classifier evaluation is performed by means of the ROC curves (cf. Appendix A). For each class (tree species) and for spatial feature vectors computed on the HSV colour space ROC curves are plotted on the same graph. Figure 5.23 depicts ROC curves for the spatial feature vector computed in the HSV colour space. ROC curves obtained for the six tree species are depicted on the same graph by different colours.

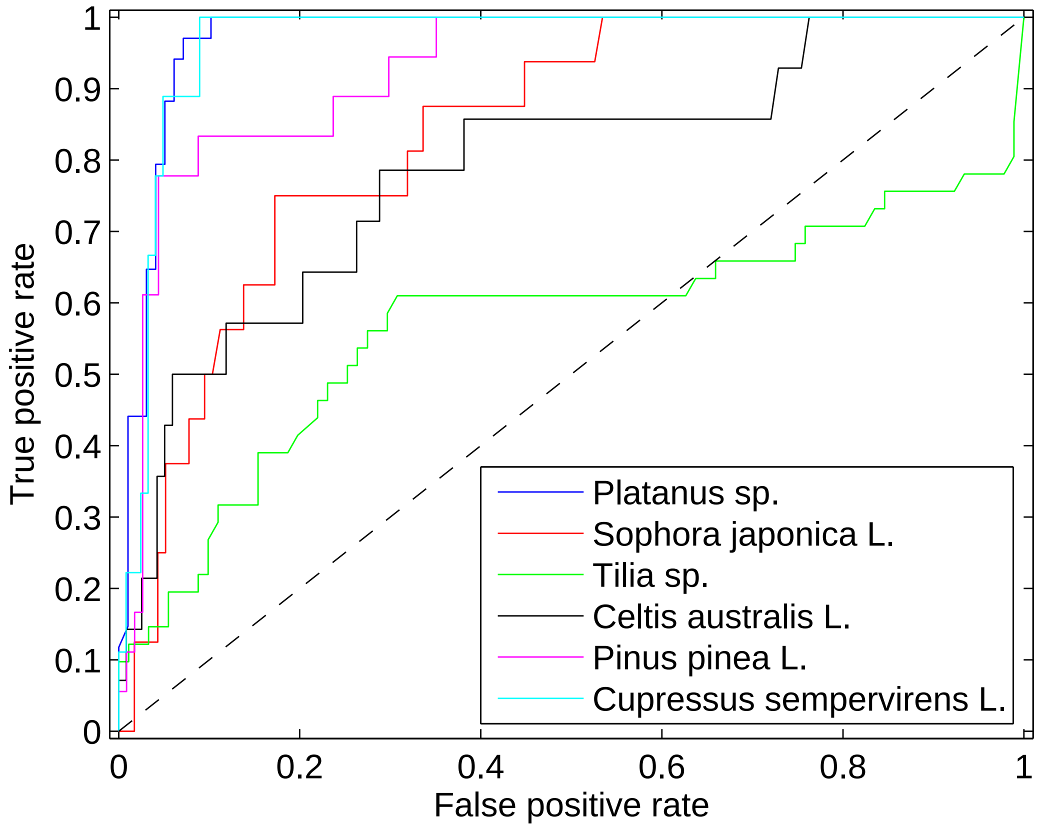

Figure 5.23: Classification performances for texture feature vectors extracted on the HSV colour space.

Spatial features computed on the HSV colour space give good performances for the *Platanus sp.* and the *Cupressus sempervirens L.* classifiers while performing less satisfying for the *Tilia sp.* which gets confused to *Celtis australis L.* and *Pinus pinea L.*.

Assessment of Classification Accuracy

Confusion matrices and user's accuracy matrices are used to asses classification accuracy for species classification based on spatial features. Table 5.13 presents the confusion matrix obtained for the six tree species from the Marseille data set while Table 5.14 presents the user's accuracy for texture feature vector computed on the HSV colour space and using a linear kernel SVM classifier. Details on different was to assess classification accuracy are given in Appendix A. Table 5.13 shows that by using texture features, *Celtis australis L.* trees are mostly mistaken by *Tilia sp.* trees, while *Cupressus sempervirens L.* trees are rather well detected.

Table 5.13: Confusion matrix for the SVM classifier and texture feature vector computed on the HSV colour space.

	Ground Truth						
	Platanus	Sophora	Tilia	Celtis	Pinus	Cupressus	# of Det. Trees
Platanus	**33**	1	6	1	0	0	41
Sophora	1	**10**	5	4	3	0	23
Tilia	0	3	**18**	2	1	1	25
Celtis	0	0	4	**5**	0	1	10
Pinus	0	2	6	2	**13**	0	23
Cupressus	0	0	2	0	1	**7**	10
# of G.T. Trees	34	16	41	14	18	9	132

Table 5.14 presents the user's accuracy for the linear kernel SVM classifier using spatial feature vectors computed on the HSV colour space. This can be computed from the confusion matrix and gives the probability that for a tree sample of a given species, the correct species of that sample is the actual species in the ground truth.

Table 5.14: User accuracy matrix for spatial features.

	Ground Truth					
	Platanus	Sophora	Tilia	Celtis	Pinus	Cupressus
Platanus	**80.5**	2.43	14.63	2.44	0	0
Sophora	4.34	**43.47**	21.73	17.39	13.04	0
Tilia	0	12.0	**72.0**	8.0	4.0	4.0
Celtis	0	0	40.0	**50.0**	0	10.0
Pinus	0	8.69	26.1	8.1	**56.5**	0
Cupressus	0	0	20.0	0	10	**70.0**

5.3.7 Towards a combined classification approach

Results obtained individually by the spectral and the spatial feature spaces encouraged the development of a combined approach benefitting from the advantages of the two feature spaces previously described. There are at least two main approaches to doing this, either by uniting the feature spaces, or by combining the outputs of each classifier. The first approach, an early fusion strategy, was implemented to evaluate the performances of tree species classification by spectral and spatial features.

Figure 5.24 gives the overview of the combined system.

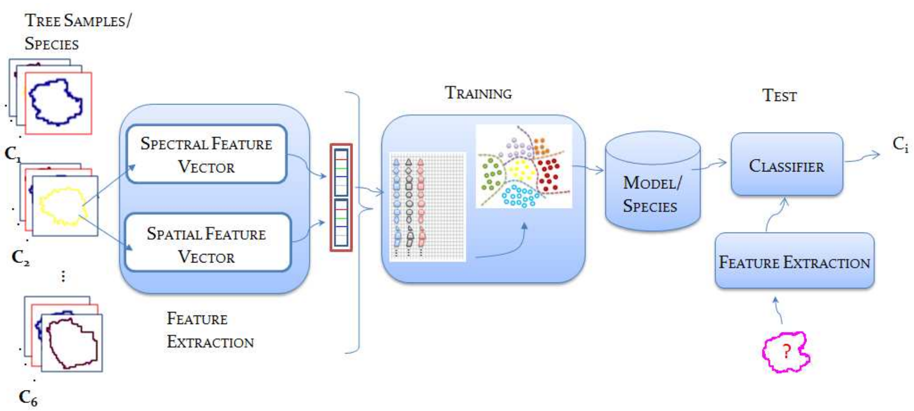

Figure 5.24: System overview for the combined tree species classification approach.

The input of the system is made up of spatial and spectral feature vectors for each sample of a tree species. They are used by the SVM classifier to learn a model from training samples for each tree species, during the training stage.

For each tree sample of unknown species, spectral and spatial features are extracted before comparing them to species models generated during training. An estimation is made by each classifier on the membership class of the test sample which is labelled as belonging to the class with the highest probability.

Models obtained for each species during the training stage are compared to features of an unknown sample. The classifier takes a decision in terms of probability. The sample is considered belonging to the class indicated by the classifier having the highest probability.

5.3.7.1 Feature extraction

Tree samples from the training data set are used to build feature vectors. Spatial and spectral features are extracted for each tree crown following the methodology previously presented for the *spectral* and *spatial* feature space and resulting feature vectors are concatenated for each tree sample. They are used during training by the SVM classifier to build a model for each corresponding tree species.

5.3.7.2 Feature transformation

Following the methodology presented in the previous sections, feature vectors were also computed in different colour spaces *RVB*, *HSV*, *XYZ* and *Lab*. Information extracted from the *IR* band was also used to characterise tree samples for all colour spaces.

5.3.7.3 Results

Before presenting the results on the Marseille database, we selected the best combination of feature vectors and colour spaces for the early fusion, in terms of overall accuracy. This was computed for all *colour space - feature vector* combinations and is presented in Table 5.15.

Table 5.15: Overall accuracy (%) for early fusion of spectral and spatial feature vectors computed on different colour spaces.

Spectral \ Spatial	RGB	HSV	XYZ	Lab
RGB	65.5	**76.2**	65.7	69.3
HSV	69.7	73.2	67.8	73
XYZ	67.9	74.8	65.2	61.1
Lab	70.6	73.9	68.8	68

Overall accuracy results presented in Table 5.15 shows that best results are obtained when combining spectral features extracted on RGB colour space with texture features computed on the HSV colour space. This case shows that best combination results are not given by the combination of best performing spectral and spatial colour spaces, i.e. Lab colour space for the spectral feature vector and HSV colour space for the spatial feature vector.

Figures 5.25, 5.26 and 5.27 present the output map for tree species obtained by the combined approach by using spectral features computed on the RGB colour space and spatial feature vectors extracted on the HSV colour space.

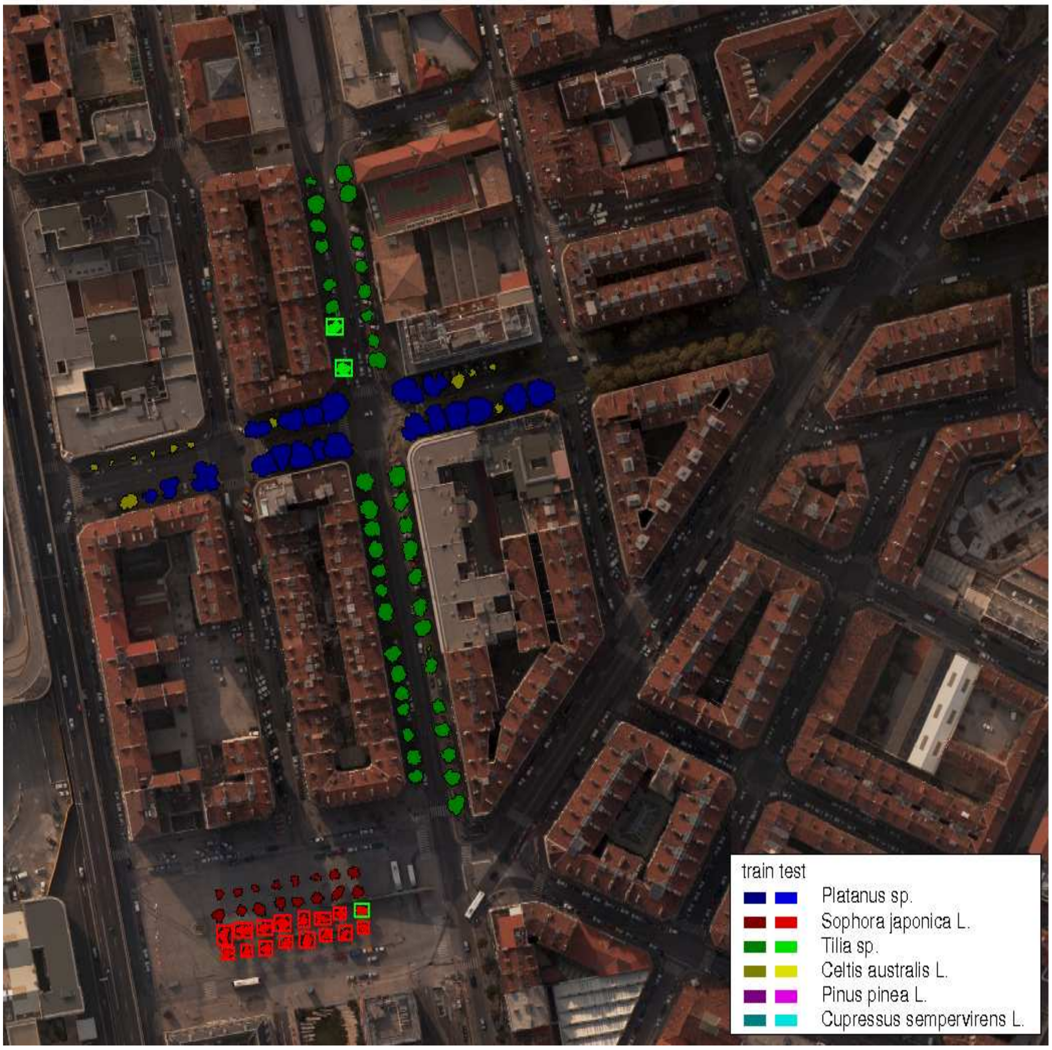

Figure 5.25: Tree species classification results obtained on the Marseille data set - site A by the combined approach using spectral features extracted on the RGB colour space and spatial feature vectors computed on the HSV colour space. Ground truth data is marked by a tree crown mask and classification results are bounded by rectangles coloured by appropriate species colour.

Figure 5.25 depicts tree species classification results obtained on site A of the Marseille data set for the combined approach. Compared to results obtained for the spatial features and presented in Figure 5.20 performances of the combined approach are highly improved and close to the ones obtained for the spectral features and presented in Figure 5.16. The two *Tilia sp.* samples were correctly classified and the 15 out of 16 samples of *Sophora japonica L.* were also correctly classified.

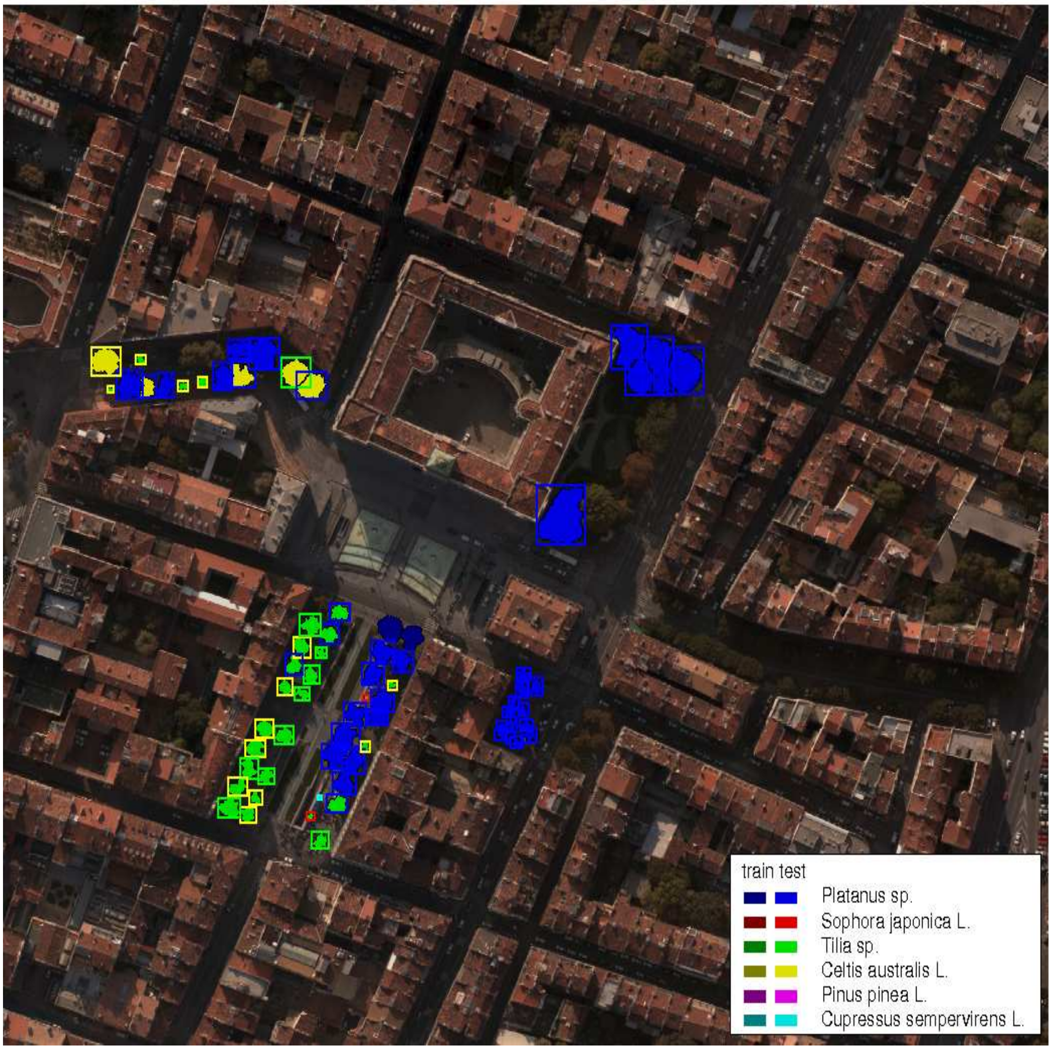

Figure 5.26: Tree species classification results obtained on the Marseille data set - site B by the combined approach using spectral features extracted on the RGB colour space and spatial feature vectors computed on the HSV colour space. Ground truth data is marked by a tree crown mask and classification results are bounded by rectangles coloured by appropriate species colour.

Results obtained for site B of the Marseille data set, are illustrated in Figure 5.26 for the combined approach. Five out of the six tree species from the Marseille database reported by the combined approach classifier, whereas only three are present in ground truth data. Compared to results obtained for spatial features we note the presence of *Sophora japonica L.* and *Cupressus sempervirens L.* samples in site B, whereas for results obtained for the spectral features, only the three species present in the ground truth data were reported in site B. All *Platanus sp.* samples are correctly classified by the combined approach classifier, like 1 sample of the *Celtis australis L.* species and 9 samples of *Tilia sp.*. The most misclassified samples are the *Tilia sp.* ones which are mistaken with *Celtis australis L.* ones.

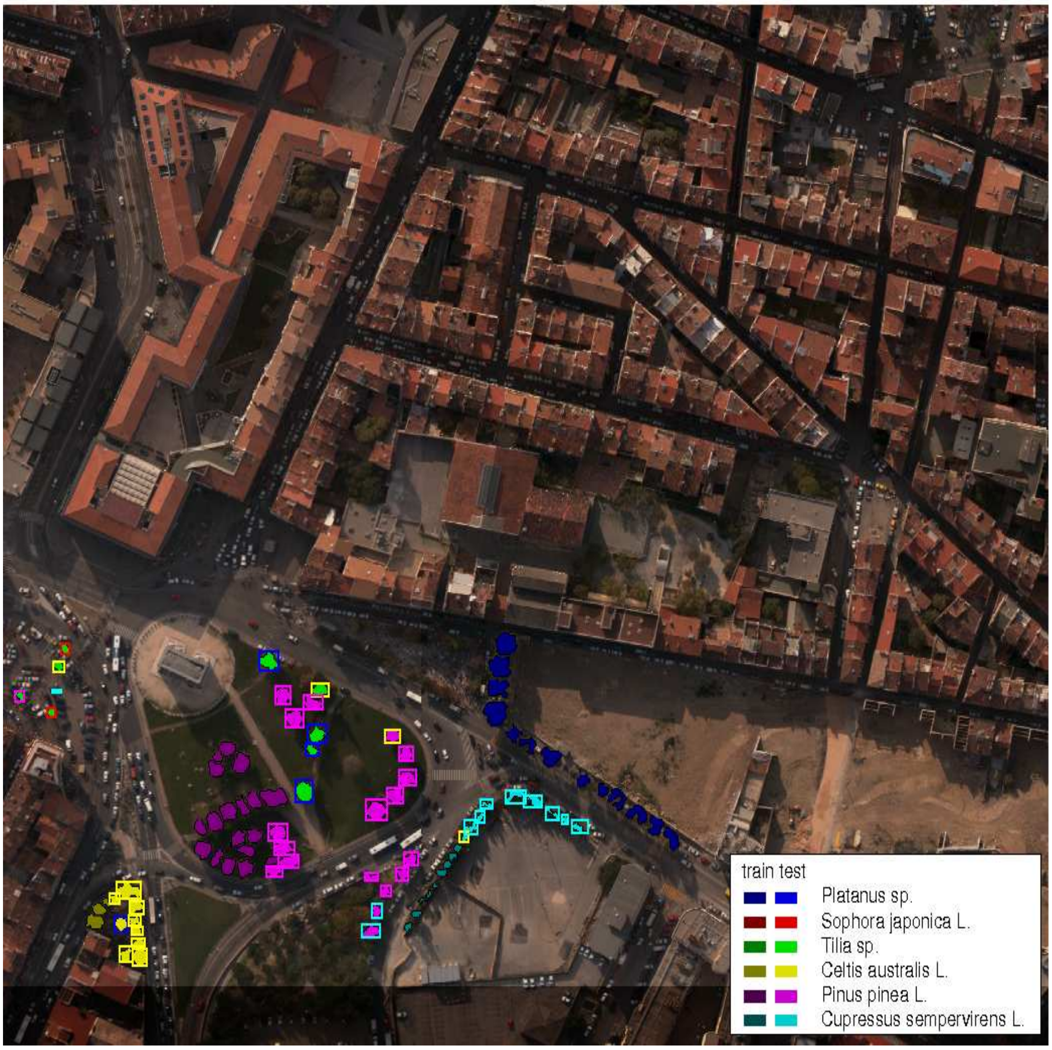

Figure 5.27: Tree species classification results obtained on the Marseille data set - site C by the combined approach using spectral features extracted on the RGB colour space and spatial feature vectors computed on the HSV colour space. Ground truth data is marked by a tree crown mask and classification results are bounded by rectangles coloured by appropriate species colour.

Tree species classification results obtained for the combined classification approach for site C of the Marseille data set are reported in Figure 5.27. An improvement in the number of correctly classified samples is noticed for the *Cupressus sempervirens L.*, the *Pinus pinea L* and the *Celtis australis L.* species compared to the spatial features classifier. Each of the *Tilia sp.* samples is misclassified, and mostly mistaken as *Platanus sp.* samples. 2 *Pinus pinea L.* samples are misclassified as *Cupressus sempervirens L.* ones and 1 as *Celtis australis L.*. The turquoise rectangle in the upper left part of the image stands for a *Tilia sp.* tree sample misclassified as *Cupressus sempervirens L.* species. As the size of the sample is very small, the ground truth data can no longer be observed and only the classification result remains visible.

5.3.7.4 Evaluation

ROC curves are plotted for each class and for each colour space. They are used to evaluate classifier performances (cf. Appendix A). Figure 5.28 presents ROC curves obtained for tree species classification for the combined approach. ROC curves obtained for the six tree species are depicted on the same graph by different colours.

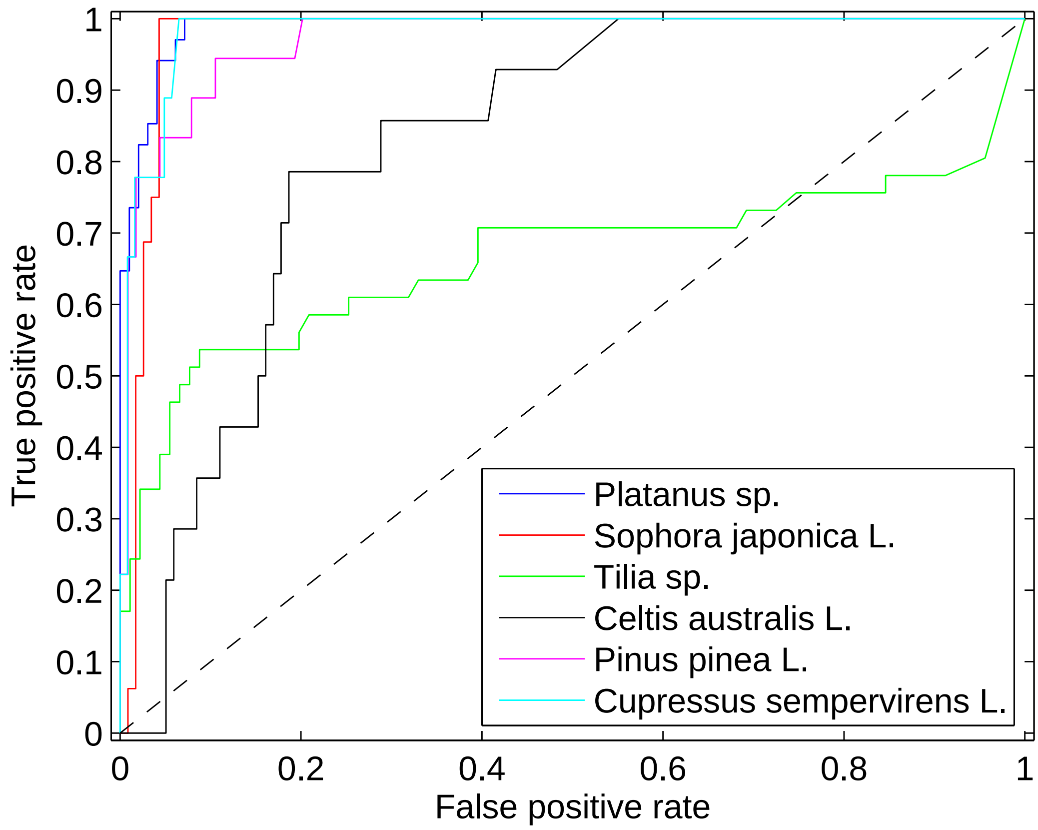

Figure 5.28: Classification performances for the combined approach to tree species classification with spectral features extracted on the RGB colour space and spatial feature vectors computed on the HSV colour space.

The combined approach gives rather good performances in separating *Platanus sp.* from *Sophora japonica L.* and *Cupressus sempervirens L.* while its performances are quite poor when in comes to *Tilia sp.* trees.

Assessment of Classification Accuracy

Confusion matrices and user's accuracy matrices (cf. Appendix A) are given below for the combined approach. Table 5.16 presents the confusion matrix while Table 5.17 presents user's accuracy for tree species classification using the combined approach, with spectral features computed on the RGB colour space and spatial ones computed on the HSV colour space. The combined approach gives the highest number of confusions between samples of *Tilia sp.* and *Celtis australis L.* but also the highest number of detected *Cupressus sempervirens L.* samples.

Table 5.16: Confusion matrix for the combined approach.

	Ground Truth						
	Platanus	Sophora	Tilia	Celtis	Pinus	Cupressus	# of Det. Trees
Platanus	**34**	0	8	4	0	0	46
Sophora	0	**15**	4	0	0	0	19
Tilia	0	1	**11**	1	0	0	13
Celtis	0	0	15	**9**	1	1	26
Pinus	0	0	1	0	**15**	0	16
Cupressus	0	0	2	0	2	**8**	12
# of G.T. Trees	34	16	41	14	18	9	132

The user accuracy matrix given below was computed from the confusion matrix and reports accuracies of individual species from a user's point of view (cf. Appendix A).

5.3.8 Discussion

The tree species classification system developed takes as input tree crown units delineated by the tree crown delineation algorithm presented in Chapter 4. A total of 267 samples of tree crowns belonging to six tree species were used to perform tree species classification. A sub-set of 213 deciduous trees belonging to four tree species and 54 coniferous ones were used to evaluate the capabilities of tree species

Table 5.17: User accuracy matrix for the combined approach.

	Ground Truth					
	Platanus	Sophora	Tilia	Celtis	Pinus	Cupressus
Platanus	**73.9**	0	17.4	8.7	0	0
Sophora	0	**78.9**	21.1	0	0	0
Tilia	0	7.7	**84.61**	7.7	0	0
Celtis	0	0	57.7	**34.6**	3.8	3.8
Pinus	0	0	6.2	0	**93.8**	0
Cupressus	0	0	16.7	0	16.7	**66.6**

classification. Tree samples for each species were divided into training and test sub-sets and were used to extract features used to perform species classification.

Separation between six species of trees from the Marseille data set was evaluated by using spectral and spatial features in a supervised classification approach based on SVM classifier. Feature vectors were composed of spectral and spatial characteristics computed on whole tree crowns, and on all training samples belonging to a class. Spectral and spatial features were extracted on four different colour spaces, namely, *RGB*, *HSV*, *XYZ*, *Lab*.

For each feature space, classification accuracy was evaluated against ground truth data. ROC curves, confusion and user's accuracy matrices accompany visual results obtained for each feature space. A combined approach using spatial and spectral features is also evaluated for the six tree species of the Marseille data set.

Classification accuracy varies with the type of input features. The results from evaluations based on the Marseille data set provide initial proofs that spectral and spatial feature vectors can accurately differentiate between tree species belonging to the same taxonomic group. The results also show that in our experiments, a training sample of approximately 28×28 pixels or less provide sufficient information to obtain a reliable sample model, as long as the training sample is representative for its class.

No attempt was made to use frequency or geometrical characteristics for the species classification approach and future studies may examine the effectiveness of such features. In an urban environment with trees of different ages and tree crowns often cut to rectangular shapes, geometric characteristics of the tree crown didn't appear discriminant enough to characterise a tree species. As for the frequency features, too little information on each tree crown resulted in not being enough to be efficiently exploited by filter banks approaches.

Further research should be carried out on a richer data set before concluding on what type of features are most appropriate to differentiate between tree species. For the combined approach, further works should be performed to investigate a late fusion strategy.

5.4 Conclusions

This chapter outlines vegetation characterisation techniques from two levels of detail. The first one, provides vegetation characterisation from a morphological point of view, whereas the second one gives the distribution of tree species in a city inferred by machine learning techniques from statistical properties of tree species.

The first level of characterisation allows an estimate of tree height, tree crown area and gives tree truck position coordinates. Such parameters are useful in visualisation applications as they can be used to integrate 3D tree models into virtual city models.

The second level of detail in vegetation characterisation is achieved through tree species classification. Tree species identification from aerial imagery is a very difficult task, even for highly experimented photo-interpreters. Due to the high variety of species and the high variability of a species characteristics it is not easy to identify reliable features for species classification. The method proposed in this chapter to cope with the problem of tree species classification evaluates spectral and spatial statistical characteristics of tree crowns.

Three classification systems were evaluated for tree species classification, which differ according to the input feature vector. The first one uses only spectral features, the second one uses only spatial features and the third one takes as input a feature vector composed of both spectral and spatial tree crown characteristics.

Due to the low number of samples for each species, results obtained should be considered with caution. Future research should be carried out using a higher number of samples for tree species classification tasks where analysis units vary in size and acquisition conditions.

Chapter 6

Concluding Remarks and Future Directions

The aim of this thesis was to develop a system capable of detecting and characterising vegetation from high resolution aerial imagery of urban areas. This chapter gives a review of what has been accomplished in this thesis (cf. Section 6.1) and outlines the implications of the new system for vegetation management in urban areas. Finally, perspectives and future directions will be drawn in Section 6.2.

6.1 Conclusions

Since the mid- '70, the need of a detailed inventory of species of trees in public parks was addressed by the city hall of Paris to IGN's photo-interpreters [IGN, Département de Télédétection, 1986], [IGN, Département de Télédétection, 1991]. The aim of the study was to establish a "green cadastral map" containing location and species of trees present in public areas. It was at the beginning of such types of applications of remote sensed photo-interpretation and most of the inventory was performed by field surveys.

With the development of the acquisition sensors and the maturity of research in analysis of urban scenes from high resolution aerial imagery [Brédif *et al.*, 2007], the vegetation component or the city lacked precise description of its characteristics [Baillard *et al.*, 1998].

The vegetation analysis system presented in this thesis fills this need, and provided specific input data for each module exists, answers to the following questions: *where in remote sensing data is vegetation located?*, *which type of urban vegetation is it?*, *which are the shape characteristics of each tree?*, *which is the species of a tree?*.

- *Vegetation extraction* in urban areas from remotely sensed imagery was the first objective of this work. Based on state of the art methods developed to answer similar questions, two approaches were studied in Chapter 3. The first one combines different spectral indexes, as the traditional NDVI, to produce masks of vegetation areas, but revealed the need of constantly adapting the indices used to data. The second method is based on a SVMs classifier with different kernel configurations and takes as input a feature vector composed of spectral reflectances of vegetation and non-vegetation pixels in the four spectral bands. Three additional colour spaces are studied in combination with the IR channel and revealed that the *Lab* one in a linear kernel configuration performed better that the NDVI index.

- Vegetation masks obtained from the first module give focus areas for the following modules. The module presented in Chapter 4 deals with *identifying types of urban vegetation*. The interest is on lawns and trees which are separated from each other by computing height variance on the DSM correspondent to vegetation areas. Tree crown borders are delineated by a region growing algorithm applied on height data (DSM). We proposed a strategy to extract seeds used for initialising the growing step which give accurate regions with a one to one correspondence to tree tops. Performances of the proposed method are compared to two state of the art methods mostly used for similar goals, the random walk image segmentation algorithm [Erikson, 2004a] and the watershed algorithm [Vincent and Soille, 1991]. The algorithm for individual tree crown delineation outperforms such traditional approaches and this is due to the seed initialisation strategy which gives accurate locations for tree tops. This is indeed the crucial part of any region growing algorithm. As it is performed on 3D height data, it is not influenced by shadings, occlusions or intensity variations often encountered in urban area imagery.

- The output of this module consists of low-height vegetation and tree crown masks. The first one corresponds to lawn areas and the second one to individual tree crown units which will be used by the following module to estimate *individual tree shape characteristics* (cf. Chapter 5). 3D tree parameters are extracted for each tree crown unit and used for visualisation purposes to enhance virtual 3D city models by a realistic representation of vegetation. Vegetation characterisation is taken a step further, by adding *tree species classification* to the whole system, provided ground truth information are available. It is important to stress that human interpreters are not able to assign a species to a tree crown only based on the tree crown outline. Spectral and spatial features computed for each tree crown unit are used to perform tree species classification based on a SVM classifier. An early fusion strategy is presented to evaluate benefits of spectral and spatial features for tree species classification in urban areas. The obtained results showed that by combining spectral and spatial features, coniferous trees can be differentiated from deciduous ones. As for the distinction between different deciduous tree species, spectral features proved sufficient for certain species, while spatial features alone revealed sufficient for other tree species.

Results obtained from all of the modules of the entire system are exploited to create realistic 3D city models by integrating tree models according to species and applying 3D shape parameters of individual trees on each model. This allows to successfully meet the *completeness* and *robustness* requirements set for the vegetation analysis system.

6.2 Perspectives

The algorithm presented in this thesis to perform individual tree crown delineation belongs to the family of region-growing approaches and gives highly accurate estimates of tree top locations. This is the crucial part of such type of methods, as the growing stage depends on the number and position of seeds. The growing part of the algorithm could be improved by extracting features at each step of height-descent strategy and merging the regions according to a rule-based strategy measuring the similarity between features.

Future works could also focus on the development of top-down segmentation approaches involving marked point processes [Perrin *et al.*, 2006]. The strategy could start from seed regions extracted by our algorithm and by introducing *a priori* knowledge into the segmentation process, like contextual and topological relationships for trees, results obtained for individual tree crown delineation could be improved. Model-based approaches like template matching [Olofsson *et al.*, 2006] could also be a valuable strategy. Starting from the extracted seed regions, a feature extraction step could be combined with the template matching one to output more accurate tree regions. 3D tree templates could also be fitted on the DSM or supplementary features computed on the colour channels could be added to improve the growing part of the algorithm.

Different types of features could be extracted from tree regions to perform tree species classification, such as texton features [Varma and Zisserman, 2003]. Future work should be considered to develop a multi-class classification strategy or to evaluate other types of classification systems. Late-fusion strategies should also be developed to evaluate the potential of fusing the output of different classifiers rather than their input.

At a global, more general view of the entire system, an interesting subject for future research could be the combination of aerial imagery with laser data which could provide a higher accuracy for the DSM and could allow the extraction of tree species characteristics which are not available from aerial imagery.

Currently, researches from two out of the three modules of the vegetation analysis system proposed in this thesis have been successfully integrated to IGN's Bati-3D ®production line [IGN, Institut Géographique National, 2008], whose aim is to produce realistic virtual 3D models from aerial remote sensed data. These are the modules developed to detect vegetation, presented in Chapter 3 and the one presented in Chapter 4 separating high- from low- height vegetation and performing individual tree crown delineation.

Future work should aim the integration of the vegetation classification module into the final system. Several questions on the specific needs of an end used still have to be analysed prior to this integration.

Main categories of users of the results obtained with the vegetation analysis system vary from local communities to urban planners. For local communities, if their demand builds up on basic visualisation needs, (i.e. the 3D view of a city and its vegetation) the first two modules of the vegetation analysis system offer sufficient details on vegetation to produce a view of the city's vegetation. If needs are for more details, such as tree species distribution for statistic purposes, two types of actions could be considered, as the case may be. If the local communities posses GIS databases of tree species, tree species classification could be considered either for generalisation purposes or database updating. In this case, the tree species classification module could be successfully used. Should no ground truth data be available, tree species clustering (unsupervised classification) could be more appropriate than classification. Future work should be considered for the development of similarity measures appropriate for tree species.

The needs of urban planners differ from those of local communities. One case which could be taken into consideration is estimating the appropriate moment when lopping interventions are necessary, especially when electricity power lines are threatened by tree branches growth [RTE, Gestionnaire du Réseau de Transport d'Electricité, 2008b,a]. In this case, tree species and species growth rate have to be known in order to decide for the best moment of intervention. The tree species classification module could be used in such cases but auxiliary information is needed (i.e. ground truth species information and species growth curves) in order to give accurate estimations of their development.

Appendix A

Classification Tools

We present in this Appendix different classification tools used throughout this thesis. It begins by a the Support Vector Machines (SVM) classification framework. It is the classification tool that we used in our pattern recognition tasks. Classifier evaluation protocol and quality assessment measures used in our experiments are then reported.

A.1 Support Vector Machines for Discrimination Problems

A.1.1 Linear Classification: SVM Principle

To illustrate the basic concepts of SVMs, we begin our presentation with the linear support vector approach for binary classification.

Let us consider the following representation for the training data:

$$S = \{(x_1, y_1), (x_2, y_2), \ldots, (x_N, y_N)\}, x \in \mathbb{R}^d, y \in \{+1, -1\} \tag{A.1}$$

where x_i is a vector in a space $\aleph \in \mathbb{R}^d$, N is the number of training samples, and y_i is the label associated to x_i ($y_i = +1$ for class c_1 and $y_i = -1$ for class c_2).

Suppose the two classes are linearly separable. This means that it is possible to find at least one hyperplane defined by a vector w with a bias b, able to separate the classes without error:

$$f(x) = w.x + b = 0 \tag{A.2}$$

where $w \in \mathbb{R}^d$, b $\in \mathbb{R}$ and . standing for the scalar product.

To find such a hyperplane, w and b should be estimated in a way that

$$y_i(w.x_i + b) \geq +1 \; if \; y_i = +1 \tag{A.3}$$

$$y_i(w.x_i + b) < -1 \; for \; y_i = -1 \tag{A.4}$$

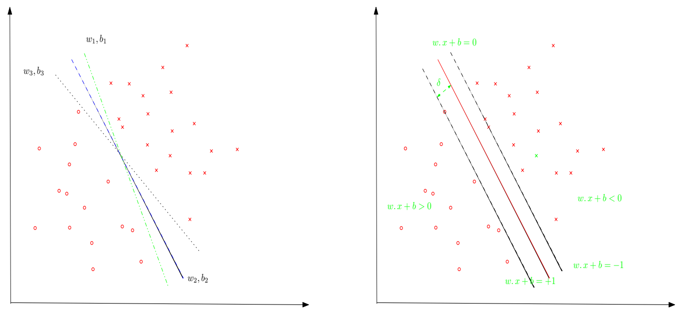

Figure A.1: SVMs for linear separable classes. Left: Several feasible hyperplanes. Right: Optimal separating hyperplane

These two inequalities can be combined under this compact notation

$$y_i(w.x_i + b) - 1 \geq 0 \tag{A.5}$$

The decision function may be expressed as [Cunningham *et al.*, 2008]

$$f_d(x) = sign(w.x + b) \tag{A.6}$$

with $f_d(x_i) = sign(y_i), \forall i \in [1, N]$

Vapnik proposed a training algorithm capable of discriminating samples without any classification errors [Vapnik, 1995]. This algorithm is based on idea that among all possible hyperplanes, there is a unique *optimal hyperplane*, maximising the minimal distance ($\delta - margin$) between the samples and the hyperplane.

Samples closest to the hyperplane are named *Support Vectors* (SV) and are defined by

$$y_i(w.x_i + b) = 1 \tag{A.7}$$

They are all equally close to the optimal hyperplane. One can prove that they are enough to compute the separating hyperplane (hence their name).

If a simple re-scale of the hyperplane parameters w and b takes place, the margin can be expressed as $\frac{2}{\|w\|}$.

The optimal hyperplane can be found by solving the following optimisation problem:

$$\underset{w}{minimise}\, b \frac{1}{2} \cdot (\| w \|)^2 \tag{A.8}$$

$$subject\ to\ y_i(w.x_i + b) \geq 1, i = 1, \ldots, N \tag{A.9}$$

This is a convex optimisation problem (quadratic criterion, linear inequality constraints). Usually the dual formulation is favoured for its easy solution with standard techniques. Using a Lagrangian formulation, the above problem can be translated to:

$$\underset{\lambda_i}{maximise} \sum_{i=1}^{N} \lambda_i - \frac{1}{2} \sum_{i,j=1}^{N} \lambda_i \lambda_j y_i y_j (x_i . x_j) \tag{A.10}$$

$$subject\ to \sum_{i=1}^{N} \lambda_i y_i = 0\ and\ \lambda_i \geq 0, i = 1, \ldots N \tag{A.11}$$

where λ_i are the Lagrange multipliers.

Under this formulation, the optimal parameters λ_i^* provide the classification function f_d:

$$f_d(x) = sign(\sum_{i \in S} \lambda_i^* y_i (x_i x) + b) \tag{A.12}$$

where S is a subset of training samples that correspond to non-zero Lagrange multipliers. These training samples are called support vectors.

A.1.2 Soft Margin

The above method is applicable to linearly separable data. In most cases, classes are not linearly separable, and the constrain of equation A.10 cannot be satisfied. The linear SVM method can be adapted: a soft margin may be used to get better efficiency in a noisy situation. In order to carry out the optimisation, a cost function can be formulated to combine maximisation of a margin and minimization of error criteria, using a set of variables called slack variables, ζ (FigureA.1)

This cost function is defined as

$$minimise\ J(w, b, \zeta) = \frac{1}{2} \parallel w \parallel^2 + C \sum_{i=1}^{N} \zeta_i \tag{A.13}$$

$$subject\ to\ y_i(w.x + b) \geq 1 - \zeta_i \tag{A.14}$$

Dual optimisation may be achieved in the same way as in the separable data case.

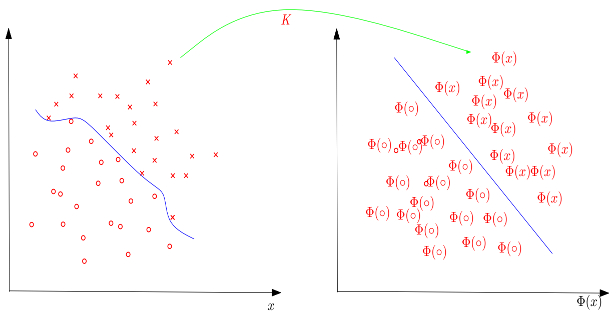

Figure A.2: Kernel Mapping : From Input Space (Left) to Feature Space (Right)

A.1.3 Kernel-Based Classification

The linear SVM classifier previously described finds linear boundaries in the input feature space. To obtain more general decision surfaces, such as non-linear discriminant functions, the Support Vector Machine maps the input vector x into a high dimensional feature space and then performs linear classification in that space. Linear boundaries in the enlarged space translate to non linear boundaries in the original space.

Let us denote the induced space $\mathscr{H}$ via a map Φ :

$$
\begin{aligned}
\Phi : \mathbb{R}^p &\rightarrow \mathscr{H} \\
x &\rightarrow \Phi(x)
\end{aligned}
$$

In the SVM framework there is no assumption on the dimensionality of $\mathscr{H}$ which could be very large, and sometimes infinite. We just suppose that $\mathscr{H}$ is equipped with a dot product. Maximising A.12 now requires the computation of a dot product, $\Phi(x)\Phi(z)$.

One would consider that mapping into a high dimensional feature space would add extra complexity to the problem. But, the inner product of the vectors in the mapping space can be expressed [Bakir *et al.*, 2007] using specific functions K in the original space:

$$K(x, z) = \Phi(x)\Phi(z) \tag{A.15}$$

$K(x, z)$ is called a *kernel function*. If a kernel function K can be found, this function can be used for training without knowing the explicit form of Φ.

The dual optimisation problem is now formed as :

$$maximise \sum_{i=1}^{N} \lambda_i - \frac{1}{2} \sum_{i,j=1}^{N} \lambda_i \lambda_j y_i y_j K(x_i, x_j) \quad (A.16)$$

$$subject\ to \sum_{i=1}^{N} \lambda_i y_i = 0\ and\ \lambda_i \geq 0, i = 1, \ldots N \quad (A.17)$$

The resulting classifier becomes :

$$f(x) = sign(\sum_{i=0}^{N} \lambda_i^* y_i K(x_i, x) + b) \quad (A.18)$$

Using kernel functions is equivalent to mapping the feature vectors into a high dimensional feature space before using a hyperplane classifier there (cf. Figure A.2). Everything about the linear case also applies to non-linear cases, using a suitable kernel, K, instead of the Euclidean dot product.

In this research, three kinds of kernels have been tested. These kernels are mathematically defined by equations A.19-A.22 [Chang and Lin, 2001].

$$1.\ Linear\ kernel\ K(x_i, x_j) = {x_i}^T . x_j \quad (A.19)$$

$$2.\ Polynomial\ kernel\ K(x_i, x_j) = ((\gamma . {x_i}^T . x_j) + 1)^d, \gamma > 0 \quad (A.20)$$

$$3.\ Gaussian\ radial\ basis\ function\ kernel\ K(x_i, x_j) = e^{\frac{1}{2}(\frac{\|x_i - x_j\|}{\sigma})^2} \quad (A.21)$$

There is no theory regarding which kernel is the best, given a problem domain. It is important to select the appropriate kernel based on the specific application.

A.1.4 SVM Multi-class Classification

The SVM method was designed to be applied only for two class problems. For multi-class problems, the linear SVM approach may be extended using many linear machines to create boundaries consisting of sections of hyperplanes. When linear discrimination is not effective, an appropriate nonlinear mapping can be found. The basic idea is to reduce the multi-class to a set of binary problems so that the SVM approach can be used. Two main approaches have been proposed:

The first approach is called *one-against-all*. In this approach, a set of binary classifiers is trained to be able to separate each class from all others. Then each data object is classified to the class for which the largest decision value was determined [Hsu and Lin, 2002]. This method trains N SVMs (where N is the number of classes) and there are N decision functions. Although it is a fast decision function it suffers from errors caused by marginally imbalanced training sets. An alternative approach proposed by [Hsu and Lin, 2002], similar to the *one-against-all* method, uses one optimisation problem to obtain N decision functions. Reducing the classification to one optimisation problem may require less SVs then a multi-class classification based on many binary SVMs.

The second approach is called *one-against-one*. In this approach, a series of classifiers is applied to each pair of classes with the most commonly computed class kept for each object. Then a max-win operator is used to determine to which class the object will be finally assigned. The application of this method requires $N(N-1)/2$ machines to be applied.

We adopted the *one-against-all* method to tree species classification task presented in Chapter 5.

Recent approaches have been developed in the *machine learning* community to tackle this multi-class optimisation problem [Bordes *et al.*, 2007]. Unlike approaches decomposing multi-class categorisation problems into multiple binary classification tasks, Crammer and Singer generalise the notion of the margin to multi-class problems [Crammer and Singer, 2002]. The notion of margin proposed yields a direct method for training multi-class predictors and based on the dual of the optimisation problem, the dual problem can be decomposed into multiple optimisation problems of reduced size.

A.1.5 Implementation Details

The SVM library used to perform classification experiments presented in Chapters 3 and 5 of this thesis is the LIBSVM [Chang and Lin, 2001]. It is a simple and easy-to-use support vector machines tool for classification, regression, and distribution estimation. It includes a graphical user interface for both classification and regression. LIBSVM can easily be linked to standalone applications. LIBSVM includes efficient multi-class classification, cross validation for model selection and probability estimates. The package includes the source code of the library in C++ and Java, and a simple program for scaling training data.

A.2 Classifier Evaluation Protocol

To compare the performances of the classifiers, accuracy measure alone is not adequate as class distributions and miss classification costs are not uniform. To evaluate the performances of the proposed approaches, Receiver Operating Characteristic (ROC) graphs have been used. A ROC graph depicts tradeoffs between hit rate and false alarm rate [Egan, 1975]. To further present classifier evaluation, the terminology used will be presented in the following [Provost and Fawcett, 1997].

Let p, n be the positive and negative instance classes, and let Y, N be the classifications produced by a classifier. Let $p(p|I)$ be the posterior probability that instance I is positive. The true positive rate (TP) of a classifier is:

$$TP = p(Y|p) \approx \frac{\text{positives correctly classified}}{\text{total positives}} \tag{A.22}$$

The false positive rate (FP) of a classifier is :

$$FP = p(Y|n) \approx \frac{\text{negatives incorrectly classified}}{\text{total negatives}} \tag{A.23}$$

On a ROC graph, true positive (TP) is plotted on the Y axis and false positive (FP) is plotted on the X axis. These statistics vary together and a threshold on a classifier's continuous output is varied between its extremes. The best model corresponds to the point on the curve which is closest to the upper left corner (TP rate equals 1 and FP rate equals 0).

A.3 Assessment of Classification Accuracy

Confusion matrices are used to asses the accuracy of the classification [Richards and Jia, 1999]. They are used in this thesis to asses the accuracy of tree species classification results for each classification scheme presented in Chapter 5.

Confusion matrices not only indicate classification accuracy but also pairs of miss classification (or confusion) between classes. They are a means of knowing the nature of miss classification, i.e. the confusion class.

Given a data set with N labelled classes and associated labels. Let L_i with $i = 1, \ldots, N$ denote the assembly of elements labelled as L_i.

Let C_j with $j = 1, \ldots, N$ be the assembly of elements classified as L_j.

The the confusion matrix CM is given by:

$$CM(i, j) = |L_i \cap C_j| \tag{A.24}$$

Each column of the matrix represents samples in a ground truth class, while each row, samples which have been classified as belonging to the actual class. On the major diagonal the number of correct classified samples for each class is given while the rest of the elements $CM(i, j)$ indicate the number of samples belonging to the L_i class classified as belonging to the L_j class.

In addition to showing errors of omission (samples belonging to the class of interest that the classifier has failed to recognise) and commission (samples from other classes that the classifier labelled as belonging to the class of interest), the confusion matrix can be used to compute other accuracy measures such as *overall accuracy*, *producer's accuracy* and *user's accuracy* [Congalton and Green, 2008]. *Overall accuracy* is the sum of the major diagonal (i.e. the correctly classified sample units) divided by the total number of sample units in the entire error matrix. Producer's and user's accuracies are ways of representing individual category accuracies. The first one gives the probability that the classifier has labelled the sample as belonging to class L_i given that the actual class is L_i and the latter gives the probability that the actual class is L_i given that the pixel has been labelled as L_i. In general terms, for a particular category, *user's accuracy* is computed by dividing the number of correctly classified samples by the total number of samples that were classified as belonging to that category while *producer's accuracy* is computed by dividing the number of samples that have been classified correctly by the total number of reference samples in that class.

Appendix B

Tree Species Ground Truth Data

The speed with which extensive areas can be mapped is a significant advantage of remote sensing. Current techniques allow the interpretation of remote sensing data to determine standard land cover types. In this thesis we present an image processing system designed for vegetation detection and characterisation in urban areas. To determine the species of trees delineated this system, ground-truth data collection is a necessity. This Appendix describes the protocol used for collecting data necessary to determine the tree species present in the examined area. It will show the distribution of 15 tree species associated to sites A, B and C presented in Chapter 2. This data is used in a classification framework both to generate tree species distribution map for the study area and to measure the accuracy of tree species map (cf. Chapter 5).

The goal of the field work is to identify sufficient information on the ground to allow an accurate interpretation of the tree species.

B.1 Fieldwork Planning and Preparation

Reference data for tree species identification was collected in September 2006 during a field acquisition campaign in the city of Marseille, France. The acquisition campaign lasted for 2 days and accounted for a total of 16 hours of work. Field data was collected between 10 a.m. and 17 p.m. local standard time.

B.1.1 Site Selection

The selection of sites was made by visual inspection of the orthoimage of the Marseille city. Four sites were chosen for field data acquisition according to following criteria:

- areas should contain tree samples on public domain
- different types of urban vegetation should be present the specific area: street trees, single trees, trees in public parks, etc.

- several tree species should coexist in the area

The sites were also chosen with respect to access conditions so that data acquisition should be possible. Figure B.1 presents the three areas chosen for field data collection.

B.2 Field Equipment and Procedures

B.2.1 Field equipment

The MATIS [1] laboratory of IGN provided equipment used for the field acquisition campaign. Generally, the type of equipment depends on the type of data to be recorded. For the goal of identifying tree species for classification purposes sample field images whole trees, distinctly presenting tree crown and trunk characteristics at a high resolution are sufficient information for a biologist to distinguish between different tree species.

Therefore, the equipment used was made up of

- Laptop with aerial acquisition campaign management software presenting data for the study area
- Digital camera
- Aerial photo data sheets

B.2.2 Procedure

The process at each tree location will take about 10 to 15 minutes, depending on sample's access conditions. Indeed, some tree samples were nor accessible as they belonged to private courtyards or they were no longer present on the ground, or they were replaced by younger trees. Therefore, an important step, and the first one was to establish a correspondence between field data and image data. Once the tree identified, its position was marked into the GIS software. Then, image data was collected for each tree, starting with the trunk, and continuing with the tree's crown and whole shape image recording. Next, leaf samples were collected and registered into an index file associating each leaf sample to the tree's location and acquired images. This was the last step of the data acquisition procedure and recordings were stored in the GIS software.

Figure B.2 presents sample images recorded for tree samples of the Marseille data set, site B.

[1] *Méthodes d'Analyses et de Traitement d'Images pour la Stéréo-restitution*

(a)

(b)

(c)

Figure B.1: Marseille sites selected for field data collection. (a) Site A. (b) Site B. (c) Site C.

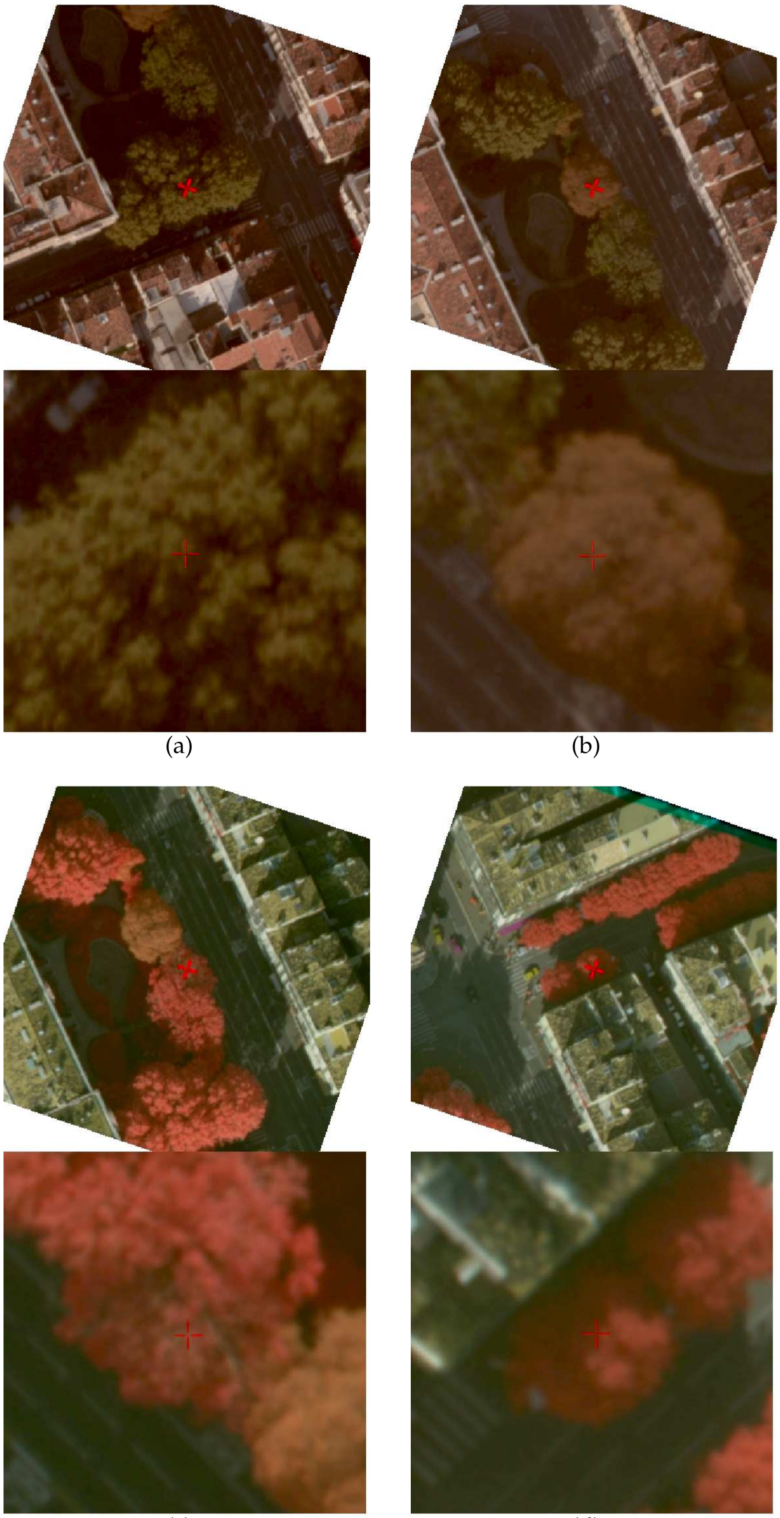
(a) (b) (c) (d)

Figure B.2: Examples of recordings made by the acquisition management software for site B, Marseille data set. Each tree marked by a red cross is linked to field recordings presented in figure B.3. (a) RGB image and enlarged crop of a *Type1* tree. (b) RGB image and enlarged crop of a *Type3* type. (c) False colour image and enlarged crop of a *Type4* tree. (d) False colour image and enlarged crop of *Type7* tree.

(a) *Type1*

(b) *Type3*

(c) *Type4*

(d) *Type7*

Figure B.3: Examples of tree recordings for site B, Marseille data set. For each tree presented in figure B.2 A set of four images recorded on ground is presented. (a) RGB image and enlarged crop of a *Type1* tree. (b) RGB image and enlarged crop of a *Type3* type. (c) False colour image and enlarged crop of a *Type4* tree. (d) False colour image and enlarged crop of *Type7* tree.

B.3 Field Data Collection

Data collection campaign focused on gathering field data of tree and vegetation species present within the study area.

B.3.1 Field Data Collection Protocol

Data types to be collected for each tree includes:

image data:

one image containing details of the tree's trunk such as colour, roughness, ...

one image of the tree's leaves

one image of the entire tree, trunk and crown

specimen data:

one leaf was collected for each tree each time this was possible

B.4 Field Data Analysis

One of the most critical steps in data collection is the post processing one, including phases like error checking and compilation of the tree species database. This was done in the lab and consisted in a thorough data evaluation. *Bad data* was eliminated from the final database and all data resulting from the fieldwork was put on a CD which was sent to the Inventaire Forestier National, for species identification.

B.5 Identification of Tree Species

Tree species were identified by the Inventaire Forestier National,(IFN) (French National Forest Inventory Agency), on the basis of data recordings made on field. The results of the tree species identification was provided to us in form of a spreadsheet containing the comment and scientific names associated to each tree label.

Table B.1 presents common and scientific names associated to tree species labels assigned during the field acquisition campaign. A total of 15 species were identified in the four areas from the Marseille data set.

From the total number of tree species in the Marseille area, there were only 6 of them with enough tree samples to perform a tree species classification approach. Examples of these tree species are given in Chapter 5, section 5.3.3.

Table B.1: Common and scientific name associated to tree species labels.

Tree species id	Common name	Scientific name
Type1	Platane	Platanus sp.
Type2	Chêne vert	Quercus ilex L.
Type3	Marronnier	Aesculus hippocastanum L.
Type4	Sophora du Japon	Sophora japonica L.
Type5	Tilleul	Tilia sp.
Type6	Micocoulier	Celtis australis L.
Type7	Mûrier	Morus alba L. ou Morus nigra L.
Type8	Pin parasol	Pinus pinea L.
Type9	Filaire	Phillyrea sp.
Type10	Laurier sauce	Laurus nobilis L.
Type11	Cyprès de Provence	Cupressus sempervirens L.
Type12	Olivier	Olea europaea L.
Type13	Figuier	Ficus carica L.
Type14	Albizia	Albizia julibrissin Durazz.
Type15	Palmier	Washingtonia robusta

Appendix C

Extended Summary in French/Resumé Etendu en Francais

Le texte retranscrit à la suite dans cette annexe correspond à la publication qui a été acceptée pour publication en 2009 dans le journal RFPT *Revue Française de Photogrammétrie et de Télédétection* édité par la SFPT *Société Française de Photogrammétrie et de Télédétection*. Bien que n'en recouvrant pas la totalité, ce texte constitue un résumé important, en langue française, des travaux présentés auparavant [Iovan *et al.*, 2009].

Introduction

La modélisation 3D des zones urbaines est un enjeu actuel important pour des nombreuses applications liées à l'aménagement du territoire, l'urbanisme ou la gestion de l'environnement. Un large éventail de techniques de traitement automatique d'images aériennes, a été proposé depuis plusieurs années pour la reconstruction 3D des environnements urbains. Ces approches sont aussi nombreuses que variées, tant en ce qui concerne le type de données utilisées que sur le plan du degré d'automatisation de la méthode. De nombreuses études ont porté sur l'analyse des bâtiments, que ce soit pour contrôler l'étalement urbain, cartographier les modes d'utilisation du territoire urbain et des infrastructures ou pour reconstruire les environnements urbains. Cependant, la plupart des modélisations se limitent aux objets créés par l'homme (bâti, route...). Ainsi, si la recherche a atteint la maturité en ce qui concerne la reconstruction d'objets fabriqués par l'homme [Taillandier and Vallet, 2005] beaucoup de défis subsistent concernant la modélisation d'autres objets tels que les arbres, les arbustes, les haies ou les pelouses. Or la végétation est également très importante pour la compréhension des zones urbaines. Les modèles urbains 3D peuvent être améliorés par l'intégration de la végétation, avec une description précise de la disposition des arbres et des espèces. Si jusqu'à récemment, la modélisation des milieux urbains s'est notamment axée sur la cartographie de l'occupation des sols et le suivi des zones urbanisées à partir des données dans le domaine visible et proche infrarouge, avec l'accès aux donnes très haute résolution spatiale, de plus en plus de recherches relèvent le défi représenté par la végétation urbaine. Ainsi, si pour des résolutions spatiales d'ordre kilométrique les applications portaient notamment sur la détection des grands ensembles paysagers, à mesure que la résolution augmente, les applications évoluent vers la classification des espèces végétales en passant par une étape de classification des terrains agricoles de grande étendue et de couverts forestiers. Pour des applications d'urbanisme, les données aériennes couleur et infrarouges sont utilisées pour analyser l'état phytosanitaire et la vitalité des arbres en milieux urbain en exploitant des informations de couleur et texture [Fuhrer *et al.*, 1981],[Hermans *et al.*, 2003], tandis que pour des applications de visualisation et reconstruction 3D [Baillard *et al.*, 1998] ces données peuvent être enrichies avec des modèles numériques d'élévation issues des données laser [Straub and Heipke, 2001]. D'autres études utilisent des données Lidar [Haala and Brenner, 1999] ou hyper-spectrales [Ouma and Tateishi, 2008] pour analyser ou classifier par espèces les types de végétation présents en milieu urbain.

Nous présentons un système hiérarchique pour analyser la végétation urbaine à partir d'images aériennes couleur et infrarouges à très haute résolution et d'un modèle numérique d'élévation. Le système proposé détecte les zones de végétation et les classifie en végétation haute et basse. Les houppiers de chaque arbre sont ensuite individualisés par un algorithme de segmentation d'images. Des paramètres géométriques (la hauteur, le diamètre de la couronne, la localisation du tronc des arbres) sont estimés pour chaque arbre. Une classification supervisée pour caractériser les espèces d'arbres est ensuite effectuée pour chaque objet ainsi extrait. Finalement, un rendu réaliste de l'environnent virtuel urbain est obtenu en intégrant des modèles virtuels d'arbres.

Site d'étude et données

Le site urbain sur lequel porte notre étude est la ville de Marseille. C'est une agglomération contenant de nombreux espaces verts (parcs, jardins), autant sur le domaine public que privé. La végétation, fortement imbriquée entre les bâtiments, est présente le long des routes ou dans les cours d'immeubles. Nous nous intéressons ici à tout type de végétation présente sur l'espace public de la ville. Nous disposons d'images aériennes couleur et infrarouges acquises simultanément par quatre capteurs différents en novembre 2004. Ces images ont une résolution de 20 cm/pixel. L'étude se situe dans un contexte multi vues, c'est-à-dire que chaque point du terrain est vu dans plus de 2 images (en moyenne entre 6 et 9). Dans les images de la Figure C.1, on peut observer une image RVB représentant le centre-ville de Marseille Figure C.1-(a) et le canal IR correspondant Figure C.1-(b).

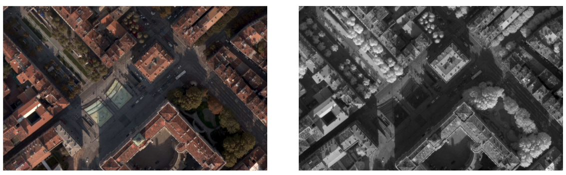

(a) (b)

Figure C.1: Centre ville de Marseille : (a) Image RVB. (b) Canal IR.

Nous disposons également d'un modèle numérique d'élévation (MNE) obtenu de façon automatique par corrélation d'images, en utilisant l'algorithme présenté dans [Pierrot-Deseilligny and Paparoditis, 2006]. Un MNE est une représentation maillée de l'altitude de l'ensemble des objets vus sur les clichés (sol, ruptures de pente, bâtiments, végétation, routes, ponts, etc.). Le contexte multi vues dans lequel nous nous situons, rend possible l'obtention d'un MNE très dense, ayant un important degré de détail, et une précision de 20 cm.

La méthodologie mise en œuvre se décompose en cinq étapes successives que nous décrirons dans la suite. La première étape consiste à identifier toute région contenant de la végétation (arbres, arbustes ou pelouses). Nous proposons une approche d'extraction de végétation reposant sur une classification supervisée, utilisant un classifieur fondé sur les séparateurs à vastes marges (SVM) [Boser *et al.*, 1992]. Une fois ces zones identifiées, la végétation haute (arbres) et la végétation basse (pelouses) sont séparées par analyse de la variance du MNE. Une méthode de segmentation des régions est ensuite appliquée pour individualiser les houppiers d'arbres. Cette méthode repose sur une analyse géométrique locale du MNE. Pour chaque arbre ainsi délimité, un vecteur de paramètres est calculé et utilisé pour déterminer leurs espèces par classification SVM. Enfin, l'ensemble des informations caractérisant la végétation extraite, permet de paramétrer et de positionner un modèle 3D de végétation réaliste.

Détéction de la végétation

Le milieu urbain est un mélange de portions de routes, de bâtiments, de zones herbacées, boisées et de sols nus. Les signatures spectrales de ces différents types d'éléments peuvent être très proches, tel que les surfaces minérales et les matériaux de construction. Leur réflectance spectrale peut connaître des variations importantes en fonction de leur couleur, brillance, orientation ou inclinaison. De plus, les conditions atmosphériques au-dessus des milieux urbains sont fortement perturbées par la présence de gaz et poussières émises par les installations industrielles. Ces facteurs induisent de grandes variations dans la réflectance spectrale apparente d'un même matériel urbain [Bannari *et al.*, 1999]. Les méthodes traditionnelles de télédétection utilisent des "indices de végétation" pour détecter la végétation. De nombreux indices sont proposés dans la littérature [Gong *et al.*, 2003], le plus utilisée étant le NDVI (Normalized Difference Vegetation Index) [Rouse *et al.*, 1974] qui par construction accentue les zones dont le niveau d'infrarouge est élevé par rapport à celui du rouge, et met en valeur la végétation. Cependant, ce type d'indice initialement développé pour le traitement d'images satellitaires n'est pas adapté au traitement d'images aériennes acquises au-dessus des agglomérations urbaines. Il apparaît en effet que certains matériaux de construction présentent, dans cet espace de représentation, une réponse proche de celle de la végétation. Pour pallier ce problème, nous avons développé une méthode robuste reposant sur une classification supervisée utilisant un SVM. Les zones d'apprentissage ont été saisies à la main et contiennent des pixels de végétation et des pixels de non-végétation. Pour chaque pixel, nous calculons un vecteur de caractéristiques à partir des valeurs de réflectance spectrale dans les 4 canaux, rouge (R), vert (V), bleu (B) et infrarouge (IR). Comme la plupart des indices spectraux utilisés dans la littérature pour détecter les zones de végétation sont des combinaisons linéaires des réflectances des pixels, nous avons choisi un noyau linéaire pour le classifieur. Les résultats obtenus pour l'approche proposée pour la détection de la végétation en milieu urbain par classification supervisée sont présentés dans la Figure C.2, pour la zone de test présenté dans les Figures C.1-(a) et (b).

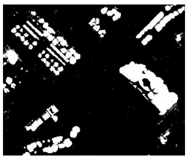

Figure C.2: Détection de végétation en milieu urbain par classification supervisée par SVM : Masque de végétation obtenue pour la zone d'étude présenté en Figure C.1.

La pertinence de l'approche que nous proposons est mise en avant par la comparaison des résultats ainsi obtenus avec les résultats obtenus pour la même zone par une combinaison des indices spectraux, illustrés dans la Figure C.3. Le masque de végétation obtenu pour la même zone utilisant l'index NDVI est présenté dans Figure C.3-(a). Au premier abord, il n'y a pas de différence notable entre ce masque de végétation et celui présenté dans la Figure C.2.

Dans le rectangle situé dans la partie supérieure de l'image présenté dans la Figure C.3-(a), des parasols bleus peuvent être identifiés. Dans l'image NDVI ces parasols seront confondus à la végétation suite à la binarisation de l'image. Le système de détection de végétation par classification supervisée permet d'éviter cette erreur. Les taux de bonnes classifications sont bons pour les deux méthodes, variant de 87.5% pour la méthode utilisant des indices spectraux à 98.5% pour la méthode de classification supervisée par SVM. Les résultats de la méthode basée sur l'indice NDVI pourraient être améliorés en combinant plusieurs indices spectraux. Ce faisant, le nombre des seuils pour la décision augmenterait avec chaque nouvel indice introduit. C'est pourquoi la méthode de classification supervisée basé sur les SVM est préférée pour l'étape de détection de végétation.

Segmentation de la végétation

Le second module de notre système a pour objectif de séparer les régions de végétation basse (les pelouses) des régions contenant la végétation haute (arbres). Pour cela, la méthode proposée exploite les variations locales du MNE. Notre

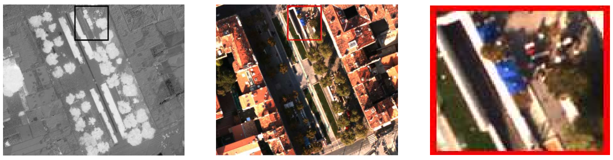
(a) (b) (c)

Figure C.3: Détection de végétation en milieu urbain par indices spectraux. **(a)** Image NDVI présentant les pixels de végétation. **(b)** Image RVB correspondante. **(c)** Extrait agrandi de l'image (b) présentant des parasols classifiés comme végétation.

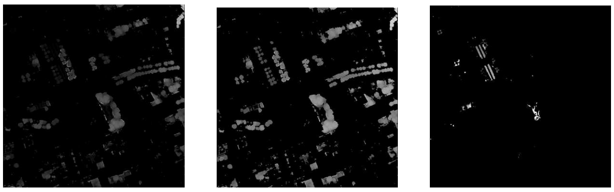
(a) (b) (c)

Figure C.4: Séparation entre la végétation haute et basse. **(a)** L'image de variance calculée sur les zones de végétation correspondantes sur le MNE. **(b)** Masque d'arbres. **(c)** Masque de pelouses.

approche repose sur la différence de rugosité entre la surface d'un arbre et d'une pelouse. L'indice de rugosité utilisé ici est obtenu à partir de la variance locale du MNE. La variance est calculée avec :

$$V = \sum \frac{(x_{ij} - M)^2}{(n-1)} \tag{C.1}$$

où x_{ij} est l'altitude du pixel (i,j) sur le MNE; n est le nombre des pixels dans le voisinage choisi et M est la moyenne des pixels dans le voisinage calculé avec :

$$M = \frac{\sum x_{ij}}{n} \tag{C.2}$$

La variance locale de l'altitude a été calculée dans un voisinage de 11x11 pixels. L'image de variance ainsi obtenue est classée en pelouses et arbres en utilisant une méthode de binarisation basée sur l'histogramme des variances. La taille de voisinage pour le calcul de la variance ainsi que le seuil pour la binarisation ont été déterminées de façon empirique. La Figure C.4-(a) présente l'image de variance calculée sur le MNE correspondant aux zones de végétation auparavant identifiées. Les résultats de la segmentation en arbres et pelouses sont présentés sous la forme de masques dans les Figures C.4-(b) et Figure C.4-(c).

Les résultats de classification obtenus pour la séparation pelouses/arbres ont été évalués grâce à une vérité terrain saisie manuellement par un opérateur humain et les résultats obtenus sont de très bonne qualité avec un taux de bonnes classifications de 97%. Ce taux est obtenu en calculant le rapport entre le nombre des pixels correctement classifiés et le nombre total des pixels.

De nombreuses recherches portent sur l'individualisation automatique des houppiers d'arbres à partir des images aériennes ou satellitaires. Parmi les différentes approches proposées, nous notons une première classe de méthodes basées objet, qui utilisent des modèles de houppiers d'arbres pour estimer la position du sommet des arbres [Pollock, 1996], [Larsen, 1997], [Perrin, 2006]. Une autre famille d'approches exploite les ombres projetées par les couronnes pour estimer leurs contours [Gougeon and Leckie, 2001] en cherchant les vallées entre les couronnes [Gougeon, 1995c] ou par croissance de régions [Erikson, 2004a]. D'autres approches reposant sur le contour utilisent une analyse multi-échelle [Brandtberg and Walter, 1998] ou des contours actifs [Horváth *et al.*, 2006a] pour individualiser les houppiers d'arbres. Enfin, d'autres méthodes utilisent l'information de maximum local pour déterminer les sommets ainsi que le nombre d'arbres [Pinz, 1998], [Wulder *et al.*, 2004].

Pour individualiser les arbres, nous avons développé un algorithme de croissance de régions, à partir du MNE correspondant aux régions de végétation haute. Notre approche est composée de deux étapes : la première est destinée à trouver le sommet de chaque arbre, appelé "graine", qui est étendue dans la seconde étape, jusqu'à atteindre la surface correspondant au houppier de l'arbre considéré.

Traditionnellement, les méthodes de croissance de régions (CR) développées pour la segmentation d'images commencent par la recherche aléatoire des graines auxquelles on ajoute successivement les pixels voisins satisfaisant un critère de similarité. Ce processus se poursuit jusqu'à ce que tous les pixels de l'image soient étiquetés. Il est possible de scinder la procédure de segmentation en deux étapes, l'une dans laquelle les pixels représentant des graines sont choisis, et une deuxième, de croissance de régions. Les performances de ce type de méthodes de segmentation sont très dépendantes du nombre de graines (le nombre de régions détectées étant égal au nombre de graines) ainsi qu'au choix du critère de similitude utilisé pour la croissance des régions.

Notre approche exploite la géométrie du MNE pour l'individualisation des arbres. L'étape de choix des graines débute par un flou gaussien sur le MNE, qui permettra de lisser la surface. Le modèle numérique d'élévation flou ainsi obtenu sera dénommé dans la suite MNEF. Le principe du choix des graines repose sur la détection des maxima locaux du MNEF. Cependant, lorsqu'on se contente d'une simple détection d'annulation de gradient, on constate que certains arbres présentent plusieurs maxima locaux, posant alors un problème de sur-détection. Nous proposons, pour résoudre ce problème, la méthode suivante : - le pixel correspondant à la hauteur maximale du MNEF constitue le point de départ de l'algorithme. Ce point correspondant au sommet de l'arbre le plus haut constituera la première graine de l'algorithme. La hauteur d'analyse h sera ensuite décrémentée d'un pas δ h et une croissance de régions autour de la première graine détectée sera effectuée pour les pixels dont la hauteur correspond à l'intervalle [h ; h + δ h[. La zone ainsi obtenue, sera dénommée "zone d'interdiction" . Elle sera composé par les pixels connexes à la région définie comme graine, dont la hauteur est comprise entre celle des pixels en limite de graine et la hauteur δ h; - ensuite, l'ensemble des zones formées par les pixels appartenant à l'intervalle [h ; h + δ h[est analysé et les zones n'étant pas connectées à une zone d'interdiction sont étiquetées comme nouvelles graines ; - l'opération sera répétée jusqu'à ce que la hauteur d'analyse atteigne zéro. On notera que les graines ne sont pas représentées par des pixels isolés mais par des groupes de pixels (dont la taille dépend de δh).

Le principe de zone d'interdiction permet de réduire sensiblement le nombre de sur-détections. La Figure C.5 illustre cette méthode.

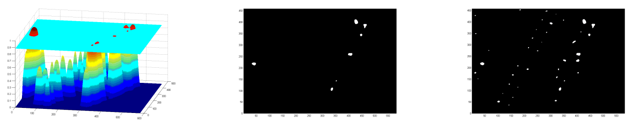

(a) (b) (c)

Figure C.5: Recherche des graines sur le MNEF. **(a)**Visualisation 3D du MNEF correspondant aux arbres: Tous les points ayant une hauteur supérieure à la hauteur de l'analyse h seront évalués pour la recherche des graines. **(b)** Visualisation 2D de la 30ème itération. **(c)**Les graines sont détectées après la dernière itération : nous pouvons observer que nous obtenons une graine pour chaque arbre.

A partir des graines ainsi obtenues, les contours de chaque houppier sont obtenus par une croissance de régions contrainte par des critères géométriques. L'approche est similaire à celle de la recherche des graines, en prenant en compte l'altitude correspondante à chaque pixel voisin des graines (sommets des arbres) : la hauteur d'analyse h est décrémentée itérativement et à chaque itération une croissance des régions est effectuée pour les pixels dont l'altitude est supérieure à h. Ce principe permet d'assurer que les pixels ajoutés par croissance appartiennent bien au même arbre.

La valeur de δh à été fixée à 3 de façon empirique pour pouvoir tester l'intégralité des graines potentielles pour chaque arbre. Cela permet d'estimer un modèle de végétation le plus fidèle à la réalité en ce qui concerne le nombre d'arbres pour une meilleure intégration dans le modèle 3D urbain.

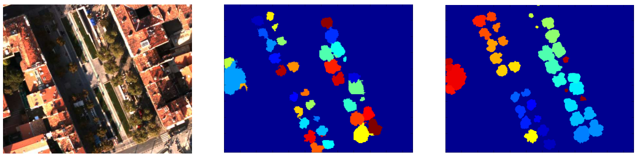

(a) (b) (c)

Figure C.6: Résultats obtenus pour l'individualisation des houppiers. **(a)** Données d'entrée. **(b)** Résultats pour la délimitation automatique des houppiers. **(c)** Données de référence pour la délimitation des houppiers.

Les résultats obtenus par cette méthode sont illustrés dans la Figure C.6-(b) sur la zone de test présentée dans la Figure C.6-(a). Les données de référence présentées dans la Figure C.6-(c) seront utilisées pour évaluer la précision de notre algorithme.

L'approche utilisée pour l'évaluation est similaire à celle présentée dans [Mei and Durrieu, 2004]. Une analyse statistique est d'abord effectuée en prenant en considération le nombre total d'arbres dans la vérité terrain, les faux négatifs (arbres manquants) ainsi que les faux positifs (les régions n'ayant pas de correspondant arbre). Nous prenons en considération les cas suivants pour l'analyse spatiale de la segmentation: segments purs, arbres sur-segmentés et arbres sous-segmentés. Les segments purs sont des segments correctement identifiés et correspondant aux arbres. Nous considérons qu'un segment est 100 % pur s'il correspond à un et un seul segment dans la vérité terrain avec une zone de chevauchement supérieure à 80 %. La sur-segmentation des arbres correspond au cas où plus d'un segment est associé à la délimitation de la vérité terrain. La sous-segmentation correspond à des segments qui comprennent une partie importante (>10 %) de plus d'un arbre. Les résultats de l'évaluation de la précision de la segmentation sont présentés dans le Tableau C.1.

Table C.1: Évaluation de la précision de la segmentation des arbres.

	Quantité	**% du nombre total d'arbres**
Arbres correctement segmentées	32	78.0
Arbres sur-segmentées	1	2.4
Arbres sous-segmentées	4	9.7
Arbres omis	4	9.7
Nombre total d'arbres	41	
Nombre total d'arbres détectes	37	

Caracterisation de la végétation

A partir des résultats obtenus par la méthode de segmentation des régions, nous pouvons estimer pour chaque arbre, le diamètre de sa couronne, la hauteur ainsi que sa localisation sur le sol. La Figure C.7 présente les caractéristiques estimées pour un arbre sur le MNE, à partir du résultat de segmentation des houppiers d'arbres correspondants.

(a) (b) (c)

Figure C.7: Estimation 3D des caractéristiques des arbres. **(a)** Estimation de surface de projection au sol de la couronne de l'arbre. **(b)** Estimation de taille de la couronne de l'arbre. **(c)** Estimation de la hauteur de l'arbre.

Le diamètre de la couronne peut être estimé comme le diamètre du segment correspondant à la couronne de l'arbre (cf. Figure C.7-(a) et (b)). Ainsi, le diamètre est calculé avec :

$$diam\grave{e}tre = 2 * \sqrt{\frac{A}{\pi}} \tag{C.3}$$

où A représente l'aire de chaque région déterminée en exploitant la taille des pixels. Nous estimons la position du tronc de l'arbre sur le sol comme étant le barycentre du segment correspondant à la couronne de l'arbre. La hauteur d'un arbre (cf. Figure C.7- (c)) est estimée comme étant l'écart entre la base de l'arbre et son sommet. L'altitude du terrain au pied de l'arbre est calculée à partir du modèle numérique de terrain (MNT), qui est une représentation numérique de toute surface topographique et qui est obtenu en utilisant l'algorithme présenté dans [Champion and Boldo, 2006]. Les sommets des arbres sont estimés comme correspondant à l'emplacement du point maximum de chaque graine extraite lors de l'étape d'individualisation des arbres. La hauteur des arbres est donc directement calculée sur le MNE normalisé (nMNE). Le nMNE est calculé comme la différence entre le MNE et le MNT.

Classification des espèces d'arbres

Le sujet de classification des espèces d'arbres à été premièrement étudié dans le domaine de l'étude forestière, où les techniques numériques d'interprétation d'images aériennes/satellitaires étaient utilisées dans des buts d'inventaire et de gestion forestière [Gougeon, 1995b]. En fonction de la résolution spatiale des données d'entrée, les objectifs de ces études portaient sur un large éventail d'applications. Alors que les données à haute résolution étaient utilisées pour une classification pixellaire des différents houppiers [Erikson, 2004a] les données ayant une faible résolution spatiale étaient le plus souvent exploitées pour reconnaître une espèce d'arbre donné [Gillis and Leckie, 1993].

La classification des espèces d'arbres en milieu urbain est un grand défi, en raison de la grande hétérogénéité spectrale dans le milieu urbain, des ombres portées des couronnes d'arbres, de la variabilité des conditions d'illumination, du mélange important d'espèces d'arbres, de la grande diversité des âges et des formes des arbres. Malgré l'intérêt croissant de la recherche au cours des dernières années, les études visent principalement l'extraction automatique de structures de végétation à partir des images aériennes [Straub, 2003a]. La méthode de classification des espèces d'arbres en milieu urbain que nous proposons est une méthode de classification supervisée utilisant les SVM. Des vecteurs de caractéristiques sont formés à partir des indicateurs de texture calculés autant pour une approche pixellaire que pour une approche par régions. Les deux approches sont présentés et les résultats obtenus sont évalués et comparés à une vérité terrain définie manuellement. Les espèces d'arbres sont définies par différentes caractéristiques, telles que la hauteur moyenne, la forme de la couronne d'un arbre, la forme et couleur des feuilles, la densité de feuilles de la couronne, les caractéristiques spectrales de la couronne. Pour classifier différentes espèces d'arbres du point de vue radiométrique, une description détaillée de leur canopée est nécessaire. La réflectance des végétaux dépend de la configuration au moment de l'acquisition des données, de la réflectance du sol, de la réflectance des feuilles, de leur architecture (qui dépend de la taille d'une feuille, de la hauteur de la canopée, de l'indice foliaire (Leaf Area Index (LAI)), de l'inclinaison des feuilles, etc.), des conditions d'illumination. Nous présentons dans ce qui suit une analyse sur le lien entre l'architecture d'une plante et des feuilles des arbres, et leur réflectance spectrale [Jacquemoud and Feret, 2007]. La réflectance spectrale se définit comme la quantité d'énergie réfléchie par rapport à celle reçue en fonction de la fréquence du rayonnement incident. La végétation réfléchit fortement dans la partie de proche infrarouge du spectre, et peu dans la région du visible. La signature spectrale d'un arbre dépend de la réflectance de ses feuilles. Elle est due à de nombreux facteurs issus de ses constituants : eau, matière sèche, chlorophylle et pigments. La chlorophylle, qui donne sa couleur verte à la végétation, est à l'origine de 70% de la réflectance totale dans le visible. Or, la chlorophylle est présente de la même façon dans les feuilles de toutes les plantes, quelque soit leur espèce. En revanche, dans l'infrarouge, le rôle de la chlorophylle est nettement moins important et la réflectance est alors surtout due à l'inclinaison des feuilles et au LAI. Ainsi, du point de vue théorique un feuillu pourrait être différencié d'un résineux dans le proche infrarouge, car le premier à une densité de feuilles supérieure au deuxième. Il est généralement possible de distinguer feuillus et résineux (adultes) et parfois identifier certaines espèces en particulier lorsque l'acquisition a eu lieu à un stade phénologique précis, tel que la floraison (qui peut donner des propriétés spectrales spécifiques pour certains arbres). Cependant, l'inclinaison des feuilles et l'indice foliaire sont difficilement mesurables sur des données ayant la résolution des données utilisées dans cette étude et acquises en novembre, quand la plupart des végétaux perdent leurs feuilles, malgré le climat méditerranéen. Les caractéristiques de taille et forme sont également des caractéristiques discriminantes entre les espèces d'arbres. En ce qui concerne la taille des arbres, même si cette caractéristique permettrait une distinction entre deux espèces à l'âge adulte, elle varie avec l'âge pour une même espèce. Quant à la forme des arbres, celle-ci ne représente pas une caractéristique discriminante pour la classification des espèces d'arbres, car souvent les arbres en ville sont taillés. Les images sont caractérisées par l'information spectrale et par la texture (c'est-à-dire la variabilité tonale dans une zone donnée), deux caractéristiques interdépendantes [Baraldi and Parmiggiani, 1995], [Haralick *et al.*, 1973]. La texture de l'image contient des informations sur l'organisation spatiale et structurale des d'objets [Tso and Mather, 2001]. D'un point de vue statistique, il existe deux catégories d'indicateurs de texture : de premier ordre (occurrence), et du second ordre (co-occurrence) [Haralick *et al.*, 1973]. Les indicateurs de premier ordre sont calculés à partir de l'histogramme de l'intensité des pixels dans un voisinage, mais ne tiennent pas compte de la relation spatiale entre les pixels. Les indicateurs de deuxième ordre sont calculés à partir de la matrice de co-occurrence de niveaux de gris (Gray Level Co-occurrence Matrix (GLCM)) qui indique la probabilité d'apparition d'un motif dans une direction et une distance donnée [Haralick *et al.*, 1973]. Pour classifier les espèces d'arbres, nous avons utilisé dans cette étude des indicateurs de texture de premier et second ordre. Ainsi, nous avons retenu la moyenne, la variance, l'asymétrie, le second moment angulaire, le contraste, la corrélation, l'entropie et l'homogénéité. Différents indicateurs de texture peuvent être calculés à partir de la matrice de co-occurrence. Chaque élément de la matrice de co-occurrence $g(i, j|d, \theta)$ décrit la co-occurrence spatiale des deux niveaux de gris (i) et respectif (j) à une distance intra pixel (d) et dans une direction θ. Une matrice de co-occurrence est définie comme suit:

$$G(d, \theta) = [g(i, j|d, \theta)] \tag{C.4}$$

L'utilisation de la matrice de co-occurrence implique le choix d'une taille de voisinage, une distance et une direction. Les résultats de classification sont fortement dépendants de la taille de la fenêtre : si elle est trop petite, l'information spatiale extraite n'est pas statistiquement valide, alors qu'une taille trop grande entraîne le recouvrement des différentes classes. Nous calculons pour chaque segment issu du processus de segmentation, les paramètres de texture de premier et second ordre. Cette approche nous permet de résoudre le problème de recouvrement des classes. Nous proposons deux approches pour le calcul des caractéristiques de texture : une approche pixellaire et une approche par région. La taille du voisinage pour le calcul des caractéristiques à partir de la matrice de co-occurrence pour l'approche pixellaire été choisie à 31x 31 pixels. Pour l'approche par région, le calcul des caractéristiques de texture se fait sur tous les pixels contenus dans un segment (correspondant à un houppier). Le choix de la distance entre les pixels est dépendant du niveau de détail de la texture analysée. Moins il y a de détails, plus la distance entre les pixels peut être augmentée. Dans le but de préserver toute différence possible entre les espèces, nous avons utilisé une distance de 1 pixel pour caractériser la texture. Le choix de la direction de calcul est important dans le cas des textures non isotropes. Les textures d'arbre étant isotropes, le calcul de co-occurrence dans une direction unique suffit (fixé ici à 0°). Le classifieur supervisé utilisé est un SVM bi-classes à noyau linéaire. Les vecteurs de caractéristiques proposés pour chaque segment sont composés des huit caractéristiques de texture de premier et second ordre mentionnées auparavant. Ils ont été calculés sur quatre espaces colorimétriques différents RVB, XYZ, Lab, IST [Sève, 1996]. La base d'apprentissage et celle de test ont été créées à partir des régions issues de la segmentation des houppiers. Les tests de classification d'espèces ont été effectués sur la même zone que celle étudiée pour la segmentation des houppiers. Cette zone contient deux espèces d'arbres : tilleuls (Tilia) et platanes (Platanus hispanica). L'apprentissage est effectué sur un ensemble de 18 segments et les tests sur 19 segments. Les Figures C.8-(a) et (b) illustrent les segments correspondant aux arbres utilisés pour la classification des espèces. Les platanes sont représentés avec une nuance plus foncée que les tilleuls.

Les résultats obtenus pour la classification d'espèces d'arbres sont présentés

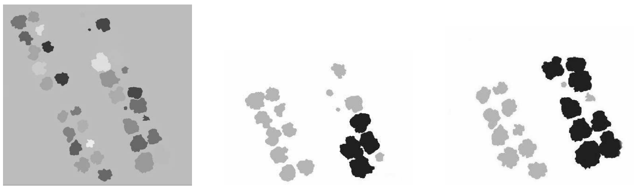

(a) (b) (c)

Figure C.8: Classification des espèces d'arbres : base d'apprentissage et de test et résultats de la classification pixellaire. **(a)** Zone d'apprentissage contenant les segments issus de la segmentation des houppiers d'arbres. **(b)** Données de référence de la zone de test utilisées pour l'évaluation des résultats de classification. **(c)** Résultat de la classification automatique des espèces d'arbres par approche pixellaire, pour le vecteur de caractéristiques calculé sur toutes les composantes dans l'espace IST.

dans le Tableau C.2 et la Figure C.8-(c), pour les vecteurs de caractéristiques (VC) calculés sur les différents espaces colorimétriques (RVB, XYZ, Lab, IST) ainsi que sur leurs composantes. Par exemple, VC / Blabel signifie que le vecteur de caractéristiques est calculé sur le canal B de l'espace colorimétrique RVB. En revanche, lorsque les vecteurs de caractéristiques sont calculés sur un espace colorimétrique, cela signifie que toutes les composantes de l'espace colorimétrique sont prises en compte.

On note les taux de bonne classification allant de 93,42% pour le vecteur des caractéristiques calculées pour une approche pixelaire, sur le composant Saturation (Slabel) de l'espace colorimétrique IST, à 100% pour une approche par régions, ce qui semble en accord avec un groupement des pixels appartenant à une classe pour une approche objet. Au contraire, nous observons que l'inverse se produit pour l'espace IST. Ceci pourrait être du à la présence de la composante Intensité (cf. VC/ Intensité) dans l'ensemble IST ou bien la discrimination entre ces deux espèces est liée à une différence de couleur des feuilles sénescentes. Malgré les résultats encourageants obtenus pour ces deux espèces, des évaluations supplémentaires devraient être réalisées afin de pouvoir conclure sur les caractéristiques discriminantes pour la classification d'espèces d'arbres.

Les résultats de chaque module présentés auparavant sont exploités pour améliorer le rendu des modèles numériques des villes en intégrant un modèle réaliste de la végétation. Les informations comme la hauteur des arbres, la position et l'espèce d'arbres, extraites de façon automatique, sont utilisées pour paramétrer les modèles numériques d'arbres. Ceux-ci sont ensuite intègres dans le modèle des villes. La Figure C.9 illustre le résultat d'un modèle de ville 3D sur notre zone d'études, contenant des modèles d'arbres correspondant à la réalité. Nous pou-

Table C.2: Évaluation de la précision de la classification des espèces.

Espace colorimétrique pour le calcul du vecteur de caractéristiques	**Approche pixellaire** **Précision de la classification (%)**	**Approche par région** **Précision de la classification (%)**
RVB	58,19	73,68
Rlabel	68,09	68,42
Glabel	52,77	68,42
Blabel	62,10	68,42
IR	52,49	57,89
DSM	70,35	63,16
XYZ	61,61	68,42
Xlabel	62,59	68,42
Ylabel	58,62	68,42
Zlabel	63,13	63,16
IST	**95,84**	94,74
Intensité	61,91	57,89
Saturation	90,53	89,47
Teinte	93,42	**100**
Lab	53,13	57,89
L_label	81,42	89,47
a_label	79,61	57,89
b_label	76,71	73,68

vons ainsi remarquer que deux types d'arbres sont présents dans cette illustration. De plus, nous pouvons remarquer que les troncs d'arbres sont correctement placés au sol et que leur emplacement correspond au barycentre de la projection au sol de la couronne de l'arbre.

Conclusions et perspectives

Nous avons présenté dans cet article un système complet d'analyse d'images pour la caractérisation de la végétation en milieu urbain. A partir des images aériennes couleurs et infrarouges ce système extrait la végétation en milieu urbain, sépare les arbres de pelouses ainsi que les houppiers des arbres entre eux, classifie les arbres en fonction de leur espèce et analyse les couronnes des arbres pour estimer les

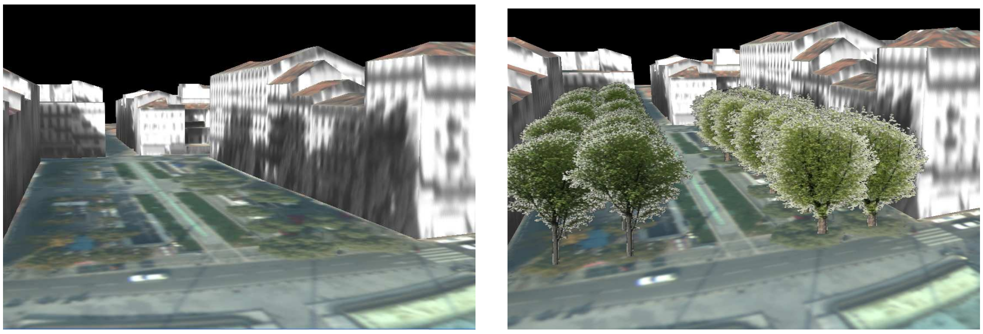

Figure C.9: Modèle urbain 3D avec un rendu réaliste sur la ville de Marseille : à gauche : modèle 3D urbain contenant les bâtiments. à droite : Modèle 3D urbain généré automatiquement et contenant les bâtiments et la végétation.

informations géométriques les caractérisant. Toutes ces données sont utilisées pour enrichir des modèles 3D urbains avec des informations concernant la végétation.

La recherche dans le domaine de la télédétection manque souvent d'informations concernant la classification des espèces d'arbres en milieu urbain. Cette étude intègre l'analyse des textures pour la classification des espèces des arbres. Les premiers résultats mettent en évidence les possibilités des systèmes d'identification et classification des espèces d'arbres en milieu urbain à partir d'images aériennes.

Nous remarquons que les caractéristiques de texture de premier et deuxième ordre sont des indicateurs discriminants pour caractériser les deux espèces d'arbres étudiées. De plus, nous notons qu'une approche de classification par régions permet une meilleure modélisation de la variance intra−classe. Cependant, des évaluations exhaustives intégrant plusieurs espèces d'arbre et nombre d'individus devraient être effectuées afin de tester la capacité de généralisation de cette approche. Nos travaux futurs seront menés dans le but d'évaluer les capacités d'optimisation de ces types de méthodes à plusieurs classes.

Bibliography

[Andersen *et al.* 2002] Andersen, H.E. ; Reutebuch, S.E. ; Schreuder, G.F.: Bayesian Object Recognition for the Analysis of Complex Forest Scenes in Airborne Laser Scanner Data. In: *International Archives of Photogrammetry Remote Sensing and Spatial Information Sciences* Volume 34 ISPRS (event), September, 9–13 2002, p. 35–41 57

[Baillard *et al.* 1998] Baillard, C. ; Dissard, O. ; Maitre, H.: Segmentation of urban scenes from aerial stereo imagery. In: *Pattern Recognition, 1998. Proceedings. Fourteenth International Conference on* 2 (1998), Aug, p. 1405–1407 4, 147, 168

[Bakir *et al.* 2007] Bakir, G.H. ; Hofmann, T. ; Schölkopf, B. ; Smola, A.J. ; Taskar, B. ; Vishwanathan, S.V.N. ; Gökhan Bakir, Bernhard Schölkopf Alexander J. Smola Ben T. (Editor) ; Vishwanathan, S. V. N. (Editor): *Predicting Structured Data*. The MIT Press, 2007 154

[Bannari *et al.* 1995] Bannari, A. ; Morin, D. ; He, D.-C.: Caractérisation de l'environnement urbain à l'aide des indices de végétation dérivés à partir des données de hautes résolutions spatiale et spectrale. In: Dubois, l.-M. M. (Editor) ; Lafrance, P. (Editor): *Télédétection des milieux urbains et périurbains : sixièmes journées scientifiques du « Réseau Télédétection » de I'AUPELF-UREF* Volume Télédétection francophonie: bilans régionaux et thématiques. Liège : John Libbey Eurotext, Paris, 2-5 octobre 1995 1995, p. 47–64 25, 26, 29

[Bannari *et al.* 1999] Bannari, A. ; Morin, D.R. ; Haboudane, D.: Analyse des effets atmosphériques sur les indices de végétation en milieu urbain. In: *Télédétection* 1 (1999), Nr. 1, p. 19–46 170

[Baraldi and Parmiggiani 1995] Baraldi, A. ; Parmiggiani, F.: An investigation of the textural characteristics associated with the gray level cooccurrence matrix statistical parameters. In: *Geoscience and Remote Sensing, IEEE Transactions on* 33 (1995), Mar, Nr. 2, p. 293–304 104, 178

[Beaubien 1994] Beaubien, J.: Landsat TM satellite images of forests: from enhancements to classification. In: *Canadian Journal of Remote Sensing* Volume 20, 1994, p. 17–26 97

[Berberoglu *et al.* 2000] Berberoglu, S. ; Lloyd, C. D. ; Atkinson, P. M. ; Curran, P. J.: The Integration of Spectral and Textural Information Using Neural

Networks for Land Cover Mapping In the Mediterranean. In: *Computers & Geosciences* 26 (2000), Nr. 4, p. 385–396 27

[Bernd 1997] BERND, J. ; POWERS, R. (Editor): *Practical handbook on image processing for scientific applications*. CRC Press LLC, 1997 104, 109

[Bicego *et al.* 2003] BICEGO, M. ; DALFINI, S. ; MURINO, V.: Extraction of Geographical Entities from Aerial Images. In: *2nd GRSS/ISPRS Joint Workshop on Remote Sensing and Data Fusion over Urban Areas*, 22-23 May 2003, p. 125–128 27, 47

[Bochow *et al.* 2007] BOCHOW, M. ; SEGL, K. ; KAUFMANN, H.: Automating the build-up process of feature-based fuzzy logic models for the identification of urban biotopes from hyperspectral remote sensing data. In: *Urban Remote Sensing Joint Event*. Paris, France, 11-13 April 2007, p. 1–8 28

[Bonham 1989] BONHAM, C. ; WILEY-INTERSCIENCE (Editor): *Measurements for Terrestrial Vegetation*. Wiley-Interscience, 1989 89

[Bordes *et al.* 2007] BORDES, A. ; BOTTOU, L. ; GALLINARI, P. ; WESTON, J.: Solving MultiClass Support Vector Machines with LaRank. In: GHAHRAMANI, Zoubin (Editor): *Proceedings of the 24th International Machine Learning Conference*. Corvallis, Oregon : OmniPress, 2007, p. 89–96 156

[Boser *et al.* 1992] BOSER, B. E. ; GUYON, I. M. ; VAPNIK, V. N.: A training algorithm for optimal margin classifiers. In: *COLT '92: Proceedings of the fifth annual workshop on Computational learning theory*. New York, NY, USA : ACM, 1992, p. 144–152. – ISBN 0-89791-497-X 36, 170

[Brack 1997] BRACK, C.L.: Forest Mensuration: Measuring trees, stands and forests for effective forest management. In: *ISBN 0 7315 2413 6*. http://fennerschool-associated.anu.edu.au//mensuration/home.htm : Australian National University, 1997. – Last accessed on the 23 of July 2009 89

[Brandtberg 2002] BRANDTBERG, T.: Individual tree-based species classification in high spatial resolution aerial images of forests using fuzzy sets. In: *Fuzzy Sets and Systems* 132 (2002), Nr. 3, p. 371–387 98

[Brandtberg and Walter 1998] BRANDTBERG, T. ; WALTER, F.: Automatic Delineation of Individual Tree Crowns in High Spatial Resolution Aerial Images by Multiple-Scale Analysis. In: *Machine Vision and Applications* 11 (1998), Nr. 2, p. 64–73 55, 173

[Brédif *et al.* 2007] Brédif, M. ; Boldo, D. ; Pierrot-Deseilligny, M. ; Maître, H.: 3D building reconstruction with parametric roof superstructures. In: IEEE (Editor): *International Conference on Image Processing* Volume 2 IEEE (event), september 2007, p. 537–540 147

[Buyantuyev *et al.* 2007] Buyantuyev, A. ; Wu, J. ; Gries, C.: Estimating vegetation cover in an urban environment based on Landsat ETM imagery: A case study in Phoenix, USA. In: *International Journal of Remote Sensing* 28 (2007), Nr. 2, p. 269–291 3

[Campbell 2002] Campbell, C.: Kernel methods: A survey of current techniques. In: *Neurocomputing* 48 (2002), October, p. 63–84 36

[Ceccato *et al.* 2001] Ceccato, P. ; Flasse, S. ; Tarantola, S. ; Jacquemoud, S. ; Gregoire, J. M.: Detecting vegetation leaf water content using reflectance in the optical domain. In: *Remote Sensing of Environment* 77 (2001), Nr. 1, p. 22–33 111

[Champion and Boldo 2006] Champion, N. ; Boldo, D.: A robust algorithm for estimating digital terrain model from digital surface models in dense urban areas. In: Förstner, W. (Editor) ; Steffen, R. (Editor): *International Archives of Photogrammetry, Remote Sensing and Spatial Information Sciences* Volume 36, Part 3. ISPRS Commission III, 2006, p. 111–116. – Bonn, Germany 11, 176

[Chang and Lin 2001] Chang, C.-C. ; Lin, C.-J.: *LIBSVM: a library for support vector machines*, 2001. – Software available at `http://www.csie.ntu.edu.tw/~cjlin/libsvm` 38, 111, 155, 156

[Chen *et al.* 2006] Chen, Q. ; Baldocchi, D. ; Gong, P. ; Kelly, M.: Isolating Individual Trees in a Savanna Woodland Using Small Footprint Lidar Data. In: *Photogrammetric Engineering and Remote Sensing* 72 (2006), Nr. 8, p. 897 53

[Cleve *et al.* 2008] Cleve, C. ; Kelly, M. ; Kearns, F.R. ; Moritz, M.: Classification of the wildland–urban interface: A comparison of pixel-and object-based classifications using high-resolution aerial photography. In: *Computers, Environment and Urban Systems* 32 (2008), Nr. 4, p. 317–326 109

[Congalton and Green 2008] Congalton, R. G. ; Green, K. ; Inc, CRC P. (Editor): *Assessing the Accuracy of Remotely Sensed Data: Principles and Practices*. 2nd Revised edition. Taylor & Francis Group, 2008 158

[Cord and Cunningham 2008] Cord, M. (Editor) ; Cunningham, P. (Editor): *Machine Learning Techniques for Multimedia: Case Studies on Organization and Retrieval*. Berlin Heidelberg : Springer-Verlag, 2008. – 285 p 36

[Cord and Declercq 2001] Cord, M. ; Declercq, D.: Three-dimentional building and modeling using a statistical approach. In: *IEEE Transactions on Image Proessing* 10 (2001), Nr. 5, p. 715–723 4

[Cortes and Vapnik 1995] Cortes, C. ; Vapnik, V.: Support-vector networks. In: *Machine Learning* 20 (1995), Nr. 3, p. 273 –297 36

[Crammer and Singer 2002] Crammer, K. ; Singer, Y.: On the algorithmic implementation of multiclass kernel-based vector machines. In: *The Journal of Machine Learning Research* 2 (2002), p. 265–292 156

[Cristianini and Shawe-Taylor 2000] Cristianini, N. ; Shawe-Taylor, J.: *Support Vector Machines and other kernel-based learning methods*. Cambridge, UK : Cambridge University Press, 2000 36

[Culvenor 2003] Culvenor, D.S.: *Remote Sensing of Forest Environments: Concepts and Case Studies*. Chap. Extracting Individual Tree Information: A Survey of Techniques for High Spatial Resolution Imagery, p. 255–278, Kulwer Academic Publishers, 2003. – google books 51

[Culvenor *et al.* 1998] Culvenor, D.S. ; Coops, N. ; Preston, R. ; Tolhurst, K.G.: A spatial clustering approach to automated tree crown delineation. In: *Proc. of the International Forum on Automated Interpretation of High Spatial Resolution Digital Imagery for Forestry*, Natural Ressources Canada, Canadian Forest Service, 1998, p. 67–80 48, 52, 55

[Cunningham *et al.* 2008] Cunningham, P. ; Cord, M. ; Delany, S. J.: *Machine Learning Techniques for Multimedia: Case Studies on Organization and Retrieval*. Chap. Supervised Learning, p. 21–50. Berlin Heidelberg : Springer-Verlag, 2008 152

[Deering 1978] Deering, D.W.: *Rangeland Reflectance Characteristics Measured by Aircraft and Spacecraft Sensors*, Texas A&M Univ, College Station, Ph.D. thesis, 1978. – 338 p 26

[Digabel and Lantuejoul 1978] Digabel, H. ; Lantuejoul, C.: Iterative algorithms. In: *Proceedings of the 2nd European Symposium of Quant. analysis of microstructures in material sciences, biology and medicine*. Caen, France, 4-7 october 1977 1978 82

[Dralle and Rudemo 1996] Dralle, K. ; Rudemo, M.: Stem Number Estimation by Kernel Smoothing of Aerial Photos. In: *Canadian Journal of Remote Sensing* 26 (1996), Nr. 7, p. 1228–1236 51

[Drimbarean and Whelan 2001] Drimbarean, A. ; Whelan, P.F.: Experiments in colour texture analysis. In: *Pattern Recognition Letters* 22 (2001), Nr. 10, p. 1161–1167 123

[Duda and Canty 2002] Duda, T. ; Canty, M.: Unsupervised classification of satellite imagery: choosing a good algorithm. In: *International Journal of Remote Sensing* 23 (2002), Nr. 11, p. 2193–2212 27

[Durupt and Taillandier 2006] Durupt, M. ; Taillandier, F.: Reconstruction automatique de batiments a partir d'un MNE et de limites cadastrales : une approche operationnelle. In: *RFIA: Reconnaissance des Formes et Intelligence Artificielle*, 2006 2

[Egan 1975] Egan, J. P. ; Carterette, E.C. (Editor) ; Friedman, M. P. (Editor): *Signal Detection Theory and ROC Analysis*. New York : Academic Press, 1975 (Series in Cognition and Perception). – 277 p 157

[Erikson 2003] Erikson, M.: Segmentation of individual tree crowns in colour aerial photographs using region growing supported by fuzzy rules. In: *Canadian Journal of Forest Research* 33 (2003), Nr. 8, p. 1557–1563 48

[Erikson 2004a] Erikson, M.: *Segmentation and Classification of Individual Tree Crowns*. Uppsala, Sweden, Swedish University of Agricultural Sciences, Ph.D. thesis, 2004 69, 97, 98, 148, 173, 177

[Erikson 2004b] Erikson, M.: Species classification of individually segmented tree crowns in high-resolution aerial images using radiometric and morphologic image measures. In: *Remote Sensing of Environment* 91 (2004), June, Nr. 3-4, p. 469–477 52

[Flamanc *et al.* 2003] Flamanc, D. ; Maillet, G. ; Jibrini, H.: 3-D City Models: an Operational Approach using Aerial Images and Cadastral Maps. In: H. Ebner and C. Heipke and H. Mayer and K. Pakzad (Editor): *ISPRS Conference Photogrammetric Image Analysis (PIA)* Volume XXXIV, Part 3/W834. Munich, Germany : Institute for Photogrammetry and GeoInformation University of Hannover, Germany, Sep 2003, p. 53–58 2

[Fuhrer *et al.* 1981] Fuhrer, J. ; Erismann, KH ; Keller, HJ ; Favre, A.: A system for quantitative determination of species and vitalities of urban trees on color-infrared photographs. In: *Remote Sensing of Environment* 11 (1981), p. 1–8 168

[Gerke *et al.* 2001] Gerke, M. ; Straub, B.M. ; Koch, A.: Automatic Detection of Buildings and Trees from Aerial Imagery Using Different Levels of Abstraction.

In: *Publications of the German Society for Photogrammetry and Remote Sensing* 10 (2001), p. 273–280 3

[Gerylo *et al.* 1998] Gerylo, G. ; Hall, R. J. ; Franklin, S. E. ; Roberts, A. ; Milton, E. J.: Hierarchical image classification and extraction of forest species composition and crown closure from airborne multispectral images. In: *Canadian Journal of Remote Sensing* 24 (1998), Nr. 3, p. 219–232 98

[Gillis and Leckie 1993] Gillis, M.D. ; Leckie, D.G.: Forest inventory mapping procedures across Canada / Petawawa National Forestry Institute. 1993 (PI-X-114). – Information Report 97, 177

[Gitelson *et al.* 1996] Gitelson, A. A. ; Kaufman, Y. J. ; Merzlyak, M. N.: Use of a green channel in remote sensing of global vegetation from EOS-MODIS. In: *Remote Sensing of Environment* 58 (1996), Nr. 3, p. 289–298. – ISSN 0034-4257 34

[Gong *et al.* 2003] Gong, P. ; Pu, R ; Biging, G. S. ; Larrieu, M. R.: Estimation of Forest Leaf Area Index Using Vegetation Indices Derived from Hyperion Hyperspectral Data. In: *IEEE Transactions on Geoscience and Remote Sensing* 41 (2003), Nr. 6, p. 1355–1362 31, 170

[Gong *et al.* 2002] Gong, P. ; Sheng, Y. ; Biging, GS: 3D Model-Based Tree Measurement from High-Resolution Aerial Imagery. In: *Photogrammetric Engineering and Remote Sensing* 68 (2002), Nr. 11, p. 1203–1212 57

[Gougeon 1995a] Gougeon, F. A.: Comparison of possible multispectral classification schemes for tree crowns individually delineated on high spatial resolution MEIS images. In: *Canadian Journal of Remote Sensing* 21 (1995), Nr. 1, p. 1–9 98

[Gougeon 1995b] Gougeon, F. A.: A Crown-following Approach to the Automatic Delineation of Individual Tree Crowns in High Spatial Resolution Aerial Images. In: *Canadian Journal of Remote Sensing* 21 (1995), Nr. 3, p. 274–284 48, 51, 97, 177

[Gougeon 1995c] Gougeon, F. A.: A System for Individual Tree Crown Classification of Conifer Stands at High Spatial Resolution. In: *Proc. of the 17th Cananadian Symposium on Remote Sensing*. Saskatchewan, Canada, June 1995, p. 635–642 51, 98, 173

[Gougeon 1998] Gougeon, F. A.: Automatic Individual Tree Crown Delineation Using a Valley-Following Algorithm and a Rule-Based System. In: Hill, D.A.

(Editor) ; Leckie, D.G. (Editor): *Proceedings of the International Forum on Automated Interpretation of High Spatial Resolution Digital Imagery for Forestry*, Natural Ressources Canada, Canadian Forest Service, February 1998, p. 11–23 48, 51

[Gougeon and Leckie 2001] Gougeon, F. A. ; Leckie, D. G.: Individual Tree Crown Image Analysis - A Step Towards Precision Forestry. In: *Proceedings of the First International Precision Forestry Symposium*. Seattle, U.S., Jun 2001 51, 173

[Gougeon and Leckie 2003] Gougeon, F. A. ; Leckie, D. G.: Forest Information Extraction from High Spatial Resolution Images Using an Individual Tree Crown Approach / Canadian Forest Service, Pacific Forestry Centre. Victoria, British Columbia, 2003 (BC-X-396). – Information Report. http://www.pfc.cfs.nrcan.gc.ca 48, 49, 51

[Green 2002] Green, P.: *Colour Engineering: achieving device independent colour*. Chap. Colorimetry and colour difference, p. 49–77, John Wiley & Sons, LTD, 2002 37, 40, 111

[Haala and Brenner 1999] Haala, N. ; Brenner, C.: Extraction of Buildings and Trees in Urban Environments. In: *ISPRS Journal of Photogrammetry and Remote Sensing* 54 (1999), p. 130–137 3, 27, 168

[Hall *et al.* 1991] Hall, F.G. ; Strebel, D.E. ; Nickeson, J.E. ; Goetz, S.J.: Radiometric rectification: Toward a common radiometric response among multidate, multisensor images. In: *Remote Sensing of Environment* 35 (1991), Nr. 1, p. 11 – 27. – ISSN 0034-4257 30

[Haralick 1979] Haralick, R. M.: Statistical and structural approaches to texture. In: *Proceedings of the IEEE* 67 (1979), May, Nr. 5, p. 786–804 100

[Haralick *et al.* 1973] Haralick, R. M. ; Shanmugam, K. ; Dinstein, I. H.: Textural features for image classification. In: *IEEE Transactions on Systems, Man and Cybernetics* 3 (1973), Nr. 6, p. 610–621 104, 121, 178

[Hermans *et al.* 2003] Hermans, C. ; Smeyers, M. ; Rodriguez, R. M. ; Eyletters, M. ; Strasser, R. J. ; Delhaye, J.-P.: Quality assessment of urban trees: A comparative study of physiological characterisation, airborne imaging and on site fluorescence monitoring by the OJIP-test. In: *Journal of Plant Physiology* 160 (2003), January, Nr. 1, p. 81–90 168

[Horváth *et al.* 2006a] Horváth, P. ; Jermyn, I. H. ; Kato, Z. ; Zerubia, J.: A Higher-Order Active Contour Model for Tree Detection. In: *Proceedings International Conference on Pattern Recognition (ICPR)*. Hong Kong, August 2006 55, 173

[Horváth *et al.* 2006b] Horváth, P. ; Jermyn, I. H. ; Kato, Z. ; Zerubia, J.: An improved 'gas of circles' higher-order active contour model and its application to tree crown extraction. In: Kalra, P. (Editor) ; Peleg, S. (Editor): *Proc. Indian Conference on Computer Vision, Graphics, and Image Processing (ICVGIP)* Volume 4338. Madurai, India : Springer-Verlag Berlin Heidelberg, December 2006, p. 152–161 55

[Hsu and Lin 2002] Hsu, C.-W. ; Lin, C.-J.: A comparison of methods for multi-class support vector machines. In: *IEEE Transactions on Neural Networks* 13 (2002), p. 415–425 111, 156

[Huete *et al.* 2002] Huete, A. ; Didan, K. ; Miura, T. ; Rodriguez, E.P. ; Gao, X. ; Ferreira, L.G.: Overview of the radiometric and biophysical performance of the MODIS vegetation indices. In: *Remote Sensing of Environment* 83 (2002), p. 195–213 24

[Hung and Ridd 2002] Hung, M.-C. ; Ridd, M. K.: A Subpixel Classifier for Urban Land-Cover Mapping Based on a Maximum-Likelihood Approach and Expert System Rules. In: *Photogrammetric Engineering & Remote Sensing* 68 (2002), Nr. 11, p. 1173–1180 28

[Hyyppa *et al.* 2001] Hyyppa, J. ; Kelle, O. ; Lehikoinen, M. ; Inkinen, M.: A segmentation-based method to retrieve stem volume estimates from 3-D tree height models produced by laser scanners. In: *Geoscience and Remote Sensing, IEEE Transactions on* 39 (2001), May, Nr. 5, p. 969–975 53

[IGN, Département de Télédétection 1986] IGN, Département de Télédétection: Etude phytosanitaire des plantations d'alignement / Institut Géographique National. Paris, 1986. – Direction des Parcs, Jardins et Espaces Verts 147

[IGN, Département de Télédétection 1991] IGN, Département de Télédétection: Cadastre Vert / Institut Géographique National. Arras, 1991. – Service des Espaces Verts 147

[IGN, Institut Géographique National 2008] IGN, Institut Géographique National: *BATI-3D ®: modélisation 3D des zones urbaines*. `http://www.ign.fr/institut/documentArticle.do?idDoc=5591864&indexRoot=8&indexChild=5`. 2008. – (Accessed on the 31st of August 2009) 2, 6, 150

[Iovan *et al.* 2008a] Iovan, C. ; Boldo, D. ; Cord, M.: Detection, Characterization and Modeling Vegetation in Urban Areas from High Resolution Aerial Imagery.

In: *IEEE Journal of Selected Topics in Applied Earth Observations and Remote Sensing* 1 (2008), September, Nr. 3, p. 206–213 6, 110

[Iovan *et al.* 2008b] Iovan, C. ; Boldo, D. ; Cord, M.: Detection, segmentation and characterization of vegetation in high-resolution aerial images for 3D city modeling. In: ISPRS (Editor): *International Archives of Photogrammetry, Remote Sensing and Spatial Information Sciences* Volume 37, July 2008 110

[Iovan *et al.* 2009] Iovan, C. ; Boldo, D. ; Cord, M.: Modélisation de la végétation en milieu urbain : détection et caractérisation à partir d'images aériennes haute résolution couleur et infrarouge. In: *Revue Française de Photogrammétrie et de Télédétection* 189 (2009), March, p. 17–27 6, 110, 167

[Iovan *et al.* 2007] Iovan, C. ; Boldo, D. ; Cord, M. ; Erikson, M.: Automatic Extraction and Classification of Vegetation Areas from High Resolution Images in Urban Areas. In: Ersboll, Bjarne K. (Editor) ; Pedersen, Kim S. (Editor): *Proc. of the 15th Scandinavian Conference on Image Analysis (SCIA)* Volume 4522. Aalborg, Denmark : Springer, Juin 2007, p. 858–867 6

[Jackson *et al.* 1983] Jackson, R. D. ; Pinter, P. J. ; Slater, P. N.: Discrimination of growth and water stress in wheat by various vegetation indices through clear and turbid atmospheres. In: *Remote Sensing of Environment* 13 (1983), p. 187–208 24

[Jacquemoud and Feret 2007] Jacquemoud, S. ; Feret, J. B.: Modélisation de la réflectance spectrale et directionnelle des couverts végétaux pour la determination de la teneur en pigments et en eau - Applications. In: *Atelier PNTS Hyperspectral*. Nantes, France, April 2007 101, 102, 177

[Jensen 1996] Jensen, J. R. ; Clarke, K. C. (Editor): *Introductory Digital Image Processing: a remote sensing perspective*. second edition. Prentice Hall, 1996 101

[Kanda *et al.* 2004] Kanda, F. ; Kubo, M. ; Muramoto, K.: Watershed segmentation and classification of tree species using high resolution forest imagery. In: *Geoscience and Remote Sensing Symposium, 2004. IGARSS'04. Proceedings. 2004 IEEE International* Volume 6, 2004, p. 3822–3825 53

[Key *et al.* 2001] Key, T. ; Warner, T.A. ; McGraw, J.B. ; Fajvan, M.A.: A comparison of multispectral and multitemporal information in high spatial resolution imagery for classification of individual tree species in a temperate hardwood forest. In: *Remote Sensing of Environment* 75 (2001), Nr. 1, p. 100–112 97, 98

[Knudsen 2005] Knudsen, T.: Technical Note: Pseudo natural colour aerial imagery for urban and suburban mapping. In: *International Journal of Remote Sensing* 26 (2005), Nr. 12, p. 2689–2698 3

[Komura *et al.* 2004] Komura, R. ; Kubo, M. ; Muramoto, K.: Delineation of tree crown in high resolution satellite image using circle expression and watershed algorithm. In: *Geoscience and Remote Sensing Symposium, 2004. IGARSS'04. Proceedings. 2004 IEEE International* Volume 3, 2004, p. 1577–1580 53

[Korpela 2004] Korpela, I.: Individual Tree Measurements by Means of Digital Aerial Photogrammetry. In: *SILVA FENNICA — A quarterly journal of forest science of the Finnish Society of Forest Science and the Finnish Forest Research Institute Monographs* 3 (2004), p. 93 51, 97, 99

[Korpela 2006] Korpela, I.: 3D Treetop Positioning by Multiple Image Matching of Aerial Images in a 3D Search Volume Bounded by LiDAR Surface Models. In: Förstner, Wolfgang (Editor) ; Steffen, Richard (Editor): *International Archives of Photogrammetry, Remote Sensing and Spatial Information Sciences.* Volume XXXVI. Bonn, Germany : E. Schweizerbartsche Verlagsbuchhandlung, September 2006, p. 191–196 51

[Kulikova *et al.* 2007] Kulikova, M. S. ; Mani, M. ; Srivastava, A. ; Descombes, X. ; Zerubia, J.: Tree Species Classification Using Radiometry, Texture and Shape Based Features. In: *Proc. European Signal Processing Conference (EUSIPCO).* Poznan, Pologne, September 2007 98

[Lamar *et al.* 2005] Lamar, W.R. ; McGraw, J.B. ; Warner, T.A.: Multitemporal censusing of a population of eastern hemlock (Tsuga canadensis L.) from remotely sensed imagery using an automated segmentation and reconciliation procedure. In: *Remote Sensing of Environment* 94 (2005), Nr. 1, p. 133–143 48, 53

[Larsen 1997] Larsen, M.: Crown Modelling to Find Tree Top Positions in Aerial Photographs. In: *Proc. of the Third Internationl Airborne Remote Sensing Conference and Exhibition* Volume 2, 1997, p. 428–435 56, 173

[Leckie *et al.* 2003] Leckie, D. ; Gougeon, F. ; Hill, D. ; Quinn, R. ; Armstrong, L. ; Shreenan, R.: Combined High-Density LiDAR and Multispectral Imagery for Individual Tree Crown Analysis. In: *Canadian Journal of Remote Sensing* 29 (2003), Nr. 5, p. 633–649 52

[Leckie 1990] Leckie, D.G.: Advances in remote sensing technologies for forest surveys and management. In: *Canadian Journal of Forestry Research* Volume 20, 1990, p. 464–483 97

[Leckie *et al.* 2005] LECKIE, D.G. ; TINIS, S. ; NELSON, T. ; BURNETT, C. ; GOUGEON, F. A. ; CLONEY, E. ; PARADINE, D.: Issues in species classification of trees in old growth conifer stands. In: *Canadian Journal of Remote Sensing* 31 (2005), Nr. 2, p. 175–190 98

[Lillesand *et al.* 2008] LILLESAND, T. M. ; KIEFER, R. W. ; CHIPMAN, J. W. ; HOBOKEN, N.J. (Editor): *Remote sensing and image interpretation*. 6th edition. John Wiley & Sons, 2008 10, 11, 19, 30, 98

[LOEMI 2009] LOEMI, website: *La caméra numérique de l'IGN : les configurations*. [online]. 2009. – URL `http://recherche.ign.fr/LOEMI/argenerique.php?AR=CAMNU&PAGE=1`. – Retrieved on the 14 of August, 2009 10

[Mallet and Bretar 2009] MALLET, C. ; BRETAR, F.: Full-waveform topographic lidar: State-of-the-art. In: *ISPRS Journal of Photogrammetry and Remote Sensing* 64 (2009), Nr. 1, p. 1–16 24

[Maltamo *et al.* 2004] MALTAMO, M. ; MUSTONEN, K. ; HYYPPA, J. ; PITKANEN, J. ; YU, X.: The accuracy of estimating individual tree variables with airborne laser scanning in a boreal nature reserve. In: *Canadian Journal of Forest Research* 34 (2004), Nr. 9, p. 1791–1801 53

[Mathieu *et al.* 1998] MATHIEU, R. ; POUGET, M. ; CERVELLE, B. ; ESCADAFAL, R.: Relationships between satellite-based radiometric indices simulated using laboratory reflectance data and typic soil color of an arid environment. In: *Remote Sensing of Environment* 66 (1998), Nr. 1, p. 17–28. – ISSN 0034-4257 32

[MATIS, IGN 2008] MATIS, IGN: *Laboratoire MATIS - Méthodes d'Analyses pour le Traitement d'Images et la Stéréorestitution*. `http://recherche.ign.fr/labos/matis/`. 2008. – (Accessed on the 31st of August 2009) 95, 96

[McBride and Reid 1988] MCBRIDE, J. R. ; REID, C.: *A Guide to Wildlife Habitats of California*. Chap. Pasture, p. 166. Sacramento, California : California Department of Forestry and Fire Protection, 1988 45

[Mei and Durrieu 2004] MEI, C. ; DURRIEU, S.: Tree Crown Delineation from Digital Elevation Models and High Resolution Imagery. In: *Proc. of the ISPRS Workshop 'Laser scanners for Forest and Landscape Assement'* Volume 36. Fribourg, Germany, oct 2004 53, 67, 175

[Meyer *et al.* 1996] Meyer, P. ; Staenz, K. ; K.I., Itten: Semi-automated procedures for tree species identification in high spatial resolution data from digitized colour infrared-aerial photography. In: *ISPRS Journal of Photogrammetry and Remote Sensing* 51 (1996), February, Nr. 1, p. 5–16 97, 98

[Michel and Lortic 1992] Michel, A. ; Lortic, B.: Typologies urbaines et télédétection satellitaire. La notion de zones en milieu urbain. In: *L'espace géographique* 21 (1992), Nr. 2, p. 167–178 24

[Ministry for the Economy, Industry and Employment 2009] Ministry for the Economy, Industry and Employment: *Competitivenes clusters in France*. `http://www.industrie.gouv.fr/liste_index/index-ang.html`. February 2009. – (Accessed on the 31st of August 2009) 2

[Myeong 2005] Myeong, S.: Improving Urban Vegetation Classification by Including Height Information Derived from High-Spatial Resolution Stereo Imagery. In: *Korean Journal of Remote Sensing* 21 (2005), Nr. 5, p. 383–392 27, 47

[Myeong *et al.* 2003] Myeong, S. ; Nowak, D.J. ; Hopkins, P.F. ; Brock, R.H.: Urban Cover Mapping Using Digital, High-Spatial Resolution Aerial Imagery. In: *Urban Ecosystems* 5 (2003), Nr. 4, p. 243–256 47

[Nichol and Lee 2005] Nichol, J. ; Lee, C. M.: Urban vegetation monitoring in Hong Kong using high resolution multispectral images. In: *International Journal of Remote Sensing* 26 (2005), Nr. 5, p. 903 – 918 97

[Olofsson *et al.* 2003] Olofsson, K. ; Bohlin, J. ; Lamas, T. ; Olsson, H.: Estimation of forest parameters by using remote sensing sigle tree detection and field plots with tree positions. In: Bevers, M. (Editor) ; Barrett, T. M. (Editor): *Systems Analysis in Forest Resources, Proceedings of the 2003 Symposium*, 2003, p. 97–104 56, 57

[Olofsson *et al.* 2006] Olofsson, K. ; Wallerman, J. ; Holmgren, J. ; Olsson, H.: Tree species discrimination using Z/I DMC imagery and template matching of single trees. In: *Scandinavian Journal of Forest Research* 21 (2006), p. 106–110 149

[Ouma and Tateishi 2008] Ouma, Y. O. ; Tateishi, R.: Urban-trees extraction from Quickbird imagery using multiscale spectex-filtering and non-parametric classification. In: *ISPRS Journal of Photogrammetry and Remote Sensing* 63 (2008), Nr. 3, p. 333 – 351 56, 168

[Paparoditis *et al.* 2006] PAPARODITIS, Nicolas ; SOUCHON, Jean-Philippe ; MARTINOTY, Gilles ; PIERROT-DESEILLIGNY, Marc: High-end aerial digital cameras and their impact on the automation and quality of the production workflow. In: *ISPRS Journal of Photogrammetry and Remote Sensing* 60 (2006), Nr. 6, p. 400 – 412. – Digital Aerial Cameras. – ISSN 0924-2716 9

[Pekkarinen 2002] PEKKARINEN, A.: A method for the segmentation of very high spatial resolution images of forested landscapes. In: *International Journal of Remote Sensing* 23 (2002), Nr. 14, p. 2817–2836 54

[Perrin 2006] PERRIN, G.: *Etude du couvert forestier par processus ponctuels marqués*, Ecole Centrale de Paris, Ph.D. thesis, october 2006 173

[Perrin *et al.* 2005] PERRIN, G. ; DESCOMBES, X. ; ZERUBIA, J.: A Marked Point Process Model for Tree Crown Extraction in Plantations. In: *Proc. IEEE International Conference on Image Processing (ICIP)*. Genova, september 2005 48, 57

[Perrin *et al.* 2006] PERRIN, Guillaume ; DESCOMBES, Xavier ; ZERUBIA, Josiane: 2D and 3D Vegetation Resource Parameters Assessment using Marked Point Processes. In: *Proc. International Conference on Pattern Recognition (ICPR)*, 2006, p. 1–4 86, 149

[Perry and Lautenschlager 1984] PERRY, C. R. ; LAUTENSCHLAGER, L.F.: Functional equivalence of spectral vegetation indices. In: *Remote Sensing of Environment* 14 (1984), p. 169–182 24

[Persson *et al.* 2002] PERSSON, Å. ; HOLMGREN, J. ; SÖDERMAN, U.: Detecting and Measuring Individual Trees Using an Airborne Laser Scanner. In: *Photogrammetric Engeneering and Remote Sensing* 68 (2002), Nr. 9, p. 925–932 54

[Pierrot-Deseilligny and Paparoditis 2006] PIERROT-DESEILLIGNY, M. ; PAPARODITIS, N.: A Multiresolution and Optimization-Based Image Matching Approach: An Application to Surface Reconstruction from SPOT5-HRS Stereo Imagery. In: *Proc. of the ISPRS Conference Topographic Mapping From Space (With Special Emphasis on Small Satellites)*. Ankara, Turkey, feb 2006 11, 169

[Pinz 1991] PINZ, A.J.: A Computer Vision System for the Recognition of Trees in Aerial Photographs. In: TILTON, J.C (Editor): *Multisource Data Integration in Remote Sensing, NASA Workshop on* Volume 3099. University of Maryland College Park, Maryland, June 14-15 1991, p. 111–124 3

[Pinz 1998] PINZ, A.J.: Tree Isolation and Species Classification. In: HILL, D.A. (Editor) ; LECKIE, D.G. (Editor): *International Forum on Automated Interpretation* *of High Spatial Resolution Digital Imagery for Forestry*. Victoria, British Columbia, Canada, February 1998, p. 127–139 50, 98, 173

[Pinz 1990] Pinz, H.: Constructing a neural network for the interpretation of the species of trees in aerial photograps. In: *Proceedings., 10th International Conference on Pattern Recognition* Volume 1, 1990, p. 755 – 757 98

[Pitkänen *et al.* 2004] Pitkänen, J. ; Maltamo, M. ; Hyyppä, J. ; Yu, X.: Adaptive methods for individual tree detection on airborne laser based canopy height model. In: *Laser scanners for forest and landscape assessment. Proceedings of the ISPRS working group VIII/2*. Freiburg, Germany, October 2004, p. 3–6 48, 50, 51, 54

[Pitt *et al.* 1997] Pitt, D.G. ; Wagner, R.G. ; Hall, R.J. ; King, D.J. ; Leckie, D.G. ; Runesson, U.: Use of remote sensing for forest vegetation management: A problem analysis. In: *Forestry Chronicle* 73 (1997), p. 459–478 49

[Pollock 1996] Pollock, R. J.: *The Automatic Recognition of Individual Trees in Aerial Images of Forests based upon a Synthetic Tree Crown Image Model*. Vancouver, Canada, University of British Columbia, Department of Computer Science, Ph.D. thesis, 1996 51, 56, 173

[Pollock 1998] Pollock, R. J.: Individual tree recognition based on a synthetic tree crown image model. In: *International forum: Automated Interpretation of High Spatial Resolution Digital Imagery for Forestry*. Victoria, British Columbia, 1998 (Conference Natural Resources Canada), p. 25–34 56

[Pollock 1994] Pollock, R.J.: A model-based approach to automatically locating tree crowns in high spatial resolution images. In: *Image and Signal Processing for Remote Sensing* 2315 (1994), December, Nr. 1, p. 526–537 55, 56

[Popescu *et al.* 2003] Popescu, S. C. ; Wynne, R. H. ; Nelson, R. F.: Measuring individual tree crown diameter with lidar and assessing its influence on estimating forest volume and biomass. In: *Canadian Journal of Remote Sensing* 29 (2003), Nr. 5, p. 564–577 50, 51, 54

[Pouliot *et al.* 2005] Pouliot, D.A. ; King, D.J. ; Pitt, D.G.: Development and evaluation of an automated tree detection–delineation algorithm for monitoring regenerating coniferous forests. In: *Canadian Journal of Forest Research/Revue Canadienne de Recherche Forestiere* 35 (2005), Nr. 10, p. 2332–2345 54

[Provost and Fawcett 1997] PROVOST, F. ; FAWCETT, T.: Analysis and Visualization of Classifier Performance: Comparison under Imprecise Class and Cost Distribution. In: *Proceedings of the Third International Conference on Knowledge Discovery and Data Mining (KDD)*. Huntington Beach, CA, 1997 157

[Richards 1993] RICHARDS, J. A.: *Remote Sensing and Digital Image Analysis: An Introduction*. 2nd. Berlin : Springer-Verlag Telos, 1993. – 340 p 27

[Richards and Jia 1999] RICHARDS, J.A. ; JIA, X.: *Remote sensing digital image analysis: an introduction*. 3rd. Springer-Verlag Berlin Heidelberg, 1999. – 439 p 157

[Robinson *et al.* 1995] ROBINSON, A. H. ; MORRISON, J. L. ; MUEHRCKE, P. C. ; KIMERLING, A. J. ; GUPTILL, S. C. ; SONS, John Wiley (Editor): *Elements of Cartography*. 6th. John Wiley & Sons, Inc., 1995. – 688 p 1, 10

[Rohde and Olson 1972] ROHDE, W.G. ; OLSON, C.E.: Multispectral sensing of forest tree species. In: *Photogrammetric Engineering and Remote Sensing* 38 (1972), December, p. 1209–1215 97, 98

[Rouse *et al.* 1974] ROUSE, J. W. ; HAAS, R. H. ; SCHELL, J. A. ; DEERING, D. W. ; HARLAN, J. C.: Monitoring the vernal advancement of retrogradation of natural vegetation / NASA / Goddard Space Flight Center, Type III Final Report. Greenbelt, Maryland, USA, 1974. – Research Report 170

[RTE, Gestionnaire du Réseau de Transport d'Electricité 2008a] RTE, GESTIONNAIRE DU RÉSEAU DE TRANSPORT D'ELECTRICITÉ: *Sous les lignes, prudence, restons à distance*. `http://www.sousleslignes-prudence.com/`. 2008. – (Accessed on the 31st of August 2009) 150

[RTE, Gestionnaire du Réseau de Transport d'Electricité 2008b] RTE, GESTIONNAIRE DU RÉSEAU DE TRANSPORT D'ELECTRICITÉ: *Travaux d'élagage de la végétation à proximité des lignes à Marseille (Bouches du Rhône)*. http://www.rte-france.com/. 2008 150

[Ruskoné 1996] RUSKONÉ, R.: *Extraction automatique du réseau routier par interprétation locale du contexte: application à la production de données cartographiques*, Université de Marne-la-Vallée, Ph.D. thesis, 1996 2

[Rutzinger *et al.* 2007] RUTZINGER, M. ; HÖFLE, B. ; PFEIFER, N.: Detection of high urban vegetation with airborne laser scanning data. In: *Proceedings of Forestsat Conference, Montpellier, France*, 2007 3

[Schardt *et al.* 2002] Schardt, M. ; Ziegler, M. ; Wimmer, A. ; Wack, R. ; Hyyppä, J.: Assessment of forest parameters by means of laser scanning. In: *ISPRS Commission III, Symposium*. Graz, Austria, September 2002, p. 302–310 53

[Secord and Zakhor 2006] Secord, J. ; Zakhor, A.: Tree detection in aerial lidar and image data. In: *International Conference on Image Processing*. Atlanta, Georgia, USA, September 2006, p. 2317–2320 54

[Segl *et al.* 2003] Segl, K. ; Roessner, S. ; Heiden, U. ; Kaufmann, H.: Fusion of spectral and shape features for identification of urban surface cover types using reflective and thermal hyperspectral data. In: *ISPRS Journal of Photogrammetry & Remote Sensing* 58 (2003), p. 99– 112 28

[Shackelford and Davis 2003] Shackelford, A.K. ; Davis, C.H.: A Hierarchical Fuzzy Classification Approach for High-Resolution Multispectral Data Over Urban Areas. In: *IEEE Transactions on Geoscience and Remote Sensing* 41 (2003), p. 1920–1931 48

[Small and Miller 1999] Small, C. ; Miller, R. B.: Digital Cities II: Monitoring the Urban Environment from Space. In: Huand, Y. (Editor): *Toward Digital Earth: Proceedings of the International Symposium on Digital Earth (ISDE)*. Beijing, China : Science Press, November 1999, p. 1–7 1

[Solberg *et al.* 2006] Solberg, S. ; Naesset, E. ; Bollandsas, O.M.: Single tree segmentation using airborne laser scanner data in a structurally heterogeneous spruce forest. In: *Photogrammetric Engineering and Remote Sensing* 72 (2006), Nr. 12, p. 1369–1378 54

[Sowmya and Trinder 2000] Sowmya, A. ; Trinder, J.: Modelling and representation issues in automated feature extraction from aerial and satellite images. In: *ISPRS Journal of Photogrammetry & Remote Sensing* 55 (2000), p. 34–47 101

[Stefanov *et al.* 2001] Stefanov, W.L. ; Ramsey, M.S. ; Christensen, P.R.: Monitoring Urban Land Cover Change : An Expert System Approach to Land Cover Classification of Semiarid to Arid Urban Centers. In: *Remote Sensing of Environment* 77 (2001), p. 173–185 47

[Straub 2003a] Straub, B. M.: Automatic Extraction of Trees from Aerial Images and Surface Models. In: *International Society of Photogrammetry Remote Sensing, Photogrammetric Image Analysis Conference* Volume XXXIV, Part 3/W8. Munich, Germany, September 2003, p. 157–166 55, 177

[Straub 2003b] Straub, B. M.: A Top-down Operator for the Automatic Extraction of Trees-Concept and Performance Evaluation. In: *International Society of Photogrammetry and Remote Sensing Comission III/WG3*. Dresden, Germany, 2003, p. 34–39 55

[Straub 2004] Straub, B. M.: A Multiscale Approach for the Automatic Extraction of Tree Tops from Remote Sensing Data. In: *International Society of Photogrammetry and Remote Sensing* Volume XXXV, Part B3. Istanbul, Turkey, 2004, p. 418–423 55

[Straub and Heipke 2001] Straub, B. M. ; Heipke, C.: *Automatic Extraction of Man-Made Objects from Aerial and Space Images*. Volume III. Chap. Automatic Extraction of Trees for 3D City Models From Images and Height Data, p. 267–277. In: Gruen, A. (Editor) ; Baltsavias, E.P. (Editor) ; Henricsson, O. (Editor): *Automatic Extraction of Man-Made Objects from Aerial and Space Images* Volume III, A.A.Balkema Publishers, Lisse/Abingdon/Exton(PA) Tokio, 2001 48, 55, 168

[Straub *et al.* 2003] Straub, B.M. ; Gerke, M. ; Pahl, M.: Automatic Mapping of Settlement Areas Using a Knowledge-Based Image Interpretation System. In: Crowley, J. (Editor) ; Piater, J. (Editor) ; Vincze, M. (Editor) ; Paletta, L. (Editor): *3rd International Conference on Computer Vision Systems* Volume 2626. Berlin Heidelberg : Springer-Verlag, April 2003, p. 355–364 3, 55

[Sugumaran *et al.* 2003] Sugumaran, R. ; Pavuluri, M.K. ; Zerr, D.: The use of high-resolution imagery for identification of urban climax forest species using traditional and rule-based classification approach. In: *Geoscience and Remote Sensing, IEEE Transactions on* 41 (2003), Sept., Nr. 9, p. 1933–1939 98

[Sève 1996] Sève, R.: *Physique de la couleur. De l'apparence colorée à la technique colorimétrique.* Paris : Masson, 1996. – 356 p 179

[Taillandier 2004] Taillandier, F.: *Reconstruction du bâti en milieu urbain: une approche multi-vues*. France, Ecole Polytechnique, Ph.D. thesis, 2004 2

[Taillandier and Vallet 2005] Taillandier, F. ; Vallet, B.: Fitting Constrained 3D Models in Multiple Aerial Images. In: *British Machine Vision Conference*. Oxford, U.K., August 2005 168

[Terrettaz and Collet 1997] Terrettaz, P. ; Collet, C.: Différenciation des tissus résidentiels à l'aide de l'indice PVI, de la morphologie mathématique et de filtrage contextuel : exemple de Genève (Suisse). In: AUPELF-UREF (Editor): *Télédétection des milieux urbains et périurbains : sixièmes journées scientifiques du « Réseau Télédétection »*, 1997, p. 123–131 26

[Thenkabail *et al.* 2004] Thenkabail, P.S. ; Enclona, E.A. ; Ashton, M.S. ; Legg, C. ; De Dieu, M.J.: Hyperion, IKONOS, ALI, and ETM+ sensors in the study of African rainforests. In: *Remote Sensing of Environment* 90 (2004), Nr. 1, p. 23–43 97

[Theodoridis and Koutroumbas 2003] Theodoridis, S. ; Koutroumbas, K. ; Press, Elsevier A. (Editor): *Pattern Recognition, 2nd edition*. 2003 36

[Thom and Souchon 1999] Thom, C. ; Souchon, J-P.: The IGN digital camera system in progress. In: Fritsch, R. (Editor): *Photogrammetric Week* Volume 99, Wichmann Verlag, Heidelberg, 1999, p. 89–94 9

[Tiede *et al.* 2005] Tiede, D. ; Hochleitner, G. ; Blaschke, T.: A full GIS-based workflow for tree identification and tree crown delineation using laser scanning. In: Stilla, U. (Editor) ; Rottensteiner, F. (Editor) ; Hinz, S. (Editor): *The International Archives of Photogrammetry, Remote Sensing and Spatial Information Sciences.* Volume XXXVI. Vienna, 2005, p. 9–14 54

[Tiede *et al.* 2006] Tiede, D. ; Lang, S. ; Hoffmann, C.: Supervised and forest type-specific multi-scale segmentation for a one-level-representation of single trees. In: *International Archives of Photogrammetry, Remote Sensing and Spatial Information Sciences* Volume XXXVI. Salzburg, Austria, July 2006 54

[Tooke *et al.* 2009] Tooke, T. R. ; Coops, N. C. ; Goodwin, N. R. ; Voogt, J. A.: Extracting urban vegetation characteristics using spectral mixture analysis and decision tree classifications. In: *Remote Sensing of Environment* 113 (2009), Nr. 2, p. 398 – 407. – ISSN 0034-4257 1

[Tournaire 2007] Tournaire, O.: *Reconstruction 3D d'objets du réseau routier en milieu urbain à partir d'images haute résolution*. France, Université de Marne-la-Vallée, Ph.D. thesis, 2007 2

[Trias Sanz 2006] Trias Sanz, R.: *Semi-automatic rural land cover classification from high-resolution remote sensing images*. Paris, France, Université Paris 5, Ph.D. thesis, March 2006. – in english 109

[Tso and Mather 2001] Tso, B. ; Mather, P. M.: *Classification methods for remotely sensed data*. New York : Taylor and Francis, 2001 104, 178

[Tso and Olsen 2005] Tso, B. ; Olsen, R. C.: Combining spectral and spatial information into hidden Markov models for unsupervised image classification. In: *International Journal of Remote Sensing* 26 (2005), Nr. 10, p. 2113–2133 27

[Tuceryan and Jain 1998] Tuceryan, M. ; Jain, A. K.: *The Handbook of Pattern Recognition and Computer Vision*. Chap. Texture analysis, p. 207–248, Word Scientific Publishing Co, 1998 104

[Tucker 1979] Tucker, C. J.: Red and photographic infrared linear combinations for monitoring vegetation. In: *Remote Sensing of Envorinment* 8 (1979), p. 127–150 26

[Turner 2006] Turner, R. S.: *An airborne Lidar canopy segmentation approach for estimating above-ground biomass in coastal eucalypt forests.*, School of Biological, Earth & Environmental Science, University of New South Wales., Ph.D. thesis, 2006 48, 57

[United Nations 2007] United Nations, Population D.: *World Urbanization Prospects: The 2007 Revision*. http://www.un.org/esa/population/publications/wup2007/2007wup.htm. 2007 1

[Vapnik 1995] Vapnik, V. N.: *The nature of statistical learning theory*. New York, NY, USA : Springer-Verlag New York, Inc., 1995 36, 152

[Varma and Zisserman 2003] Varma, M. ; Zisserman, A.: Texture classification: Are filter banks necessary? In: *2003 IEEE Computer Society Conference on Computer Vision and Pattern Recognition, 2003. Proceedings* Volume 2, 2003 149

[Vincent and Soille 1991] Vincent, L. ; Soille, P.: Watersheds in digital spaces: an efficient algorithm based on immersion simulations. In: *Pattern Analysis and Machine Intelligence, IEEE Transactions on* 13 (1991), Jun, Nr. 6, p. 583–598 53, 55, 69, 148

[Voss and Sugumaran 2008] Voss, M. ; Sugumaran, R.: Seasonal Effect on Tree Species Classification in an Urban Environment Using Hyperspectral Data, LiDAR, and an Object-Oriented Approach. In: *Sensors* 8 (2008), p. 3020–3036 98

[Wang *et al.* 2004] Wang, L. ; Gong, P. ; Biging, GS: Individual tree-crown delineation and treetop detection in high-spatial-resolution aerial imagery. In: *Photogrammetric Engineering and Remote Sensing* 70 (2004), Nr. 3, p. 351–357 55

[Wania 2008] Wania, A.: *Urban vegetation: detection and function evaluation for air quality assessment*. France, Université Louis Pasteur, Ph.D. thesis, 2008. – in english 28, 97

[Warner *et al.* 1998] Warner, T.A. ; Lee, J.Y. ; McGraw, J.B.: Delineation and Identification of Individual Trees in the Eastern Deciduous Forest. In: Hill, D.A.

(Editor) ; Leckie, D.G. (Editor): *Automated Interpretation of High Spatial Resolution Digital Imagery for Forestry*. Victoria, British Columbia, Canada, 1998, p. 81–91 52

[Weinacker *et al.* 2004] Weinacker, H. ; Koch, B. ; Heyder, U. ; Weinacker, R.: Development of Filtering, Segmentation and Modelling Modules for LIDAR and Multispectral Data as a Fundament of an Automatic Forest Inventory System. In: *Proceedings of the ISPRS working group VIII/2, Laser-Scanners for Forest and Landscape Assessment* Volume 36. Freiburg, Germany, October 2004, p. 50–55 3, 49, 53

[Wolf (Straub), B. M. and Heipke, C. 2007] Wolf (Straub), B. M. and Heipke, C.: Automatic extraction and delineation of single trees from remote sensing data. In: *Machine Vision and Applications* 18 (2007), Nr. 5, p. 317–330 55

[Work Group Computer Graphics and Media Design, Dresden University of Technology 2007] Work Group Computer Graphics and Media Design, Dresden University of Technology: *Xfrog Public Plants*. `http://web.inf.tu-dresden.de/ST2/cg/downloads/publicplants/`. 2007. – (Accessed on the 26 of January 2007) 96

[Wu 2003] Wu, J.: *Rotation invariant classification of 3d surface texture using photometric stereo*. Edinburgh, UK, Heriot-Watt University, Ph.D. thesis, 2003 100

[Wulder *et al.* 2000] Wulder, M. ; Niemann, K.O. ; Goodenough, D.G.: Local Maximum Filtering for the Extraction of Tree Locations and Basal Area from High Spatial Resolution Imagery. In: *Remote Sensing of Environment* 73 (2000), Nr. 1, p. 103–114 50

[Wulder *et al.* 2004] Wulder, M.A. ; White, J.C. ; Niemann, K.O. ; Nelson, T.: Comparison of Airborne and Satellite High Spatial Resolution Data for the Identifcation of Individual Trees with Local Maxima Filtering. In: *International Journal of Remote Sensing* 25 (2004), Nr. 11, p. 2225 – 2232 48, 173

[Xiao *et al.* 2004] Xiao, Q. ; Ustin, SL ; McPherson, EG: Using AVIRIS data and multiple-masking techniques to map urban forest tree species. In: *International Journal of Remote Sensing* 25 (2004), Nr. 24, p. 5637–5654 97

[Xie *et al.* 2008] Xie, Yichun ; Sha, Zongyao ; Yu, Mei: Remote sensing imagery in vegetation mapping: a review. In: *Journal of Plant Ecology* 1 (2008), Nr. 1, p. 9–23 24, 27, 28, 29

[Xu 2008] Xu, H.: A new index for delineating built-up land features in satellite imagery. In: *International Journal of Remote Sensing* 29 (2008), Nr. 14, p. 4269–4276 3

[Xu *et al.* 2005] Xu, M. ; Watanachaturaporn, P. ; Varshney, P.K. ; Arora, M.K.: Decision tree regression for soft classification of remote sensing data. In: *Remote Sensing of Environment* 97 (2005), Nr. 3, p. 322 – 336. – ISSN 0034-4257 26

[Yansong *et al.* 2004] Yansong, B. ; Xiaowen, L. ; Changzuo, W. ; Jihua, W. ; Liangyun, L.: The Method Research of City Vegetation Information Abstraction Based on High-Resolution IKONOS Image. In: *International Geoscience and Remote Sensing Symposium*. Alaska, USA : IEEE, Piscataway NJ, ETATS-UNIS, September 2004 48

[Yu *et al.* 2006] Yu, Q. ; Gong, P. ; Clinton, N. ; Biging, G. ; Kelly, M. ; Schirokauer, D.: Object-based Detailed Vegetation Classification with Airborne High Spatial Resolution Remote Sensing Imagery. In: *Photogrammetric Engineering and Remote Sensing* 72 (2006), Nr. 7, p. 799–811 109

[Yu *et al.* 2004] Yu, X. ; Hyyppä, J. ; Kaartinen, H. ; Maltamo, M.: Automatic detection of harvested trees and determination of forest growth using airborne laser scanning. In: *Remote Sensing of Environment* 90 (2004), Nr. 4, p. 451–462 53

[Zhang and Foody 1998] Zhang, J. ; Foody, G. M.: A fuzzy classification of sub-urban land cover from remotely sensed imagery. In: *International Journal of Remote Sensing* 19 (1998), Nr. 14, p. 2721–2738 27

[Zhang and Feng 2005] Zhang, X. ; Feng, X.: Detecting urban vegetation from IKONOS data using an object-oriented approach. In: *Proc. International Geoscience and Remote Sensing Symposium (IGARSS)* Volume 2, IEEE, July 2005, p. 1475 – 1478 1

[Zhang 2001] Zhang, Y.: Texture-Integrated Classification of Urban Treed Areas in High-Resolution Color-Infrared Imagery. In: *Photogrammetric Engineering and Remote Sensing* 67 (2001), December, Nr. 12, p. 1359–1365. – Journal of the American Society for Photogrammetry and Remote Sensing 3, 48

[Zhou and Troy 2008] Zhou, W. ; Troy, A.: An object-oriented approach for analysing and characterizing urban landscape at the parcel level. In: *International Journal of Remote Sensing* 29 (2008), Nr. 11, p. 3119–3135 3

[Zhu *et al.* 2003] Zhu, G. ; Bian, F. ; Zhang, M.: A Flexible Method for Urban Vegetation Cover Measurement based on Remote Sensing Images. In: *ISPRS*

Joint Workshop High Resolution Mapping from Space. Hannover, Germany : ISPRS, 2003 27

[Zhu *et al.* 2005] Zhu, X. ; He, C. ; Pan, Y. ; Zhang, J.: Detecting urban green space from landsat7 ETM+ data by using an unmixing algorithm of support vector machine. In: *Proc. International Geoscience and Remote Sensing Symposium (IGARSS)* Volume 2, IEEE, July 2005, p. 1467–1470 28

Résumé

La modélisation 3D des zones urbaines est un enjeu actuel important pour des applications liées à l'aménagement du territoire, l'urbanisme ou la gestion de l'environnement. Les méthodes de traitement automatique d'images aériennes proposes depuis plusieurs années pour la reconstruction 3D d'environnements urbains se limitent aux objets créés par l'homme. Or, la végétation est également très importante pour la compréhension des zones urbaines. Cette thèse présente le développement d'un système hiérarchique d'analyse d'images aériennes couleur et infrarouge pour la détection et la caractérisation de la végétation en vue de la modélisation 3D des milieux urbains. Le premier module de ce système a pour fonction de détecter les zones de végétation. L'approche adoptée repose sur une méthode de classification supervisée utilisant les Séparateurs à Vaste Marge (SVM) que nous comparons aux approches traditionnelles de télédétection. Les modules suivants ont pour but de caractériser ces zones de végétation. La séparation en végétation haute (arbre) et végétation basse (pelouse) repose sur un critère de texture calculé sur le modèle numérique de surface (MNS). Ensuite, une étape d'extraction des houppiers faisant intervenir un algorithme de croissance de régions intégrant des caractéristiques géométriques d'arbres est présentée. Des paramètres morphologiques (la hauteur, le diamètre de la couronne, la localisation du tronc des arbres) sont estimés pour chaque houppier. Les différentes espèces d'arbres sont ensuite déterminées par un système de classification supervisée. Dans ce domaine, nous avons étudié l'apport des caractéristiques radiométriques, de texture, ainsi que de leur fusion. L'ensemble des informations extraites par ce système (paramètres morphologiques, type de végétation et espèce) est utilisé pour enrichir un modèle 3D urbain avec des modèles de végétation réalistes.

Mots clés : Analyse d'images, images aériennes multi-vues, reconstruction 3D, reconnaissance de formes, classification de texture, segmentation d'images, caractérisation de la végétation, modèle urbain 3D

Abstract

Automatic 3D reconstruction of urban areas is an active research topic in distinct application areas and an issue of primary importance in fields such as urban planning, disaster management, or telecommunications planning. Significant progress has been made in recent years concerning the automatic reconstruction of man-made objects or environments from multiple aerial images. Yet, a lot of challenge concerning the modelling of other objects present on the terrain surface, such as trees, shrubs, hedges, or lawns still exists. An accurate reconstruction of such types of vegetation areas is a challenge due to their complex nature and to their intricate distribution between man-made objects in dense urban areas. This thesis presents an image analysis system for vegetation detection and characterisation from high resolution colour infrared aerial imagery for 3D city modelling. The aim of the system's first module is to extract vegetation areas. The approach developed is based on a Support Vector Machines (SVM) classifier and its performances are compared to traditional remote sensing methods for vegetation detection. The system's following modules aim at characterising vegetation areas thus identified, according to their morphology. Separation into high- (tree) and low- (lawn) height vegetation areas is based on texture characteristics computed on the digital surface model (DSM). Individual tree crown delineation is performed by using a region-growing algorithm based on geometrical characteristics of trees. 3D morphological characteristics (height, crown diameter, tree trunk position) are estimated for each tree crown. A supervised classification to characterise each tree by its species is performed on each tree crown. The set of parameters extracted by each of the modules are used to enrich 3D city models by virtual realistic tree models.

Keywords: Image analysis, multi-view aerial images, 3D reconstruction, shape recognition, texture classification, image segmentation, vegetation characterisation, 3D city model.